IMPACTS OF DESICCATION CRACKING AND CLIMATE CHANGE ON HIGHWAY CUTTING HYDROLOGY

By

Andrew J. Booth

School of Civil and Building Engineering

A Doctoral Thesis

Submitted in partial fulfillment of the requirements for the award of

Doctor of Philosophy of

Loughborough University

June 2014

Abstract

Climate change is predicted to have a global effect on temperatures and precipitation rates throughout the world. The UK Climate projections expect that in the United Kingdom this will lead to warmer, drier summers and wetter winters, where events of extreme rainfall are more common. These changes are expected to impact on slope hydrology, and concurrently slope stability. In the United Kingdom this impact is expected to be negative, whereas in other countries, such as Italy and France it could lead to slopes being more stable. Infrastructure slopes in the UK range in age and construction quality, they are susceptible to serviceability problems, characterised by heterogeneous material properties and can fail unexpectedly due to progressive reduction in soil shear strength. In this thesis the effects of climate change on a highway cutting in the south of England are modelled, using numerical methods. A finite element model is created and developed in the software package GeoStudio VADOSE/W. The model has been validated against observed pore water pressure trends and magnitudes and is shown to be able to accurately replicate the behaviour. By incorporating the effects of desiccation cracking on the soil's material properties, by the means of bimodal soil water characteristic curve and hydraulic conductivity function, the replication of these trends is improved even further. A series of future climate series were created using the UKCP09 Weather Generator 2.0. These series were implemented with the VADOSE/W model as climate boundary conditions and models were run, and the results compared to control, current climate results. The results were investigated by the means of statistical analyses which revealed that climate change will have some significant effects on the slope's hydrology, increasing magnitudes of evapotranspiration greatly which can have further significant effects on the magnitude of suctions developing in the slope throughout the summer. It is thought that the results suggest that climate change will not have significant negative effects on slope stability. However it is important to remember that the results only apply with certainty to the specific slope and climate change scenario investigated here. The methods used and developed within this thesis can be extended to other locations, in the UK and internationally, analysing the effects of different climate change scenarios.

Contents

List of figures

List of tables

List of notation

A	Inverse of relative humidity at soil surface (Section 2.8.4.1)
A	Total area of cracked soil (Section 2.10.1)
A_c	Total area of cracks
AE	Actual evaporation
AET	Actual evapotranspiration
AEV	Air entry value
AT	Actual transpiration
D	Depth to phreatic surface
E_e	Elastic modulus with respect to change in effective stress
E_a	Vapour removal parameter
FEM	Finite element method
H	Total hydraulic head
H_s	Elastic modulus with respect to change in suction
HCF	Hydraulic conductivity function
I	Net infiltration
K_w	Hydraulic conductivity
K_r	Relative hydraulic conductivity
K_s	Saturated hydraulic conductivity
K_x	Hydraulic conductivity in x direction
K_y	Hydraulic conductivity in y direction
LAI	Leaf area index
LTA	Long term average
P	Precipitation
PBM	Physically-based model

PE	Potential evaporation
PI	Plasticity index
PLF	Plant limiting function
PML	Plant moisture limit
PRU	Potential root uptake
PSD	Pore series distribution
PT	Potential transpiration
Q	Applied boundary flux
Q_n	Net incoming radiation
R	Runoff
R_s	Contractile skin radius of curvature
RE	Recharge to water table
S	Storage (Section 2.8.1)
S	Actual nodal root uptake (Section 2.8.4.2.2)
SPSS	Statistical Product and Service Solutions
SWCC	Soil water characteristic curve
T	Transpiration
T_s	Surface tension of water
VWC	Volumetric water content
W_W	Wind speed
X_{max}	Maximum crack width for capillary law to still apply
a	Van Genuchten curve fitting parameter
a_d	Drying value of a
a_w	Wetting value of a
c'	Effective cohesion
c'_p	Effective cohesion at peak
c'_{cs}	Effective cohesion at critical state
c'_r	Effective cohesion at residual
dof	Degrees of freedom
f_w	Ratio of actual to hydrostatic suctions
h	Water pressure head
i	Gradient of hydraulic potential
m	Van Genuchten curve fitting parameter

n	Van Genuchten curve fitting parameter
q	Specific flux
r	Effect size
t	Time
t	T-test statistic (Section 6.5.1.1.1)
u_a	Air pressure
u_w	Pore water pressure
u_v^{air}	Near surface air vapour pressure
u_{v0}^{air}	Saturated vapour pressure
u_v^{soil}	Near surface air vapour pressure in soil
x	Horizontal distance
y	Vertical distance
y_c	Crack depth
Γ	Slope of saturation vapour pressure versus temperature curve
ϕ'	Angle of shearing resistance
ϕ'_p	Angle of shearing resistance at peak
ϕ'_{cs}	Angle of shearing resistance at critical state
ϕ'_r	Angle of shearing resistance at residual
η	Psychrometric constant
θ	Volumetric water content
θ_r	Residual volumetric water content
θ_s	Saturated volumetric water content
σ'	Effective stress
ϑ_c	Crack porosity
ϑ_s	Soil porosity
ν	Poisson's ratio
ρ	Density of soil
ρ_w	Density of water
σ	Total stress
τ_p	Peak shear stress
τ_r	Residual shear stress
χ	Effective stress parameter
ψ	Suction

Terminology

Climate   Climate is the average weather expected over a long period of time, typically 30 years.

Hydrology   The study of the movement of water through the environment, which can pertain to surface water flow, ground water flow, infiltration, precipitation and more.

Vadose Zone   The zone between the ground surface and the phreatic surface where water pressures are negative.

Weather   Weather is the temperature, precipitation (rain, hail, sleet and snow) and wind, which change hour by hour and day by day.

1 Introduction

The Intergovernmental Panel for Climate Change (IPCC) has confirmed that the earth's atmosphere is warming (IPCC, 2007). It is well known that most landslides are directly or indirectly triggered by adverse climatic factors (Briceno et al., 2007), such as heavy rainfall events (Wasowski et al., 2007). With a changing climate it is essential to determine the exact relations between slope failure and climate change conditions; the understanding of this may significantly contribute to proposals of appropriate remedial measures and management policies (Briceno et al., 2007). In the last century there has been a significant increase in the number of reported landslides; in individual countries such as Canada (Geertsema et al., 2007) and Italy (Wasowski et al., 2007), and also worldwide (CRED, 2009; Petley, 2012). These increases have been linked to climate change, with extreme precipitation events, such as the winter of 2000/2001 in the United Kingdom thought to be a determining factor.

It is important to consider that different regions of the world will experience different types of climate change. For example, in southern Italy the projections show a strong trend of decreasing mean yearly precipitation (Wasowski et al., 2007), whereas in the United Kingdom the UKCP09 projections (UK Climate Projections, 2009) suggest little to no change in mean yearly precipitation but a significant decrease in summer precipitation with a increase in winter precipitation, particularly extreme events. There also remains the question if the increases observed in landslides are actually a result of climate change or other causes. In the south of Italy, Wasowski et al. (2007) conclude that the observed increase in landslides is actually due to land use changes and not climate change, believing that climate change would actually make slopes more stable due to the decrease in projected rainfall. Similar results have been found

by Malet et al. (2007) in the south east of France, where the projected climate change is for much drier summers resulting in a decrease in soil water content and an increase in slope stability.

The meaning of the term 'landslide' in the English language is very broad, possibly including slope instability in man-made or natural slopes, deep and shallow failure, sudden failure or progressive failure, rock slides, debris flow and more, each with its own set of distinct parameters and triggering mechanisms. It would therefore be incongruous to make a catchall statement such as "landslide occurrence in the future will increase due to climate change" (Briceno et al., 2007). Briceno et al. (2007) conclude that it is of utmost importance to improve knowledge within:

- Causes of critical behaviour, through detailed hydrogeological and geomechanical modelling.
- The potential impact of climate change on landscape and vegetation cover.
- The gathering of more monitoring data of all kinds in order to determine the real behaviour of landslide movements.

In this thesis the focus will be on hydrogeological modelling; investigating the effects of climate change on the hydrology of man-made infrastructure slopes. The main focus of the work will be in the United Kingdom, drawing on the work of Rouainia et al. (2009) and Davies et al. (2008a; 2008c), however it is anticipated that the methods developed will be applicable not only in the United Kingdom, but also internationally.

Infrastructure slopes in the United Kingdom are subject to a seasonal climate that causes variation in pore water pressures throughout the year. Field observations have shown that high, negative pore water pressures are synonymous with the summer months, with these often dissipating to hydrostatic pore water pressures by winter (Anderson and Kneale, 1980; Ridley et al., 2004a). The negative pore water pressures are synonymous with volume change; the soil shrinks as moisture is removed from the soil. Serviceability problems can result from these volume changes, for example railway lines can be taken out of line and level causing disruption to the network (Glendinning et al., 2009a; Loveridge et al., 2010). These issues are particularly common in the south of England where highly plastic clays, such as London Clay, are prevalent (Loveridge et al., 2010).

2

Heavy precipitation in the winter rewets slopes, dissipating suctions and bringing the slope closer to the point of failure, reducing the factor of safety as the soil weakens. A more recently recognised failure mechanism affecting infrastructure slopes is progressive failure, which has been linked to seasonal variation in the climate (Skempton, 1964). Cyclical pore water pressures cause progressive softening in over consolidated clay slopes. Seasonal cyclic stress changes, synonymous with the shrink-swell behaviour of clay slopes subject to alternating wet winters and dry summers, cause downslope movement, strain softening (as the plastic strains are irreversible) and eventually collapse (Kovacevic et al., 2001; Nyambayo et al., 2004; Loveridge et al., 2010).

Climate change will affect the United Kingdom. Significant projections for the climate include warmer, drier summers and winters that are wetter with more extreme precipitation events. The UKCP09 projections from the Met Office Hadley Centre show that effects in the south of England will be particularly severe (UK Climate Projections, 2009). Climate change is expected to have negative impacts on infrastructure slopes in the United Kingdom. Greater seasonality in the climate from summer to winter is likely to result in larger pore water pressure cycles. The size of these cycles has been linked to climate change and it is thought that delayed failure may become more problematic and frequent an occurrence in the future.

Numerical methods, such as the finite element method, have been employed to model these types of slopes with static boundary conditions and material properties often used. For example, steady state hydraulic boundary conditions representing probable summer and winter surface pore water pressures have been applied (Kovacevic et al., 2001; Nyambayo et al., 2004). However, in reality the slope-atmosphere interactions are far more complex than this. The processes of evaporation, transpiration, infiltration, runoff and subsurface flow all contribute to the subsurface hydrology of the slope. Physically-based models (PBMs) have been recommended as the best way to model these slopes (Dijkstra and Dixon, 2010; Fredlund et al., 2010a). These models combine a temporal climate process system for evaluation of the water

balance with a hydrogeological system and multi-layered soil system that can cope with variations in soil properties and soil water content.

Some authors have used these kinds of models to analyse the effects of vegetation and climate on railway earthworks (Briggs, 2011), or the possible effects of climate change on natural and infrastructure slopes (Collison, 2000; Davies et al., 2008c; Rouainia et al., 2009). None of these models have considered the effects of desiccation cracking on the hydraulic properties of the soil. These cracks allow easier infiltration of moisture into the slope, effectively increasing the permeability of the soil. It has been suggested that simulations based on intact soil material could differ considerably from those based on the soils that develop near the ground surface with time (Fredlund et al., 2010a).

The aim of the work presented in this thesis is to develop a physically-based model that accounts for the temporal and spatial variability of climate and material properties. The model is developed with the intention of using it to analyse the effects of climate change on infrastructure slopes in the United Kingdom. The model can then be used as a basis for modelling similar problems in the United Kingdom and internationally.

1.1 Objectives

1) Identify an infrastructure slope in the United Kingdom for which extensive pore water pressure data, material properties and climate data is available and develop a physically-based model in a suitable finite element software package and use the obtained data to validate the model.

2) Identify and review potential methods for including the effects of desiccation cracks of the hydraulic properties of soil.

3) Develop an improved soil hydraulic property model and implement into the already existing physically-based model, and then validate the results against the observed pore water pressure data for the slope.

4) Identify the most suitable, up-to date method for generating series of future climate data. Use this to create series of temporal, present and future climate data sets for the location of the slope.

5) Combine the developed physically-based model, which includes the soil properties considering the effects of desiccation, with the generated climate data to analyse the effects of climate change on infrastructure slopes in the United Kingdom.

6) From the results of these analyses, draw conclusions that further the understanding of the effects of climate change on infrastructure slopes and make recommendations for further work.

1.2 Layout of the thesis

In addition to this chapter this thesis comprises six further chapters. A literature review chapter, three methodology, results and analysis, and discussion chapters, a methodology overview chapter and finally, the conclusions and recommendations for further work chapter.

Chapter 2 – Literature review. In this chapter a detailed investigation into and review of the current state of knowledge of the research area are carried out. The review focuses on infrastructure slope problems, slope hydrology, atmosphere/slope interactions, unsaturated soil (mechanics and hydrology), effects of desiccation cracking and climate change. At the end of this chapter the proceeding methodology is described briefly.

Chapter 3 – Methodology overview. In the overview of the methodology brief descriptions of the general approach to the work in this thesis and then more specific ideas for each chapter are presented.

Chapter 4 – Development and validation of the Newbury cutting hydrological model. A numerical hydrology model of the Newbury bypass cutting slope is

developed and validated in this chapter. The results are analysed and deficiencies in the model identified.

Chapter 5 – Effects of desiccation cracks. Improvements are made to the model developed in the previous chapter. The effects of hysteresis and desiccation cracking on the hydraulic behaviour of the soil is considered and included in the model.

Chapter 6 - Modelling the effects of climate change on the Newbury cutting. Soil property models including the effects of desiccation, developed in the previous chapter, are implemented into a study investigating the effects of climate change on the Newbury cutting slope.

Chapter 7 – Conclusions and recommendations. In the final chapter conclusions from the results and analyses are given. Some recommendations for further work are also made.

2 Literature review

2.1 Chapter Outline

This chapter reviews previous work and the current understanding in the area of embankment and cuttings and their hydrology and stability. The chapter begins with an overview of typical infrastructure earthworks in the United Kingdom and then discusses the types of slope stability issues affecting these slopes and also other problems that are encountered. Observations of the hydrological behaviour, particularly seasonal pore water pressure cycles, in infrastructure slopes and actual failures of these slopes are then described.

The next sections move onto describing the requirements of modelling and replicating the hydrological behaviour of infrastructure slopes; starting with a description of the effects of climate, and how these effects may be quantified. Unsaturated soils are described, focussing on the effects on soil strength and soil hydrology that a soil being in the unsaturated state has. Desiccation cracking, which is a phenomenon synonymous with unsaturated soil, is described; considering the influence on material properties and subsequent effects on slope hydrology.

Forecast climate change for the United Kingdom is reviewed, using the UKCP09 climate change projections. The possible effects of climate change on natural and man-made slopes internationally are considered and then specifically the effects on the hydrology of infrastructure slopes are looked at. The methods of implementing these effects into numerical models are studied. Numerical modelling software is identified, with the intention of selecting the most suitable one for the proceeding

work. In the final section the finite element software package VADOSE/W is introduced.

Section	Title
2.2	Earthworks in the United Kingdom
2.3	Problems Encountered
2.4	Characterising Permeability
2.5	Progressive failure
2.6	Pore water pressure measurements in infrastructure slopes
2.7	Observed failures of infrastructure slopes in the UK
2.8	Atmosphere and slope interactions
2.9	Unsaturated soil
2.10	Desiccation cracking
2.11	Climate change
2.12	Numerical methods and software

Table 2-1: Literature review section headings.

2.2 Earthworks in the United Kingdom

There are approximately 20 000 km of infrastructure embankments and cuttings in the United Kingdom, owned by Network Rail, The Highways Agency, British Waterways and London Underground Limited (Perry et al. 2003a; 2003b), making up about one third of the total asset value for transport infrastructure (Clark et al., 2006). There are approximately equal lengths of both cuttings and embankments (Table 2-2). Of the total main transport network, including motorways, railways and A-roads, more than 7% is located in areas with a moderate to significant landslide potential (Dijkstra and Dixon, 2010).

Infrastructure owner	Total length of embankments (km)	Total length of cuttings (km)
Network Rail	5000	5000
Highways Agency	3500	3500
British Waterways	1100	1100
London Underground	60	60

Table 2-2: Infrastructure earthworks and owners in the UK (after Perry et al., 2003a; 2003b).

Railway and highway earthworks in the UK are beginning to suffer, due to age (most railway earthworks are around 150 years of age (Perry et al., 2003a), and also a lack of proper investment in maintenance and repair (Glendinning et al., 2009a). However, an increasing demand for timeliness and reliability from existing transport networks has led to the introduction of financial penalties for railways (Perry et al., 2003b). Awareness has been raised of the need to maintain earthworks, and as a result the amounts spent on appraisal, maintenance and repair has increased. In 1993/1994 the UK Department of Transport estimated that £11 600 000 was spent on remediation of earthworks (Glendinning et al., 2009a); this figure had risen to at least £50 000 000 by 1998/1999, although the totals are likely to be even higher as records at the time were incomplete (Perry et al., 2003a; 2003b). More up to date figures are not available; however a recent Freedom of Information Request (Highways Agency, 2013) revealed that between 2003 and 2012 the total amount spent on repairs of highways in England by the Highways Agency increased from £726m to £809m, with a peak in 2010 of £1,307m.

It is impractical to replace all these earthworks (Clarke et al., 2006), therefore proper maintenance and repair is essential. In a monetary sense planned maintenance and repair is preferable to unplanned. Once compensation has been taken into account, costs of up to ten times greater have been recorded for unplanned over planned maintenance (Glendinning et al., 2009a).

Earthworks are affected by the climate; it is well documented that periods of extreme rainfall result in more earthwork failures (Loveridge et al., 2010). In proceeding sections it will be shown that the climate in the United Kingdom is predicted to change (Section 2.11), with more extreme wet weather events, and greater seasonal variation in climate, anticipated to occur each year. With this changing climate there will need to be a changing appreciation of the earthworks that are at risk and when they will be at risk.

2.2.1 Past and present design and construction

The majority of the rail network in the United Kingdom was built in the early to mid-19th century, with construction peaking in the 1850's (Perry et al., 2003a). Between 1834 and 1841 some 660 miles of railway were built in England, involving the excavation of approximately 54 million m^3 of material to form cuttings, the majority of the excavated material was then used to form the embankments (Skempton, 1996). These cuttings and embankments were constructed before the advent of modern soil mechanics theories and thus there was little or no understanding of the processes occurring within an embankment during or after construction (Glendinning et al., 2004a; Ridley et al., 2004a). Based on publications from the time of construction, Skempton (1996) gives a detailed account of how cuttings and embankments were constructed during the railway boom of the mid-19th century.

On the best method of embankment construction at the time Skempton (1996, p.35) says…

"The best way of building an embankment, especially in clay, would have been to form the bank in shallow layers, say 2 to 4 ft. thick, running out each of them to the full length, and following with the upper layers after each of the lower ones was laid and compacted with 'beetles' or punners". Indeed, this method was used in places; however it was often considered that this was too slow a process, and not suited to the combined operations of cuttings and embankments on a large scale (Skempton 1996). Instead the most commonly used method in the mid-1830s was to "run out the bank to its full height at once, by end-tipping from the advancing head of the bank" (Skempton 1996, p.35). The embankments of the time were being built in thick layers without compaction (Vaughan et al., 2004).

Problems were often encountered very soon after construction, with settlement of embankments being the least of the issues. Slips occurring in embankments and cuttings were common during construction and in the years soon after. Of embankments Skempton (1996, p.41-42) says "slips within the body of an embankment were nearly always restricted to clay fills (poorly compacted by modern standards) and resulted principally from softening of the clay lumps by absorption of

rain water", and on cuttings "superficial slips were common in clay cuttings either in rainy seasons during construction or in the first or second winter afterwards".

When slips occurred during construction, typically when tipped to a height greater than 5 metres (Kovacevic et al., 2001), the builders, with no understanding of the causes of the failures, would simply keep on building until the embankment stayed up, probably due to partial consolidation and gain in strength (Vaughan et al., 2004).

Copyright not obtained

Figure 2-1 shows a cross section of a typical historical railway embankment, compared to a modern highway embankment. Ballast fill covers the top of the slope and vegetation is allowed to grow uncontrolled. As well as the high permeability ballast being used, the poor compaction of this fill also leads to a permeability that is relatively high, allowing ease of infiltration of moisture after rainfall and increased landslide potential (Loveridge et al., 2010). Vegetation on railway embankments and cutting has grown largely unchecked since the 1950s (Loveridge et al., 2010), leading to many serviceability problems, related to the moisture removal by high water demand vegetation such as large trees (Glendinning et al., 2009).

Figure 2-1: Modern highway embankment (left) compared with historical railway embankment (right) (after O'Brien, 2007 cited in Loveridge et al., 2010).

2.2.1.1 Design and construction of modern highway slopes

In stark contrast to railway embankments, built well before the advent of modern soil mechanics, motorway embankments have been constructed since 1960 resulting in a higher standard of construction. Embankment fill is well compacted and placed on a suitable foundation, with soft materials removed prior to construction (Loveridge et al., 2010). Vegetation growth is also closely managed; embankments and cutting slopes are seeded with grasses in accordance with the Specification for Highway Works and selected shrubs and trees can also be planted (Greenwood et al., 2004; Glendinning et al., 2009). Major instability of modern embankments is rare (Loveridge et al., 2010), however minor instability, mostly related to shallow failures in the top portion of the embankment fill is reported (Parsons and Perry, 1985; Perry, 1989).

The design and planning of infrastructure slopes currently takes place based upon static information, such as maps, soil parameters and soil water conditions (Dixon et al., 2006). This information essentially provides a snapshot of the current conditions and assumes steady state conditions (Blight, 2003; Dixon et al., 2006). When considering the design life span of these slopes in the United Kingdom and the potential of climate change and other factors the use of steady state conditions becomes questionable. Dixon et al. (2006) highlight the potential impact of a changing climate, specifically temperature and precipitation, and its effects on the soil water balance.

2.2.2 Slope stability of infrastructure slopes

Landslides can occur at a range of scales, from shallow to deep-seated failures (Dijkstra and Dixon, 2010). Both cuttings and embankments are susceptible to both types of failure. Smethurst (2003) distinguishes between the two with the following definitions:

- Shallow failures, which can be up to 2.0 metres deep, are mostly contained within the embankment or cutting slopes. The failures tend to be translational in shape.
- Deep-seated failures occur at depths greater than 2.0 metres and are rotational in shape. The failure surface will often penetrate outside the slope and can damage nearby infrastructure or property.

Slope stability is driven by the external and internal hydrologies of the slope and changing material properties from time of construction (Glendinning et al., 2009a). However, deep and shallow types of failure differ in the triggering patterns (i.e. rainfall intensity and pore water pressure profiles), and therefore require different hydrological models when being analysed; Dijkstra and Dixon (2010) say…

"Shallow landslides, particularly those that show regular reactivation, form an important category of slope movement for the determination of critical climate thresholds and required detailed modelling of effective rainfall required to initiate movement. The lag time for significant increases in pore pressure to reach deeper failure surfaces makes the establishment of critical climate thresholds more complex. Several events could be required to trigger instability, and therefore issues such as antecedent rainfall or, more importantly antecedent soil moisture contents and pore pressures need to be determined". Loveridge et al. (2010) have summarised the different types of failure affecting infrastructure slopes in the United Kingdom in Table 2-3.

Infrastructure Slope	Deformation	Instability		Comment
		Shallow	Deep	

Highway cutting	✘	✔	✘ (not yet?)	Rare problems experienced; typically crossing landslides or other geohazards
Highway embankment	✘	✔	✘ (not yet?)	
Rail cutting	✘	✔	✔	Many failed – on average Network Rail manages 50 earthworks failures per year across Great Britain
Rail embankment	✔	✔	✔	

Table 2-3: Failure mechanisms compared with earthwork type (after Loveridge et al., 2010).

Deep-seated failures are often 'delayed'. This is a recognised phenomenon where failure can occur many years after construction; typically 40-50 years (Loveridge et al., 2010). Delayed failures have been observed in many railway and highway cuttings and embankments (Skempton, 1996). One such example of this type of failure is the A1 cutting slope near Dromore, Northern Ireland (Hughes et al., 2007). The cutting was in lodgement till, a stiff, heavily over consolidated clay. The slope failure occurred approximately 30 years after construction, following a prolonged period of heavy rainfall.

Age is shown to play an important part in determining whether a slope is susceptible to failure. The age of a slope will determine whether pore pressures are equilibrated and also the quality of construction. Parsons and Perry (1985, p.63) state that '...critical condition of a slope will arise at an age that will depend on the degree of over-consolidation, the rate of pore pressure equilibration and design factors such as the height and gradient of the slope and methods of drainage'. Major instability of more recently constructed highway embankments has been relatively rare (Loveridge et al. 2010), although not unheard of.

As discussed in Section 2.2.1, delayed failure of many railway cuttings and embankments has been observed, typically 40 – 50 years after construction. It has been postulated that as motorway infrastructure approaches and exceeds this age, similar failures may begin to occur within the infrastructure constructed since the 1960s (Loveridge et al., 2010), although with the modern construction methods that are now used it remains to be seen whether the time to failure (and the actual occurrence of failure) remain the same. Glendinning et al. (2006) explain how this potential problem is in part thought to be caused by the very low permeability present in the newly constructed embankments, particularly in the over-consolidated clay prevalent in the UK. After construction, very high suctions are often prevalent, providing apparent stability to the slope. Due to the low permeability of the soil, these suctions take a long time to equilibrate, typically 10 – 15 years. The suctions will eventually equilibrate and become positive at some points, leading to potential slope instability.

2.3   Problems Encountered

Embankments and cuttings constructed from high-plasticity clays are affected by seasonal changes in pore water pressure. These changes are driven by seasonal variation in climate, but can also be affected by the presence of vegetation on the slope, where mature, high water demand vegetation has the greatest affect. Seasonal pore water pressure variance leads to seasonal volume change, causing shrinkage and swelling in the clay, leading to a multitude of serviceability problems. Over a number of years, repeated shrink-swell cycles can lead to strain-softening and a reduction in strength of the soil, sometimes preceding ultimate slope failure by progressive/delayed failure. Glendinning et al. (2009b) identify three key effects that are driven by seasonal changes in pore water pressure (two of which have already been mentioned):-

1.   Deformations to the slope and, in the case of rail embankments the overlying track.

2. Cracking of the slope surface in the summer, leading to infiltration pathways available for the autumn.

3. Strain softening of clay materials in the slope as a result of shrinkage and swelling, which may lead to progressive failure of the slope.

In this section serviceability and ultimate failure, vegetation, soil type and soil permeability are looked at, particularly focussing on how they affect slope hydrology and slope stability. These areas of interest have been identified by numerous authors as being critical when considering either the actual stability of infrastructure slopes, or the parameters that influence the stability (Glendinning et al., 2009a; Glendinning et al., 2009b; Clarke and Smethurst, 2010; Dijkstra and Dixon, 2010; Loveridge et al., 2010) In proceeding sections more detailed reviews of the identified problems are presented.

2.3.1 Serviceability and ultimate limit states

Infrastructure slope failure may be defined in terms of serviceability limit state (SLS), which is measured by failure to meet ride quality performance and ultimate limit state (ULS), measured by catastrophic failure (Glendinning et al., 2009a). Differential vertical movements of the order of tens of millimetres have been recorded, causing serious problems for track alignment and ride quality on railways (Glendinning et al., 2009a; Loveridge et al., 2010). Ultimate failure often occurs during periods of intense rainfall. For example, during the extremely wet winter of 2000/2001 in the United Kingdom many slope failures occurred, causing disruption of the road and rail networks (Dixon et al., 2006). More recently, many landslides occurred in the extremely wet year of 2012, with a large proportion of these affecting man-made slopes such as road and railway embankments and cuttings (Pennington and Harrison, 2013). In the United Kingdom, 2012 was the second wettest year since records began (Met Office, 2013). The more recently understood phenomenon of delayed/progressive failure also affects these slopes, especially where high-plasticity clays dominate (Skempton, 1964; Kilsby et al., 2009; Clarke and Smethurst, 2010; Loveridge et al., 2010).

High-plasticity clays are a particular problem due to their high shrink-swell potential (Loveridge et al., 2010). The climate and slope vegetation have an important role to play in causing SLS or ULS problems; seasonal pore water pressures changes are driven by the seasonality of climate and water extraction by the vegetation, causing volume changes (leading to SLS problems) and also the prospect of strain softening leading to delayed failure (Glendinning et al., 2009b; Clarke and Smethurst, 2010).

2.3.2 Role of vegetation

Vegetation has always been recognised as affecting infrastructure in the United Kingdom, with issues of leaves on the line and sighting being the traditional focus (Glendinning et al., 2009b). However, it is now widely recognised that vegetation has a major impact on the engineering performance of slopes; whether they be for rail or highways (Smethurst et al., 2006; Glendinning et al., 2009a; Glendinning et al. 2009b). The impacts of vegetation can be split into mechanical and hydrological effects (Glendinning et al., 2009b). Some are viewed as beneficial to slope stability and some are seen as detrimental. Table 2-4 outlines the mechanical and hydrological impacts, splitting them into what are considered beneficial or detrimental to the performance of infrastructure slopes in the UK.

	Beneficial	**Detrimental**
Mechanical	Root reinforcement. Surcharging of the slope base.	Loading of the upper part of the slope. Uprooting or overturning.
Hydrological	Large suctions generated by mature trees. Prevention of pore water pressure build-up. Canopy and thatch effects can intercept rainwater.	Seasonal shrink swell cycles, exacerbated by out of phase nature of water demand leading to SLS and ULS problems/issues.

Table 2-4: Beneficial and detrimental impacts of vegetation on slopes (Greenwood et al., 2004; Ridley et al., 2004b; Glendinning et al., 2006; Glendinning et al., 2009b; Clarke and Smethurst, 2010).

Vegetation severely affects serviceability of slopes. High water demand vegetation growing on clay embankments extracts water from the slope, causing differential shrinkage settlements, taking the railway track out of line and level (Clarke and Smethurst, 2010). In the United Kingdom, peak water demand by vegetation in the summer is out of phase with the season of greatest rainfall in the winter, which intensifies seasonal fluctuations in soil moisture content (Smethurst et al., 2006; Glendinning et al., 2006). The presence of vegetation on a slope and the seasonality of its water demand can cause strain softening to occur as the soil goes through its shrink-swell cycles, which is indicative of progressive failure (Smethurst et al., 2006).

High water demand trees may also have beneficial impacts when it comes to the hydrology of slopes. High suctions are developed within the soil during the period of high water demand. During summer, suctions in excess of 250 kPa have been observed in slopes covered with high water demand trees, with water uptake extending to significant depths between 3 m and 5 m (Glendinning et al. 2009b; Briggs, 2011). Once summer ends, and the season of greatest rainfall begins, the soil profile begins to re-wet. It was shown that the suctions generated by mature trees growing in the low permeability clays prevalent in southern England are large enough to prevent full re-wetting of the soil in winter and spring, and thus suctions can persist throughout these seasons (Smethurst et al., 2006). There are potentially very significant implications for the management or removal of these types of tree (Kilsby et al., 2009; Loveridge et al., 2010). Suctions generated by light shrubs or grass are generally much lower than those developed by large trees and are therefore rarely sustained through winter (Smethurst et al., 2006).

Vegetation has some mechanical impacts and also canopy effects. For example, roots can often be seen holding together slopes that may otherwise degrade; tree roots can bind the soil to resist erosion and movement (Greenwood et al., 2004; Glendinning et al., 2009b). Vegetation can also act as a canopy over the slope; intercepting rainwater before it reaches the soil surface (Glendinning et al., 2009b).

As the climate changes, the role that vegetation plays in influencing slope stability could also change. Rouainia et al. (2009, p.81) suggest one of the possible effects, stating that '"the habits of vegetation are likely to change, with the potential of causing volume changes at greater depths as rooting to greater depths occurs during periods of drought". It is also postulated that small changes in temperature (just 1-2 degrees) could alter the type of vegetation, water use and rooting characteristics (Glendinning et al., 2006).

2.3.3 Problem soils

Serviceability problems can be created by soils with a large shrinkage potential (Clark and Smethurst, 2010; Loveridge et al., 2010). Delayed and progressive failure occurs in slopes constructed of or in soil that exhibits strain-softening behaviour. The overconsolidated, high-plasticity clays prevalent in southern England (Figure 2-2 a)) possess both of these properties. It is the combination of the seasonality of British climate from summer to winter and the properties that make these soils so problematic. Slope failures have been observed in London, Gault, Weald, Oxford, Kimmeridge, Reading and many more clays in southern England (Parsons and Perry, 1985).

AMPTHILL CLAY FORMATION
BARTON GROUP
GAULT FORMATION
KELLAWAYS FORMATION
KIMMERIDGE CLAY FORMATION
LAMBETH GROUP
LIAS GROUP
LONDON CLAY FORMATION
MERCIA MUDSTONE GROUP
OXFORD CLAY FORMATION
WADHURST CLAY FORMATION
WEALD CLAY FORMATION
WEALDEN GROUP

LOW
MEDIUM
HIGH
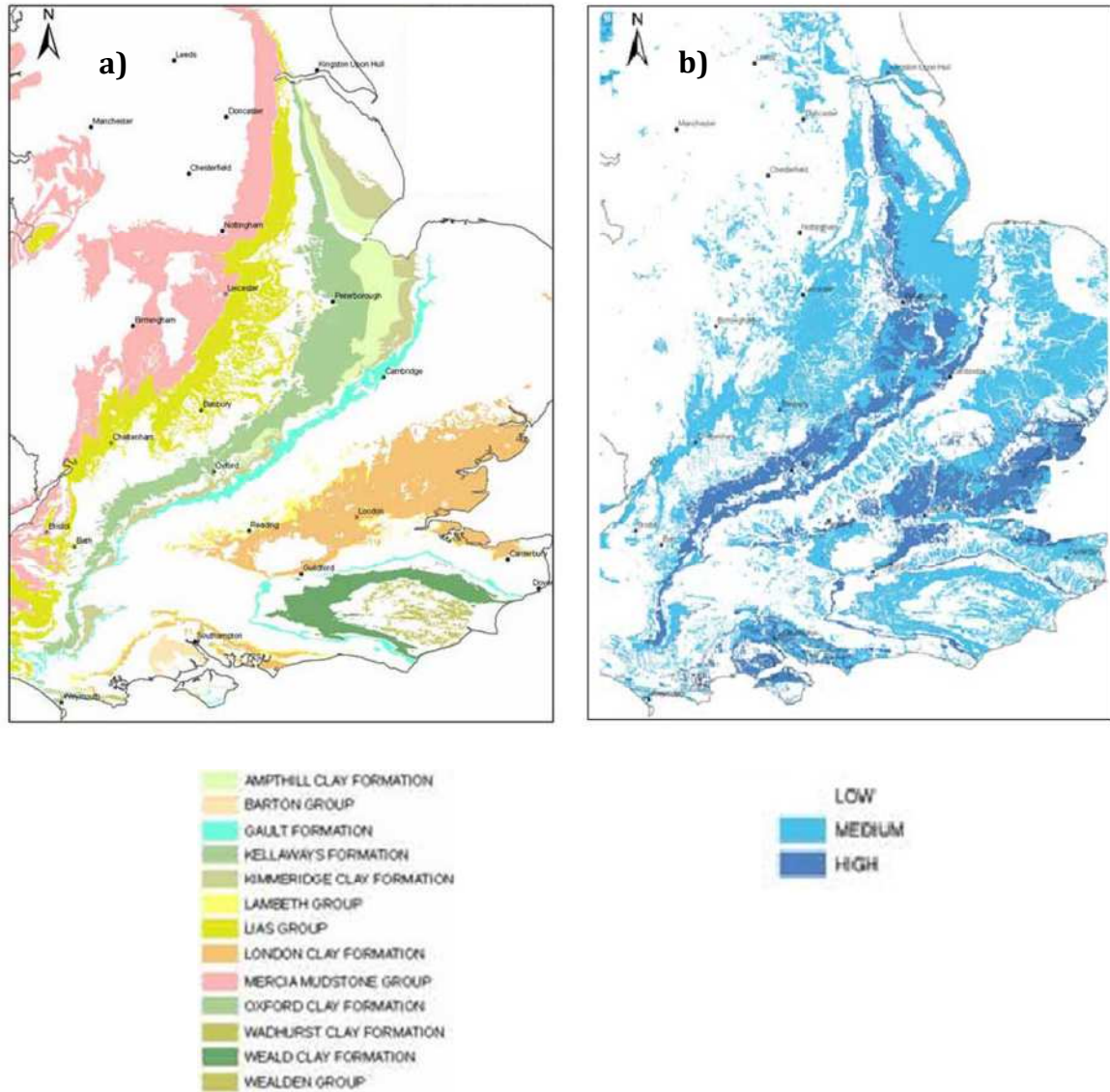
Figure 2-2: a) The clay formations of south east England, susceptible to shrink-swell behaviour and b) the shrink-swell hazard potential of soils in southern England (Reproduced with the permission of the British Geological Survey ©NERC. All rights Reserved).

Embankments and cuttings created from and within these soils experience high negative pore pressures after construction. The low permeability of the soil means that it can take many years, 10-15 years on average (Glendinning et al., 2006), for the pressures to equilibrate. In the following sections, these types of soil, their properties and the effects they have on the behaviour of slopes are investigated in greater detail; looking at soil permeability, how shrink-swell behaviour influences serviceability, the causes of delayed and progressive failure and also how the soil interacts with vegetation.

Shrinkage and swelling of soils is a major problem; in the United Kingdom alone it is estimated that in the last 10 years shrink-swell behaviour has cost the economy £3 billion (British Geological Survey, 2013). Figure 2-2 b) shows the shrink-swell hazard potential of soils in southern England. Areas of high shrink-swell potential are shown in dark blue. From this figure it is clear that large areas of the region are affected by these soils; the London, Oxford and Gault Clay formations appear to be particularly problematic. There are also large areas at medium risk (lighter blue), with the Kimmeridge, Lias and Weald formations being within this group. The at-risk soils are characterised by high plasticity, being able to absorb large quantities of water and swelling greatly. Table 2-5 shows a number of clay soils found in the United Kingdom and some measured values of plasticity index (Smethurst et al., 2006; Hughes et al., 2007; Atkinson, 2007; Zielinski et al., 2011; British Geological Survey, 2013).

Soil	Plasticity Index	Characterisation
Gault Clay	30 – 70	High to extremely high plasticity
London Clay	35	High plasticity
Reading Clay	32	High plasticity
Oxford Clay	28	High plasticity
Kimmeridge Clay	27	High plasticity
Weald Clay	23	Intermediate plasticity
Lodgement Till	20	Intermediate plasticity
Galston Clay	19	Intermediate plasticity

Table 2-5: Some clay soils in the United Kingdom and their plasticity characteristics.

2.4 Characterising Permeability

The coefficient of permeability of the soil is very important in determining transient pore water pressure response to rainfall. In a homogeneous material the response rates would primarily be determined by the balance between rainfall, soil thickness and diffusivity (Dijkstra and Dixon, 2010), however the clay soils found in the United Kingdom commonly show significant spatial heterogeneity and the occurrence of soil

structure, soil cracks and often, granular material such as sands and gravels strongly affecting the relationship (Nyambayo et al., 2004; Dijkstra and Dixon 2010). It is very important to have reliable permeability data to model the interaction between the climate and the pore water pressure response. Numerous works have tried to provide these measurements, some of which are described in Section 2.4.1.

It is noted that when dealing with unsaturated soils, what is commonly known as 'permeability' is most often referred to as the 'hydraulic conductivity'. In this thesis the term 'hydraulic conductivity' is more commonly used, as the hydraulic properties of unsaturated soils are mostly dealt with. However, in this section saturated soils are being considered, meaning that the more common term 'permeability' is most often used, with some exceptions; for example Collison et al. (2000) refer to the 'saturated conductivity'.

2.4.1 Permeability of clay Soils

The effects of anisotropy on permeability data have been highlighted by tests carried out by Smethurst et al. (2006). In-situ and lab tests were carried out on Grey and Weathered London Clay; the in-situ permeability was obtained from bailing out tests carried out in hand-augered boreholes 3.0 m deep, the lab tests were on undisturbed samples from depths of 0.5, 1.0, 1.5, 2.0 and 3.0 m carried out at effective confining pressures of 10, 15, 20, 25 and 35 kPa in triaxial apparatus. Table 2-6 summarises the results from these tests.

Property	Grey London Clay		Weathered London Clay	
	Range (m/s)	Average (m/s)	Range (m/s)	Average (m/s)

Saturated vertical permeability from triaxial tests	3.9×10^{-11} to 6.6×10^{-10}	2.3×10^{-10}	5.0×10^{-10} to 1.6×10^{-9}	8.7×10^{-10}
Saturated vertical permeability from borehole bail-out tests	2.3×10^{-9} to 4.4×10^{-9}	3.9×10^{-9}	3.6×10^{-8} to 5.0×10^{-8}	4.3×10^{-8}

Table 2-6: Permeability meaurements of Grey and Weathered London Clay from insitu and laboratory tests; after Smethurst et al. (2006).

Two important associations are seen in these results. Firstly, permeability is shown to be higher in the Weathered Clay. Secondly is the difference between the measured permeability from the insitu and laboratory tests. The insitu permeabilities are typically one to two orders of magnitude greater than the lab permeabilities. Smethurst et al. (2006) ascribe this to the effects of anisotropy and fabric that could not be fully captured in the triaxial samples.

Collison et al. (2000) has summarised the mean saturated conductivity of a Weald Clay located within the site of a landslide at Roughs field in southern England. Permeabilities for three zones are published; the root zone, landslide debris zone and the intact Weald Clay (Table 2-7). No detail is given on the method used to obtain these measurements other than a reference to an unpublished technical report. The magnitude of the permeability (x 10^{-9} m/s) in the intact clay is similar to that of the London Clay measured in the in-situ tests by Smethurst et al. (2006). In the root zone however, the permeability is shown to be four orders of magnitude greater than the intact clay. Collison et al. (2000) attribute this to the presence of cracks which are prevalent in the upper surface of the soil.

Zone	Mean saturated conductivity (m/s)
Root zone 0-30 cm	1.3×10^{-5}

Landslide debris 30-200 cm	8.7×10^{-7}
Weald Clay > 200 cm	7.8×10^{-9}

Table 2-7: Soil properties for the Roughs Field landslide, after Collison et al. (2000).

Anderson and Kneale (1980) have published permeability properties of a Kimmeridge Clay and Clay-loam from a highway embankment. The soil described as a clay-loam by the authors is taken from a 0.25 m deep 'mantle' at the uppermost section of the slope and is the result of transport and deposition of the material at the site. The Kimmeridge Clay sample taken from a depth of 1.0 m, and prevalent throughout the remainder of the slope, was relatively homogeneous with some in-filled fissure material and small inclusions had a very low permeability of 3.68×10^{-10} m/s. The clay-loam had a significantly higher permeability of 9.8×10^{-6} m/s.

Dixon and Bromhead (1999) carried out an investigation into the pore water pressure regimes in actively eroding London Clay coastal slopes, installing 56 standpipe piezometers at a range of depths down to 60 m below original ground level. As part of this study calculations of in-situ permeability were made to explore the relationship of decreasing permeability with depth for London Clay. Permeability was measured at depths up to 57.1 m below the original ground level. Table 2-8 shows a number of the results obtained.

Piezometer	Depth below original ground level (m)	Permeability (m/s)
P1	5.9	3.5×10^{-10}

P9	19.2	2.8×10^{-11}
P11	36.1	2.1×10^{-11}
P45	57.1	9.6×10^{-12}

Table 2-8: Summary of a number of the measured permeability values, after Dixon and Bromhead (1999).

Although there were no measurements at shallower depths than 5.9 m the relationship between depth and permeability is clear; as depth increases the permeability decreases. Over a depth change of approximately 50 metres the permeability drops by two orders of magnitude. Dixon and Bromhead (1999, p.659) have listed "weathering, increasing effective stress (decreasing void ratio) and conditions of formation/deposition" as mechanisms affecting the relationship.

2.5 Progressive failure

Strain softening materials such as rock, dense sands and over-consolidated clays are subject to a type of slope failure known as progressive or delayed failure (Sterpi, 1999). When a cutting is excavated in over-consolidated clay (O-C), collapse can be delayed by pore pressure equilibration as the soil expands (Vaughan and Walbancke, 1973); as the pore pressures increase mean effective stress reduces and the stress state approaches failure, with the strength of the soil at time of collapse being significantly less than the peak strength that may have been measured in the laboratory (Potts et al., 1997).

Due to the pre-existing overburden pressure, over-consolidated clays exhibit a denser state of packing than normally-consolidated (N-C) clay, with lower water content, and therefore greater shear strength at the same effective stress. During the shearing process, over-consolidated clays tend to expand, particularly after the peak strength

has been surpassed. This volume expansion results in an increasing water content

Copyright not obtained

(
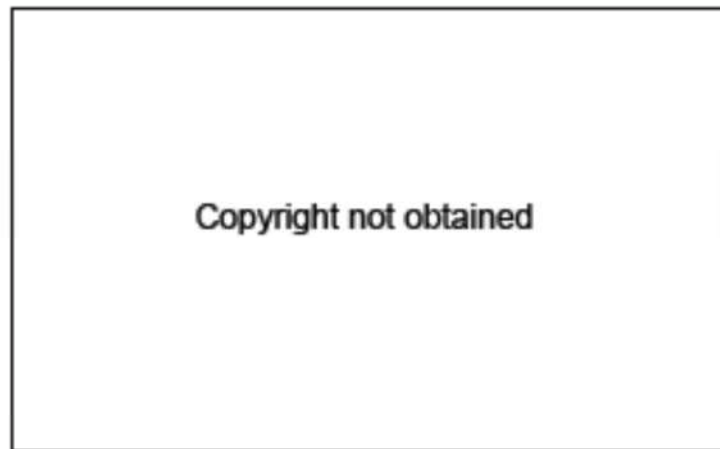
Figure 2-3), which explains some of the drop in strength from peak (Skempton, 1964). The term to describe the increase in volume of over-consolidated clays with shearing is *'dilatancy'*. If at some point within a clay slope the shear stress exceeds the peak strength at any point, then the strength at this point will continue to decrease. As the strength at this point is now less than peak, stresses must be redistributed to some other points, causing peak strength to be surpassed here as well. By this process the shear zone propagates throughout the slope, and a failure surface progressively develops along which the average soil strength is somewhere between the peak and residual strength (Conte et al., 2010).

Copyright not obtained

Figure 2-3: Relationships between displacement and shear stress and water content and between normal effective stress and shear strength for normally consolidated (N-C) and over-consolidated (O-C) clays. After Skempton (1970).

The critical state concept (Roscoe et al., 1958) represents an idealisation of observed patterns of behaviour of saturated clays in triaxial compression tests (Craig, 2004). Some of these patterns are visible in

Copyright not obtained

Figure 2-3 where c' and ϕ' are the effective cohesion and the effective angle of shearing resistance respectively, with the subscripts p, s and r representing peak, critical state and residual values respectively. Saturated clay, whatever its original condition, at the critical state, any further increment in shear strain will not result in any change in water content (Skempton, 1970). Over-consolidated clay will expand during shear, until the critical state is reached, at which point it continues to deform at constant stress and constant volume. Conversely, normally consolidated clay will contract on shear, until the critical state is reached. At the critical state the shear strength of the over-consolidated clay essentially correlates to the peak strength of the normally consolidated clay, as the water content in this state is equal to that attained by the clay due to dilatancy.

Leroueil (2001) has suggested slopes in over-consolidated clays exhibit four stages of behaviour; 1) pre-failure where the slope has yet to experience failure, which should apply to most engineered slopes (Take and Bolton, 2011), 2) first-time failure, 3) post-failure, which includes all soil displacements from the on-set of first-time failure until the soil mass comes to rest (Take and Bolton, 2011) and 4) reactivation stages, in which the slope failure occasionally becomes active along the pre-existing failure

Copyright not obtained

surface.

Figure 2-4 depicts these stages diagrammatically. At the different stages of collapse the soil will be characterised by different shear strength parameters, but what these parameters should be has long been an important discussion in the literature. Skempton (1977) has presented peak ($c'_p = 7\ kPa, \phi'_p = 20^o$), critical ($c'_s = 0\ kPa, \phi'_s = 20^o$) and residual ($c'_r = 1\ kPa, \phi'_r = 13^o$) effective shear strength parameters for London Clay. Clearly this wide range of values between peak and

residual strengths means that those chosen for design will have significant implications for the cost and safety of proposed slopes schemes (Take and Bolton, 2011).

Copyright not obtained

Figure 2-4: Stages of slope instability. After Leroueil (2001).

Skempton (1964) originally recommended using the residual state strength values to design for first-time failure. By using these values the possibility of failure could be completely avoided. However, back-analyses of first-time slope failures of cuttings in London Clay by Skempton (1970; 1977), showed a similarity between the strength at failure and the fully softened strength or the critical state strength

Copyright not obtained

(

29

Figure 2-5). Skempton (1970) states that the displacement required to reduce an overconsolidated clay to its fully softened, critical state condition is several times greater than the displacement at peak strength, but is considerably less than that corresponding to the residual strength

Copyright not obtained

(
Figure 2-3).

Copyright not obtained
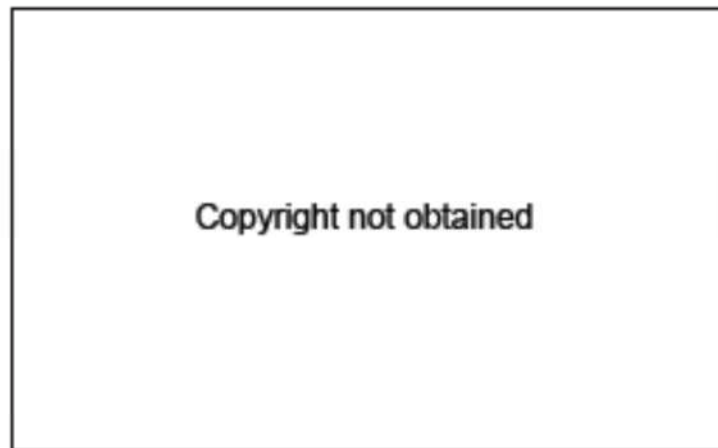
Figure 2-5: Strength of London Clay at first-time failure of cuttings. After Take and Bolton (2011) and Skempton (1977).

There are several mechanisms by which this initial reduction in shear strength may be brought about. Pore water pressure equilibration is well known. This mechanism occurs in cut slopes, which after construction can exhibit pore water pressures lower than the ultimate equilibrium values, because of the unloading effect of excavation (Vaughan and Walbancke, 1973). As pore water pressures equilibrate to their long term value softening of the clay occurs, along with a reduction in strength to the critical state, precluding failure of the slope. Failure of cuts in overconsolidated clays may therefore be delayed primarily by the rate of pore water pressure equilibration (Vaughan and Walbancke, 1973). Delayed failure has been observed in London Clay cuttings 40 – 50 years after excavation (Skempton, 1977), although the time for equilibration and failure may be less for shallower cuttings; in the order of 10 years for cuttings less than 4.5 metres deep (Chandler and Skempton, 1974).

Skempton (1964) identifies seasonal variation of water content as another mechanism that reduces strength of clay. Seasonal cyclic stress changes, synonymous with the shrink-swell behaviour of clay slopes subject to alternating wet winters and dry summers, cause outward movement, strain softening (as the plastic strains are irreversible) and eventually collapse (Kovacevic et al., 2001; Nyambayo, 2004; Loveridge et al., 2010). The mechanism depends on the number and severity of shrink-swell cycles and the magnitude of the end of winter pore water pressures (Kovacevic, 2001). Nyambayo et al. (2004) demonstrated that all things being equal an embankment which experiences small seasonal pore water pressure changes is likely to stand-up for a longer period before collapse, compared to an embankment that experiences large pore water pressure changes. Progressive failure brought about by seasonal shrink-swell cycles may be difficult to detect and occur unexpectedly, as; 1) the reduction of strength with cycling allows collapse to occur at lower pore water pressures than associated with pore water equilibration (Kovacevic, 2001) and 2) the movements which cause cumulative strain and the progressive development of the rupture surface are small and could be masked by larger vertical movements, and therefore it is unlikely that collapse could be predicted from measurements of deformation.

An explanation of how shrink-swell cycles lead to progressive failure is offered by the more recently discussed process of creep in the form of down-slope ratcheting (Clarke and Smethurst, 2010; Dijkstra and Dixon, 2010; Loveridge et al., 2010; Take and Bolton, 2011). In this mechanism sequences of swelling and shrinkage lead to downslope creep, accompanied by progressive regional softening within the zone affected by seasonal moisture movements (Take and Bolton, 2011). Prior to rupture regional softening of the slope will be due to the repeated mobilisation of dilatancy in successive wet seasons. If this occurs repeatedly the softening will eventually be enough to cause failure under conditions that, if peak strength of the soil was to be assumed, would certainly not predicate failure.

Skempton (1964) suggested that the effects of these seasonal shrink-swell cycles may be limited to shallower depths. However, if as predicted seasonal variation in the climate becomes more severe (see Section 2.11.2), affecting moisture content at greater depths in the slope then climate change could increase the likelihood of delayed failure occurring (Rouainia et al., 2009). As a possible example of this kind of impact, O'Brien et al. (2004) noted that in their numerical modelling of progressive failure there was a tendency for failures to develop in slopes that had been anticipated as relatively stable. They attributed this to the magnitude and extent of cyclic pore water pressures they imposed on the model, which were more likely representative of extreme weather conditions; i.e. once every 5 or 10 years, rather than annually. Therefore these kinds of results could be indicative of the effects of climate change if it does influence the occurrence of extreme weather conditions.

2.5.1 Numerical and laboratory modelling of progressive failure

Numerical modelling studies on progressive failure in infrastructure slopes have been carried out (Potts et al., 1997; Kovacevic et al., 2001; Nyambayo et al., 2004; O'Brien et al., 2004; Davies et al. 2008c; Rouainia et al., 2009). These studies have shown that slopes subject to varying climates are susceptible to progressive failure, with failure generally initialising at the toe of the slope and progressing from there. The studies have focussed on the different mechanisms instigating progressive failure; Potts et al. (1997) consider the effects of pore water pressure equilibration whereas Kovacevic

et al. (2001) and Nyambayo et al. (2004) look at the effects of the cyclic pore water pressures and shrink-swell cycles. Take and Bolton (2011) have carried out centrifuge tests on a clay slope subject to successive wet and dry seasons to analyse the effects of creep and down-slope ratcheting.

Potts et al. (1997) modelled delayed collapse of cut slopes in a Brown London Clay due to dissipation of suctions, assuming strain-softening behaviour of the soil. Progressive failure was found to be predominant, with the roll of the climate controlled hydraulic boundary condition being of significant importance. By increasing the magnitude of suctions at the surface boundary condition from 10 kPa to 20 kPa the stability of a 3:1 slope was increased by more than half

Copyright not obtained

(
Figure 2-6).

Copyright not obtained

Figure 2-6: Effect of increasing the surface suction from 10 kPa to 20 kPa on the stability of a 3:1 slope. After Potts et al. (1997).

Kovacevic et al. (2001) analysed the effects of seasonal climate on old railway embankments constructed of London Clay. The study found that collapse tends to

occur in winters with long wet periods when surface suctions have fallen to 0 kPa and the slope has rewetted. Kovacevic et al. (2001) conclude that the progressive collapse failure mechanism depends on the number and severity of the shrink/swell cycles and end of winter pore water pressures.

Nyambayo et al. (2004) has conducted comparable studies, which also consider the influence of the bulk permeability of the soil on progressive failure. The model was a 7 m high embankment, constructed from London Clay, with a London Clay foundation. Seasonality of the United Kingdom climate was represented by imposing alternate 6 month summer and winter pore water pressure boundary conditions. Each complete cycle included a summer and a winter, thereby simulating 1 year. To investigate the influence of permeability, the analyses were repeated with three values of permeability; low (1e-9 m/s), intermediate (1e-8 m/s) and high (1e-7 m/s). Results found that an embankment with a high permeability is more susceptible to progressive failure. Analysis of summer and winter pore water pressures showed that pore water pressures in the clay fill recovered during the winter for the high permeability clay but did not in the low permeability fill, showing that pore pressure cycles were less for the low permeability clay. When subjected to 13 years of alternate winter and summer pore water pressure profiles, a progressive failure mechanism had progressed into the embankment with high permeability

Copyright not obtained

(
Figure 2-7), whereas the embankments with intermediate and low permeability experienced little to no strain. Nyambayo et al. (2004, p.907) concluded that "all things being equal, an embankment which experiences small seasonal pore water

pressure changes is likely to stand-up for a longer period before collapsing, compared to an embankment that experiences large pore water pressure changes".

Copyright not obtained

Figure 2-7: Contours of sub-accumulated deviatoric plastic strains predicted for high permeability during cycles 1-13. After Nyambayo et al. (2004).

Take and Bolton (2011) carried out centrifuge tests on a model Kaolin Clay slope subject to variations in rainfall and humidity corresponding to successive wet and dry seasons. These tests were carried out to investigate the role of seasonal moisture cycles in progressive failure. Widespread dilation and softening of the soil was observed accompanying creep in the form of down-slope ratcheting which lead ultimately to progressive failure at the toe of the slope. Back analyses of the mobilised strength showed that clay slopes which temporarily mobilise an average stress ratio in excess of the critical state stress ratio during any portion of the year may eventually be brought to failure under the action of seasonal variations of pore water pressure.

2.6   Pore Water Pressure Measurements in Infrastructure Slopes

Up until recently there has been a lack of good measurements in infrastructure slopes that could be used in assessments of slope stability (Ridley et al., 2004b). However, in more recent times as the need for these measurements has become more apparent, a

number of slopes in the United Kingdom have been instrumented and monitored to take pore water pressure measurements.

Ridley et al. (2004a) published measurements of positive and negative pore water pressures in two types of embankments in the United Kingdom. The embankments are an old railway embankment located on the East London Line between Surrey Quays and New Cross and a recently constructed highway embankment of the M23 motorway, close to Gatwick Airport. The make-up of the railway embankment is ash, overlying London clay on a gravel foundation, the only significant vegetation on the embankment being grass. Piezometers were placed in the core and slopes of the

Copyright not obtained

 embankment.

Figure 2-8 shows maximum (solid data points) and minimum (open data points) recorded during the period December 1997 to September 1999.

Copyright not obtained

Figure 2-8: Pore pressures in an old railway embankment, after Ridley et al. (2004a).

Copyright not obtained

Figure 2-8 shows that pore pressures in the embankment core are significantly higher at all times of the year but there is less seasonal variation than within the embankment slopes. Negative pore water pressures are maintained throughout the year in the side slopes with the greatest variation at the slope surface (from a maximum suction of 7m head to a minimum ≈ 0.5m head), probably due to the effects of evapotranspiration and runoff from the slope surface.

The monitored highway embankment is constructed from a Weald Clay overlying a gravel foundation. A total of 18 modular piezometers were placed in two sections, one which had recently been planted with small trees and the second with just grass. This slope has a long history of slope failure, underlined by two adjacent sections to the instrumented one which had recently failed and been repaired.

Copyright not obtained

Figure 2-9 shows pore water pressure measurements at a depth of 1.0 m at two locations on the slope with tree cover (top of slope and upper mid-slope).

Figure 2-9: Pore water pressures in a highway embankment, after Ridley et al. (2004a).

The trend of pore water pressures is clear. Maximum suctions occur either late in summer or early autumn, dependent upon the climate that year. Maximum suctions were observed at the mid-slope locations for all year. Pore water pressures return to positive values relatively quickly, with the rate being greatest at the mid-slope locations. Ridley et al. (2004a) state that the quick re-wetting of the soil profile is probably due to cracks penetrating from the surface after summer drying. Seasonal variation is greatest at the mid-slope location.

Walbancke (1976, cited in Vaughan et al., 2004) has observed pore water pressures under various grassed embankments and cuttings.

Figure 2-10 shows maximum winter pore water pressures to be generally hydrostatic with the water table being approximately at the slope surface. The minimum observed pore water pressures are positive below a certain depth with large suctions present closer to the surface. Variation is comparable to that observed by Smethurst et al. (2006); the greatest seasonal variation occurs near to the surface, decreasing in a non-linear fashion as depth increases.

Figure 2-10: Pore water pressures below grassed embankment and cutting slopes, after Walbancke (1976) cited in Vaughan et al. (2004).

Copyright not obtained

Figure 2-8 shows that the same relationship was observed by Ridley et al. (2004a) in pore water pressure measurements within the slopes of an old railway embankment. The actual measurements for any given slope in any given year will be dependent upon material properties, vegetation present and antecedent climate conditions but it is clear that there is a frequently observed relationship between seasonal variation in pore water pressures in infrastructure slopes and depth.

2.6.1 Newbury cutting

A highway cutting slope has been extensively instrumented and monitored (Smethurst et al., 2006) in southern England. The cutting forms part of the relatively recently constructed A34 Newbury bypass. The slope is built in London Clay of 20 m thickness, with the top 2.5 m being heavily weathered. Instruments were installed throughout the slope to monitor soil water content, pore water pressure, soil temperature, the free water surface, rainfall, runoff and climatic data.

Figure 2-11 shows the location, type and number of instruments installed at the site.

Copyright not obtained

Figure 2-11: Plan of the Newbury cutting site slope showing the location of instruments, after Smethurst et al. (2006). Instruments are split into group A, B, C and D.

Monitoring took place over a wet winter (2002-2003) and an exceptionally dry summer (2003). Results are shown by group of instruments A – D (

Figure 2-11). Figure 2-12 shows pore water pressure measurements from the piezometers located at group A at the top of the slope. The effects of the wet winter and proceeding dry summer are clear; positive pore water pressures are recorded at all instruments after two months of heavy rainfall (300 mm in November and December 2002), then during the very dry summer evapotranspiration was greater than rainfall resulting in suctions of up to 25 kPa developing, which despite heavy rainfall in November and December 2003 have mostly not returned to positive pore water pressures by 31 December 2003.
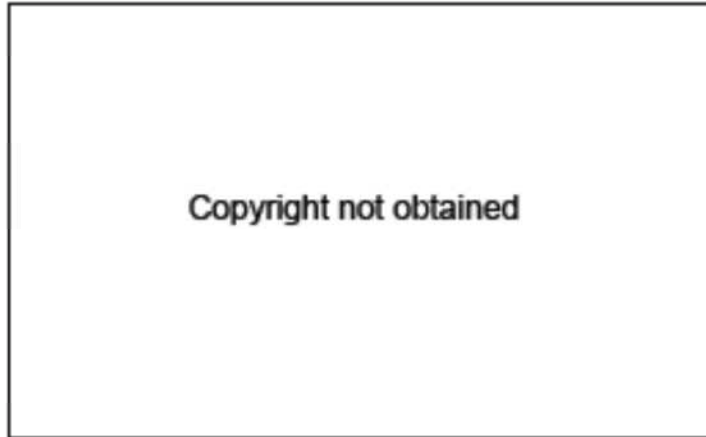
Figure 2-12: Vibrating wire piezometer readings from group A, after Smethurst et al. (2006).

Figure 2-13 and

Figure 2-14 show tensiometer and equitensiometer readings from instrument group C and maximum and minimum pore water pressure profiles measured by the piezometers and tensiometers at each instrument group.

Figure 2-13 shows measurements of suction for group C, at approximately mid-slope, at depths of 0.3 m and 0.6 m. At 0.3 m suctions develop rapidly at the beginning of June up to the tensiometers maximum measureable value of 90 kPa, suctions develop more slowly at 0.6 m reaching 90 kPa by the end of July. Suctions greater than 90 kPa were measured by the equitensiometer installed at 0.3 m depth; up to 440 kPa was recorded in September. The results from the equitensiometer show that standard tensiometers that record suctions up to 90 kPa may not be sufficient to fully capture the development of suctions in the vadose zone. Data from the equitensiometer

should be used with care (Smethurst et al., 2006), as the data is very sensitive to the water content-suction relationship of the ceramic material used in the equitensiometer. Smethurst et al. (2006) therefore advise that the data should be treated as indicative only, rather than quantitative.

Copyright not obtained

Figure 2-13: tensiometer and equitensiometer readings from instrument group c, after Smethurst et al. (2006).

Copyright not obtained

Figure 2-14 shows profiles of minimum and maximum pore water pressures with depth recorded at all instrument groups by the piezometers and tensiometers. Maximum pore water pressures were recorded in January 2003, generally being hydrostatic below a water table at no more than 0.5 m depth. Minimum pore

pressures were recorded at the end of September 2003, with suctions developing to a depth of at least 4 m. The greatest suctions are found in the top 1.0 m, decreasing rapidly with depth. This top 1.0 m represents the soil drying zone, caused by the direct removal of water by plant roots and is also most affected by evaporation from the soil surface.

Copyright not obtained

Figure 2-14: Maximum and minimum pore water pressures measured by piezometers and tensiometers at all instrument group locations, after Smethurst et al. (2006).

2.6.1.1 Numerical modelling of the Newbury cutting

Davies et al. (2008a) have created a numerical model of the Newbury bypass cutting slope. Surface pore water pressures were calculated using SHETRAN (Ewen et al., 2000). This program requires soil and vegetation properties, and weather data at a user defined time-step (per second, per minute, per hour, per day etc.) to calculate the surface boundary flux and the surface pore water pressures. Weather data at an hourly time-step was used for this work. This data was obtained from a weather station approximately 20 miles from the site and soil properties for London Clay were obtained from Croney (1977). Evapotranspiration, runoff and surface pore water pressures are calculated in SHETRAN and then transferred to Flac TP flow (Itasca, 2002), a finite difference software, which calculates the subsurface saturated and unsaturated flow and pore water pressure response.

48

The model was run for one year of climate data (2003) and temporal pore water pressures calculated throughout the slope and then compared to those observed by Smethurst et al. (2006). Figure 2-15 and Figure 2-16 show the pore water pressure profiles at a mid-slope location for end of September 2003 and end of December 2003 respectively. The profiles show the maximum suctions occurring at the end of summer and the minimum suctions occurring in the winter.
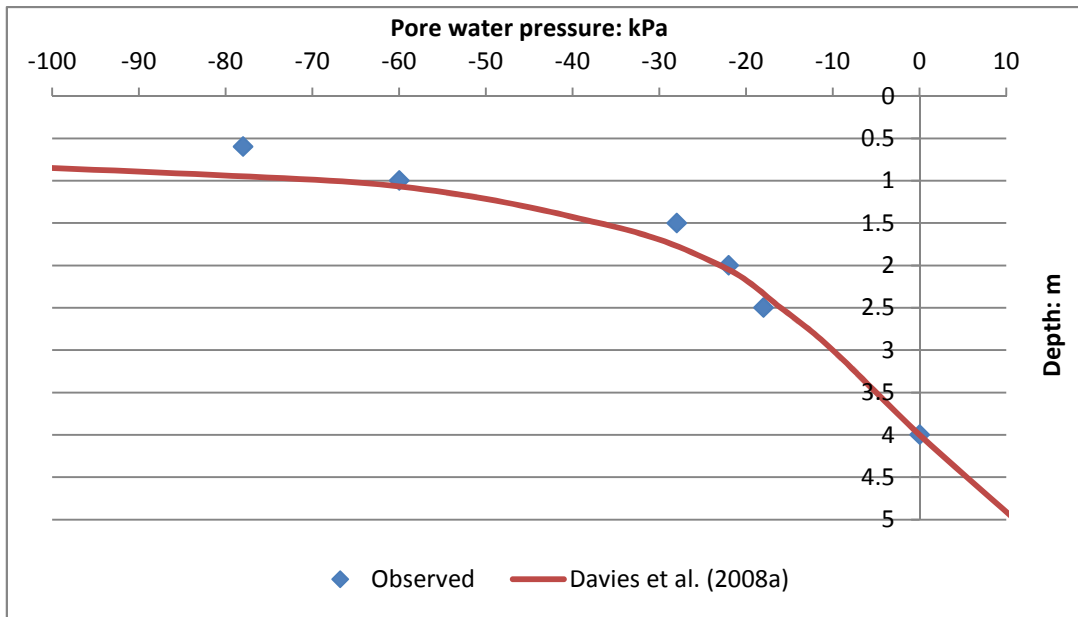
Figure 2-15: Calculated and observed pore water pressures at instrument group C, end of September 2003.

The results for the end of September 2003 correlate well with those observed by Smethurst et al. (2006); particularly well at a depth of 1.0 m and below. A maximum suction of 250 kPa was calculated at a depth of 0.3 metres (omitted for clarity), which does not initially compare well to the observed value of 440 kPa, but it must be remembered that Smethurst et al. (2006) recommend that this high suction be considered indicatively only.
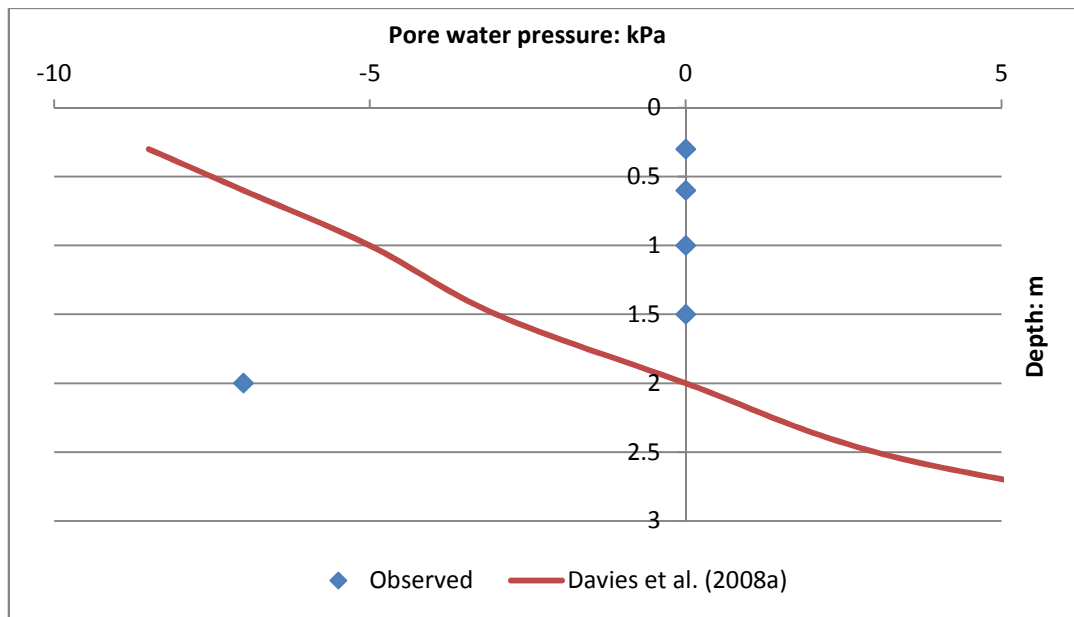
Figure 2-16: Calculated and observed pore water pressures at instrument group C, end of December 2003.

The model has not replicated the pore water pressures as well at the end of December 2003. The observed pore water pressures show suctions have dissipated by the end of December; the numerical model has not managed to capture this. Davies et al. (2008a) suggest that the issues in replicating the suctions at the end of December 2003 arise from the lack of inclusion of the effects of desiccation cracking on the hydraulic properties of the soil. In section 2.10 it will be shown that these cracks may be critically important in influencing the slope hydrology and should always be considered when developing slope hydrology models of slopes.

2.7 Observed Failures of Infrastructure Slopes in the UK

The autumn of 2000 was the wettest up to that point in England and Wales since records began (Met Office, 2012). In the period 1 September to 30 November, an average of 503mm rainfall fell, which was 196% of the 1961-90 average. In southern England up to 250% of this average fell. The winter following this (2000-2001) was characterised by prolonged periods of wet weather with numerous high intensity rainstorms (Bracegirdle et al., 2007). For example, in south eastern England between 1 February and 8 February up to 200% of the month's average total rainfall fell (Met Office 2011). This extreme wet weather heightened the risk of slope instability, and the outcome was extensive earthworks failures affecting infrastructure. In the period November 2000 to April 2001 the Highways Agency reported about 60 slope failures,

and there were more than 100 reported failures on the national rail network (Ridley et al., 2004b). These instances of slope instability had severe detrimental effects on the UK's infrastructure, disrupting and delaying road and rail networks (Dixon et al., 2006).

2.7.1 British Motorway Survey 1980-1983

An extensive survey of earthwork failures on selected lengths of British motorway was carried out in the period 1980-1983 (Parsons and Perry, 1985). The survey was carried out in areas where overconsolidated clays predominate, on cuttings and embankments, aiming to identify the basic factors affecting the stability of these slopes and to quantify any long-term problems. Despite the age of the survey it is still relevant today. The slopes investigated are constructed to the same standard as those today, and they are within the soils that have been identified as being particularly susceptible to SLS and ULS problems (Section 2.3.3). Also, the majority (>70%) of existing highways cutting and embankments were constructed before the 1990s (Loveridge et al., 2010), meaning that the effects on theses slopes are still of particular interest.

Geology	Failure rate (%)	Predominant slope (v : h)
Cuttings		
Gault Clay	9.7	1 : 2.5
Oxford Clay	3.2	1 : 2
Reading Beds	2.7	1 : 3
Lower Coal Measures	1.4	1 : 2
Plateau Gravel	1.1	1 : 3
Boulder Clay	1.0	1 : 3
Embankments		
Gault Clay	9.1	1 : 2.5
Reading Beds	7.8	1 : 2
Kimmeridge Clay	6.1	1 : 2
Oxford Clay	5.7	1 : 2

London Clay	4.4	1 : 2

Table 2-9: Geologies encountered with failure rates greater than 1 per cent and the predominant failed slope geometry (after Parsons and Perry, 1985).

In the earthworks surveyed, which varied in age from 3 to 22 years, significant incidence of slope failure in both cuttings and embankments was identified, although failure rates for embankments were generally higher than for cuttings. Four factors affecting these failures were studied; geology, age of earthwork, geometry of slope and orientation of slope. High failure rates, in the range 4-8 per cent, were exhibited by embankments of Kimmeridge Clay, Oxford Clay and London Clay. Failure rates in Gault Clay were found to be the highest; over 9 per cent in cuttings and embankments, and therefore, the only geology where cutting failure rates exceed embankment failure rates. Table 2-9 summarises the geologies with failure rates greater than 1 per cent, along with the predominant slope geometry. Failure rate is calculated as the proportion of the total length of cutting or embankment examined that was observed to have failed at some point.

Very high failure rates were found in some slopes of certain geology, age and slope geometry. More than half of cutting slopes in Gault Clay (slope of 1 : 3, and age 22 years) and Oxford Clay (slope of 1 : 1.75, aged 22 years) had failed at some location. Steeper slopes in these materials were found to have lower failure rates, showing that there is possibly a critical slope geometry for which failure is most likely. In embankments, high failure rates were observed in particular geometries of Gault, Oxford, Kimmeridge and London Clay. Regarding height of slope; those of height greater than 5 m have the highest failure rate for the majority of geologies and slope geometries.

In the study of slope orientation there was found to be little correlation between slope orientation and failure rate. Some variation was observed but there was no consistent pattern for any geology type, other than the Reading Beds which showed greater failure rates for those slopes oriented to the North.

2.7.2 Pore water pressures and stability of a motorway embankment

Anderson and Kneale (1980) have published daily precipitation data

Copyright not obtained

(

Figure   2-17)   and   pore   water   pressure   measurements

Copyright not obtained

(

Figure 2-18) for a motorway embankment site leading up to and after a shallow surface slip that occurred in March 1978. The embankment forms part of the M4 motorway west of Swindon and is constructed of Oxford and Kimmeridge clay. The slope was instrumented with twenty-two tensiometers at depths of 25 cm, 60 cm and

100 cm; such depths were chosen because earlier observed slips had occurred at

Copyright not obtained

depths up to one metre.

Figure 2-17 shows daily precipitation in the month leading up to the slope failure and proceeding days, arrows represent the corresponding pore water pressure profiles for that date.

Copyright not obtained

Figure 2-17: Daily precipitation before and after the March 1978 landslip (Anderson and Kneale, 1980).

Figure 2-17 and

Figure 2-18 show a correlation between precipitation amounts, pore water pressures and likelihood of slope failure. The set of measurements on 03/03/1978 show the pore water pressures on the day of the slide; it can be seen that the phreatic surface is at its highest point and the negative pore water pressures above this are at a minimum. By studying the antecedent rainfall pattern before the slope failure

(

Figure 2-17) it is shown that there was persistent precipitation for the preceding 12 days. The third measurement on 09/03/1978 comes after a short dry period of 6 days; from the pore water pressure profile it can be seen that the slope has drained considerably and the phreatic surface is now at its lowest point and negative pore water pressures have once again returned to their maximum.

Copyright not obtained

Figure 2-18: Pore water pressure measurements before and after the March 1978 landslip (Anderson and Kneale, 1978).

Anderson and Kneale (1980) make two observations from their findings: firstly, measureable changes in pore water pressure and suction are found to have occurred with depth, with no lateral variation in the pore water pressures and suctions being apparent over the time monitoring took place (explaining why profiles are sufficient to represent the data), secondly the landslide occurred at a time when the saturated zone was at its maximum extent. In addition it is noted that antecedent rainfall is very important in affecting likelihood of slope failure; the maximum intensity of rainfall leading up to failure on the 3.3.1978 is 5 mm per 24 hours and a total of 21.9 mm in 10 days. This implies that mean intensity is close to the clay permeability and most of the precipitation will have been able to infiltrate the slope. Subsequent rainfall occurred on 12-15 March and in these days maximum intensity was considerably higher (5mm per 7 hours on each of the four days), however, the levels of saturation attained on 3 March were not achieved.

2.8 Atmosphere and slope interactions

In Section 2.7 the link between climate and slope stability was made. Landslides are often mobilised during periods of intense rainfall and the response of slopes to extreme rainfall events is well documented (Ng and Shi, 1998; Ridley et al., 2004; Dijkstra and Dixon, 2010; Oh and Vanapalli, 2010; Rahardjo et al., 2010). In this section it will be shown how the climate interacts with soil slopes, and it will be discovered that precipitation is not the only force affecting the slope's hydrology and stability.

The flux boundary condition at a soil surface is important for many problems in geotechnical engineering, such as saturated/unsaturated groundwater flow, slope stability and volume change in expansive soils (Tratch et al., 1995). The ability to quantify this flux correctly, means these problems can be addressed far more rigorously and accurately (Fredlund et al., 2010). Precipitation, in the form of rainfall or snow, provides the source of moisture to the flux boundary. Knowledge of this term alone is not sufficient to model the effects of the flux boundary on slope hydrology (Dijkstra and Dixon, 2010). Other climate parameters, such as temperature, relative humidity, wind speed and net solar radiation, which drive the evaporative and transpiration losses, have important effects and must also be accurately quantified.
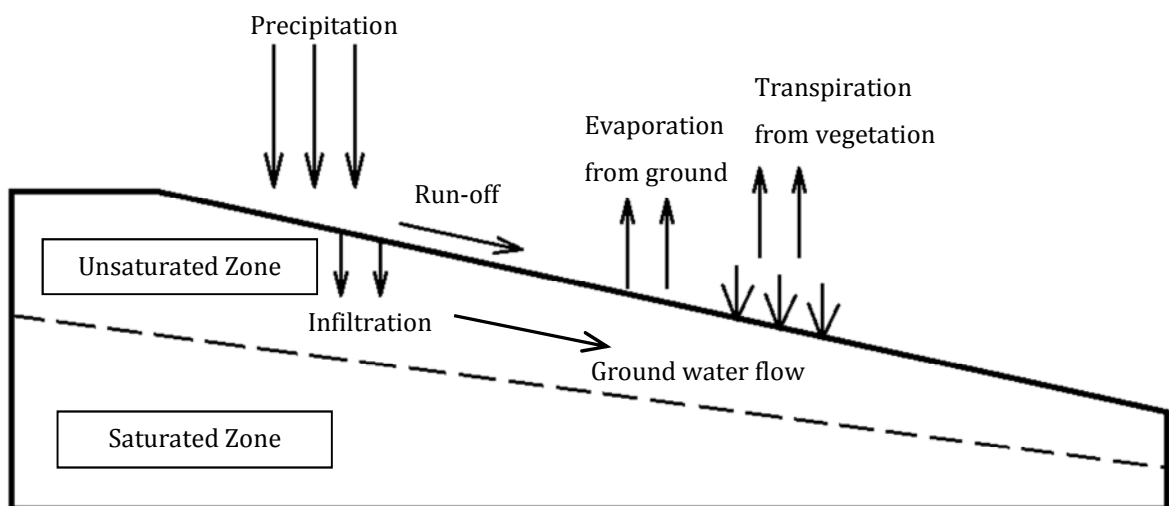
Figure 2-19: 2-dimensional model of the hydrological processes affecting a slope's hydrology.

At the ground surface water will either be entering the ground resulting from precipitation or leaving it via evapotranspiration. It can also be shed across the ground surface through runoff. *Figure* 2-19 represents the processes affecting the hydrology of a slope. The quantities of each term that contribute to moisture entering or leaving the ground can be expressed in terms of net infiltration. Net infiltration can be expressed by (Fredlund et al., 2010a):-

<div align="right">

Equation 2-1

</div>

Net infiltration (I) = Precipitation (P) – Actual Evaporation (AE)
– Transpiration (T) – Runoff (R)

2.8.1 Water balance equation

The net infiltration equation is useful, in that it shows the current effects of each of the terms at a given time of the year at the ground surface; however the annual soil system water balance considers the complete system, and the effects of seasonal changes (Blight, 2003). The annual soil system water balance suggested by Blight (2003) is given by Equation 2-2 in which the summation is carried out over at least a full year:-

<div align="right">

Equation 2-2

</div>

$$\sum (P - R) + S - \sum AET = RE + losses$$

Where P = precipitation, R = run-off, ET = actual evapotranspiration, S = change in stored water within the soil, RE = recharge to the water table. Losses could be due to inaccuracies in measurements or ill-defined boundary conditions.

Although Equation 2-1 and Equation 2-2 seemingly simplify the problem, in reality each individual term can be very complex to calculate. In Section 2.8.2 to Section 2.8.4 each of the individual terms is described, along with the method of quantification. On its own the water balance is a useful tool in that it allows the user to estimate possible effects on the slope hydrology. However, to calculate actual changes in pore water pressures throughout the slope and how these effect possible land sliding requires a

more rigorous approach. This approach must acknowledge the role of material properties, and how these may vary temporally and spatially as well as effects of vegetation and a variable climate (Dijkstra and Dixon, 2010; Fredlund et al., 2010a).

2.8.2 Precipitation

Precipitation is the easiest to quantify, being obtained directly from weather station measurements. These measurements should be obtained from the site or as close to the site in question as possible. Fredlund et al. (2010a) raise a number of important issues to be considered when deciding what precipitation data should be chosen and how it should be applied to any geotechnical engineering problem:-

1. Even though total precipitation in any two years may be the same the pore water pressure response could be very different depending upon the precipitation distribution through the year and antecedent soil moisture conditions. Therefore it is necessary to perform any modelling simulations using several years of independent climate data.

2. Conventionally, precipitation measurements have been collected on a daily basis. This method does not allow for the quantification of storm events as, for example, it does not identify the difference between the same amounts of precipitation falling in 10 minutes or 10 hours. Every effort should be made to record hourly (or even sub-hourly) precipitation data.

3. Another motivation for the use of hourly/sub-hourly precipitation measurements is in order to compute separation between infiltration and runoff. The time steps that are part of the numerical model could be in the order of minutes and the total time period over 10 years. Consequently, computer simulations can take a significant time to run.

2.8.2.1 Snow

The effects of snowfall on the water balance are generally not considered in the United Kingdom, particularly for locations in the south of England (Collison et al., 2000; Smethurst et al., 2006; 2012). However the effects of snow and particularly rapid snow melt can be important. Reports of landslides triggered by rapid snowmelt

are not rare, particularly in very mountainous countries such as Italy (Fiorucci et al., 2011) and Japan (Kawagoe et al., 2009).
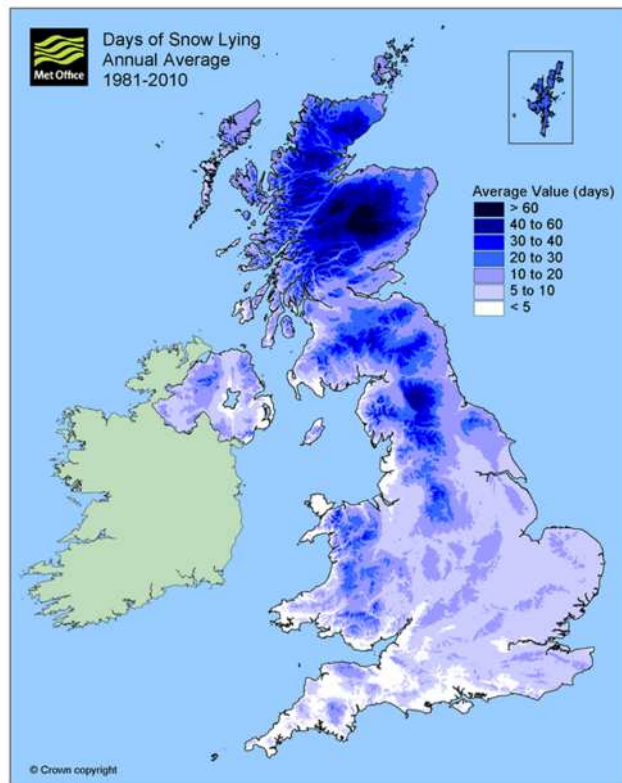
Figure 2-20: Days of snow lying - annual average 1981-2010. Contains public sector information licensed under the Open Government Licence v1.0.

Figure 2-20 shows the annual average number of days when snow was lying between 1981 and 2010 for the whole of the United Kingdom. For the majority of the southern half of England the number of days ranges from < 5 to 20, with only upland areas exceeding this. In the future the amount of snow falling in the United Kingdom is expected to decrease significantly, due to climate change. There could be a decrease in the mean winter snowfall rate of 65–80% over mountain areas and 80–95% elsewhere (UK Climate Projections, 2009).

2.8.3 Runoff

Water can be lost from the system through runoff. Runoff is water that cannot infiltrate the ground and will therefore be shed across the surface. Runoff occurs when the rainfall intensity is greater than the infiltration capacity of the soil (Clarke

and Smethurst, 2010), the amount of runoff in a rainfall event can therefore be calculated as:

$$Runoff = Cumulative\ Rainfall - Cumulative\ Infiltration$$

2.8.4 Evapotranspiration

Evapotranspiration from the soil is perhaps the most difficult of the terms to define. Evapotranspiration is the cumulative removal of water from the system by evaporation from the soil surface and transpiration from vegetation present on the slope. Evapotranspiration depends upon the interactions between the elements of the plant-soil-atmosphere system. It is dependent upon the plant type, climate, soil characteristics and current soil water conditions (Smethurst et al., 2006) and would be very difficult to measure directly. Fortunately, equations exist that can estimate evapotranspiration with reasonable confidence.

Before introducing the equation for actual evapotranspiration, an important concept shall initially be discussed; that of potential evapotranspiration. Potential evapotranspiration is the amount of water that would be removed from the soil surface if water was freely available. It is defined by Tratch et al. (1995, p.773) as "the maximum potential cumulative sum of bare soil evaporation and plant transpiration". Actual evaporation is often less than potential evapotranspiration, sometimes significantly so. In Section 2.8.4.1 and Section 2.8.4.2 methods for quantifying evaporation and transpiration are described.

2.8.4.1 Quantifying evaporation

Penman (1948) developed an equation (Equation 2-4) for the prediction of evaporation from saturated surfaces. The equation has shown good accounts of calculating evaporation in the United Kingdom and at other sites throughout America and Europe (Penman, 1948). This equation calculates the 'potential evaporation' as water is freely available due to saturation at the surface. The equation is based on

climate variables commonly collected from weather stations such as relative humidity, air temperature, wind speed and net radiation.

$$PE = \frac{\Gamma Q_n + \eta E_a}{\Gamma + \eta}$$

Where PE = potential evaporation in mm/day, Γ = slope of saturation vapour pressure vs. temperature curve kPa/⁰C, Q_n = net radiation at the saturated ground surface mm/day, η = psychrometric constant kPa/⁰C, $E_a = 2.625(1 + 0.146W_W).(u_{v0}^{air} - u_v^{air})$ mm/day, W_W = wind speed km/hr, u_v^{air} = vapour pressure in air above saturated ground surface kPa, and u_{v0}^{air} = saturated vapour pressure at the mean air temperature kPa.

Equation 2-4 shows that the vapour pressure gradient between the saturated ground surface and the air above the water becomes the primary mechanism for evaporation (Fredlund et al. 2010). As Equation 2-4 applies only to saturated surfaces an adjustment is required so that is can be applied to surfaces that are unsaturated, so as to calculate the 'actual evaporation'.

Actual evaporation from the soil surface may actually be significantly less than that calculated by the equation for potential evapotranspiration if the surface is not saturated and water is not freely available. In this case a modified version of the Penman equation (Penman, 1948) is required, one of which was developed by Wilson (1990 cited in Fredlund et al., 1990, p.6). This modified equation (Equation 2-5) takes the reduced relative humidity in the soil at the ground surface into account.

$$AE = \frac{\Gamma Q_n + \eta E_a}{\Gamma + \eta A}$$

Where AE = actual evaporation in mm/day, $E_a = 0.35(1 + 0.15W_W).u_v^{air}.\left(\frac{u_{v0}^{air}}{u_v^{air}} - \frac{u_{v0}^{air}}{u_v^{soil}}\right)$ mm/day, u_v^{soil} = vapour pressure in the soil at ground surface kPa, and A is the inverse of the relative humidity at the soil surface.

2.8.4.2 Quantifying transpiration

If vegetation is present on the slope surface then moisture shall also be extracted from the soil profile by the process of transpiration. If the vegetation is of sufficiently high demand then transpiration from plants can be significantly higher than the actual evaporation from the soil surface (Fredlund et al., 2010a). When considering the effects of vegetation on slope hydrology the following parameters must be taken into account in any function:-

1. Rooting depth/zone.
2. Growing season of the vegetation.
3. Partition of potential evapotranspiration flux into evaporation and transpiration components.
4. The current soil water content.

The rooting depth is important as it defines the depth into the soil profile to which moisture can be extracted be the vegetation. The rooting zone for grasses in clay soils was observed to be typically 0.6 – 0.9 m (Smethurst et al., 2006); for trees observations have been made of water extraction up to depths of 3 m (Briggs, 2010).

Evaporation and transpiration are both driven by the incoming solar radiation and the potential flux will be split between the two, depending on the ratio of the surface area of the vegetation's leaves to the soil surface area. This ratio is known as the Leaf Area Index (LAI), given by Equation 2-6. Table 2-10 shows how the LAI can be used to determine the split of incoming solar radiation between evaporation and transpiration (Tratch et al., 1995).

Equation 2-6

$$LAI = \left(\frac{surface\ area_{leaf}}{surface\ area_{soil}}\right)$$

LAI Value	Potential Transpiration	Evapotranspiration Split
$LAI < 0.1$	$PT = 0$	*No transpiration*
$0.1 < LAI < 2.7$	$PT = PE\left(-0.21 + 0.7LAI^{1/2}\right)$	*Combination of evaporation*

63

		and transpiration
$2.7 < LAI$	$PT = PE$	Transpiration only

Table 2-10: Relationship between Leaf Area Index and evapotranspiration split.

Where *PT* = potential transpiration rate and *PE* = potential evaporation rate.

2.8.4.2.1   Plant moisture limiting function

When soil is unsaturated and the water content falls below a certain level the ability of the roots to extract moisture from the soil is reduced. This value, known as the limiting point is typically a suction of around 50 kPa; in the field limiting points of 0 – 100 kPa suction have been observed (Loveridge et al., 2010). The roots will continue extracting water at an ever decreasing rate down to the wilting point; the water content at which the roots will no longer be able to take up water from the soil. Typically the wilting point occurs at a suction of 1500 kPa (Adu-Wusu et al., 2007; Fredlund et al., 2010a). The relationship between the waters ability to extract water and the suction in the soil is usually represented as a 'plant moisture limiting' (PML) function (Figure 2-21).
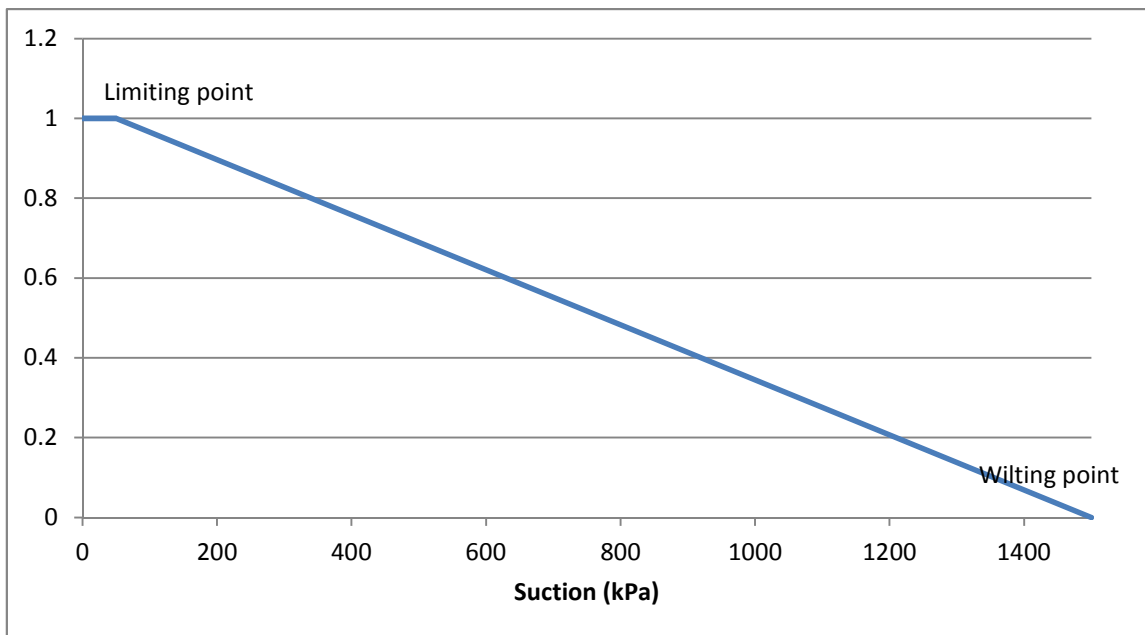
Figure 2-21: Plant moisture limiting function.

The PML function shown in Figure 2-21 has a limiting point of 50 kPa and a wilting point of 1500 kPa suction.

2.8.4.2.2   Root extraction model

Extraction of water by roots from the soil profile should be incorporated into any slope hydrology model by the means of a vegetation moisture flux model. One such technique is used by the Met Office's MORECS (Hough and Jones, 1997). MORECS simulates extraction of water by root action by removing water directly from the ground surface. The method by which MORECS represents water extraction is its weakness when considering it for use with slope hydrology modelling; by using the combined approach and removing all water directly from the slope surface MORECS cannot recreate accurate pore water pressure profiles (Briggs, 2010; Loveridge et al., 2010) which occur when there is simultaneous drying at the surface and extraction at depth by roots. Therefore, for better replication of these profiles, a root extraction model should be implemented which will treat evaporation and transpiration as two separate processes, with evaporated water being removed at the surface and transpired water removed at depth.

Tratch et al. (1995) have developed such a model. The theoretical approach uses a combination of inputs to predict transpiration rates. The inputs are the Leaf Area Index function, potential root uptake flux and a Plant Moisture Limiting function. The potential root uptake flux is determined by the method shown in Table 2-10. To realistically model the root uptake the flux must be distributed through the soil profile that is occupied by the vegetative root structure (Tratch et al., 1995). This is done by distributing the total potential root uptake flux into nodal fluxes in a predetermined shape, known as the 'shape function' (Figure 2-22).
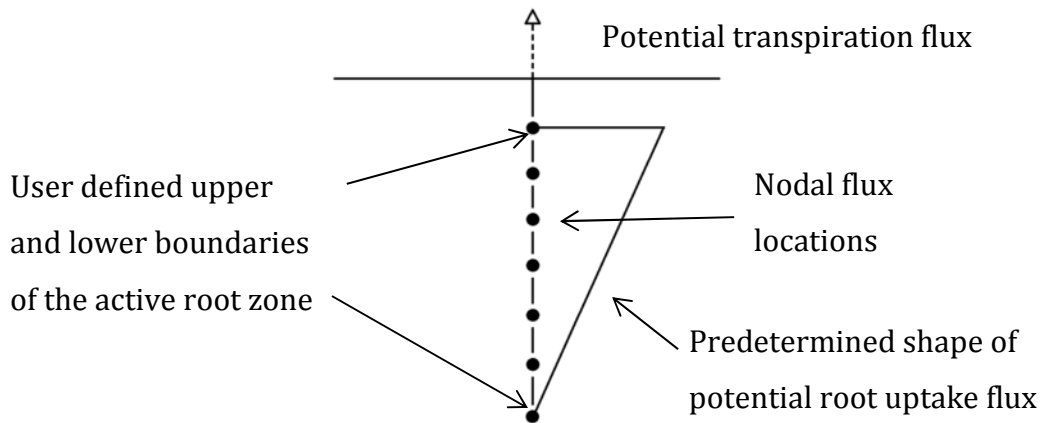
Figure 2-22: Example of a predetermined shape function and nodal flux locations (after Tratch et al., 1995).

The potential nodal flux rates are now dependent upon the potential transpiration flux, the location of the node with respect to the top and bottom of the active root zone and the node spacing and the predetermined shape of potential root uptake distribution (Tratch et al., 1995). The PML function (Section 2.8.4.2.1), which accounts for the lack of freely available water, is now introduced to modify the individual potential nodal fluxes to actual nodal fluxes.

Equation 2-7

$$S = PRU.PLF$$

Where S = actual nodal root uptake sink term m/s, PRU = potential root uptake flux m/s, and PLF = plant limiting factor. Actual nodal fluxes can now be estimated throughout the entire soil profile that the roots occupy.

2.8.5 Physically-based models

Dijkstra and Dixon (2010) advocate the use of Physically-Based Models (PBMs). These models include a climate process system (for evaluation of the water balance), a land-use–vegetation system (to quantify transfer of water at the near surface), a regional hydrogeological system (allowing a refinement of the local water balance) and a multi-layered soil system that can cope with variations in soil properties and soil water content. The main advantage of these models is that the hydrological processes are explicitly considered and simulated hydrology is used as input for the pore pressure conditions in the slope stability analysis.

Proceeding sections deal with some of the requirements of PBMs; specifically those which are intended to investigate the effects of climate change on slope hydrology and stability. In Section 2.9 the mechanical and hydraulic properties of unsaturated soil are described, including methods of accounting for their behaviour in PBMs. In Section 2.10 the phenomenon of desiccation cracking is introduced; which are found to be potentially critical in their effect on slope hydrology. Section 2.11 investigates climate change and methods of implementing it into PBMs.

2.9 Unsaturated Soil

An unsaturated soil is one where the void spaces between the soil particles are filled partially by air and water. An unsaturated soil is a multi-phase material; the phases being the solid soil particles, the liquid water and the gas air. Understanding the role of unsaturated soil in slope stability and hydrology is of utmost importance; and therefore this section explores the mechanics and hydrology of these soils and how they differ to their saturated counterpart.

2.9.1 Mechanics

The properties of an unsaturated soil differ to that of fully saturated soil due to the presence of the contractile skin (or air-water interface) between the water phase and the air phase. To understand the effects of this contractile skin, it is easiest to consider a single water molecule situated within the air-water interface; this molecule will be subjected to different forces to one that lies within the interior of the water as illustrated in Figure 2-23.

67
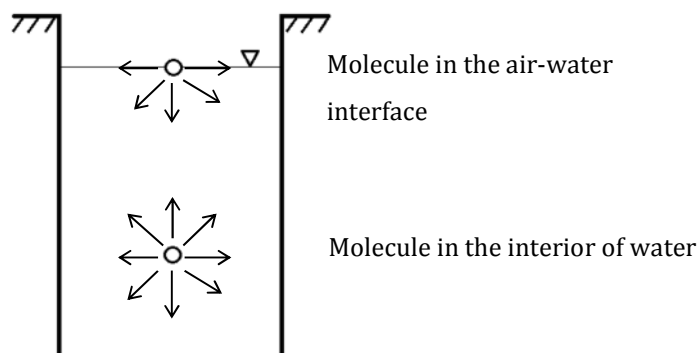
Figure 2-23: Water molecule situated in air-water interface and interior, after Fredlund and Rahardjo (1993).

As Figure 2-23 shows, the molecule at the interface is subjected to unbalanced forces towards the interior of the water whereas the molecule within the interior is in equilibrium. Therefore there must be a further force acting on the air-water molecule so as for it to be in equilibrium. This force is a tensile pull generated along the contractile skin causing the skin to act as an elastic membrane. By considering the forces acting on a two dimensional contractile skin (Figure 2-24), an expression for the curvature of the membrane can be developed.
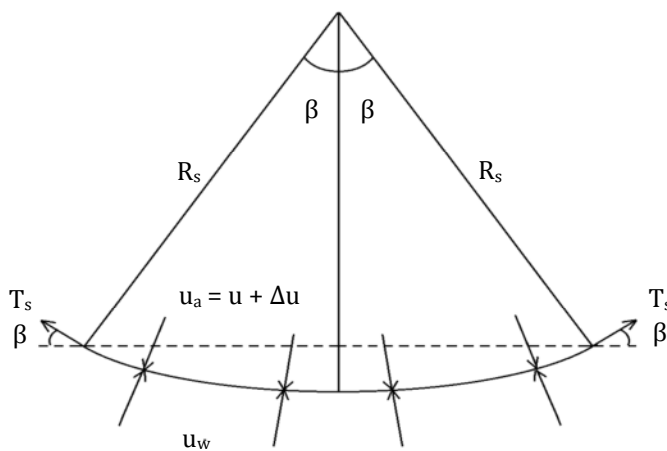
Figure 2-24: Representation of the forces acting upon the contractile skin after Fredlund and Rahardjo (1993).

Where u_w is the water pressure and $u_a = u_w + \Delta u$ is the air pressure (therefore Δu is the pressure difference between water and air), T_s is the surface tension of water and R_s the radius of curvature of the contractile skin.

There is a pressure difference across the contractile skin that can be related to T_s and R_s by considering force equilibrium in the vertical direction:

Equation 2-8

$$2T_s \sin \beta = 2\Delta u R_s \sin \beta$$

This can be rearranged to give:

Equation 2-9

$$\Delta u = \frac{T_s}{R_s}$$

This describes the situation in a 2D surface. For a 3D surface (assuming radius of curvature is equal in all directions) the expression is:

Equation 2-10

$$\Delta u = \frac{2T_s}{R_s}$$

Δu is the pressure difference between air and water. In a partially saturated soil the air pressure is greater than the water pressure. This pressure difference causes the contractile skin to curve in accordance with:

Equation 2-11

$$(u_a - u_w) = \frac{2T_s}{R_s}$$

This pressure difference $u_a - u_w$ is known as the matric suction and plays a very important role in determining the mechanical behaviour of an unsaturated soil. From the above equation it can be seen that if the matric suction increases (as the water content and consequently the water pressure decreases) the tensile pull along the contractile skin increases (assuming that the radius of curvature is constant), this increasing tensile pull results in an increase in the strength of the soil. Much experimental evidence exists to support this assertion (Escario and Saez, 1986; Gan and Fredlund, 1988; Maatouk et al., 1995; Cui and Delage, 1996).

The mechanical behaviour of a soil, whether it is saturated or unsaturated, can be described by the state of stress within the soil, with the use of stress state variables (Fredlund, 1993). Due to the more complex behaviour of unsaturated soils it has proved difficult to establish an expression for effective stress based in stress state variables as simple as that of Terzaghi's for saturated soils (Terzaghi, 1936). Bishop (1959) has proposed an equation based on two stress state variable and a soil property parameter to give the effective stress of an unsaturated soil:

Equation 2-12

$$\sigma' = (\sigma - u_a) + \chi(u_a - u_w)$$

Where σ' = the effective stress, σ = total stress, u_a = air pressure, u_w = water pressure and χ = effective stress parameter. The effective stress parameter is strongly dependent on the soil structure (Khalili and Zargarbashi, 2010), and describes the contribution of the matric suction to the macroscopic stress of the solid skeleton or the effective stress.

The stress state variables in this equation are:

$$(\sigma - u_a) = net\ stress$$
$$(u_a - u_w) = matric\ suction$$

2.9.2 Hydrology

Figure 2-25 shows a section through a slope. Within this slope there will be zones of soil that are saturated and zones that are unsaturated, the extent of each varying throughout the year as external and internal forces, such as the climate or vegetation, influence the hydrology. Fluid flow through these zones is described by two separate, but related equations.
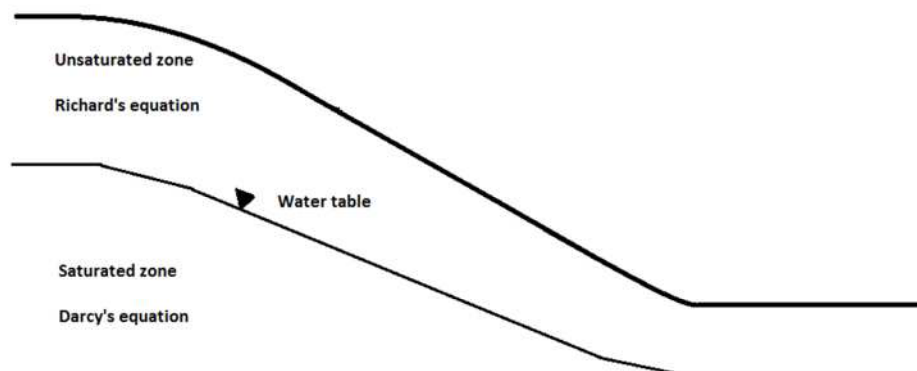
Figure 2-25: Section through a slope, showing the saturated and unsaturated zones.

Darcy's law, published by Henry Darcy in 1856, describes the flow of a fluid through a fully saturated porous medium and can be applied to soils. Water flows through a fully saturated soil in accordance with:

$$q = -k\frac{\delta H}{\delta y}$$

Where q = the specific flux m/s, k = the coefficient of permeability m/s (often referred to as saturated hydraulic conductivity), and $\frac{\delta H}{\delta y}$ = total hydraulic head gradient in the y direction.

In a saturated two dimensional soil, the governing equation for seepage is given by the Laplace's equation $K\nabla^2 H = 0$ or:

$$K_x\frac{\partial^2 H}{\partial x^2} + K_y\frac{\partial^2 H}{\partial y^2} = 0$$

Where K_x, K_y are coefficients of hydraulic conductivity in the x and y directions respectively, H is the total hydraulic head. When a source or sink Q is added then the Laplace equation becomes Poisson's equation.

$$K_x\frac{\partial^2 H}{\partial x^2} + K_y\frac{\partial^2 H}{\partial y^2} + Q = 0$$

Once a soil becomes unsaturated, Darcy's equation can still be applied, but in a different form. The permeability (k) is replaced by the hydraulic conductivity (K), which varies with changes in soil water content. Thus the solution of this equation requires knowledge of two relationships; 1) between the hydraulic conductivity and pressure head and 2) between the volumetric water content and pressure head. The Richards equation (Richards, 1931) establishes a relationship between the temporal changes of water content in a soil with the pressure gradient:

Equation 2-16

$$\frac{\delta}{\delta x}\left[K_{(\psi)}\frac{\delta h_\psi}{\delta x}\right] + \frac{\delta}{\delta y}\left[K_{(\psi)}\left(\frac{\delta h_\psi}{\delta y}+1\right)\right] = \frac{\delta\theta}{\delta t}$$

Where θ = volumetric water content, t = time (s), h = water pressure head (m), x = horizontal distance (m), $K_{(\psi)}$= hydraulic conductivity as a function of negative pressure head (ms^{-1}), y = vertical distance (m) where the positive orientation of the vertical direction is up.

This equation is highly non-linear as hydraulic conductivity changes significantly as the water content increases and decreases. Hydraulic conductivity in an unsaturated soil is highly dependent on the water content of the soil as the water flows along a web of interconnected conduits of water already present in the soil (Ng and Shi 1998). As water content increases, the size and number of these conduits increases therefore enhancing the ability of the soil to conduct water.

To utilise the Richard's equation the relationship between water content and hydraulic conductivity must be known for the particular soil being considered. In Section 2.9.3 the relationship between volumetric water content and hydraulic conductivity in discussed in more detail, and the theory of the soil water characteristic curves and the hydraulic conductivity functions is introduced.

2.9.3 Volumetric water content and hydraulic conductivity relationships

Figure 2-26 and Figure 2-27 show typical relationships for suction – volumetric water content and suction – hydraulic conductivity respectively. Henceforth, the curve for suction – water content will be known as the soil water characteristic curve (SWCC) and the curve for suction – hydraulic conductivity, the hydraulic conductivity function (HCF).
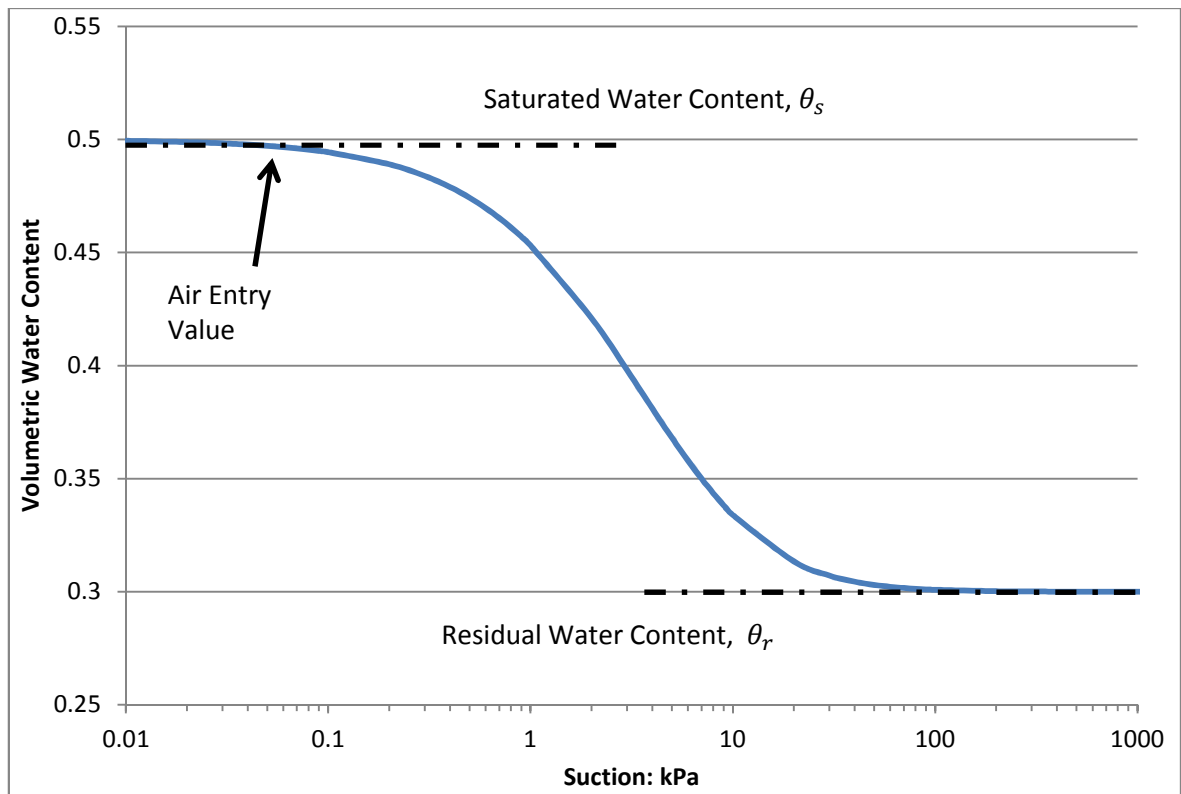
Figure 2-26: Typical soil water characteristic curve for a clay soil.

The root of the non-linearity of the Richard's equation becomes clear when these graphs are studied. The SWCC and HCF are non-linear and are coupled. Volumetric water content, suction and hydraulic conductivity are all dependent on one another; a decrease in volumetric water content leads to an increase in suction and a decrease in hydraulic conductivity, an increase in volumetric water content leads to a decrease in suction and an increase in hydraulic conductivity.
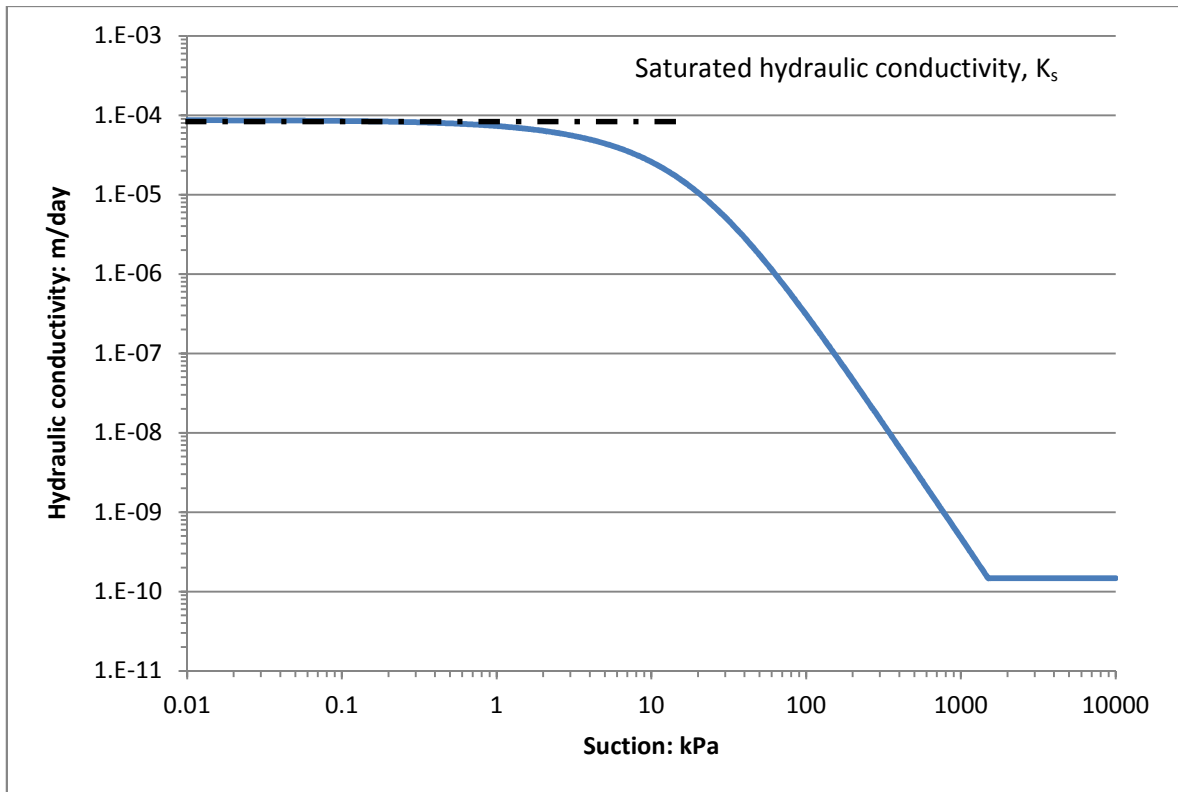
Figure 2-27: Typical hydraulic conductivity function for a clay soil

An SWCC (Figure 2-26) describes the volume of voids that remain water filled as a soil drains. The main features of the curve are; the air entry value (AEV), slope of the function and the residual water content. The AEV defines the negative water pressure at which the largest pores of the soil begin to drain freely. A soil with large, uniform pores will begin to drain before one with small pores and therefore will have a lower AEV. The slope of the function describes the rate at which water drains from the soil; analogous to the AEV, soils with large pores, such as sands, drain quicker than clay soil with small pores and therefore will have a steeper function and a lower AEV. The residual water content is the water content at which a further increase in negative water pressure will not result in significant changes in the water content. Accurately representing the SWCC in the unsaturated range is of utmost importance in a seepage analysis. Reliable measurements of the material properties described above and a method of describing the SWCC with these are required.

Measuring the hydraulic conductivity function for an unsaturated soil is extremely difficult (Abbaszadeh, 2010) and therefore estimation of these functions from an SWCC has become a more attractive procedure (Fredlund et al., 2010a). Predictive

models that fulfil these criteria are available. In Section 2.9.3.1 and Section 2.9.3.2 methods of forming the SWCC and HCF are introduced.

2.9.3.1 SWCC Predictive Models

There are a number of popular SWCC predictive models available. Some of the best known are van Genuchten (1980) and Fredlund and Xing (1994), which are described in this section. Other often used models exist (Millington and Quirk, 1961; Brooks and Corey, 1964). During the extensive literature review it was found that for similar works to this thesis the van Genuchten (1980) or Fredlund and Xing (1994) were used most often.

Van Genuchten (1980)

One of the most frequently used predictive models is that of Van Genuchten (1980). Closed-form equations to predict the SWCC and HCF for a soil based on the saturated and residual water contents and 3 curve fitting parameters have been proposed. The governing equation for the soil water characteristic curve is as follows:

Equation 2-17

$$\theta_w = \theta_r + \frac{\theta_s - \theta_r}{[1 + (\alpha h)^n]^m}$$

Where θ_w = volumetric water content, θ_r = residual water content, θ_s = saturated water content, h = pressure head (cm) of water (these need to be input as positive values despite representing negative pressures), and *a, n* and *m* are the curve fitting parameters.

The curve fitting parameters define the fit and gradient of the curve; *n* controls the slope of the volumetric water content function, *a* is a pivot point about which the n parameter changes the slope of the function and has the units cm⁻¹. The final parameter *m* affects the sharpness of the sloping portion as it enters the lower plateau where:

Equation 2-18

$$m = 1 - 1/n$$

Fredlund and Xing (1994)

The Fredlund and Xing (1994) method is also a closed-form equation that can be used to predict the soil water characteristic curve for suctions between 0 kPa and 1.0×10^6 kPa. The governing equation for the soil water characteristic curve is as follows:

Equation 2-19

$$\theta_w = C_\Psi \frac{\theta_s}{\left\{ \ln\left[e + \frac{\Psi^n}{a} \right] \right\}^m}$$

Where θ_w = volumetric water content, C_Ψ = correction function, θ_s = saturated water content, Ψ = negative pore water pressure, and a, n and m are the curve fitting parameters.

The correction function allows a progressive decrease in water content at high suctions, forcing the function through a water content of 0 at a suction of 1.0×10^6 kPa. The curve fitting parameters a, n and m have slightly different meanings to those in the van Genuchten (1980) equation. The a parameter is the inflection point of the function, the n parameter controls the slopes of the function and m controls the residual water content. These functions are determined by:

Equation 2-20

$$a = \Psi_i$$

Equation 2-21

$$m = 3.67 \ln\left(\frac{\theta_s}{\theta_i}\right)$$

Equation 2-22

$$n = \frac{1.31^{m+1}}{m\theta_s} 3.72 s \Psi_i$$

Where Ψ_i =suction corresponding to the water contemn occurring at the inflection point of the curve and *s* = the slope of the line tangent to the function that passes through the inflection point.

Many reviews of these models are available (Leong and Rahardjo, 1997; Zapata et al., 2000; Cloke et al., 2003; Nam et al., 2009), covering many different soil types and other predictive models not mentioned in this section. Invariably, the authors of these works conclude that the van Genuchten (1980) or Fredlund and Xing (1994) equation are the most effective for predicting the soil water characteristic curve of the soil in question.

2.9.3.1.1 Role of the van Genuchten parameters

A parametric study of the effects of changing each of the parameters on the SWCC was carried out by this Author. Figure 2-28 and Figure 2-29 show SWCCs produced over a suction range 0 – 100 000 kPa on a logarithmic scale as a result of the parametric studies. Residual water content is set at 0.3 and saturated water content at 0.5 which are values typical of those found in the literature for London Clay (Rouainia et al., 2009; Davies et al., 2008a).

Figure 2-28 shows the effect of changing the *n* parameter which controls the slope of the function. The values used in the parametric study are; Very small (n = 1.1), Small (n = 1.5), Middle (n = 3) and Very large (n = 6) as suggested by van Genuchten and Nielsen (1985). The value of *a* has been kept constant at a value of 100 kPa and *m* varies with *n* according to Equation 2-18. As the value of n increases, the steepness of the soil water characteristic curve increases. A steeper slope reflects the smaller suction range over which moisture is removed from soils with uniform pore sizes and would be typical of a soil predominately consisting of sand. The less steep curve generated by n = 1.25 would be typical of a clay soil, where the pores between the individual particles are very small and less uniform than that of a sandy soil and accordingly, moisture drains far less easily from the soil at lower suctions.

The curves produced are similar to those published by Leong and Rahardjo (1997), with increasing values of *n* the curve steepness increases. Differences arising are due to the way the *m* parameter has been handled. Leong and Rahardjo (1997) hold the parameter at a constant value of 1 whereas in the curves the value of *m* is allowed to vary with *n*.
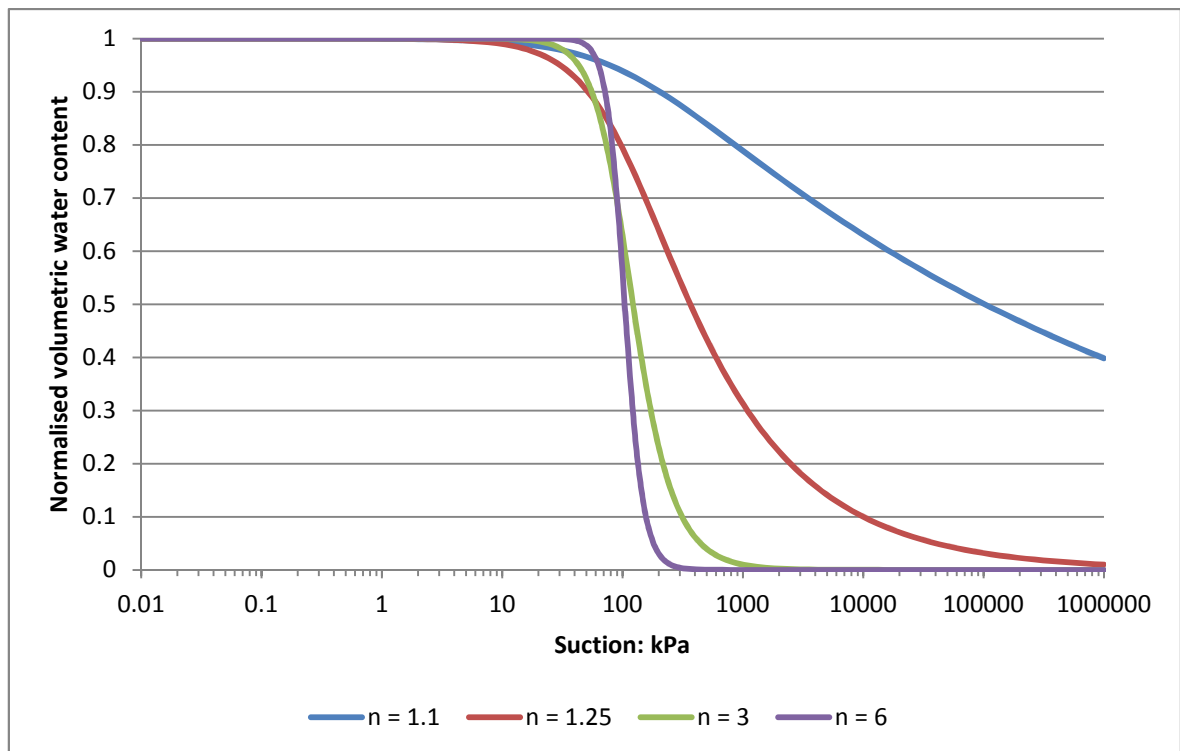
Figure 2-28: Results of the parametric study on the n parameter and the effects on the soil water characteristic curve.

Figure 2-29 shows the effects of changing the *a* parameter. The values of *a* used in this part of the parametric study have been taken from material properties published in the literature (van Genuchten, 1980; van Genuchten and Nielsen, 1985; Stankovich and Lockington, 1995). The values represent a sand (a = 3 kPa), a silty soil (a = 7 kPa) and a clay (a = 64 kPa). A curve with a value of a = 1000 kPa has been included for reference. The values of *n* and *m* have been kept constant at 2 and 0.5 respectively.
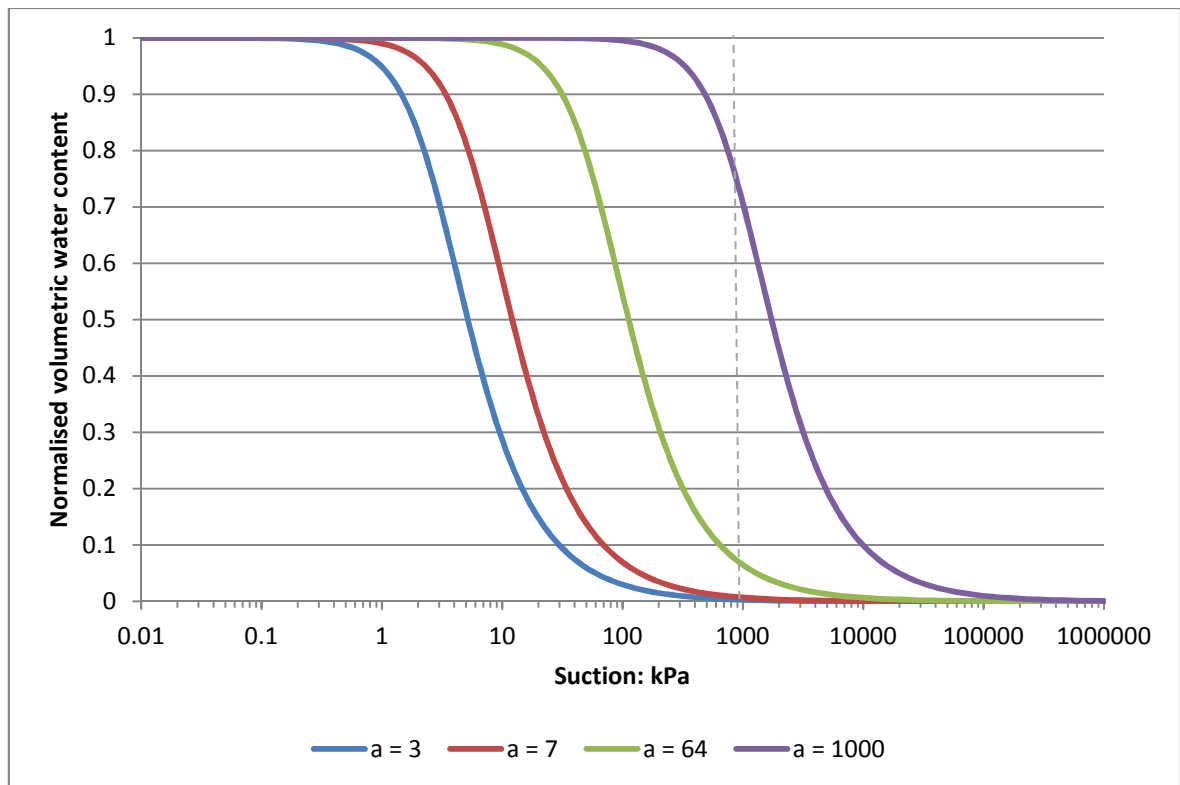
Figure 2-29: Results of the parametric study on the a parameter and the effects on the soil water characteristic curve.

The effects of changing the '*a'* parameter on the SWCC are clear, and also how this parameter relates to the type of soil and its characteristics. The lower the value of *a* the earlier the curve falls from the saturated water content; a low value of *a* represents a soil that has large, uniform pore spaces where the soil can begin draining freely at a low suction. Higher values of *a* epitomise soil where the pore sizes are much smaller and the distribution is less uniform such as clays, with these soils water cannot begin draining freely until higher values of suction are reached. Again, the curves mirror the results of Leong and Rahardjo (1997); the curves are all the same shape, only changing position as a result of the increasing value of *a*. Leong and Rahardjo (1997) point out that *a*, which is commonly construed to be analogous to the AEV of the soil, is not. This is shown clearly in Figure 2-29; the grey line is plotted for a value of 1000 kPa which does not line up with the location of the AEV for the curve where *a* = 1000 kPa.

2.9.3.2 HCF Predictive Model

Once the SWCC has been obtained, a hydraulic conductivity function may also be produced for the soil. The van Genuchten (1980) method proposes a closed form equation to describe the hydraulic conductivity of a soil as a function of the suction:

$$K_w = K_s \frac{\left[1 - \left(ah^{(n-1)}\right)(1 + (ah^n)^{-m})\right]^2}{\left(((1+ah)^n)^{\frac{m}{2}}\right)}$$

Where K_w = hydraulic conductivity, K_s = saturated hydraulic conductivity, h = pressure head (cm) of water (as for the SWCC equation, these must be positive values), and a, m and n are curve fitting parameters used in the SWCC equation. In this form of the equation the units differ from that of the SWCC. Hydraulic conductivities are measured in cm/day and the curve fitting parameter 'a' has the units of cm^{-1}.

2.9.3.3 Example Functions

van Genuchten curve fitting parameters used to fit SWCC and HCF curves for varying soil types are available (van Genuchten, 1980; van Genuchten and Nielsen, 1985; Nandagiri and Prasad, 1996). Two curves have been produced (Figure 2-30) based on the parameters from van Genuchten (1980) for a Silt Loam (Table 2-11).

Parameter	Value
θ_r	0.131
θ_s	0.396
a (cm^{-1})	0.00423
n	2.06
m	0.515
K_s (cm/day)	4.96

Table 2-11: Soil properties and curve fitting parameters of a Silt Loam G.E.3 published in van Genuchten (1980).

Equation 2-17 and Equation 2-23 have been used to produce the curves below against a logarithmic scale of pressure head. The *n* parameter used is quite small, meaning the SWCC is not very steep and water therefore drains from the soil over a large suction range. The relatively small *a* parameter (with units of inverse of pressure) also means that water does not start draining from the soil until a large pressure head is reached which is reflected in the hydraulic conductivity function. The relative hydraulic conductivity was plotted ($K_r = K_w/K_s$) on a logarithmic scale with a value of 1 representing saturated hydraulic conductivity. The relationship between the SWCC and HCF can be seen clearly; whilst the soil still has high volumetric water content of around 0.39, k_r does not decrease by any significant amount but once water starts to drain from the soil the hydraulic conductivity falls exponentially; at a negative pressure head of 10 cm $K_r = 0.93$ and at 200 cm $K_r = 0.11$.
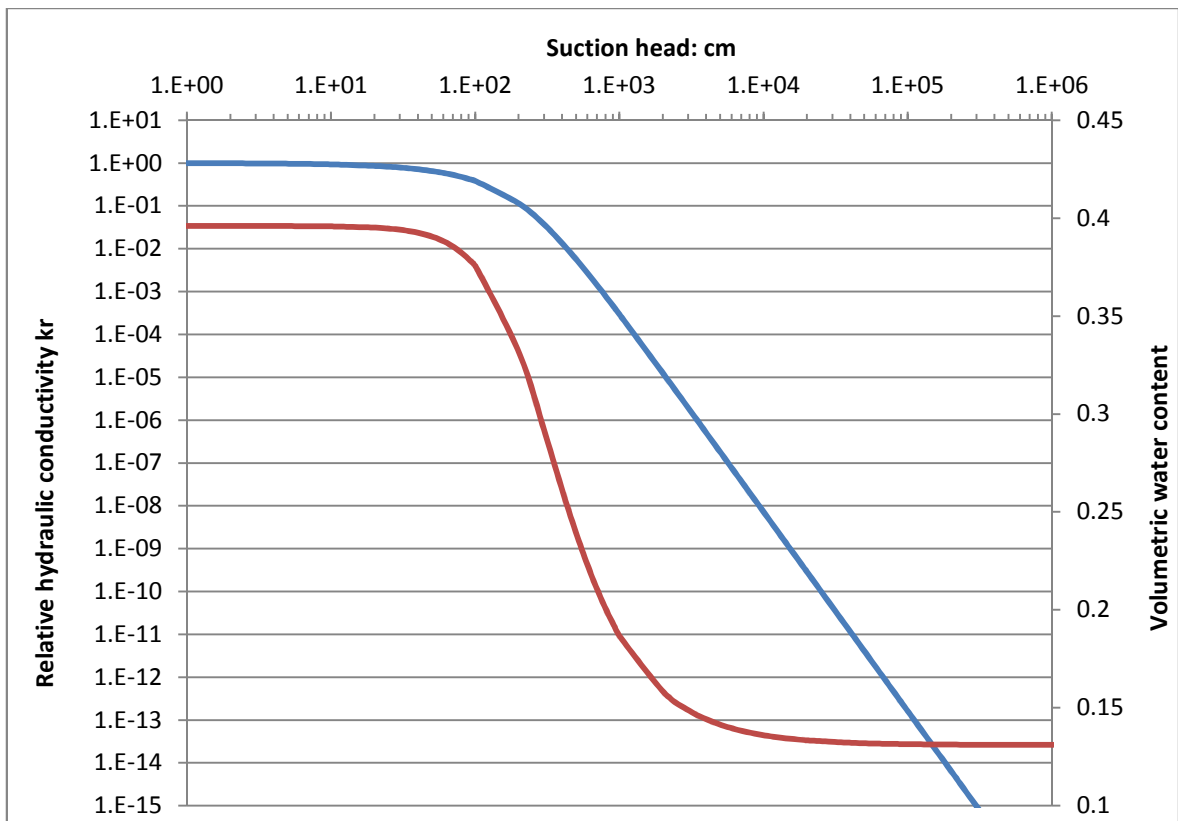
Figure 2-30: Soil water characteristic curve, and relative hydraulic conductivity function, of a silt loam based on soil properties and curve fitting parameters published in van Genuchten (1980).

2.9.3.4 Hysteresis

When determining the shape of a soil water characteristic curve in the lab, depending on whether the soil starts wet or dry and is then dried or wetted the shape of the curve will be different and thus the relationship between water content and suction. Figure 2-31 shows an example of this; if the soil is dried from a saturated state the main drying curve is followed, and if the soil is wetted from the residual state then the wetting curve is followed. If the starting point is an intermediate position on one of the main curves then a different path is taken again, these are shown by the scanning curves in Figure 2-31. The primary scanning curves are indicative of the path of wetting or drying when the main paths are reversed, whereas the secondary scanning curves are indicative of the path taken when the primary scanning curves are reversed. All points on and in between the main curves are possible equilibrium positions and therefore the equilibrium state is dependent upon the history of the system (Hendriks, 2010). This phenomenon is called hysteresis.

Generally in laboratory testing, only the main drying curve will be measured due to cost, time limitations and the difficulty of measuring the wetting curve (Fredlund et al., 2011). Due to the actual hysteretic nature of the SWCC this can lead to inaccuracies in the prediction of suction when an empirical formula such as van Genuchten's (1980) is used. Figure 2-31, which shows typical wetting and drying curves for clay, reveals the difficulties arising when only using the drying part of the SWCC to predict the magnitude of suctions in a soil hydrology problem. The graph shows that at the same volumetric water content, depending on whether the soil is wetting or drying, the values of suction can be very different. The difficulties are further compounded by the scanning curves.
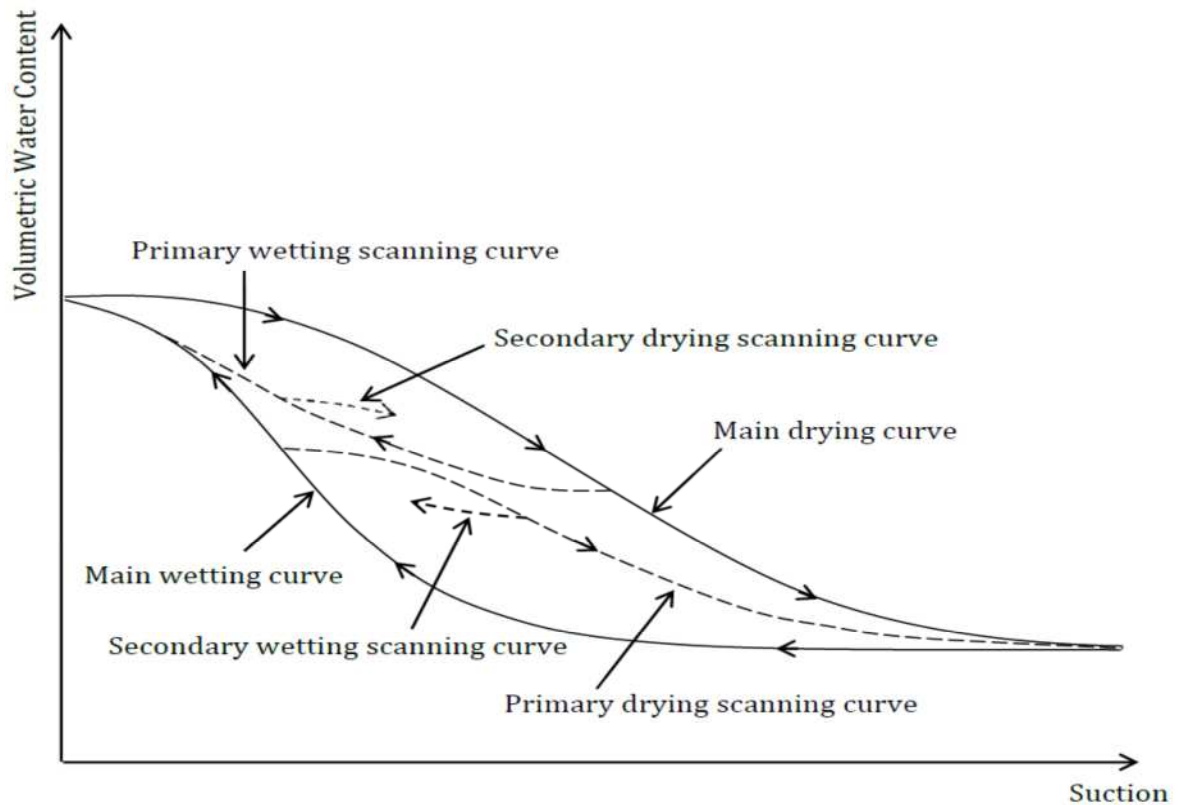
Figure 2-31: Wetting and drying soil water retention curves for a clay soil showing primary and secondary scanning curves.

Fredlund et al. (2011, p. 187-188) suggest five possible assumptions that could be applied when using an SWCC to estimate in-situ soil suctions and how these would affect the analysis of the results.

1. Ignore hysteresis and only use the drying part of the SWCC. This would give an estimate of the maximum likely soil suctions.

2. Measure the drying part of the SWCC and approximate the wetting part by estimating the size of the hysteresis loop at the inflection point. This methodology would provide an estimate of both the maximum and minimum likely suctions with the maximum being more accurate.

3. Measure both the drying and wetting parts of the SWCC in the laboratory. This would provide estimate of the maximum and minimum likely suctions with equal accuracy.

4. Determine a median SWCC halfway between the drying and wetting curves. Using this curve will then give a median estimate of the value of soil suction.

5. Use a more rigorous mathematical equation to describe the drying, wetting and scanning parts of the SWCC which can be very difficult to achieve

(Dingman, 2002), and may not actually be worthwhile as it is impossible to know whether the soil is on one of the scanning curves or one of the main curves (Fredlund et al., 2011).

Disregarding assumption 1 it would seem that assumption 2 would be the simplest to achieve whilst still being able to obtain estimates for maximum and minimum likely suctions. Due to the congruent nature of the shape of the two parts of the SWCC it is possible to apply an appropriate lateral shift to the drying curve to obtain the wetting curve (Fredlund et al., 2011).

Considering the van Genuchten (1980) equation and Figure 2-28 and Figure 2-29, it can be shown that it is the 'a' fitting parameter that controls the lateral position of the SWCC. By establishing the suitable lateral shift it is possible to calculate an appropriate value for the 'a' parameter to fit the wetting curve of the SWCC. Fredlund et al. (2011) have suggested a procedure for obtaining the wetting part of the soil water characteristic curve.

The first step is to establish the drying part of the SWCC; this can be done using any SWCC equation, such as the van Genuchten (1980) closed form equation. The classification properties of the soil are used to obtain an estimate for the magnitude of the required lateral shift from the drying curve to the wetting curve. Fredlund et al. (2011) suggest the following values of lateral shift:

- 25% shift for sands
- 50% shift for silt
- 100% shift for clays

To calculate the value of 'a' for the drying curve Equation 2-24 is used.

Equation 2-24

$$log(a_w) = log(a_d) - \frac{\varepsilon}{100}$$

Where a_w is the wetting value of a, a_d is the drying value of a and ε is the per cent value of lateral shift.

2.10 Desiccation Cracking

Preferential flow describes the phenomena whereby water moves along certain pathways, while bypassing other volume fractions of the porous soil matrix (Gerke, 2006). Gerke (2006) identifies four types of preferential flow; 1) macropore flow, 2) unstable flow, 3) "finger"-like flow and 4) funnel flow. Macropore flow describes the flow of water through roots, worm burrows, fissures or cracks. The flow in desiccation cracks falls into this category. Cracks provide preferential pathways for water infiltration and can considerably increase soil hydraulic conductivity (Rayhani et al., 2008; Li and Zhang, 2011). The majority of cracks developing in a clay soil will be vertical in nature, extending from the surface downwards. However, horizontal cracks are also observed within the soil mass, which can contribute to high lateral infiltration (Greve et al., 2010). Water can enter cracks directly from rainfall or by interception of runoff (Romkens and Prasad, 2006; Greve et al., 2010).

The existence of cracks in a soil can lead to poor estimates of runoff and infiltration (Arnold et al., 2005), and in most soil-water-plant-atmosphere models their effects are inadequately described (Novak et al., 2000). Not accounting for the effects of desiccation cracking would lead to underestimated infiltration and overestimate of surface runoff. Indeed, tests have shown that the infiltration capacity of a cracked clay soil was more than twice that of the same soil without cracks (Novak et al., 2000).

It is believed that desiccation cracking of soil may become more extensive and problematic in the future if the longer, drier and warmer summers for the United Kingdom identified in Section 2.11 come to bear (Dijkstra and Dixon, 2010). Desiccation cracks are induced by evaporation and the consequent shrinking of the soil. Shrinkage caused by changing moisture content is the major factor triggering soil cracking.

The clay soils prevalent in southern England are particularly susceptible to cracking because of their high plasticity; results of plate tests have shown that severity of cracking increases with increasing clay content (Albrecht and Benson, 2001). Networks of desiccation cracks can directly control the soils hydraulic properties, by

85

allowing rapid infiltration of rainfall, giving elevated pore water pressures within the upper surface zone of the slope (Clarke and Smethurst, 2010; Tang et al., 2011). By allowing easier infiltration of water, cracks effectively increase the hydraulic conductivity of the soil. The effects of soil cracking on hydraulic conductivity can in turn have a negative effect upon slope stability (Dijkstra and Dixon 2010; Zhang et al., 2011), when rain falls, water will fill the cracks, softening and weakening the soil leading to possible failures in excavations, slopes, dams, and infrastructure slopes (Fang, 1994).

2.10.1 Desiccation crack behaviour and properties

Desiccation cracks develop as soil dries and shrinks. If the tensile stresses developing at the time of shrinkage exceed the tensile strength of the soil at any point then cracking will occur (Nahlawi and Kodikara, 2006). Despite significantly affecting the performance of clay soils in geoengineering applications and also being of importance in disciplines such as agricultural engineering, mining engineering and materials engineering (Costa et al., 2008), field evidence is wide ranging, generally incomplete and sometomes conflicting (Nahlawi and Kodikara, 2006). Arnold et al. (2005) attribute this to a lack of sound experimental methods and complementary mathematical equations. Consequently, understanding and modelling of the cracking process and crack effects on soil hydrology has been poorly developed (Costa et al., 2008).

Crack geometry changes with time, as a function of the soil water content (Novak et al., 2000). Shrink/swell behaviour results in deepening of the cracked zone (Rayhani et al., 2008). Tests have shown that most shrinkage occurs during the saturated phase of the drying process, which is a universal behaviour independent of the soil type and the pore fluid type (Costa et al., 2008; Hu et al., 2008).

Water flows in cracks through the soil, and there remains the question whether the water in these preferential flow paths will be under the influence of capillary or gravitational forces (Gerke, 2006). Gerke (2006) states that crack sizes can range from capillary to non-capillary, meaning that different equations would be used to

describe different flow types. To describe the flow in capillary sized cracks many authors state that the Darcy/Richards equations (Equation 2-13 and Equation 2-16) are applicable and have used this approach themselves (van Genuchten, 1993; Novak et al., 2000; Gerke and Fredlund et al., 2010b; Li et al., 2011). However, for large, non-capillary sized cracks these equations will likely not be valid (Novak et al., 2000; Arnold et al., 2005). In this case the flow is gravitational and may be modelled by a kinematic wave equation (van Dam, 2000; Greco, 2002; Romkens and Prasad, 2006).

Figure 2-32 shows a 2-dimensional crack network in a desiccated soil, with the water table located at depth D. The crack depth is denoted by y_c. The proportion of the soil (by area) that is cracked is the crack porosity, ϑ_c. Li and Zhang (2010) define the crack porosity as:

Equation 2-25

$$\vartheta_C = \frac{A_c}{A}$$

A_c is the total area of the cracks in the soil (through the cross section) and A is the total area of the cracked soil. Therefore the soil porosity ϑ_S is given by:

Equation 2-26

$$\vartheta_S = 1 - \vartheta_C$$

These definitions of porosity refer only to the cracked portion of the soil. Therefore, in the idealised crack network of Figure 2-32, on the following page, the crack porosity is calculated for the area of soil which the cracks occupy, or y_c. In field conditions, where crack depths will not be uniform, the maximum crack depth is used to calculate the total area of cracked soil (through the cross section).
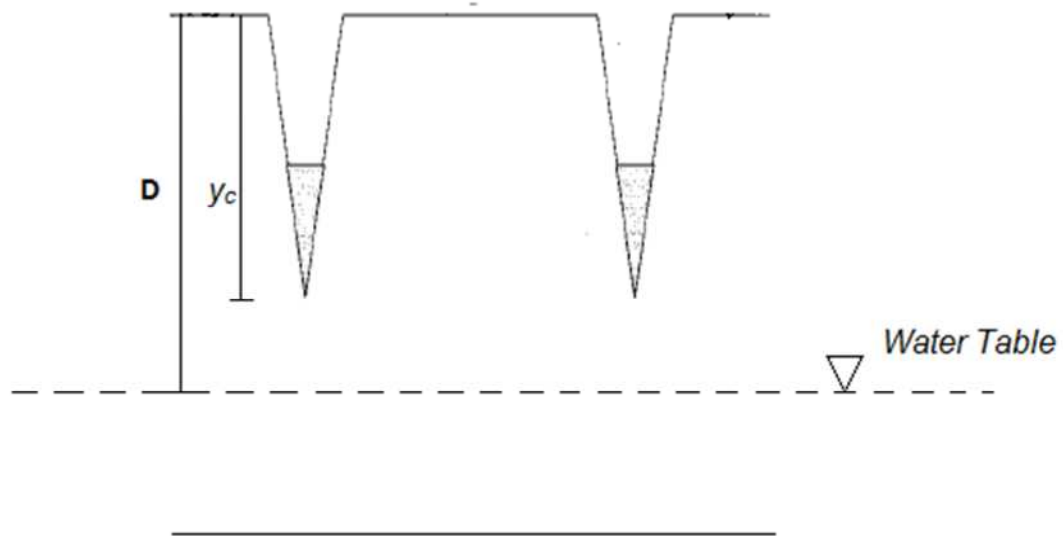
Figure 2-32: A 2-dimensional crack network.

Crack porosity can increase as a result of more cracks appearing in the soil or the size of existing cracks growing. As moisture content of the soil falls, cracks will grow and new cracks will appear. Arnold et al. (2005) monitored crack volume in a clay soil over a period of two years; with the following findings:

- A maximum crack area of 82 mm^2 over a depth of 4.5 m, or a crack porosity of 0.018. This means that through a cross section of the soil 4.5 m deep and 1.0 m wide, the total area that was cracked was 82 mm^2.

- Crack volume changed with depth – over 70 % of cracking was observed in the top 1.5 metres of the soil profile.

- Crack volume varied seasonally, reaching a maximum in later autumn and a minimum during winter.

2.10.2 Influence of desiccation cracks on slope hydrology

Maximum desiccation of a clay slope/ located in the United Kingdom often occurs in September, at the end of summer (Nyambayo et al., 2004). The cracks forming in the soil as a result of this process could possibly extend right to the base of the vadose zone by the end of summer (Clarke and Smethurst, 2010). The surface flux on a slope will be sensitive to cracks which change the soil's hydraulic properties and should therefore be considered in any surface flux model (Abbaszadeh et al., 2010; Fredlund

et al., 2010a). Not accounting for these cracks can lead to poor estimation of runoff and infiltration quantities; these processes both contribute to water storage trends in the slope that differ significantly from those of intact soil (Kohne et al., 2002; Abbaszadeh et al., 2010).

Networks of desiccation cracks can directly control the soils hydraulic properties, by allowing rapid infiltration of rainfall, giving elevated pore water pressures within the upper surface zone of the slope (Clarke and Smethurst, 2010; Tang et al., 2011). By allowing easier infiltration of water, cracks effectively increase the hydraulic conductivity of the soil.

2.10.2.1   Desiccation crack effects on hydraulic conductivity

Cracking of soils is important to the design of clay liners for landfill covers and in agriculture, and it is within these two fields that significant research has been carried out on the effects of soil cracking on hydraulic conductivity.

Albrecht and Benson (2001) conducted hydraulic conductivity tests on desiccated samples of eight different naturally occurring soils used as clay liners in the United States. The soils ranged from low plasticity (PI = 11) to very high plasticity (PI = 46), showing an increase in clay content of the soils as PI increases (from 12% clay to 53% clay). It was found that the soils of greater plasticity, and therefore greater clay content, cracked the most, whereas the soil of lowest plasticity contained no visible cracking. The soils that exhibited cracking showed increases of hydraulic conductivity of up to 2 orders of magnitude after just one cycle of drying, ultimately increasing by up to 3 orders of magnitude.

Omidi et al. (1996) carried out laboratory studies on two soils to evaluate the effects of desiccation cracking on the hydraulic conductivity of compacted soils. The soils were a high plasticity Beaumont Clay and a low plasticity Illite Silty Clay, both from the United States. The higher plasticity soil had greatest shrinkage of 16.4%, with the Illite soil shrinking by 11.7%. Undesiccated hydraulic conductivity was measured in small and large permeaters, whilst desiccated hydraulic conductivity was measured

in the large permeater only. The table below shows ratios of conductivity for undesiccated and desiccated soils in large permeaters to laboratory values, plus the ratio of conductivity for desiccated soils in large permeaters to the same undesiccated soils in large permeaters.

	Beaumont soil	Illite soil
K_{UL}/K_{lab}	39.3	8.3
K_{DL}/K_{lab}	452.0	21.7
K_{DL}/K_{UL}	11.5	2.6

Table 2-12: Results of conductivity tests on cracked soils (after Omidid et al., 1996).

Where K_{UL} = hydraulic conductivity of undesiccated samples measured in large permeaters, K_{lab} = hydraulic conductivity of undesiccated samples measured in small permeaters and K_{DL} = hydraulic conductivity of desiccated samples measured in large permeaters after two drying cycles.

Hydraulic conductivity is greater in the desiccated samples of both soils. The high plasticity Beaumont soil shows a greater increase. However, when comparing results obtained from the large permeaters the increase in hydraulic conductivity is much reduced, from 452 times greater to 11.5 times greater for the Beaumont soil. This highlights that laboratory measured hydraulic conductivity cannot always be used to predict conductivities likely to occur in the field. Small laboratory permeaters may grossly underestimate the conductivity of soil with a high amount of shrinkage (Omidi et al., 1996).

Even once cracks 'close', bulk hydraulic conductivity of the soil is observed to still be at a greater magnitude than that of the same soil that has not been cracked. Anderson et al. (1982) measured the saturated hydraulic conductivity of Oxford Clay (PI = 44) in an un-cracked state and a previously cracked state. The soil that had not been cracked had saturated hydraulic conductivity of 4 x 10^{-7} m/s at the surface and 1 x 10^{-9} m/s at 1.0 metre depth. The same soil, which had been cracked, but in a closed crack

state, had a saturated permeability of 5.2 x 10^{-5} m/s. Rayhani et al. (2007) measured the hydraulic conductivity and dimensions of cracks in un-cracked and cracked clay soils. The results showed that the dimension of cracks increased with increasing plasticity index and clay content and the hydraulic conductivity in the cracked soils increased with increasing plasticity index and cycles of drying and wetting. They also found that the hydraulic conductivities of the cracked soils, once saturated, were still at least one order of magnitude greater than that of the un-cracked soil.

Three explanations for this behaviour have been identified in the literature. Abbaszadeh (2010) and Kuna et al. (2013) have both observed that cracks often fill with eroded material from the soil surface. This material, at a much lower density than the intact soil, provides essentially no resistance to infiltration. Thus, when cracks close, there will still be parts of the soil whole with much greater conductivity than the intact part. It is also unlikely that cracks will fully close on wetting/saturation of the soil profile (Gerke, 2006; Li and Zhang, 2011), meaning that preferential pathways will still be present for infiltration. There is also the matter of how cracks close; it has already been mentioned that cracks are often observed to close from the surface (Favre et al., 1997; Greve et al., 2010). This gives the impression that cracks are closed when in reality deeper parts of the crack network would still be present (Greve et al., 2010).

Laboratory measurement of the hydraulic conductivity function of an unsaturated soil is extremely difficult and the presence of cracks only reinforces this (Abbaszadeh, 2010; Fredlund et al., 2010b). Abbaszadeh (2010) suggest that once the SWCC of the soil is established for the cracked soil, predictive models can be used to determine the HCF. However, determining the SWCC for the cracked part of the soil presents problems of its own (Fredlund et al., 2010b).

2.10.2.2 The effects of desiccation cracks on the soil water characteristic curve

Fredlund et al. (2010a) consider the effect that soil cracking will have on the soil water characteristic curve (SWCC), and hydraulic conductivity function. They predict

91

that the SWCC could take on a bimodal character

(

Figure 2-33); with similar effects on the hydraulic conductivity function where the increase in K_s due to cracks will have to be taken into account.

Figure 2-33: Possible effects of cracking on SWCC and hydraulic conductivity function, after Fredlund et al. (2010).

These changes will have significant impacts on any numerical modelling attempts. The effects of cracking should be included in models. Fredlund et al. (2010, p.3) state that "numerical modelling simulations based on the properties of originally intact materials can be considerably different from the soils that develop near ground surface with time". Therefore the development of soil-water characteristic curves and permeability/hydraulic conductivity functions for cracked soils is crucial to the study of stability of cracked soil slopes (Li et al., 2011).

2.10.2.3   Bimodal soil water characteristic curves

There are already numerous mathematical models in existence that represent unimodal soil-water characteristic curves, some of which have already been described in Section 2.9.3.1 (Brooks and Corey, 1964; van Genuchten, 1980; Fredlund and Xing, 1994;). These models are applicable to soils that are well graded with cumulative pore-size distribution and pore-size density curve that

are unimodal

(

Figure 2-34). Some soils, however, are gap graded and therefore these models are not applicable. Gap-grading occurs when particle sizes of the coarse grains are far larger than the sizes of the fine grains and the fine grains do not completely fill the pore formed by the coarse grains (Zhang and Chen, 2005). The soils can be said to be of 'dual-porosity'.

Figure 2-34: Structures, pore-size distributions and pore-size density curves for unimodal and bimodal soils, after Zhang and Chen (2005).

From a continuum mechanics stand-point the cracked soil behaves as if it is a combination of two materials, averaged over the whole volume (Fredlund et al.,

2010b). Dual-porosity models have been proposed as an applicable method to describe the hydraulic properties of structured porous media, such as cracked soils (Kohne et al., 2002; Fredlund et al., 2010a). When using this approach, two SWCC functions are superimposed to create one function for the cracked soil (Durner, 1994; Mallants et al., 1997; Kohne et al., 2002; Fredlund et al., 2010b;). Separate functions are developed for the intact part of the soil and the cracks with separate parameters for each (Durner, 1994; Kohne et al., 2002). For example the AEV of the cracks is much lower than that of the intact soil (Abbaszadeh et al., 2010).

Gerke and van Genuchten (1993) developed a one-dimensional model which simulates preferential movements of water and solutes in structured soils. The approach taken is to assume that the medium can be separated into two distinct pore systems, both of which are homogeneous media with transient water flow governed by the Richards equation but with their own distinct set of hydraulic properties. The model requires the definition of three hydraulic conductivity functions; K_f for the fracture network, K_m for the matrix system and K_a to describe the exchange of water between the two pore systems. This method requires estimates of hydraulic and transfer parameters which are difficult to measure experimentally and may not be used to model SWCCs of soils with large grains that prohibit routine measurement of SWCCs (Zhang and Chen, 2005).

Zhang and Fredlund (2003) presented a water retention curve for unsaturated fractured rocks. The model uses expressions for pore-size distribution of the rock matrix and distribution of fracture aperture to create water retention curves for each phase. The water retention curve for the fractured rock mass is obtained by combining these two separate curves and then weighting each one by their porosities to give:

Equation 2-27

$$\theta(\psi) = \vartheta_{sm}\Phi\left(\frac{\ln\left(\frac{C}{\psi}\right) - \lambda_m}{\varsigma_m}\right) + \vartheta_{sf}\Phi\left(\frac{\ln\left(\frac{C}{\psi}\right) - \lambda_f}{\varsigma_f}\right)$$

Where ϑ_{sm} is the matrix porosity, ϑ_{sf} is the fracture porosity, ψ is the value of suction, λ_m and ς_m are mean and standard deviation of ln(r), where r is the pore-size distribution, λ_f and ς_f are the mean and standard deviation of the ln(r), where r is the distribution of the fracture aperture, Φ is the cumulative function of the standard normal distribution and C = 2T cosα where T is the surface tension of water and α is the angle of contact between water and soil particle. As with the previous method (Gerke and van Genuchten, 1993) this requires measurements that are difficult to obtain.

Zhang and Chen (2005) have developed a method for predicting bimodal or multimodal SWCCs. The method utilises unimodal SWCCs for the characteristic soil components that correspond to the respective pore series. Using either the van Genuchten (1980) or Fredlund and Xing (1994) equation for a SWCC, SWCCs for the small pore series and large pore series can be formed; these are combined, with each being weighted based upon their volumetric water content at saturation (or porosity), to give the SWCC for the whole soil mass. For example, when using the van Genuchten equation the expression for the bimodal soil takes the following form:

Equation 2-28

$$\theta(\psi) = \vartheta_{sl} \left[\frac{1}{1 + (a_l \psi)^{n_l}} \right]^{m_l} + \vartheta_{ss} \left[\frac{1}{1 + (a_s \psi)^{n_s}} \right]^{m_s}$$

Where a_l, n_l, and m_l are fitting parameters for the large-pore series, a_s, n_s, and m_s are fitting parameters for the small-pore series and ψ is the suction. Weighting factors ϑ_{sl} and ϑ_{ss}, are the porosity of the small-pore series and the large-pore series respectively.

Copyright not obtained

Figure 2-35: Measured and predicted soil-water characteristic curves using van Genuchten function for sand-diatomaceous earth mixtures (after Zhang and Chen, 2005).

Verification of the function was carried out; experimental data obtained by Burger and Shackelford (2001a; 2001b) was used. Soil-water characteristic curves were measured for different mixtures of sand and diatomaceous earth pellets.

Copyright not obtained

Figure 2-35 shows the measured and predicted SWCCs a number of different mixtures alongside the fitted SWCCs from Equation 2-28. The SWCCs predicted by the proposed model fit the experimental data well. The model of Zhang and Chen (2005) can be used to predict the SWCCs of bimodal or multimodal soils; however, it does not possess a permeability function. This function is vital if the effects of cracking on hydrological processes in slopes are going to be modelled.

2.10.2.4   The capillary law maximum crack aperture

The models presented in the previous section all assume that flow in the cracks is governed by the capillary law. This law will only apply to cracks up to a certain aperture (Greve et al., 2010). Beyond this aperture the water in the crack cannot bridge between the two sides, due to the limits of surface tension of water, and the capillary law cannot be applied (Li et al., 2011). Li et al. (2011) have recommended the maximum crack aperture for which the capillary law will still apply, by considering the vertical force equilibrium of the capillary water in the crack plane (Figure 2-36).
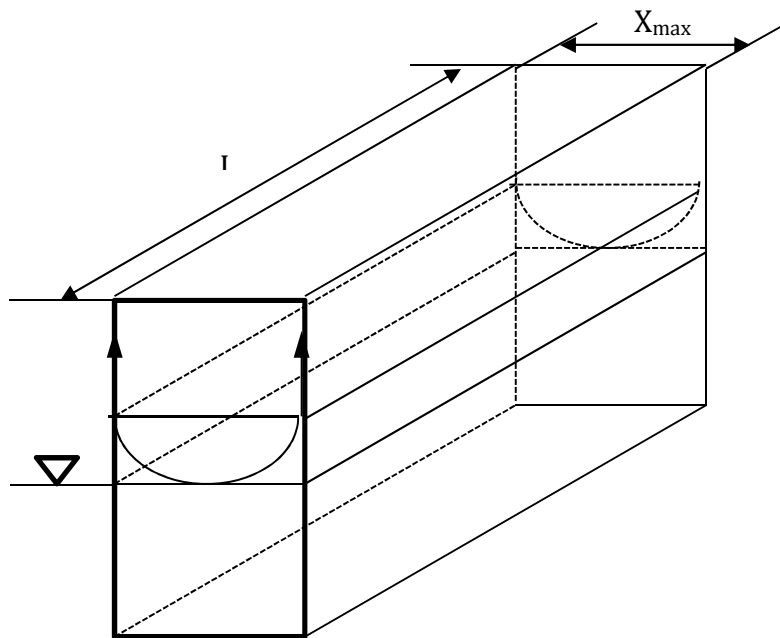
Figure 2-36: Physical model to determine maximum crack aperture for which the capillary law still applies, after Li et al. (2011).

Assuming that the meniscus is cylindrical and the contact angle is zero, the minimum capillary height is a half of X_{max}. Therefore, based on force equilibrium in the vertical direction, the resultant of the water surface tension is responsible for holding the weight of the water column, and hence:-

Equation 2-29

$$2TL = \gamma_w \left(X_{max} \left(\frac{X_{max}}{2} L - \frac{1}{2} \frac{\pi X_{max}}{4} L \right) \right)$$

Which can be simplified (see Appendix A for full simplification) to give:-

$$X_{max} = 4.32 \sqrt{\frac{T}{\gamma_w}}$$

At 20°C the surface tension of water is T = 0.0728 N/m which gives a maximum crack aperture of 11.8 mm.

2.10.2.5   Implementation of bimodal functions for desiccated soil

To implement one of these methods in a numerical model fitting parameters for the chosen closed-form equation would be required to define the crack part of the SWCC. Gerke and van Genuchten (1993) used the values in Table 2-13 for the fitting parameters of the crack in their study of a dual-porosity solute transport model.

Fitting Parameter	Value
Residual Water Content	0
Saturated Water Content	0.5
a	0.1 cm^{-1}
n	2
m	0.5
K_s	20 m/day

Table 2-13: Suggested fitting parameters for the crack part of a bimodal SWCC.

2.10.2.6   Estimating Crack Depth

Fredlund and Rahardjo (1993) have suggested an analytical equation for calculating the maximum crack depth based on the water table depth, soil suction profile and soil properties.

Equation 2-31

$$y_c = \frac{D}{1 + \dfrac{v\rho H_m}{f_w \rho_w E_e}}$$

Where y_c is the maximum crack depth, D is the depth from ground surface to the phreatic surface, v is Poisson's ratio, ρ is the total density of the soil and ρ_w is the density of water. E_e and H_m are the elastic moduli with respect to a change in effective stress $(\sigma - u_a)$ and matric suction $(u_a - u_w)$ respectively. The variable f_w allows the actual suction profile to be represented as a percentage of the hydrostatic suction profile.

Copyright not obtained

Figure 2-37 shows two soil suction profiles above a water table; hydrostatic suctions and an idealised suction profile where suctions are greater than hydrostatic.

100

Copyright not obtained

Figure 2-37: Idealised suction profile, with the suction varying linearly to the water table, after Fredlund and Rahardjo (1993).

From this diagram it is established that f_w is the ratio of the actual suctions to hydrostatic suctions. f_w increases as suctions increase, underlining the point that greater suctions lead to a greater extent of cracking in a desiccated soil. Fredlund and Rahardjo (1993) note that values of f_w = 1.0 and 2.0 result in a cracking depth of approximately 20 % and 34 % of the water table depth respectively when v = 0.35 and E_e/H_m = 0.17.
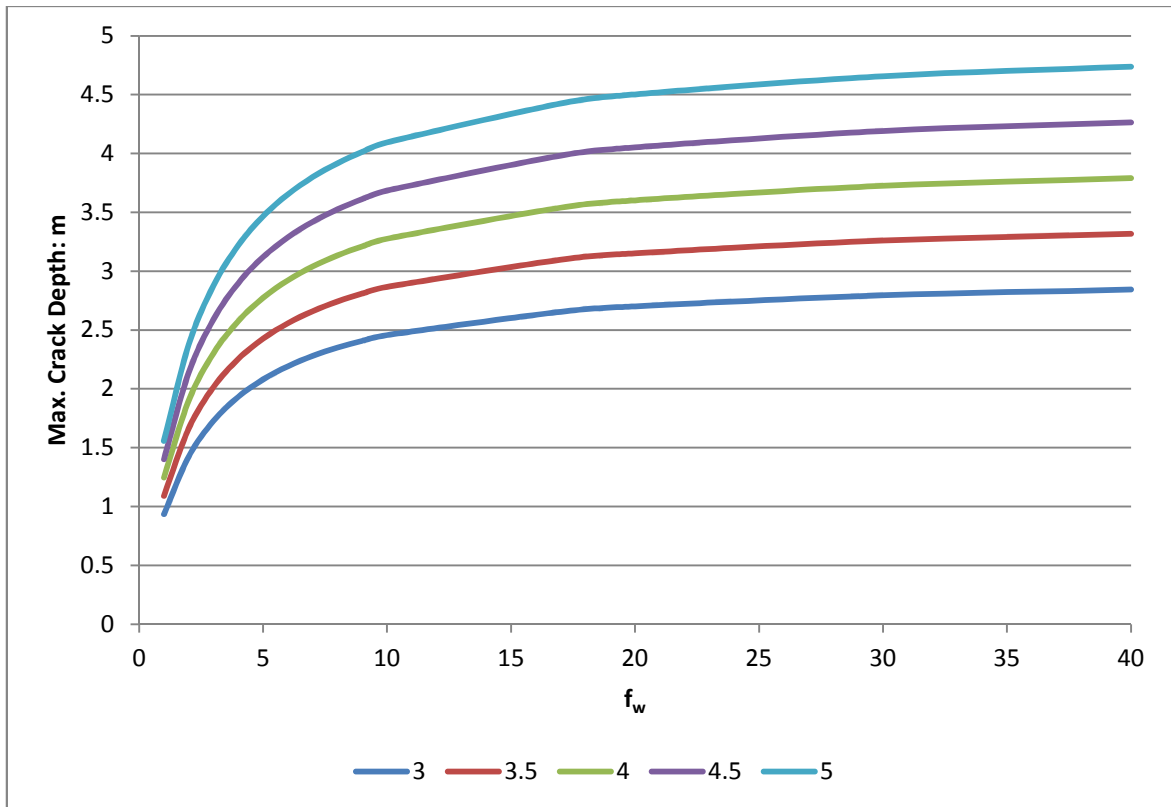
Figure 2-38: Relationship between water table depth, f_w and maximum crack depth.

Figure 2-38 was produced by this author to illustrate the relationship between the water table depth D, f_w and the maximum crack depth y_c according to Equation 2-31. The plot shows how, for different depths of water table, increasing suctions influence the depth of cracking. The plot reveals that according to Equation 2-31:

- Maximum crack depth cannot exceed the depth of the water table.
- At values of f_w greater than 10 crack depth increases, as a ratio of the water table depth, are much reduced.
- The depth of the water table plays just as significant a role as the magnitude of suctions in determining the maximum depth of cracking.

Currently, little research has been carried out to validate this approach. The equation primarily provides an insight into the physics related to the problem (Fredlund and Rahardjo, 1993).

2.10.3 Previous works

102

Collison et al. (2000) tried to account for the effects of soil cracking on slope hydrology by prescribing different soil properties to different soil layers of a slope hydrology/stability model (Table 2-14) of the Roughs field landslide in South East England. By giving the top soil layer (0.3 metres deep) higher saturated conductivity water was able to bypass to the second layer, thus representing the preferential infiltration pathways provided by desiccation cracks.

Soil Layer	Depth	Saturated Conductivity
Cracked root zone	0 – 30 cm	$1.3_x 10^{-5}$ m/s
Landslide debris	30 – 200 cm	$8.7 x 10^{-7}$ m/s
Weald Clay	>200 cm	$7.8 x 10^{-9}$ m/s

Table 2-14: Soil properties used in slope hydrology model of the Roughs field landslide.

This approach was relatively simplistic in that it assumes a constant crack depth throughout the year of only 0.3 metres, whereas in reality crack depth varies as the moisture content of the soil varies (Novak et al., 2000). This will hinder the models capability to capture the effects of cracking on slope hydrology, such as the increased infiltration rates.

Fredlund et al. (2010b) used the bimodal functions described in section 2.10.2.3 to model the suction changes beneath a slab foundation placed on various cracked soil profiles, subject to evaporation and infiltration surface flux conditions and with varying initial conditions. The conditions analysed were; intact soil: no cracks, cracked surface soil with initial suction less than AEV and cracked surface soil with initial suction greater than AEV. Analyses for crack depths of 1 m and 2 m were performed. Evaporation and infiltration rates were both 4 mm/day and applied for a total of 7 days to each model. The major findings of these analyses were:

1) In evaporation cases with cracked soil the suctions along the ground surface increase. When crack density was increased the difference in suction between the soil covered by the slab and uncovered decreased as horizontal flow dominated.

2) In the evaporation cases suctions in the cracked soil profile were essentially uniform, whereas in the un-cracked soil they varied nonlinearly, reflecting the substantial difference in hydraulic conductivity between intact and cracked soils.

3) Increases in suction were greatest in the first day of the evaporation cases, but slowed after this as the soil dried and the hydraulic conductivity decreased.

4) In the infiltration cases, with a cracked soil, there was much higher hydraulic conductivity in the cracked soil than the intact soil resulting in moisture flowing predominantly in the cracked soil, with substantial horizontal flow for larger crack densities.

5) Similarly to the evaporation case suctions, in the cracked layer become distributed uniformly as moisture infiltrates, with suctions in the intact layer being nonlinear in nature.

6) The magnitudes of soil suction changes are sensitive to the crack density. As this increases, in both the evaporation and infiltration cases, the total changes in suction increase.

7) In some cases, namely when the crack density is low and initial suctions are greater than the AEV of the cracks, and infiltration is occurring, suctions beneath the slab do not decrease but stay relatively stable throughout the 7 days. This is because the hydraulic conductivity does not increase to a level where horizontal flow becomes prevalent.

The results from the model begin to give an understanding of the effects of desiccation cracks on the hydrology of a cracked soil and how various factors, such as crack density and initial conditions influence the behaviour. Results have currently not been validated, which is proving to be difficult due to lack of appropriate data (Fredlund et al., 2010b).

2.11 Climate Change

In his significant paper, Arrhenius (1896) became the first person to describe the link between atmospheric gases such as carbon dioxide, methane and water vapour and the warming of the Earth's atmosphere, also speculating on the effect that manmade combustion has on the temperature of the Earth. The term 'greenhouse effect' was

coined, illustrating the effect of the heat barrier in the upper atmosphere created by the gases.

2.11.1 UKCP09 and climate change in the UK

On a worldwide scale, climate change is expected to alter temperatures and rainfall patterns (IPCC, 2007). In terms of the United Kingdom, much of the country is expected to experience drier, warmer summers and wetter winters (IPCC, 2007; UK Climate Projections, 2009). Intense rainfall events, particularly in the winter, are expected to become more severe and more frequent. These positions are taken based on probabilistic projections from general circulation models (GCMs). Climate change projections for the United Kingdom are provided by the UK Climate Change Projections (UK Climate Projections, 2009) based at the Met Office Hadley Centre. The Met Office Hadley Centre climate model; HadCM3, is a fully coupled Ocean-Atmosphere GCM. The HadCM3 (or Hadley Centre Coupled Model version 3) GCM was developed in 1999 (Gordon et al., 2000; Pope et al., 2000).

2.11.1.1   UKCP09 climate change projections

UKCP09 is the fifth generation of climate change information for the United Kingdom. UKCP09 climate change projections provide annual seasonal and monthly climate averages, including temperature and precipitation, over 25 km squares, for seven 30 year time periods and for three separate emissions scenarios. The greenhouse gas emissions scenarios; low, medium and high, are based on the IPCC Special Report on Emissions Scenarios (SRES) scenarios (Nakicenovic et al., 2000).

Climate change projections can be visually presented through various means, including customisable maps and probability density functions (PDFs). The PDFs are line graphs that show the relative probability of different amounts of climate change. Probability in the UKCP09 predictions must be treated carefully; the percentages given do not indicate the absolute chance of a certain change occurring. They specify the percentage of model runs that fall at or below that value. Therefore a change of

4.5 ^{0}C at a 90% probability level is indicating that 90% of the model runs fall at or below that value and 10% of the model runs are above that value.

The following maps (Figure 2-39 to Figure 2-41) show a number of probabilistic climate change projections for the whole of the United Kingdom at a number of probability levels for the 2050s at a high emissions scenario. The climate change variables that are plotted reflect the key expectations of climate change in the United Kingdom; warmer, drier summers and wetter winters (particularly intense rainfall events). The variables that have been plotted are:-

1. Change in mean summer temperature (Figure 2-39).
2. Change in mean summer precipitation (Figure 2-40).
3. Change in total precipitation on the wettest day of winter (Figure 2-41).
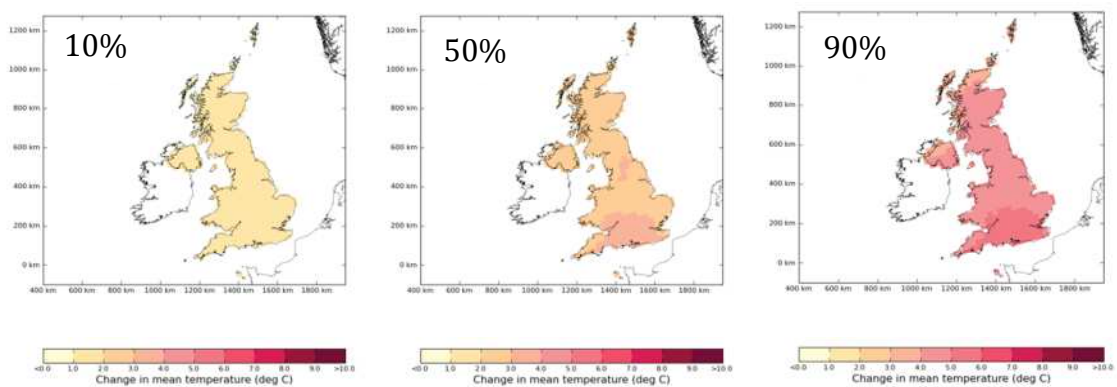
Figure 2-39: Change in mean summer temperature at 10, 50 and 90 % probability levels.

Figure 2-39 shows an increase in the mean summer temperature for the whole of the United Kingdom at all probability levels. At a 10 % probability level the increase is between 1 and 2 ^{0}C for the whole country. As the probability level increases there are some regional differences in the change. At the 50 % probability level the south of England becomes more severely affected than other regions; an increase of up to 4 ^{0}C could be seen in this region. In the rest of the country the increase is up to 3 ^{0}C in all regions. At the 90 % probability level the increase is most marked in Southern England. The change is shown to be between 5 and 6 ^{0}C in this region whereas for the majority of the rest of the country the change is between 4 and 5 ^{0}C, and in the north of Northern Ireland and Scotland between 3 and 4 ^{0}C.
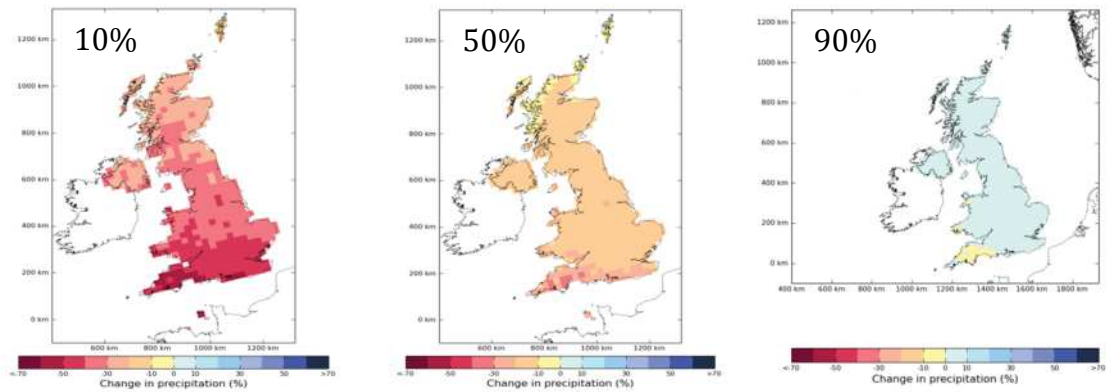
Figure 2-40: Change in mean summer precipitation at 10, 50 and 90 % probability levels.

Figure 2-40 shows the change in mean summer rainfall at three probability levels for the high emissions scenario projection. At the 10 % probability level there is a considerable change in the mean summer rainfall, especially in the south of England where there could be between 60 and 50 % less precipitation. In the rest of the country there could be between 40 and 10 % less. At the 50 % probability level there are still significant changes in the mean summer precipitation, again most noticeably in Southern England. There could be between 40 and 20 % less precipitation in this region, and between 20 and 0 % less in the rest of the country. At a 90 % probability level most regions of the country would see no decrease in the mean summer precipitation apart from the south west where a decrease of up to 10 % could happen.
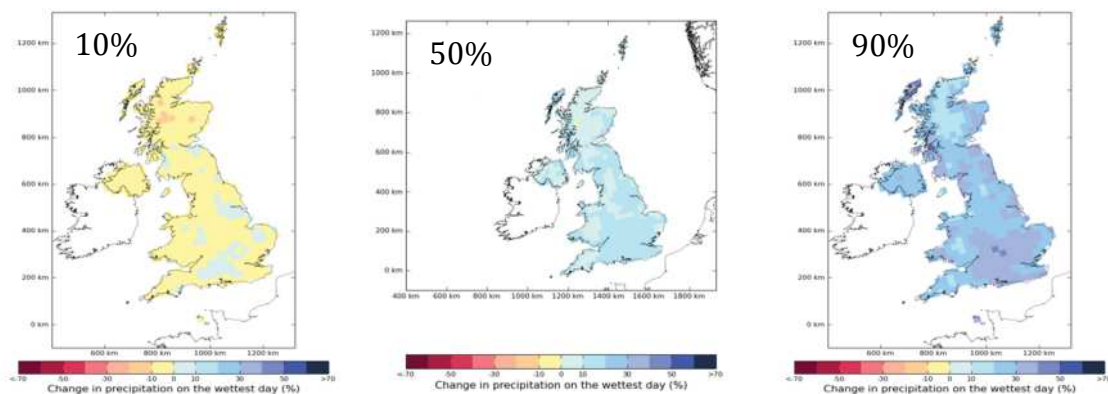
Figure 2-41: Change in total precipitation on the wettest day of winter at 10, 50 and 90 % probability levels.

Figure 2-41 shows change in total precipitation on the wettest day of winter at three probability levels. The maps show that once more the south of England could be the most severely affected. At the 10 % probability level changes are not significant; there could be between a 10 % decrease and 10 % increase throughout the country. At the 50 % probability level more significant increases are observed; between 0 and 20 % throughout the whole country. At the 90 % probability level the greater effects in the south of England are most noticeable. There is up to a 50 % increase in the total precipitation on the wettest day of winter in this region in some parts and at least between 20 and 40 % for the majority of the remaining parts. The rest of the country could also see considerable increases in the total precipitation on the wettest day of winter; most regions seeing an increase of between 10 and 40 %, with the Western Isles of Scotland seeing up to a 50 % increase.

2.11.1.2   Focus on Southern England

The south of England has been identified as the region in the United Kingdom that could be most severely affected by climate change. The following set of graphs (Figure 2-42) look at the effects of climate change on this region in more detail. PDFs have been produced for the same three climate variables as in Section 2.11.1 for one 25 km square. The square chosen is the location of the Newbury bypass cutting, located in southern England, which has been the focus of much research, having been extensively instrumented and monitored by Smethurst et al., (2006; 2012).
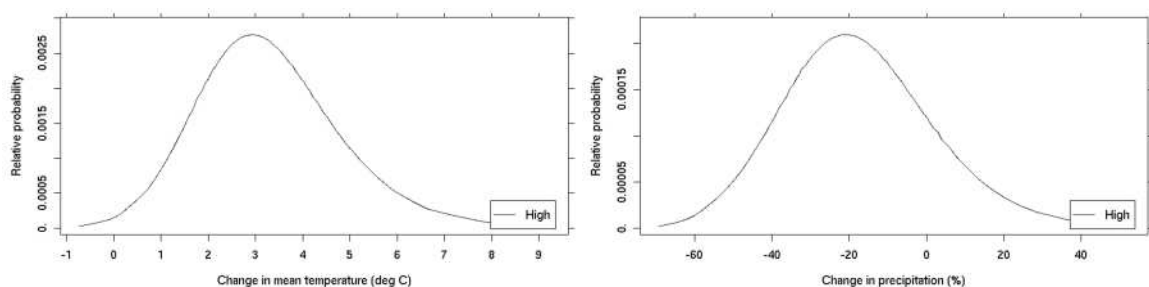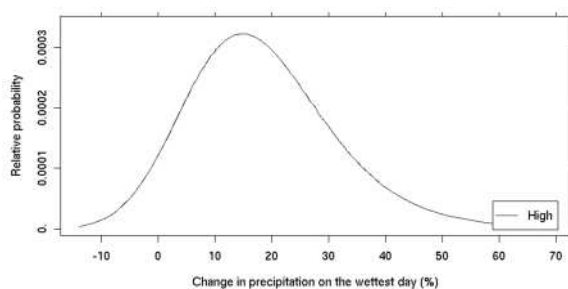
Figure 2-42: PDFs of change in mean summer temperature, change in summer precipitation and change in precipitation on the wettest day of winter.

At a high emissions scenario at this location in the south of England the most probable change in mean summer temperature is an increase of approximately 3 ^{0}C. The PDF of change in summer precipitation shows that at the high emissions scenario the most likely change would be a decrease of 20 % at this location. The PDF for the change in total precipitation on the wettest day of winter shows that the most likely increase would be around 15 % if the high emissions scenario was to occur.

Analysis of the produced maps and PDFs has shown that according to the Hadley Centre climate model HadCM3 the United Kingdom will be significantly affected by climate change by the 2050s if a high emissions scenario occurs. The region experiencing the greatest changes to its current climate will be the south of England, where it was shown that mean summer temperatures are likely to increase, mean summer precipitation will decrease and the intensity of single precipitation events in the winter is likely to increase. The Newbury bypass cutting, located in the South of England would be affected by climate change. In Section 2.11.2 possible effects on infrastructure slopes are discussed, particularly considering the three climate variables that have been focussed upon in this section of the literature review.

2.11.2 Effects of climate change on slope stability

Climate change will likely influence the future behaviour of slopes in the United Kingdom (Collison et al. 2000; Clarke et al. 2006; Dixon et al. 2006; Glendinning et al. 2009a; Loveridge et al. 2010) and internationally (Briceno et al., 2007; Geertsema et al., 2007; Hulten et al., 2007). Some recent extreme climate events, such as the very wet winter of 2000/2001 in the UK, and the recordings of increased slope failures has

prompted speculation with respect to how climate change will affect slope stability (Clarke et al., 2006). 2012 was the second wettest year on record in the United Kingdom (Met Office, 2013). Rainfall was well above average in summer and winter resulting in many landslides.
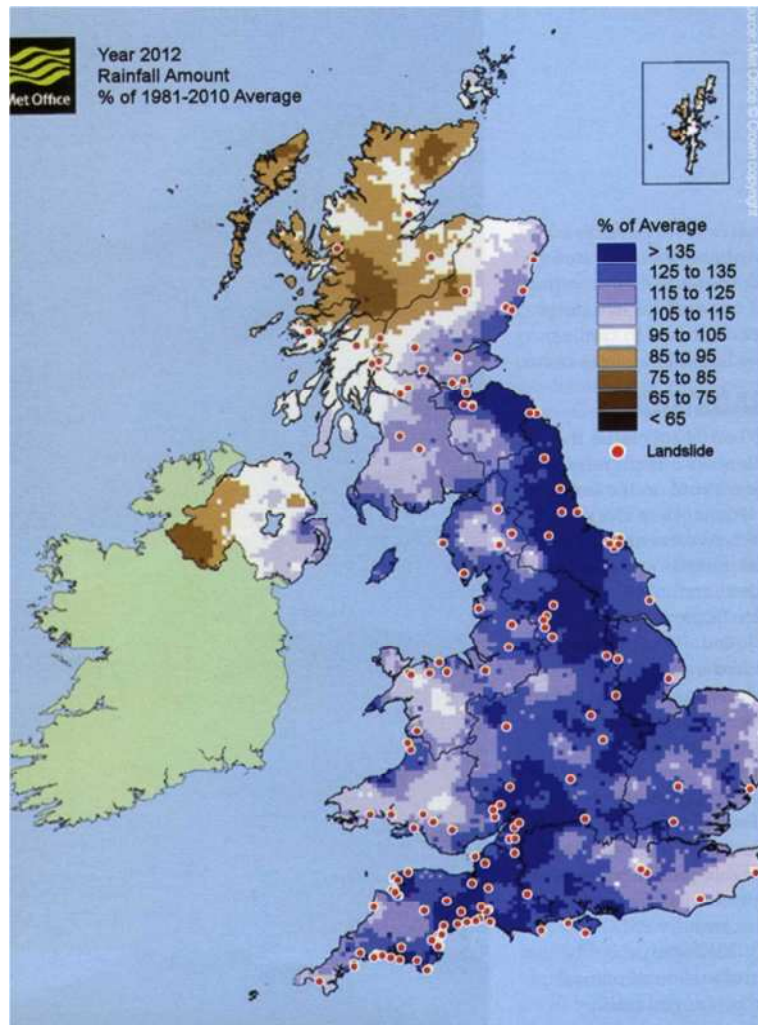
Figure 2-43: Map showing the location of landslides in the UK in 2012 and the total annual rainfall as a per cent of the1981 - 2010 long term average. After Pennington and Harrison (2013).

Figure 2-43 shows the location of reported landslides in the United Kingdom in 2012, compared to the total annual rainfall as a per cent of the 1981 – 2010 long term average (Pennington and Harrison, 2013). There is a clear correlation between the total annual rainfall and the frequency of reported landslides.

Pore water pressures are one of the major controlling factors of slope stability. These pressures, which vary spatially and temporally, are dependent upon the climate. Temporal distribution of evapotranspiration and precipitation are the two main influencers of pore water pressures (Collison et al., 2000; Dixon et al., 2006). Both of these are forecast to change, and therefore expected to impact upon pore water pressures and soil water balances. Indeed the changes are occurring at such a rate that the use of steady state information is thought to be no longer relevant for design (Dixon et al., 2006).

Numerous authors have suggested that climate change will result in more frequent landslides. Geertsema et al. (2007) analysed historic records of landslides and climate trends in northern British Columbia, Canada. They observed that landslides of the delayed type have been increasing in frequency and that these landslides occur in decades of above average precipitation, concluding that a warmer and wetter climate is likely to be accompanied by increased landslide activity. Chen (2007) studied the correlation between rainfall distribution and landslides in Taiwan, so as to investigate a possible relation between climate change and increased landslide activity. It was noted that there was an increased frequency of typhoons hitting Taiwan, with an associated increase in rainfall intensity and accumulated rainfall. During this time of changing climate there has also been an increase in the number of landslide events, mostly of the debris flow type, occurring. In the United Kingdom Mills et al. (2007) have investigated the influence of climate change on historical and projected frequency of landslides. Their findings suggested that there has been an increase in the frequency and extent of rapid response landslides in the last one hundred years.

Copyright not obtained

Figure 2-44: Total number of mass earth movement events reported since the beginning of the 20th Century; from The International Disaster Database (CRED, 2009).

Copyright not obtained

Figure 2-44 shows all the reported mass earth movements reported globally since the beginning of the 20th Century, collated by The Centre for Research on the Epidemiology of Disasters (CRED, 2009). There has been a clear increase in the number of reported landslides in the last 30 – 40 years. Petley (2012) has presented similar findings, albeit disagreeing with the total, demonstrating an increase in the number of reported landslides yearly between 2004 and 2010

Copyright not obtained

(

Figure 2-45). The method used by Petley (2012) to record landslides differs from that used by CRED (2009). Between 1 January 2004 and 31 December 2010 Petley (2012) records 2620 non-seismic, fatal landslides, causing a total of 32,322 deaths, whereas CRED (2009) records only 130 landslides and 7,431 deaths. The numbers vary so wildly because the International Disaster Database only includes events where a minimum of ten fatalities have been recorded.

Figure 2-45: Total number of landslides recorded between 2004 and 2010 and the associated number of fatalities, after Petley (2012).

It is suggested that increased landslide frequency is caused by climate change but there are likely other reasons. For example Mills et al. (2007) suggest that the increased frequency of landslides in Scotland is actually caused by other human activity, such as land management that is 'ripening' slopes so when combined with intense rainfall events failure occurs.

Serviceability problems affecting infrastructure slopes are expected to become more frequent. Larger shrink-swell cycles are a likely outcome of changing climate, caused by greater seasonal variation of the climate and increased rates of evaporation and transpiration by plants (Clarke and Smethurst, 2010). Clarke et al. (2006) suggest some of the monetary implications of ignoring climate change in future design could be:-

- Higher maintenance costs.
- Costs relating to contractual arrangement with infrastructure not meeting the design life.
- Indirect costs associated with reputation and public perception.

Ultimate failure is related to shrink-swell cycles, which could potentially be irreversible, leading to progressive failure (Take and Bolton, 2011). It is suggested that the possible greater magnitude of shrink-swell cycles, as a result of greater seasonal variation in climate, will lead to ULS failure in shorter times (Nyambayo et al., 2004; Rouainia et al., 2009). It is believed that desiccation cracking of soil may become more of a problem in the future if the longer, drier and warmer summers that are forecast for the United Kingdom occur (Dijkstra and Dixon, 2010). Networks of

113

desiccation cracks can directly control soil hydraulic properties, by allowing rapid infiltration of rainfall, giving elevated pore water pressures within the upper surface zone of the slope (Anderson et al., 1982; Clarke and Smethurst, 2010; Tang et al., 2011). The effects of soil cracking on hydraulic conductivity can in turn have a negative effect upon slope stability (Dijkstra and Dixon, 2010; Zhang et al., 2011).

2.11.3 Modelling the effects of climate change

Predicting the impact of climate change on one particular slope is difficult. Slopes of different material (and therefore permeability) and location (thus experiencing differing current climates and levels of climate change) will respond in different ways and at different time scales (Buma and Dehn, 1998; Collison et al., 2000). The study of UK climate change projections carried out in Section 2.11.1 showed different levels of climate change all over the country, highlighting the potential difficulty in including its effects. Models that consider the variability of and the changing climate along with well represented material properties are essential to develop a better understanding of the potential effects of climate change on the stability of infrastructure slopes. General circulation models (GCMs) linked to hydrology and stability models are one such method that is recognised as being a positive approach to this problem (Buma and Dehn, 1998).

Collison et al. (2000) have used such an approach to assess the likely impact of climate change on landslide activity in south east England. A combination of a GCM and a geographical information system (GIS) combined slope hydrology/stability model was used. The method was implemented to analyse the response of the water table in a section of the Lower Greensand escarpment which has a long history of frequent landslide activity. The GCM, an earlier version of the Hadley Centre model (HadCM2), showed an increase of yearly precipitation of 11 % from 2000 to 2080 and an increase in total evapotranspiration of 13 % for the site location. The coupled GCM and slope hydrology/stability model did not predict any negative consequences on

the frequency of large landslides. Climate scenarios were generated for each of the following periods; 1990-2019, 2020-2049 and 2050-2079. It was concluded that the effect of increased evapotranspiration would maintain a high soil moisture deficit and prevent the water table from rising above the shear surface of the landslide. However this method did not properly include the effects of desiccation cracking, which could play a major role in affecting the hydrology of infrastructure slopes in the United Kingdom. The top 30 centimetres of the soil profile was considered for 'bypass' flow, allowing a percentage of the rainfall to bypass this part of the soil directly to the layer below. Although considering the effects of cracking, it does not reflect the actual behaviour in the field where the occurrence of cracking is spatially and temporally variable and moisture does not actually bypass the cracked portion of the slope but passes through it at a greater rate than it would if cracks were not present.

Davies et al. (2008c) have investigated the effects of climate change on the hydrology and progressive failure of a typical railway embankment located in the United Kingdom. By using a previously developed numerical method (Davies et al., 2008a) in conjunction with the EARWIG weather generator (Kilsby et al., 2007) the mechanical response of a typical railway embankment to present and future climate scenarios was investigated. The EARWIG weather generator provides daily rainfall, temperature, humidity, wind and sunshine data for 5 km squares throughout the UK (see Section 2.11.4). This software was used to produce two climate scenarios:

1. Present day climate scenario.
2. High emissions 2080s scenario.

The hydrological response of the embankment to each climate scenario was modelled. The calculated temporal pore water pressures were then used to analyse the mechanical response. The results of the analyses showed the embankment with a present day weather scenario failing after just 5 years, whereas the embankment with the future, high emissions, weather scenario was stable for the entire 20 year cycle. It was found that periods of greatest movement coincided with periods of high pore water pressure and that the lower end of winter pore water pressures in the future slope resulted in increased stability.

In conclusion, Davies et al. (2008c) stated that climate change may not have devastating effects on stability of infrastructure embankments. The overall effect of climate change was a reduction in water infiltrating the embankment. Desiccation cracking was not taken into account in this modelling. It has been suggested that desiccation cracking may become more severe in the future with a changing climate (Section 2.10) with repercussive effects on the soil permeability and the amount of water able to infiltrate the slope.

Rouainia et al. (2009) have carried out similar work to O'Brien et al. (2008c). They have developed a numerical hydrological model to accurately predict seasonal changes of pore water pressures in an infrastructure slope due to a changing climate. The meteorological coupled hydraulic modelling was achieved using SHETRAN (Ewen et al., 2000). Surface pore water pressures, as a result of the local weather, could be transferred to FLAC TP-flow (Itasca, 2002) which then modelled subsurface flow and the resulting pore water pressures and suctions. The model was validated with data from the Newbury bypass cutting (Smethurst et al., 2006). The hydrological model was coupled with a Mohr-Coulomb strain softening model which allowed the mechanical response of the slope to pore water pressure variance to also be modelled.

Analyses were carried out to investigate how a future climate would affect progressive failure of an infrastructure embankment. The effects of two climate boundary conditions on the hydrological and mechanical response of a diagnostic railway embankment located in Newbury in southern England were compared. The boundary conditions, generated by the Earwig software (Kilsby et al., 2007) that generates meteorological weather variables for climate impact assessments, were:
1. Present day climate 2003 scenario.
2. Future climate scenario based on worst case emissions scenario for 2080.

Each boundary condition was applied to a diagnostic railway embankment that was 7 m high with a 1:2.5 slope and strain softening behaviour of the embankment material was simulated for 20 years.

Figure 2-46: a) Temporal pore water pressures at the slope toe, and b) mid-slope horizontal displacement for each boundary condition, after Rouainia et al. (2009, p.86-87).

Figure 2-46 a) and b) show calculated pore water pressures at the toe of the slope and mid-slope horizontal displacement respectively for each of the boundary

conditions.

Figure 2-46 a) shows that much higher summer suctions developed in the embankment when the future climate boundary condition was applied due to increased evapotranspiration and run-off. With the future climate applied suctions at the toe of the slope persisted throughout winter, whereas with the present climate applied, suctions were recovered every year. The size of pore water pressure cycles was much greater with the future climate applied, with a maximum cycle of 100 kPa. The cycles with the present climate applied were much less; 50 kPa being the maximum.

Figure 2-46 b) shows that horizontal mid-slope displacements progressively increase until failure occurs at the beginning of the fifth winter when the present climate is applied. After 20 years the future climate slope is still stable. Overall displacements are quite small, this is because the high summer suctions cause the slope to shrink back to near its original position.

Figure 2-46 a) does show that pore water pressure cycles are greater when the future climate is applied, but as pore water pressures are always negative, the stability of the embankment is actually better. This analysis has shown that climate change may not have a devastating effect on the progressive failure of infrastructure embankment. However there are two caveats to this conclusion that need to be considered; the effects of desiccation cracking were not fully implemented into this model and an increase in bulk permeability approach was taken, which would not account for the temporal variability of cracking.

Internationally, numerous researchers have used similar methods to investigate the effects of climate change on slope stability. There has been studies on landslides in Italy (Wasowski et al., 2007), Liechtenstein (Tacher and Bonnard, 2007), Sweden (Hulten et al., 2007) and France (Buma and Dehn, 1998; 1999; Malet et al., 2007). These studies have tended to focus on the effects of climate change on natural slopes but the findings provide an insight into the varied effects that different kinds of climate change will have throughout the world.

In Sweden, Hulten et al. (2007) used climate scenarios from the Sweden Meteorological and Hydrological Institute's (SMHI's) Rossby centre to investigate the possible impacts of changes in precipitation on landslide events. The scenarios showed that in Sweden climate change is likely to result in increased precipitation and heavy rainfall events increasing the probability of mud flows and landslides.

Buma and Dehn (1999) used GCM and limit equilibrium methods to analyse the effects of climate change on the stability of a small landslide in the south east of France. The GCM (ECHAM4/OPYC3) was used to create present climate data and then in conjunction with the IPCC emissions scenario IS92a future climate. Mean annual precipitation was projected to decrease from 721 mm observed 1928 – 1970 to 635 mm by 2069 – 2099. The Janbu limit equilibrium method was used to back calculate a threshold ground water level to trigger the landslide and combined with a hydrological model. Landslide recurrence was found to decrease drastically with the future climate scenarios applied (Table 2-15), suggesting that due to climate change this landslide will become more stable.

Precipitation input series	1928-1970 (observed)	1971-2000 (scenario)	2021-2050 (scenario)	2069-2099 (scenario)
Mean annual precipitation (mm)	721	712	648	635
Landslide recurrence (years)	12	60	1000	5000

Table 2-15: Recurrence intervals for landslide in south east France with climate change effects, after Buma and Dehn (1999).

Davies et al. (2008c) and Rouainia et al. (2009) have both made use of the EARWIG weather generator. Weather generators are used to create series of future climate variables. In Section 2.11.4 weather generators are discussed in more detail and it will be shown that the EARWIG weather generator is now considered to be obsolete.

2.11.4 Weather Generators

Weather generators were used in the works discussed in Section 2.11.3. A weather generator is a method for creating time series of weather variables for specific locations at a daily or higher resolution (Kilsby et al., 2007). The Environment Agency Rainfall Weather Impacts Generator (EARWIG) method is one such weather generator, used by Davies et al. (2008c) and Rouainia et al. (2009). EARWIG is a daily resolution weather generator that was initially developed for use in climate impact assessments on agricultural and water system management, but was also found to be beneficial in studying the impacts of climate on slope hydrology and stability. The weather generator can produce series of meteorological variables rainfall, temperature, humidity, wind and sunshine, as well as potential evaporation at a daily time resolution. Climate series can be produced for the entire United Kingdom at a 5 km grid resolution. The weather generator produces control (present day) series based on the 1961 – 1990 baseline and future series based on the now superseded UKCIP02 scenarios for 3 time slices, centred on the 2020s, 2050s and 2080s.

The EARWING weather generator was out-dated with the release of the UKCP09 Weather Generator version 2.0 in 2011 (UK Climate Projections, 2009; 2012). The Weather Generator 2.0 is based on the same well established methodology as EARWIG. The weather generator allows the user to generate statistically plausible daily time series for 5 km grid squares that are consistent with the UKCP09 baseline climate (1961 – 1990) and the UKCP09 probabilistic projections (Section 2.11.1).

There are a number of differences between the Weather Generator 2.0 and EARWIG:
- Based on the latest climate projections for the United Kingdom – UKCP09 rather than UKCP02.
- More time slices – 2020s, 2030s, 2040s, 2050s, 2060s, 2070s and 2080s.
- No wind projections - Considered to have too large an uncertainty range to be considered as part of the UKCP09 probabilistic climate projections.
- Fully explores the range of uncertainty in the climate – Each weather generator run must sample at least 100 model variants.

This introduction of at least 100 model runs is the major difference from the EARWIG method. This random element is contained in the methodology to deal with aspects of daily climate that are not explained by climate persistence. The random element allows different, but equally statistically plausible, future climate series to be generated, allowing different climate eventualities to be evaluated. The weather generator creates its 100 series by randomly selecting change factors from the probability distribution function (PDF). Figure 2-47 shows an example PDF where the red dots represent randomly selected change factors. By randomly sampling at least 100 change factors it enables the weather generator output to represent a wide spread of percentile values and represent the entire probability distribution.

The upshot of this methodology is that from each weather generator run there must be at least 100 baseline climate series and at least 100 future climate series. This has implications for any modelling work, as to correctly implement these series each one must be analysed separately. A simple overview of the Weather Generator 2.0 process is presented in Appendix A. For a detailed explanation of the methodology of the Weather Generator 2.0 see the UK climate projections Weather Generator report (Jones et al., 2010).

2.12 Numerical Methods and Software

The finite element method and finite difference method are numerical methods developed to find approximate solutions to partial differential equations. Therefore, if differential equations arise in a geotechnical problem, these numerical methods can be used to solve it. The Richards equation (Equation 2-32), which represents the flow of water in an unsaturated soil, is one such non-linear partial differential equation. This equation, due to its non-linearity, would be extremely difficult and time-consuming to solve by analytical means. Therefore the finite element method or finite difference method could be an ideal solution to solving problems implementing the Richards equation.

Equation 2-32

$$\frac{\delta}{\delta x}\left[K_{(\psi)}\frac{\delta h_\psi}{\delta x}\right] + \frac{\delta}{\delta y}\left[K_{(\psi)}\left(\frac{\delta h_\psi}{\delta y} + 1\right)\right] = \frac{\delta\theta}{\delta t}$$

A number of programmes with the ability to solve the Richards equation over many time steps have been identified. These programmes are listed in Table 2-16, including a summary of the essential features.

Programme	Features
Comsol Subsurface Flow Module	• Simulates fluid flow below ground or in other porous media. • 2D and 3D capabilities.

	• Flow in saturated and unsaturated material governed by Darcy and Richards equations. • SWCCs defined by van Genuchten or Brooks and Corey closed form equations. • Can be coupled with other physics interfaces such as the Geomechanics Module to model soil softening.
Flac two-phase flow	• 2D finite difference capable of modelling saturated and unsaturated subsurface flow. • Can be coupled with strain-softening soil material properties.
GeoStudio VADOSE/W	• Models fluid flow from the environment, across the ground surface, through the unsaturated vadose zone and into the local groundwater regime. • Uses Darcy and Richards equations for saturated and unsaturated flow. • Considers evaporation, root transpiration at depth, infiltration and runoff. • Total head, pressure head, flux or climate boundary conditions. • SWCCs defined by van Genuchten, Fredlund and Xing or user. • Can be coupled with a stress analysis but has no strain-softening material properties.
Plaxis 2D PlaxFlow	• Models groundwater flow with Darcy and Richards equations. • SWCCs defined by van Genuchten or user-defined. • Various boundary conditions for flow (seepage, head, prescribed boundary flux, infiltration/precipitation, drains and wells)

Table 2-16: Programmes capable of modelling unsaturated flow with the Richards equation.

All the programmes listed in Table 2-16 are capable of modelling saturated and unsaturated subsurface flow, possessing the ability to solve Darcy's and Richard's equations and also various methods of defining the soil water characteristic curve and hydraulic conductivity function. There is most evidence of successful employment of Geostudio VADOSE/W and FLAC two-phase flow when modelling similar problems as to that planned for this work (e.g. Ng and Shi, 1998; Davies et al., 2008a; 2008c; Rouainia et al., 2009; Briggs, 2010; Loveridge et al., 2010; Briggs, 2011; Kilsby et al.,2011) and therefore these two were considered further.

'Flac TP flow' is a finite difference method. The finite difference method, similarly to finite elements, is a numerical method which can be used to solve partial differential equations. Flac TP flow does not have an inbuilt model for capturing meteorological and vegetation dependent surface boundary fluxes. It is possible to modify the programme with the programming language FISH to allow this capability; a very time consuming process. It is therefore preferential to couple with a hydrological model, such as SHETRAN, that has this capability. In this method (as used by Davies et al., 2008a; 2008c; Rouainia et al., 2009; Kilsby et al., 2011), SHETRAN, using climate data together with soil and vegetation data predicts interception, evapotranspiration, run-off and subsurface flow. Pore pressures (below the root zone) can then be transferred to Flac-TP flow which then models flow in the unsaturated and saturated zones.

GeoStudio is an implicit, finite element, software package that consists of numerous modules for solving different types of geotechnical problem. VADOSE/W is one these modules and is specifically designed for solving unsaturated flow problems. Climate boundary conditions can be applied directly to the model, as well as vegetation properties and soil properties. There is also the option to link VADOSE/W with one of the other modules, such as SLOPE/W which analyses slope stability as a function of the pore water pressures calculate by VADOSE/W and the soil strength properties. This programme has been successfully employed by previous authors (Briggs, 2010; Loveridge et al., 2010; Briggs, 2010). Geostudio VADOSE/W possesses the following features that are desirable for this work:-

- Models saturated and unsaturated flow utilising the Darcy and Richards equations.

- Numerous methods to define the soil water characteristic curve and hydraulic conductivity function to suit the user's needs.

- Most importantly it has a fully implemented, coupled climate boundary condition that uses precipitation, evapotranspiration, wind, temperature in conjunction with material properties to calculate the soil water balance and thus pore water pressures.

- By modelling the removal of moisture by roots with depth rather than just at the surface the effects of vegetation are realised more realistically.

Therefore, due to these points and the availability of software Geostudio VADOSE/W was chosen for this work.

2.13 Literature Review Summary

The literature review has provided an in depth study of the current understanding of the subjects of climate change, slope stability and how they are linked. Within this section, a summary of what has been learnt is provided, culminating in the identification of a gap in the knowledge.

The literature review began by considering the existing infrastructure earthworks in the United Kingdom and the problems that they currently encounter, finding that:

- There are extensive infrastructure earthworks in the United Kingdom, some of which are over 150 years old, constructed before the advent of modern soil mechanics. These slopes are susceptible to SLS failure and ULS failure.

- The high plasticity clays prevalent in the south of England are problematic due to their high shrink/swell potential, creating serviceability problems due to volume change and also being influenced by progressive/delayed failure.

- Some of the more recently constructed infrastructure slopes, particularly those on the motorway network, are now approaching an age where they could possibly be affected by delayed failure. However, with the advent of modern construction methods this may not be the same problem that it was for the railway slopes constructed in the early 19th century.

- Slope failures are often observed after extreme rainfall events; the timing being dependent upon the antecedent pore water pressures in the slope.

The link between the atmosphere, slope interactions and slope hydrology processes was investigated in detail. It was found that:

- The interactions between slopes and the atmosphere are complex and simply considering the effects of precipitation is insufficient. The processes of evaporation, transpiration from vegetation and runoff must all be considered.

- The water balance method on its own is a useful tool but should be linked to a hydrogeological system with fully defined vegetation and soil properties to be able to calculate temporal changes in pore water pressures due to the effects that the atmosphere has on slope hydrology.

- Physically-based models (PBMs) were identified as a method of achieving this. PBMs, by implementing a climate process system, land use vegetation system hydrogeological system and a multi layered soil system, are powerful tools to model the effects of a dynamic climate on the hydrology and stability of slopes.

Climate change was considered, globally, nationally and regionally.

- Worldwide, climate change is expected to alter temperatures and rainfall patterns.

- In the United Kingdom projections suggest that the country will experience drier, warmer summers and wetter winters.

- The total annual precipitation is not forecast to change significantly; it is the temporal distribution of precipitation that shall be affected. There could be less precipitation in the summer and more high intensity rainfall events in the winter.

- The south of England will be one of the most severely affected regions of the UK. By the 2050s there could be an increase in mean summer temperature of between 5 and 6 ^{0}C, between 50 % and 60 % less precipitation falling in the summer and the wettest day of winter may experience 50 % more precipitation.

Climate change is expected to affect slope hydrology with subsequent effects on slope stability. The major findings that lead to this conclusion are:

- Pore water pressures, which vary spatially and temporally, are a major contributing factor to the stability of slopes.

- With a changing climate the temporal distribution of evapotranspiration and precipitation is forecast to change. These are the main influencers on pore water pressures and therefore there are expected to be impacts upon the spatial and temporal distribution of pore water pressures with concurrent effects on the slope stability.

- It is thought that a changing climate will lead to a greater frequency of landslides, and in some places on the planet an increased frequency is being observed.

- In the United Kingdom serviceability and ultimate limit state failures are expected to become more frequent. The increased seasonality of climate from summer to winter will lead to greater shrink/swell cycles with associated volume change problems.

- Climate change could also have detrimental effects on soil properties; in particularly through the process of desiccation cracking, which influences soil permeability. The warmer drier summers forecast in the future will lead to more extensive desiccation cracking. Increased desiccation cracking increases the permeability of the soil meaning that moisture can infiltrate the soil with greater ease, possibly increasing pore water pressures and leading to slope instability.

- Climate change will have different effects in different regions of the world, and therefore different effects on slope stability. Some countries in Europe could see much less precipitation totals which is predicted to result in more stable slopes.

As mentioned above, physically-based models have been identified as an effective method of studying the effects of climate change on slope hydrology and stability. Past uses of this type of methodology have been investigated; looking at models used to investigate the effects of climate change and also modelling of slopes in the present day.

- Numerical methods have been identified as the best technique for solving the highly non-linear Richards equation that describes fluid flow in an unsaturated soil. The finite element method is one such technique.

- The Newbury bypass cutting has been modelled by various researchers. Temporal pore water pressures were calculated and compared to the observed values. It was found that the model performed well when calculating the maximum suctions developing at the end of summer but poorly when replicating the dissipation of suctions that occurs throughout winter.

- Numerical modelling works focussing on the effects of climate change have found that slopes in the future may actually become more stable, contrary to popular opinion. Utilising weather generators, present day and future climate scenarios have been applied to infrastructure slopes.

- The effect of the future scenarios was a decrease in the total water infiltrating the slope, resulting in lower pore water pressures and more stable slopes.

- Desiccation cracking and its effects on soil properties have not been included in any of the works. It is believed that the inclusion of desiccation cracking is critical to a proper understanding of the effects of climate change on slope hydrology and stability.

- The effects of these cracks on the hydraulic properties of soil could be included by using bimodal SWCCs and HCFs. Some authors have already developed these equations and implemented them with some success. However, validation of the modelling results has so far not been carried out.

3 Methodology Overview

The aim and objectives of this thesis were presented in the introduction (Section 1.1). These were developed from the findings of the literature review (Section 2.13). By looking at the objectives and the literature review, the methodology has been developed. In this section the general approach to the methodology is presented and then some specificity is introduced.

3.1.1 General approach

The general approach is to use the finite element software package VADOSE/W to create a numerical model of the Newbury bypass cutting that can be used for creation and validation of a method for including the effects of desiccation cracking on the hydrology of infrastructure slopes. The numerical model, with the effects of desiccation included, will then be used to analyse the effects of climate change on the slope hydrology and stability.

3.1.2 Specific approach – Chapter 4

In chapter 4 the initial numerical model was developed in the finite element software package VADOSE/W. This program was identified as appropriate for this work (Section 3.1.5). This involved creating a Physically-Based Model, with the appropriate systems identified in the literature review (Section 2.8.5), including:

- Climate process system that can evaluate the water balance from climate data inputs. This system is already built into the software package. Climate data for

the site in question had to be obtained, including precipitation, temperature, wind and humidity.

- A vegetation system to quantify the removal of water from the system at the near-surface by root action. This required the identification of a root depth function, plant moisture limiting function, growing season and leaf area index function (Section 2.8.4.2).

- Regional hydrogeological and soil system that can refine the water balance at any location and cope with variations in soil and soil water that affect the soil hydraulic properties. This was achieved by defining the soil water characteristic curve and hydraulic conductivity function (Section 2.9.3) with the closed form predictive models of van Genuchten (Section 2.9.3.1 and 2.9.3.2).

Once the PBM was developed it could be run for 1 year of climate data, and the results compared against the observed values (Section 2.6.1) and those calculated by other authors (Section 2.6.1.1) to validate the model.

3.1.3 Specific approach – Chapter 5

In this chapter further development of the Newbury cutting model is made, introducing the effects of desiccation cracks on soil's hydraulic properties. Bimodal equations had been identified in the literature review as a possible method of achieving this (Section 2.10.2.3). Bimodal equations were developed for the soil water characteristic curve and the hydraulic conductivity function. Parameters to fit the curves were required, including the crack porosity (Section 2.10.1) and the van Genuchten parameters (Section 2.10.2.5).

The bimodal soil properties were implemented into the Newbury cutting numerical model and run with 1 year of climate data. To validate the model and see if the inclusion of bimodal properties improved the model results could be compared with those from Chapter 4 and the observed values.

Once the initial results from the bimodal model are obtained further improvements to the model can be made. This is done by carrying out sensitivity analyses on:

- Van Genuchten parameters
- Crack porosity
- Crack depth

3.1.4 Specific approach – Chapter 6

The objective of Chapter 6 is to analyse the effects of climate change on the slope hydrology of the Newbury bypass cutting, implementing the bimodal soil properties developed in Chapter 5 and the UKCP09 weather generator. The following steps are taken to achieve this:

- So as to account for varying crack depths, due to differing climate scenarios from the weather generator, test and validate the crack depth estimating equation identified in the literature (Section 2.10.2.6).
- Run the UKCP09 weather generator to create 100 series of present day and future climate scenarios (Section 2.11.4). From each series extract 1 year of climate data and implement as a VADOSE/W climate boundary condition.
- Results are obtained from each model and compared to their future or present day counterpart. Pore water pressures, crack depth estimation and pore water pressure cycle magnitude are considered.
- From these results conclusions about the effects of climate change on infrastructure slopes will be made.

3.1.5 VADOSE/W

The finite element software package GeoStudio has been chosen to carry out the intended work within this thesis. The package contains all the essential features that have been identified in the literature review to model the effects of climate change on the hydrology of infrastructure slopes. VADOSE/W is currently the only numerical 2D model capable of calculating actual evaporation based on first principle physical relationships not empirical AE formulations that are developed for unique soil types, soil moisture conditions, or climate parameters.

Within the GeoStudio suite are eight products, including VADOSE/W which is described as "finite element CAD software product for analysing flow from the environment, across the ground surface, through the unsaturated vadose zone and into the local groundwater regime". VADOSE/W is the most suitable of the eight packages to carry out the work as it possesses the following features:

- Climate boundary condition creation.
- Vegetation boundary condition creation.
- Hydraulic material properties.
- Easily definable initial conditions.

The one identified weakness of VADOSE/W is that it cannot be coupled with a strain-softening model to capture the effects of progressive failure. However, as this would be out of the scope of this work it is deemed that VADOSE/W is suitable to meet the aim and objectives of the work. In Appendix A a more in-depth description of the method by which VADOSE/W solves groundwater flow equations is given, including presentation of the finite element water flow equations.

3.1.5.1 Climate boundary conditions

The ability to define and apply comprehensive climate data was identified as being of extreme importance to model effects of climate change on slope hydrology. VADOSE/W allows the user to create a climate boundary condition based upon their measured or generated daily climate data of any length of time. This climate boundary condition includes all the variables that were identified as influencing the hydrology of a slope:

- Minimum and maximum daily temperatures.
- Minimum and maximum daily relative humidity.
- Average wind speed.
- Daily precipitation.

3.1.5.2 Vegetation boundary conditions

Vegetation is believed to be particularly effective in influencing slope hydrology and accurate representation of its behaviour is necessary to model accurately. VADOSE/W includes all the functions that are required to achieve this:

1. Leaf Area Index function (Section 2.8.4.2).
2. Plant Moisture Limiting function (Section 2.8.4.2.1).
3. Root depth function (Section 2.8.4.2.2).

The ability of the vegetation model to remove water at depth was identified as a very important factor; evaporated water should be removed from the slope surface and transpired water removed from within the slope depending on the rooting depth. The model of Tratch et al. (1995) is used in VADOSE/W. This root extraction model allows the user to define root depth distribution relative to the rooting depth.

3.1.5.3 Hydraulic material properties

Hydraulic material properties in the form of the soil water characteristic curve and hydraulic conductivity function are essential. VADOSE/W possesses a number of methods to estimate a SWCC:

1. Grain size.
2. Sample functions.
3. Closed form equations.

The grain size method and sample function method are not recommended for use in final design (Geo-Slope, 2007) but rather in initial tests of sensitivity to material properties. There are two closed form equations based on actual measured material properties available in VADOSE/W; the van Genuchten (1980) equation and the Fredlund and Xing (1994) equation.

The van Genuchten (1980) equation included in VADOSE/W is of a slightly different form to that referenced in Section 2.9.3.1 (Equation 2-17) and uses different units for some of the parameters. The governing equation used in VADOSE/W is:

Equation 3-1

$$\theta_w = \theta_r + \frac{\theta_s - \theta_r}{\left[1 + \left(\frac{\Psi}{a}\right)^n\right]^m}$$

In this form of the equation pressure is used rather than head; Ψ = suction in kPa (positive values must be used). The parameter a has units of kPa. It is very important to ensure that the units of a are consistent between the data source and what should be used in VADOSE/W. It was observed that in the literature the parameter a generally has units of cm^{-1} and therefore must be converted into kPa by:

Equation 3-2

$$a\,(kPa) = \frac{1}{a\,(cm^{-1})} * 0.09807$$

VADOSE/W has three methods for estimating the hydraulic conductivity function, two of these methods are:

Fredlund and Xing (1994) – integrates along the curve of the soil water characteristic curve to give a hydraulic conductivity function as described in Section 2.9.3.1.

van Genuchten (1980) – the closed form equation described in Section 2.9.3.1 using the same parameters defined for the SWCC.

3.1.5.4 Infiltration and runoff

If precipitation over a time step is less than the anticipated actual evaporation over the time step, then the applied surface flux boundary condition will be equal to the precipitation value minus the actual evaporation and a negative flux will be applied to the node. If the precipitation minus any actual evaporation is a positive value, then a positive (infiltrative) surface flux will be applied as a boundary condition.

If the positive flux boundary condition is such that the solved pressures at the surface become positive, then the solution is allowed to converge to this positive pressure condition and subsequently the surface node is changed to a head boundary condition

and the time step is REPEATED. After it has converged with its new head boundary condition, the solver checks to see if the computed flux is more or less than that which was applied when the original flux boundary was used (GeoStudio, 2007). If the nodal flux is less than the original amount, then runoff is calculated as:

Runoff = Precipitation - AE - Infiltration.

There are two possible ways in which VADOSE/W can deal with runoff. Either of these is selectable by the user. Re-infiltration on the slope surface will not occur in either of these options.

1) Ignore the volume of water that is calculated as runoff. In this case, the water leaving the system as runoff is not available for reapplication at any point in the model and is removed completely from the system.

2) The calculated runoff can be stored downslope in any troughs or depressions, where it can be reapplied as infiltration in subsequent time-steps. At the extents of a model ponding can only occur if the mesh is horizontal or slope upwards. In this method the duration of overland flow and the depth of the flow are ignored meaning that runoff is immediately ponded at the nearest location and can be reapplied at the next time-step.
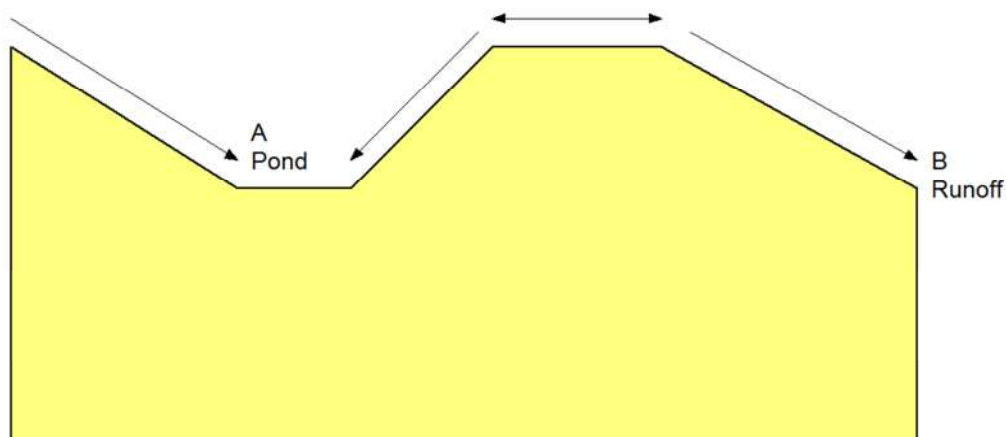
Figure 3-1: Ponding possible at A, but not at B.

In Figure 3-1, assuming that option 2 is chosen, ponding will occur at point A because it is a trough within the model geometry. Reapplication of the calculated runoff to the system will occur at this location. At point B there will be no reapplication because at the extents of the model it is sloped.
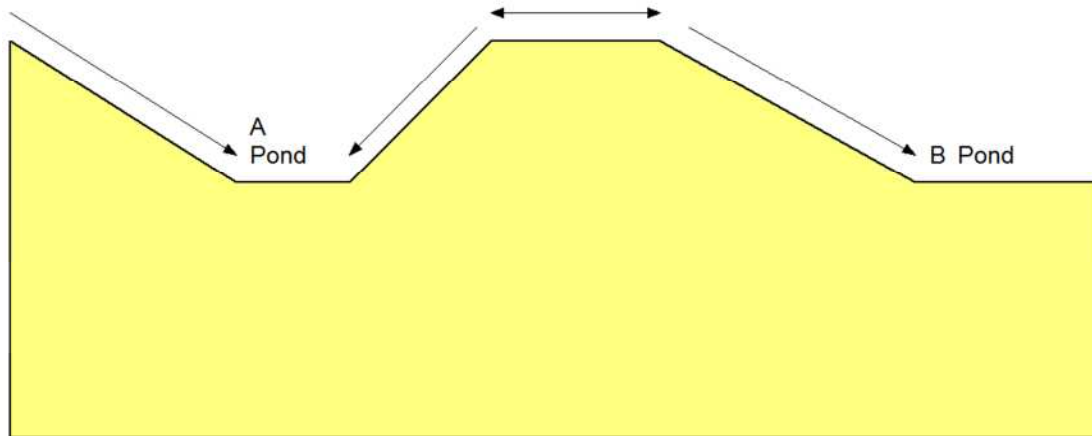
Figure 3-2: Ponding possible at A and B.

In Figure 3-2, if option 2 is chosen, ponding and reapplication of runoff will occur at A and B. At B this happens because the mesh extents are now horizontal. If option 1 is chosen in the model setup then ponding or reapplication of runoff does not occur anywhere, regardless of model geometry.

3.1.6 Computer and processor

The computer used to carry out all the analyses described in the following chapters had the following specification:

- Intel Core i7-3770K CPU @ 3.5 GHz
- RAM – 16.0 GB

4 Development and Validation of the Newbury Cutting Hydrological Model

4.1 Chapter outline

To validate the finite element software VADOSE/W a model of the Newbury Cutting has been developed. The purpose of this model was to validate a slope hydrological approach used in VADOSE/W. The model needs to be capable of replicating the hydraulic behaviour of the slope, particularly the temporal variability of pore water pressures, positive and negative, throughout the year. The Newbury cutting is located on the A34 Newbury by-pass in the south of England (OS grid reference SU 4435 6403). This cutting has been well instrumented and monitored since October 2002 by researchers at the University of Southampton (Smethurst et al., 2006; 2012) and has been modelled in previous works with some success (Davies et al., 2008b; Rouainia et al., 2009). These factors make the slope ideal for a validation model.

This chapter is structured as follows:-
- The Newbury cutting slope is described – Section 4.2,
- The numerical model is developed in Section 4.3, split into the following sections:
  - Initial model geometry – Section 4.3.1
  - Initial finite element mesh – Section 4.3.2
  - Material properties – Section 4.3.3
  - Surface boundary conditions – Section 4.3.4
  - Initial hydraulic conditions – Section 4.3.5
  - Side boundary conditions – Section 4.3.6

137

      ○   Development of the finite element mesh – Section 4.3.7

- The model is run and the results are presented – Section 4.4

- The results are discussed in detail – Section 4.5

4.2 Slope Description

The slope is 8 metres high, has a slope length of 28 metres and a slope angle of 16º (Figure 4-1). The cutting was constructed in 1997, excavated entirely within London Clay which is 20 m thick, the top 2.5 m of which is highly weathered. The weathered clay is spatially variable, changing from stiff orange brown clay to clayey silt over small distances and depths. The London Clay contains several bands of silty clay up to 50 mm thick and bands of large flints. The London Clay overlies the Reading formation of the Lambeth Group deposits. These deposits are a stiff or very stiff fissured clay, compact silt, and dense or very dense sand deposited in overbank (fine-grained) or channel (sand) settings (British Geological Survey, 2013). The cutting was chosen by Smethurst et al. (2006) for monitoring due to its "relatively uniform soil conditions and vegetation characteristics". Vegetation, covering the whole slope, is primarily grass, with some small shrubs with a maximum rooting depth of 1.0 m. When monitoring of the slope began vegetation was generally less than 0.5 metres high, but by the beginning of 2009 some shrubs were approaching 1.5 – 2.0 metres in height (Smethurst et al., 2012). Fringing the crest of the slope is mature Beech, oak and silver birch trees.
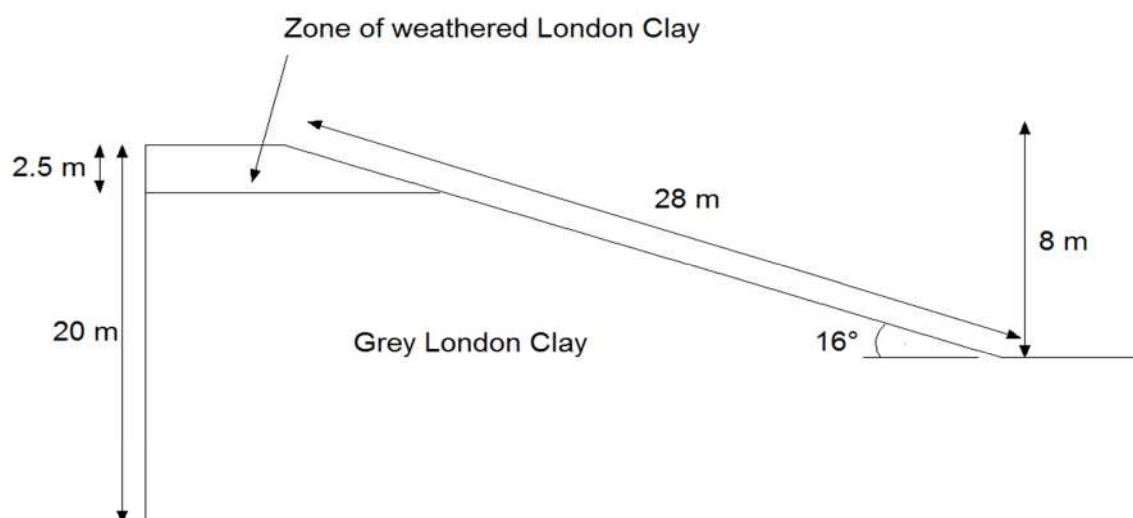
Figure 4-1: Slope cross section, after Smethurst et al. (2006).

Details of material characterisation (Section 2.4.1) and instrumentation for monitoring of climate and temporal pore water pressure distributions (Section 2.6.1) have been provided in the literature review. The results obtained by a previous author (Davies et al., 2008a), who created a numerical model of the Newbury bypass cutting can also be found (Section 2.6.1.1).

4.3 Numerical Model

Using the slope geometry, hydrological material characteristics such as permeability and soil water retention behaviour and climate data and vegetation properties such as the root depth distribution and growing season, a numerical hydrological model of the Newbury cutting can be developed in VADOSE/W. In summary the data used and where it has been sourced from is:-

- Slope geometry (Smethurst et al., 2006).
- Material characteristics (Croney, 1977; Smethurst et al., 2006; Davies et al., 2008b; Rouainia et al., 2009).
- Climate data (Smethurst et al., 2006; Rouainia, pers. comm. 2012).
- Vegetation data (Briggs and Courtney, 1985; Glendinning et al., 2006; Smethurst et al., 2006; Davies et al., 2008b).

4.3.1 Initial Geometry and boundaries

The initial model geometry is shown in Figure 4-2. The bottom boundary is located 20 m below the crest of the slope, representing the boundary between the London Clay and the underlying Lambeth Group deposits. Side boundaries are initially placed approximately 10 metres from the crest and toe of the slope so as to reduce the mesh size required in the first runs; a sensitivity analysis was carried out on the location of the boundary conditions so as to establish the optimum location for modelling efficiency.

The boundary conditions to the side of the main point of interest, i.e. the slope, are undefined, due to the there being no existing data regarding the hydraulic conditions at the side boundaries. In this case it is recommended by Geo-Slope (2007) to define

these 'far field' boundary conditions by extending the problem boundaries away from the point of interest, increasing the size of the mesh to a point where they no longer influence computed results.

The bottom boundary condition will also be defined as a no-flow condition. If adequate field data does not exist to prescribe a flow across this boundary it is common practice to assume that the lower boundary of a modelled hill slope is impermeable rock (Cloke et al., 2007). This was the approach taken by Rouainia et al. (2009) in their modelling of the Newbury cutting (Rouainia, pers. comm, 2012). By taking this approach it assumes that relative saturated hydraulic conductivities of the London Clay and the underlying Lambeth groups are different enough to provide a no flux condition.
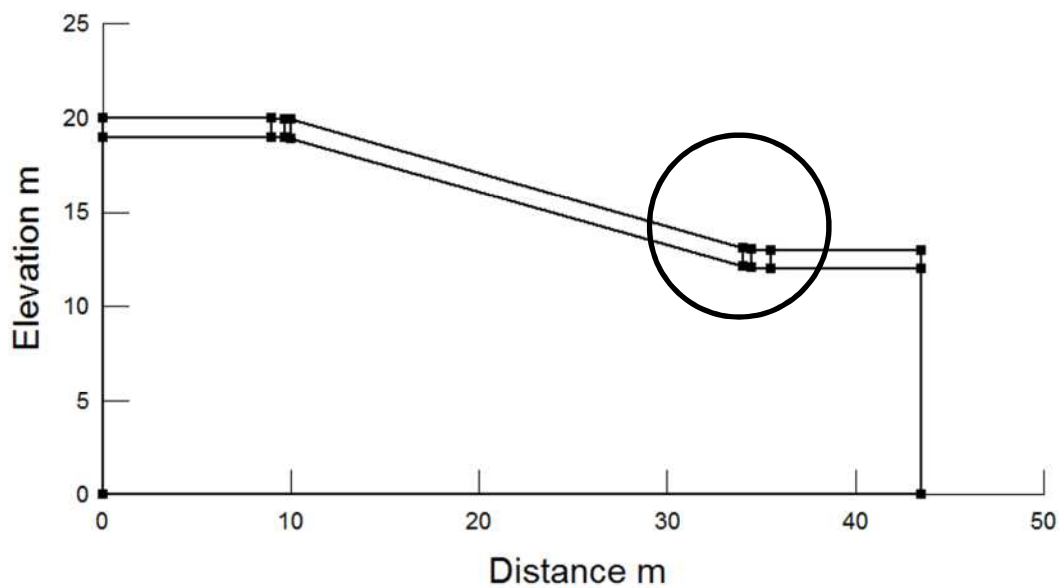
Figure 4-2: Initial model geometry.

The region shown in Figure 4-2 at the surface of the slope, part of which has been circled, is the 'surface layer'. When the surface of a slope is subject to a variable climate soil conditions can change dramatically over a short period of time; for example, during a summer storm event the ground surface can rapidly change from an extremely dry state to a saturated state. To numerically deal with these rapid and dramatic boundary changes it is necessary to have fine discretisation near the ground surface, as well as appropriate time steps. VADOSE/W has a procedure to produce the mesh in this layer that does not detriment the efficiency of the rest of the mesh by

creating areas of unnecessarily fine discretisation. The surface layer deals with the effects of precipitation, evaporation and moisture extraction by root action and therefore needs to be the same thickness as the maximum rooting depth of the vegetation.

In the case of this problem, the roots of the vegetation on the slope reach a maximum depth of 1.0 m and the surface layer is defined as this thickness (Smethurst et al., 2006). It is noted that in this model the effects of desiccation cracking are not taken into account and therefore the thickness of the surface layer is not affected by this consideration. Sensitivity analyses were carried out on number of elements required in the surface layer and the rest of the model. These analyses are described in detail in Section 4.3.7.

4.3.2 Initial finite element mesh

The initial mesh was automatically generated by VADOSE/W. The mesh is presented in Figure 4-3. This is a mesh of quadrilateral and triangular elements, with an average size of 2.0 metres. Not shown are the elements that make up the surface layer, which are very thin and would therefore not be visible at this scale. In this region fine discretisation is required to account for the rapid and dramatic boundary changes that can occur at the surface due to the climate boundary condition. Geo-Slope (2007) recommends using quadrilateral elements in the surface layer for two reasons; 1) the primary unknown (total hydraulic head in this case) gradients are usually steeper in a direction perpendicular to the surface and 2) dealing with plant root zones in the model necessitates that element nodes in the surface layer all fall on vertical lines.

Therefore in the whole model the elements used are first order quadrilateral elements in the surface layer and first order quadrilateral and triangular elements in the rest of the model. Geo-Slope (2007) advises that first order elements are suitable for problems where the primary unknown is a scalar value. In the case of this analysis the unknown variable that VADOSE/W solves is the total hydraulic head, a scalar variable; therefore first order elements, with a linear distribution of the primary unknown are implemented in this model. Figure 4-3 also highlights regions of the

mesh where quadrilateral and triangular elements are used, and shows how the primary unknown variable is distributed linearly within the elements.
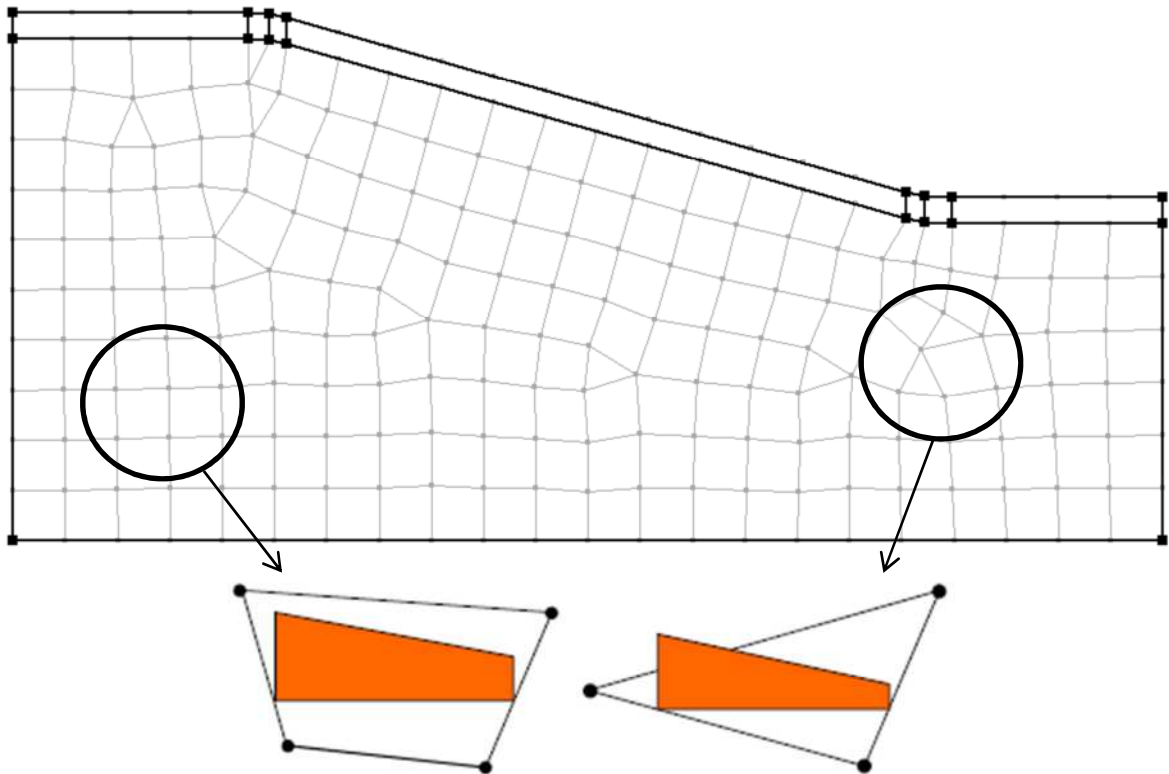
Figure 4-3: Initial finite element mesh - 421 elements, 458 nodes. Field variable distribution of the primary unknown in first order quadrilateral and triangular elements, after Geo-Slope (2007).

4.3.3 Material Properties

Material properties required for a hydrological model were discussed in Section 2.9.3 of the literature review. The material properties that are required for a VADOSE/W hydrological model are the soil water characteristic curve (SWCC) and hydraulic conductivity function (HCF). The SWCC defines the relationship between soil water content and the suction, and the HCF the relationship between the hydraulic conductivity and the suction. Smethurst et al. (2006) initially suggested the use of soil water characteristic curves from undisturbed London Clay samples published by Croney (1977).

VADOSE/W possesses two methods to define an SWCC with closed-form equations (Section 3.1.5); the van Genuchten (1980) closed-form equation and the Fredlund and

Xing (1994) closed form equation. The van Genuchten (1980) closed form equations are perhaps more commonly used to define these functions, having been used in previous modelling attempts of the Newbury cutting (Davies et al., 2008b; Rouainia et al., 2009) and by other authors (Briggs, 2011). Davies et al. (2008b), Rouainia et al. (2009) and Briggs (2011) all used the van Genuchten parameters equivalent to the Croney (1977) data to form suitable SWCCs for London Clay (Table 4-1).

Parameter	Value
Residual water content, θ_r	0.28
Saturated water content, θ_s	0.45
a	22.41 kPa
n	1.443
m	0.307

Table 4-1: van Genuchten parameters for London Clay.

In the literature review it was discovered that reviews of possible methods to define the SWCC invariably recommend the van Genuchten (1980) closed-form equation (Section 2.9.3.1.). As data is also readily available to define the SWCC of the London Clay forming the Newbury cutting it was decided to use the van Genuchten equations to develop the SWCC and HCF. The form of the van Genuchten equation used in VADOSE/W to define the SWCC is:

Equation 4-1

$$\theta_w = \theta_r + \frac{\theta_s - \theta_r}{\left[1 + \left(\frac{\psi}{a}\right)^n\right]^m}$$

Once the parameters (Table 4-1) are input into Equation 4-1 the SWCC can be generated between any required suction (Figure 4-4).
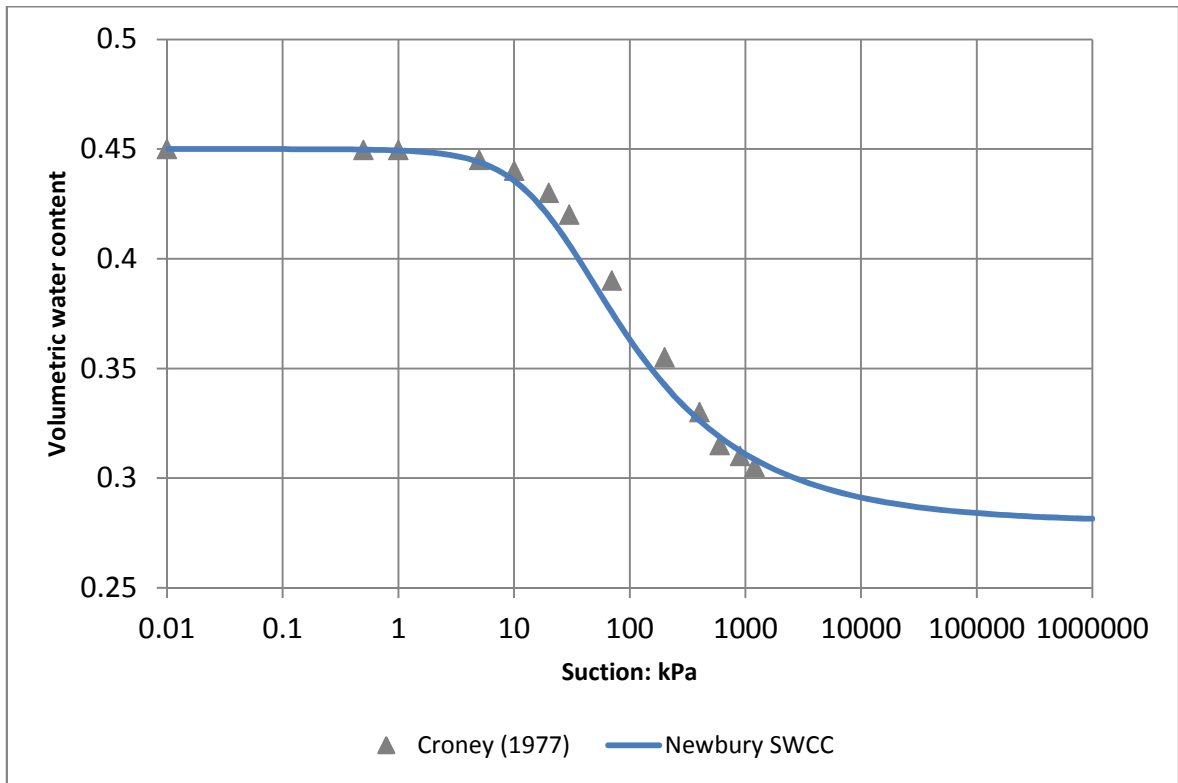
Figure 4-4: Soil water characteristic curve for the Newbury cutting London Clay generated by VADOSE/W using the parameter values given in Table 4-1 and Equation 4-1. Comparison is made to the measured data from Croney (1977) from which the parameter values are derived.

The van Genuchten equations are also used to form the hydraulic conductivity function. Equation 4-2 uses the same parameters as the SWCC (Table 4-1) with the addition of the saturated hydraulic conductivity parameter K_s:

Equation 4-2

$$K_w = K_s \frac{\left[1 - \left(a\Psi^{(n-1)}\right)\left(1 + (a\Psi^n)^{-m}\right)\right]^2}{\left(\left((1 + a\Psi)^n\right)^{\frac{m}{2}}\right)}$$

On site bail out tests showed an average saturated hydraulic conductivity in the London Clay of the order 10^{-9} m/s. This was the value initially used by Davies et al. (2008a) and Rouainia et al. (2009) in their attempts at modelling the Newbury cutting; however they both found that this value did not reproduce the suctions that were observed within the cutting by Smethurst et al. (2006). It was found that by increasing the saturated hydraulic conductivity by orders of magnitude; initially to

144

10^{-8} m/s and then finally 10^{-7} m/s the suction profiles during the summer were better modelled. This approach is justified by Rouainia et al. (2009) as it allows for the macroscopic effects of fissures, sand lenses and other heterogeneous features that were not detected by the laboratory and in situ methods used to measure the soil's permeability.

In this work a saturated hydraulic conductivity of 1 x 10^{-7} m/s was used throughout the whole soil domain. This value results in the hydraulic conductivity function shown in Figure 4-5.
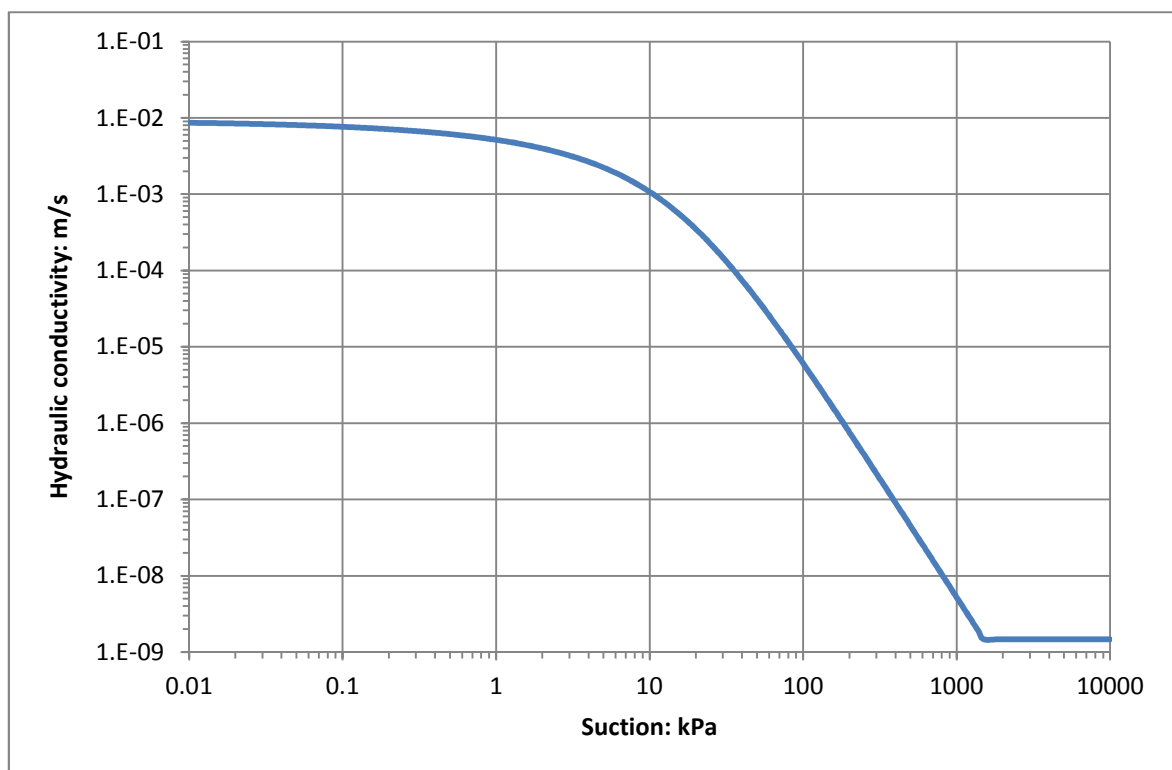
Figure 4-5: Hydraulic Conductivity Function for London Clay using the parameter values from Table 4-1 and Equation 4-2, where K_s = 1e-7 m/s.

These material properties are applied to the whole soil domain. Once this application of soil properties has been completed, the model mesh can be generated and the surface vegetation and climate boundary conditions applied.

4.3.4 Surface Boundary Condition

A boundary condition, including infiltration, evaporation, transpiration and runoff is applied across the whole surface. In this VADOSE/W analysis the surface boundary condition consists of transient weather and vegetation data and vegetation properties.

4.3.4.1 Climate Data

The requirements for a VADOSE/W climate boundary condition were discussed in Section 3.1.5. In VADOSE/W a climate boundary condition consists of the following daily weather variables:

- Maximum and minimum temperature.
- Maximum and minimum relative humidity.
- Total precipitation.
- Start and end of precipitation period.
- Energy data source.

Hourly weather data was obtained (Rouainia, pers. comm. 2012) for the years 2003 – 2006. Due to being unable to obtain the daily weather data measured on site by Smethurst et al. (2006), data from the nearest Met Office weather station had to be used. This weather data is from the Larkhill Met Office weather station, which is approximately 20 miles from the Newbury cutting site, and is the same data used by Davies et al. (2008a). The hourly weather variables available for the site are:

- Precipitation
- Temperature
- Wind speed
- Relative humidity
- Potential evapotranspiration (PET)

All of which are required to create a climate boundary condition in VADOSE/W. Potential evapotranspiration is used by VADOSE/W as the energy data source. Rather than using a net radiation value, that is not available for this site, VADOSE/W can convert the PET value to an equivalent energy value that is used to calculate the actual evaporation (AE). This is achieved using Equation 4-3.

Equation 4-3

$$AE = PET \left(\frac{h_r - \frac{u_v^{air}}{u_v^{soil}} h_A}{1 - \frac{u_v^{air}}{u_v^{soil}} h_A} \right)$$

Where h_r is the relative humidity at the solid surface and h_A is the relative humidity of the air.

There are potential problems with using this data, as it may not be representative of the Newbury cutting site. Figure 4-6 shows the monthly precipitation totals for the Newbury cutting site, measured by Smethurst et al. (2006; 2012) and the Larkhil Met Office weather station. As the graph shows, the totals are similar but with small differences throughout the year. Newbury is generally wetter, with only August having marginally more precipitation for Larkhill. This could have repercussions for the modelling results, as pore water pressures are influenced directly by precipitation.
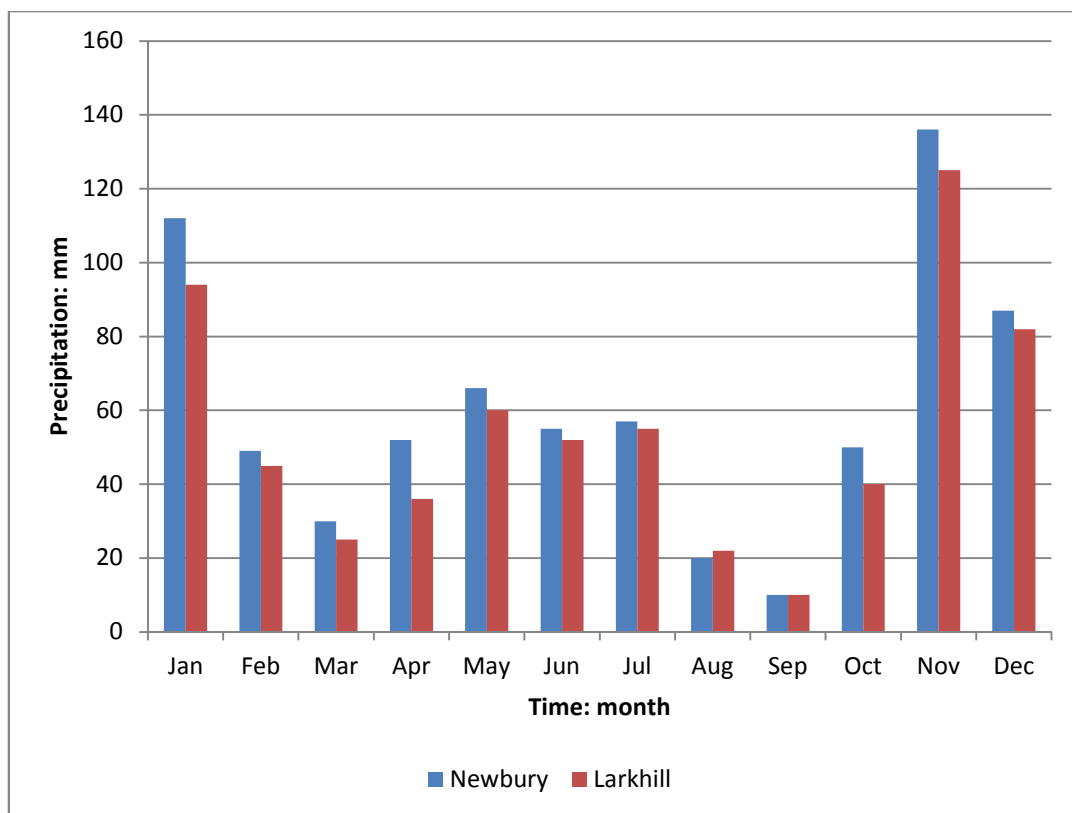
Figure 4-6: Comparison of monthly precipitation at Newbury cutting site and that recorded at the Larkin Met Office weather station for 2003.

Figure 4-7 shows the PET calculated at the Newbury cutting compared to that calculated at the Larkhill weather station. The figure shows that Larkhill PET is consistently higher. The reason for this discrepancy is the aspect of the Newbury cutting slope in conjunction with sheltering by trees at the top of the slope (Davies et al., 2008a). This serves to reduce the effect of wind on the PET. To account for this in the calculation of PET from the Larkhill weather station wind speeds have been reduced by half (Davies et al., 2008a; Rouainia, pers. comm., 2012), meaning that the potential evapotranspiration rates matched those recorded on site by Smethurst et al. (2006), which is also shown on

Figure 4-7..

Figure 4-7: Calculated PET at the Newbury cutting site compared to PET calculated from Larkhill weather station for maximum wind speed and reduced wind speed. After Davies et al. (2008a)

Figure 4-8 shows the climate data set window used to define the climate boundary conditions in VADOSE/W. The Newbury climate data has been input; the first few days can be seen at the bottom of the window. Other features of the climate boundary data set that must be defined are the location latitude and climate data distribution pattern. Location latitude is used by VADOSE/W to define the rising and falling of the sun. The latitude of the Newbury bypass cutting is 51.4 degrees.

The distribution pattern defines the distribution of climate data throughout each day. A sinusoidal pattern that distributes the potential evapotranspiration, air temperature and relative humidity between the sunrise and sunset times and the precipitation between the times specified by the user has been used here. This is recommended as the most rigorous approach where steep wetting and drying fronts are expected (Geo-Slope, 2007) and has therefore been chosen for this work.
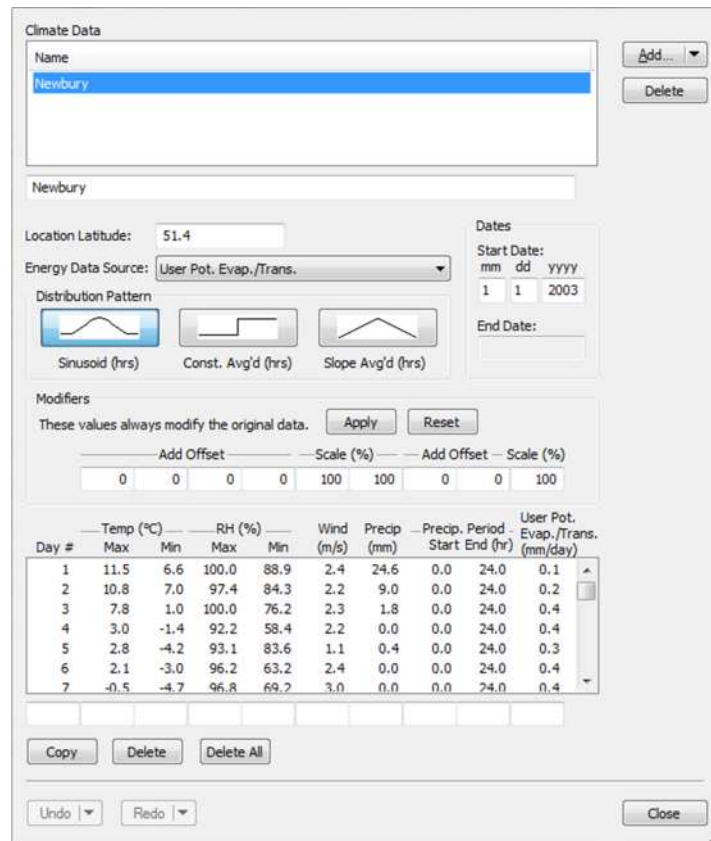
Figure 4-8: Climate data set window for Newbury cutting slope model.

VADOSE/W only allows the use of daily climate data and therefore the hourly data that is available must be scaled to daily time frame. Different methods to achieve this are used for each of the variables:

- The hourly precipitation data is summed for the entire day to give the daily total.
- For minimum and maximum daily temperature the minimum and maximum hourly values are identified and these are used.
- The minimum and maximum daily relative humidity the same approach as for temperatures is taken.
- The hourly wind speeds are averaged over the day to establish the daily wind speed to be used in the analysis.
- Hourly potential evapotranspiration data is summed for the entire day to give the daily total.

In the literature review (Section 2.8.2) it was stated that hourly or sub-hourly rainfall data would be optimal for this type of analysis (Fredlund et al., 2010). In this work daily rainfall data was used throughout. It is acknowledged here that this may have

negative impacts on the replication of the hydrological behaviour and the pore water pressures and suctions by, for example, not properly representing extreme precipitation events that occur over a period of time much shorter than one day. The implications of this decision are considered throughout; for example in the discussion of the chapter (Section 4.5.3.2) and the discussion in Chapter 5 where the ability of the model to correctly calculate the runoff is considered (Section 5.8.2.1).

The next step is to describe the length of the rainfall event, which is achieved by defining the start and end hour of the precipitation period. In this initial validation analysis the precipitation events are assumed to last for the entire day with a sinusoidal distribution. Extracting the precise length of rainfall events from the climate data is a difficult process and prone to errors; therefore this model is also being used to validate the method of applying the precipitation over the entire day. By using the sinusoidal pattern the total precipitation for the day is distributed throughout the whole day as in Figure 4-9 where the total rainfall applied is the area under the curve.
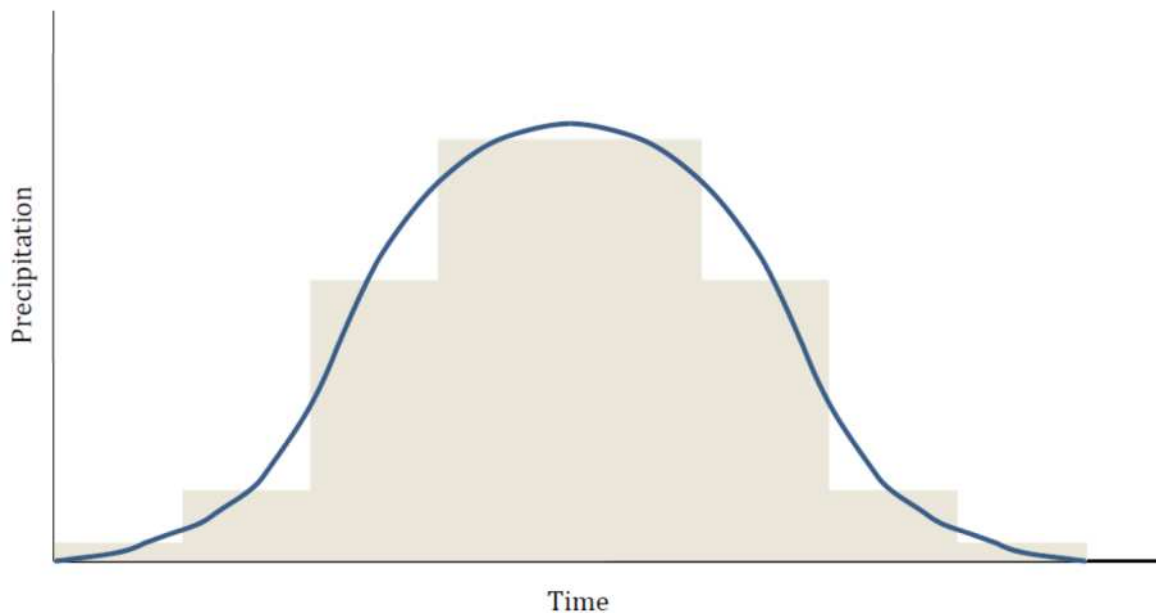
Figure 4-9: Precipitation distributed in a sinusoidal pattern throughout the day.

4.3.4.2 Vegetation Properties

Vegetation properties are defined as part of the surface boundary condition in VADOSE/W, with a root depth function that allows water to be removed from depth rather than just the surface boundary. To define a vegetation boundary condition the following are required:

- Leaf area index (LAI)
- Growing season
- Plant moisture limiting function (PML)
- Root depth function and distribution

The LAI determines the fraction of incident solar radiation driving evaporation from the bare soil or transpiration from vegetation and is combined with the growing season to give the LAI function. The growing season is defined by inputting the first and last day of the vegetation's growing season. Plant moisture limiting function determines the vegetation's ability to extract moisture from the soil as suction increases; it consists of vegetation stress onset and the wilting point. The limiting factor falls from 1 at the stress onset to 0 at the wilting point. The root depth function defines the depth to which moisture is being removed from the soil profiles throughout the year and is related to the growing season of the vegetation.

Leaf Area Index Function

Table 4-2 shows the properties used to define the LAI function that has been used in this work. Vegetation on the Newbury cutting slope consists primarily of grass and herbs. A LAI of value of 1 is suggested for this type of vegetation (Glendinning et al., 2006; Davies et al., 2008b). The growing season for an ungrazed, uncut grass such as the one present on the Newbury slope generally lasts from the beginning of March until the end of October (Briggs and Courtney, 1985).

Property	Value
Leaf Area Index	1

First day of growing season	60
Last day of growing season	304

Table 4-2: Properties and values to define the leaf area index function.

LAI and growing season are combined to form the LAI function which varies the value of the LAI throughout the year to control the amount of water transpired from the vegetation. Figure 4-10 shows the LAI function that was used for the Newbury cutting model.
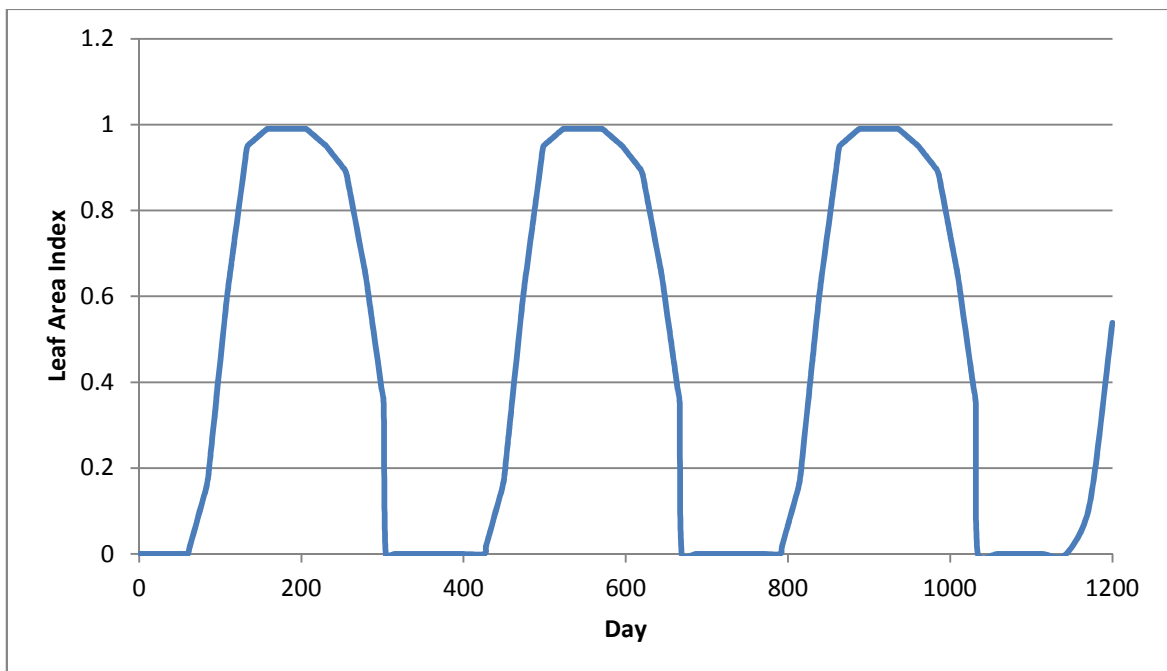
Figure 4-10: Leaf Area Index function for the Newbury cutting vegetation defined with the values shown in Table 4-2.

This function shows the LAI varying over three years; the function can be cycled for as many years as are required by the model, meaning that just the one function needs be defined.

Plant Moisture Limiting Function

The plant moisture limiting function is simply defined by the vegetation stress onset and the wilting point. Smethurst et al. (2006) used values of 45 kPa suction and 1500

kPa suction respectively for the vegetation stress onset and the wilting point. The plant moisture limiting function is a linear relationship between the suction and limiting factor (Figure 4-11).
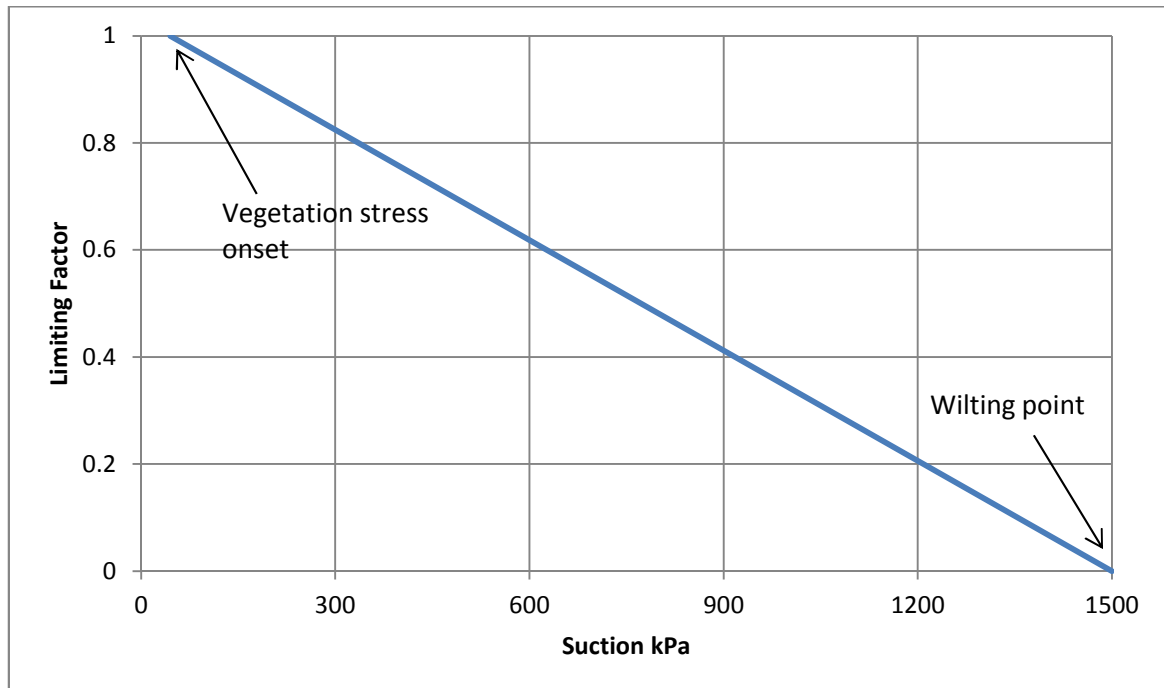
Figure 4-11: Plant Moisture Limiting function for the Newbury cutting vegetation where the vegetation stress onset is 45 kPa and the wilting point is 1500 kPa.

Therefore, from Figure 4-11, it can be seen that if the suction in the soil surrounding the roots is approximately 500 kPa then the ability of the vegetation to remove moisture from this soil will be reduced by 0.5.

Root Depth Function and Distribution

The root depth function will define the depth at which the roots will be active throughout the year. The upper boundary of the root zone is the soil surface, while the lower boundary is indefinite and irregular. Growth of the above ground vegetation is mirrored by activity in the root system (Briggs and Courtney, 1985), meaning that extraction of moisture form the soil by roots changes with the growing season of the vegetation.
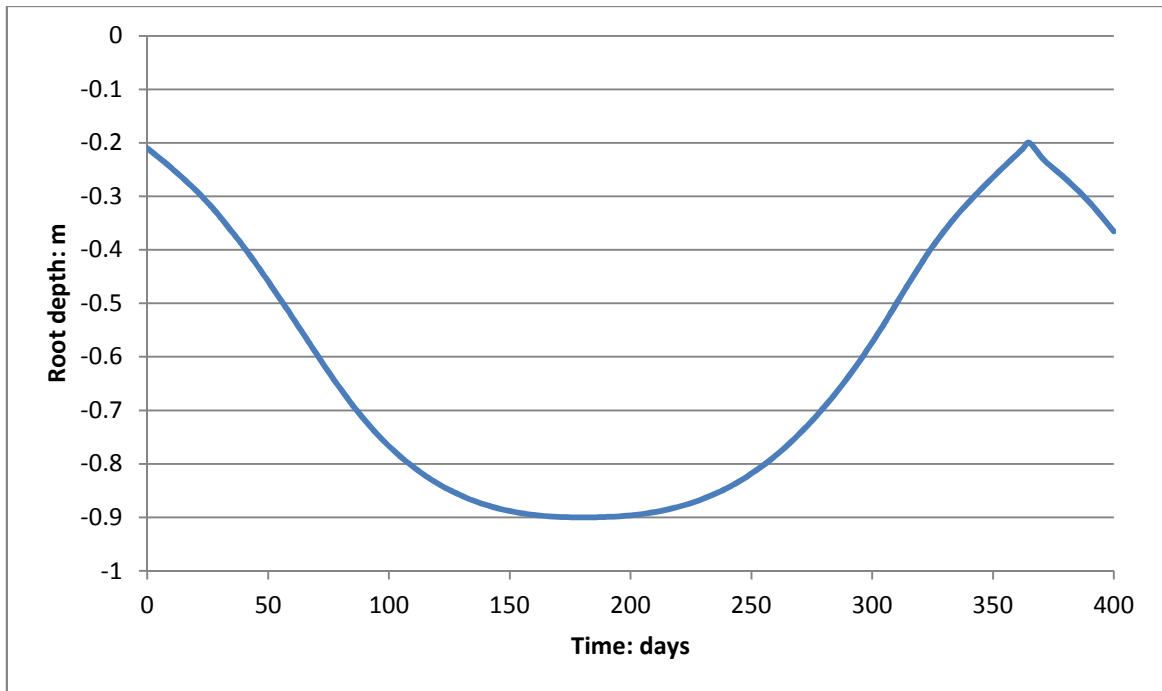
Figure 4-12: Root depth function showing maximum depth of root activity throughout the year.

The maximum root depth is mid-year (182 days) in the function (Figure 4-12). Similarly to the LAI function the root depth function is cycled so that it repeats for the following year if required.

4.3.5 Initial Hydraulic Conditions

In a transient analysis initial hydraulic conditions are essential to the VADOSE/W model. Initial conditions can have significant effects on the solution and it is therefore very important that they are suitably defined. Smethurst et al. (2006) recorded pore water pressure profiles (Figure 4-13) at the four instrumentation groups at the beginning of January 2003 and from these profiles the position of the water table at this time can be determined.
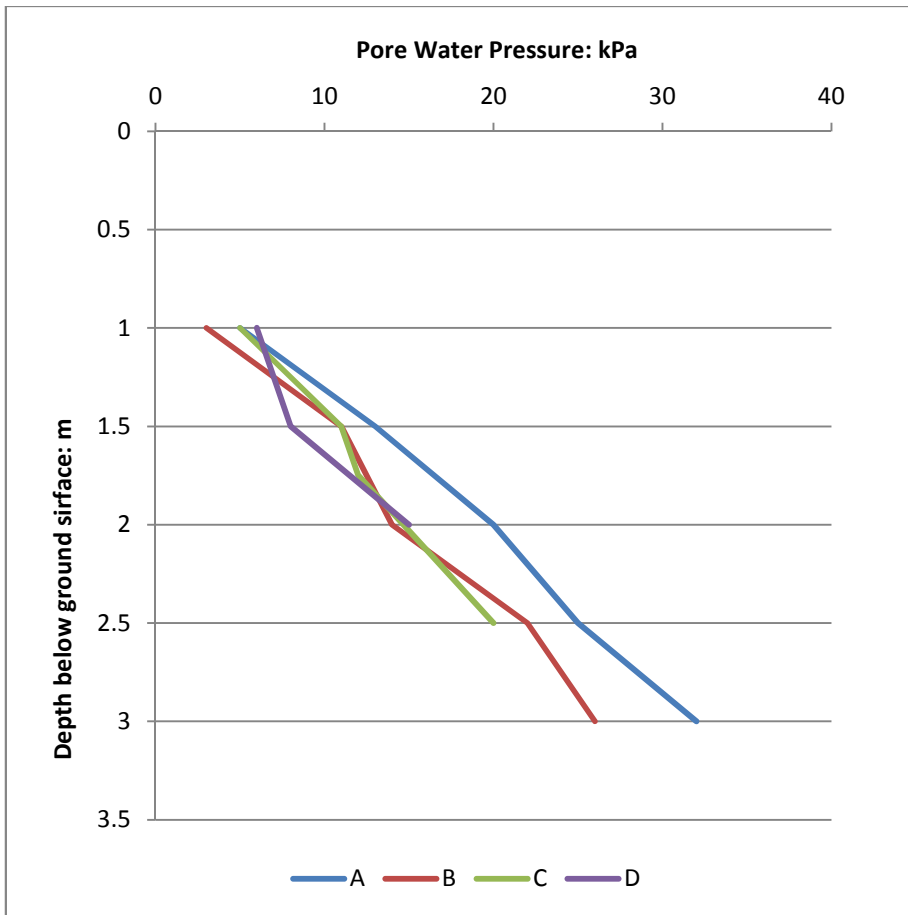
Figure 4-13: Distribution of pore water pressure with depth at the beginning of January 2003 at all instrument groups, where the locations are those shown in

Figure 2-11 . After Smethurst et al. (2006).

Smethurst et al. (2006) observed that pore water pressures in early January 2003 were generally hydrostatic below a water table at most 0.5 m below the ground/slope surface. Instruments had not been installed in the top 1.0 metres of the slope when these measurements were made and therefore there are no values above this depth. The data shown here was used to define the initial state of the system, using hydrostatic pore water pressures, with the phreatic surface located at a depth of 0.5 metres below the slope surface at all locations.

4.3.6 Far Field Boundaries

The far field boundary conditions are undefined; therefore the boundaries need to be placed at a distance from the point of interest (the slope) that does not affect the

computation of pore water pressures. A sensitivity analysis of various locations of these boundaries has been carried out. The analysis looks at how sensitive the pore water pressures and suctions developing in the slope are to the location of the boundaries. Table 4-3 gives details on the dimensions and the total number of elements in the mesh of each model. The mesh in each model is the default mesh generated by VADOSE/W for that model, except for in the surface layer where the number of elements in the vertical direction is stipulated as 10.

Model Descriptor	Distance from crest: m	Distance from toe: m	Total no. of elements
10 m	10	10	421
20 m	20	20	609
30 m	30	30	785
40 m	40	40	962
50 m	50	50	1137

Table 4-3: Details of the models in the far field boundaries sensitivity analysis.

In Appendix B sketches of each model can be found. Each model was run for one year (2003) with the Newbury climate boundary condition applied (Section 4.3.4). One year was chosen so that pore water pressures during the summer and winter could be observed. Figure 4-14 to Figure 4-16 show pore water pressure profiles generated at three locations on the slope; crest of the slope, mid-slope and the toe of the slope at the end of summer and winter. These three locations were chosen so that the effects within the whole slope could be considered; as the results show the influence of the location of the side boundaries is variable throughout the slope.
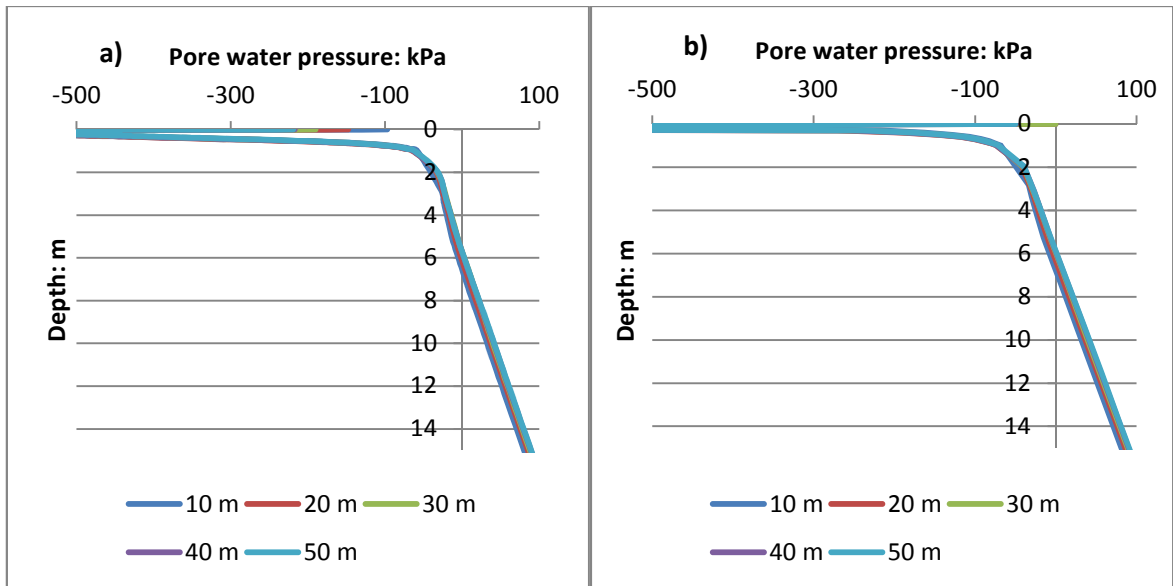
Figure 4-14: Results of the boundary location sensitivity analysis; showing pore water pressure profiles at the crest of the slope for a) end of summer, and b) winter.

In general it was found that the magnitude of negative pore water pressures were very sensitive to changes in the position of the side boundaries, but positive pore water pressures were less so. Figure 4-14 shows the results at the crest of the slope. It was found that the boundaries had to be extended to 50 metres before no change in the calculated pore water pressure profiles was observed at the end of summer or the end of the year.
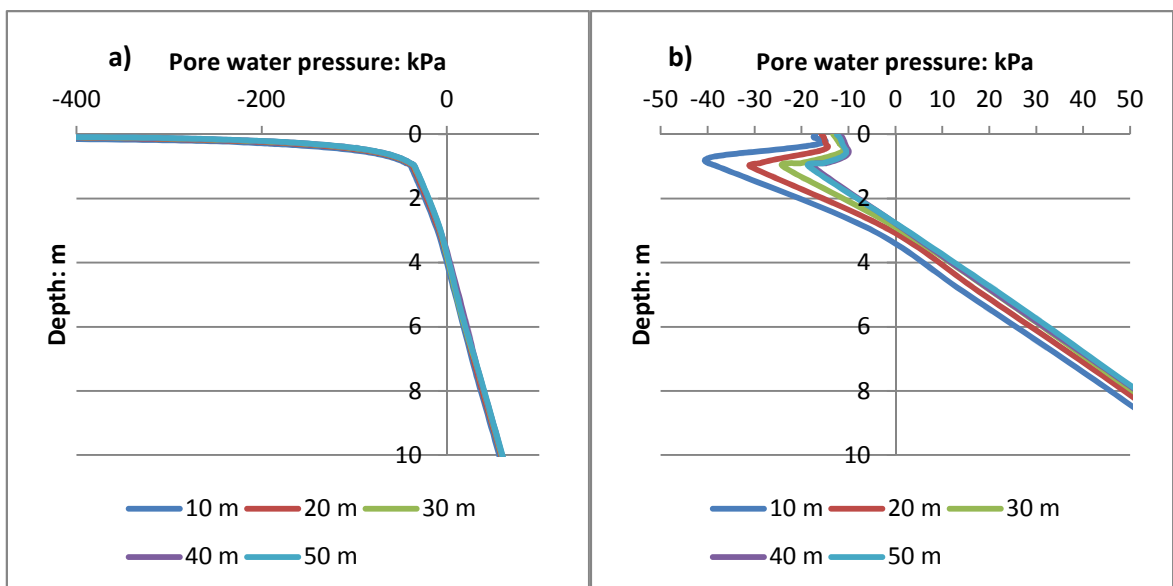
Figure 4-15: Results of boundary location sensitivity analysis for mid-slope; showing pore water pressure profiles for a) end of summer, and b) winter.

159

Similarly for the crest of the slope, at the mid-slope locations it was found that once the side boundary location was increased from 40 metres to 50 metres the effect on the pore water pressures profiles was negligible (Figure 4-15). Figure 4-16 shows the results at the toe of the slope. At the toe of the slope it was found that the influence of boundary location was not as great as at the crest of the slope or mid-slope. In fact there was very little change in the calculated suctions from the initial boundary location at 10 metres to the final one at 50 metres.
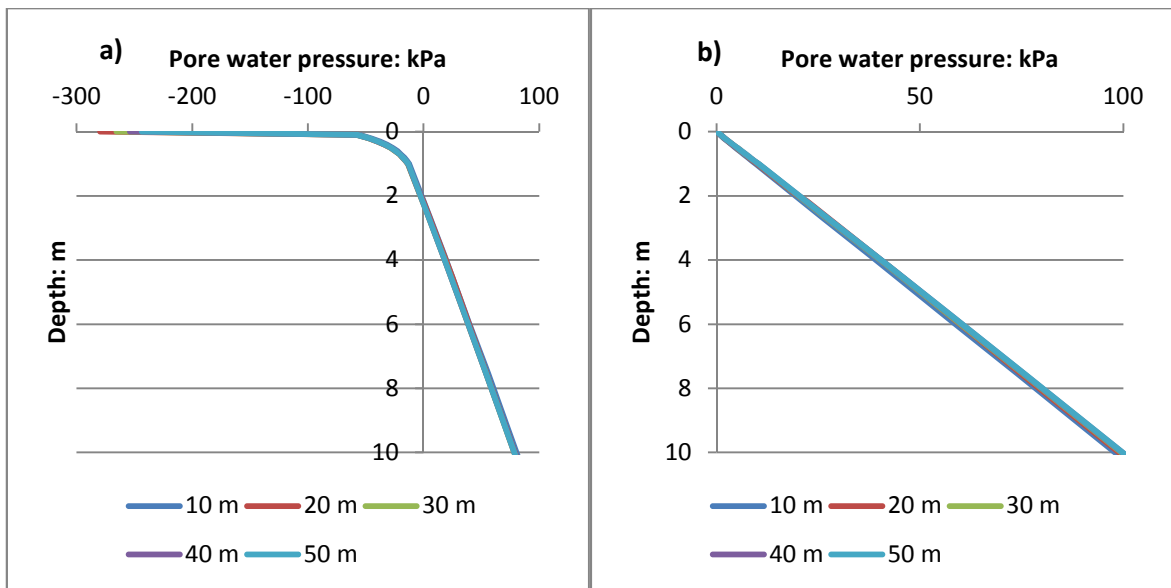
Figure 4-16: Results of boundary location sensitivity analysis at the toe of the slope; showing pore water pressure profiles for a) end of summer, and b) winter.

The results have shown that the side boundaries should be placed 40 metres away from the slope before any further increase in the distance will not influence any of the calculated pore water pressures at any location within the slope. Figure 4-17 shows the final model geometry with the side boundaries at the required location. Also shown on this figure is the finite element mesh automatically generated by VADOSE/W. In the following section the steps taken to refine this mesh are described.
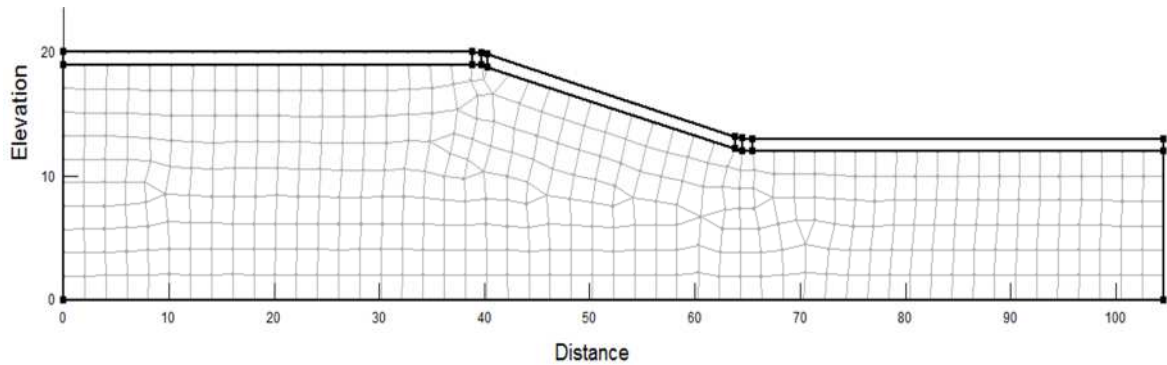
Figure 4-17: Final model geometry with an initial finite element mesh – 1237 elements, 1309 nodes.

4.3.7 Meshing

Finding the most efficient mesh for this model is an important step. An efficient mesh will maximise the models performance whilst minimising the time taken to run the model. It would be possible to simply create an extremely fine mesh for this model, however as the available computing power is limited this is not an acceptable option.

There will be areas within this model where a fine mesh is not required, for example areas where there is little change in pore water pressure with time. The aim of this sensitivity analysis is to create the most efficient mesh for the model, which will be achieved by identifying the minimum number of elements where increasing the number of elements would produce no change in the results, therefore meaning that results are mesh independent.

In this analysis the greatest pore water pressure changes are occurring in the surface layer, which is expected. Therefore, fine discretisation is required in the surface layer (Geo-Slope, 2007). The sensitivity analysis in Section 4.3.7.1 aims to produce a mesh in the surface layer that produces appropriate results with the least number of elements possible. Although efficiency in the mesh is important in practice, it is of more importance in research that correct and consistent results are obtained. Therefore, the quality of the results will always take precedence over the speed at which these results are calculated.

161

4.3.7.1 Surface Layer

A sensitivity analysis was carried out on the number of finite elements forming the surface layer of the VADOSE/W Newbury cutting validation model. It is recommended to have the surface layer elements 5 to 6 cm thick (Geo-Slope, 2007), which equates to between 16 and 20 elements thickness in the surface layer of this model. Models of 10, 15, 17 and 20 elements thickness in the surface layer have been created (Table 4-4) and will be run for 365 days with the Newbury climate data applied (2003).

Elements in surface layer	Total number of elements in model	Total number of nodes in model
10	421	458
15	541	583
17	589	633
20	661	708

Table 4-4: Model information for surface layer mesh density sensitivity analysis.

Pore water pressure profiles have been produced at the mid-slope location after 275 days and 365 days (end of summer and end of the year) for each of the model runs (Figure 4-18). Studying Figure 4-18 it can be seen that increasing the number of elements vertically significantly affects the results. By increasing the number of elements from 10 to 20 the suction at 1 metre depth at 365 days falls from 37 kPa to 16 kPa.
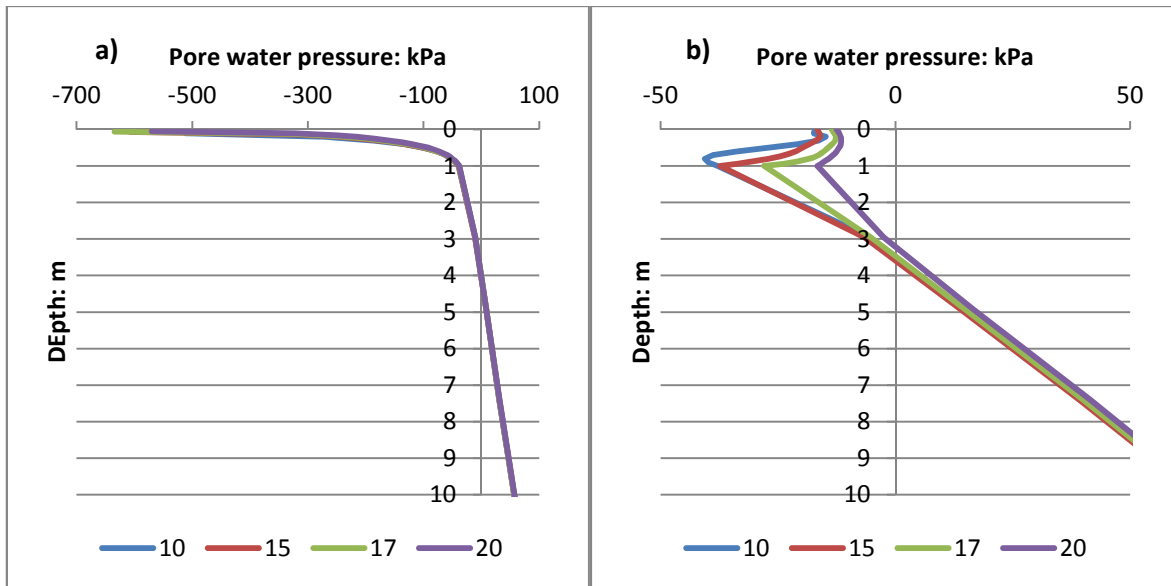
Figure 4-18: Results of the surface layer mesh sensitivity analysis; showing pore water pressure profiles at mid-slope, for a) summer (all profiles overlap), and b) winter.

Looking at Figure 4-18 it can be seen that pore water pressures in the winter are more sensitive to the number of elements vertically in the surface layer than those in the summer. Increasing the number from 17 to 20 elements still has significant effects, showing that the results are still mesh dependent, particularly at a depth of 1 m where the suction decreases from 28 kPa to 17 kPa. The decision was taken to conduct further analyses with 23 and 25 vertical elements in the surface layer.

Elements in surface layer	Total number of elements in model	Total number of nodes in model
23	733	783
25	781	833

Table 4-5: Model details for secondary surface layer mesh sensitivity analysis.

Figure 4-19 shows the pore water pressure and suction profiles generated for these two supplementary models plus the model with 20 elements. The profiles show that increasing the number of elements from 23 to 25 does not influence the results, meaning that mesh independence has been achieved. Therefore to maintain the same level of accuracy when replicating the pore water pressures in the slope it is not

163

necessary to have any more than 23 vertical elements in the surface layer. In the final model run 23 vertical elements were used in the surface layer.
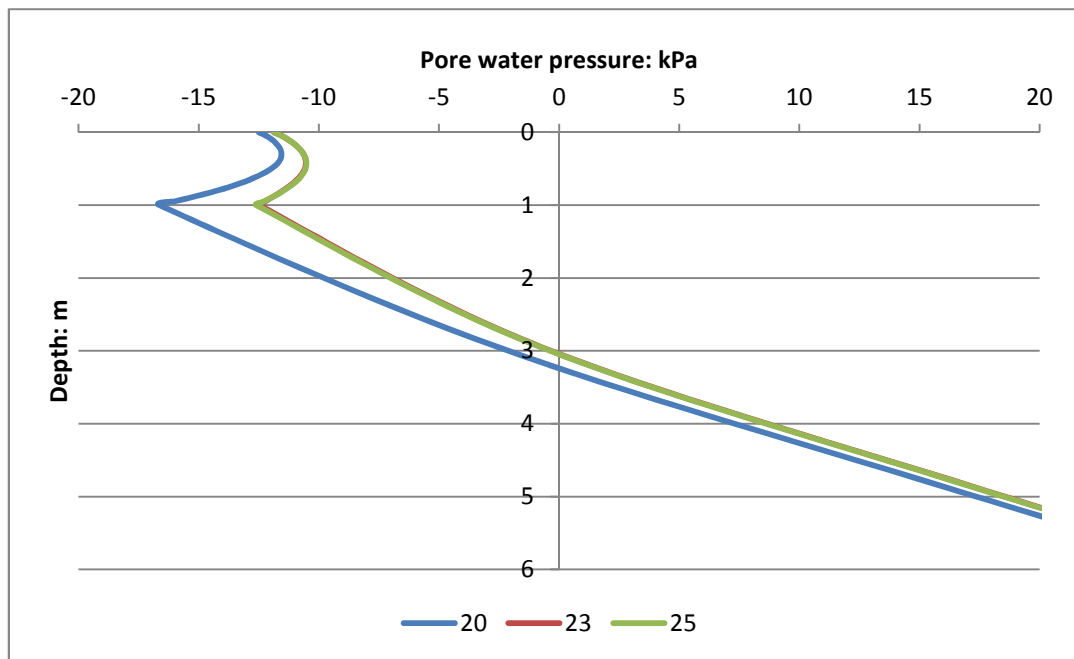
Figure 4-19: Results of the supplementary surface layer mesh sensitivity analysis; showing pore water pressure profiles at mid-slope with 20, 23 and 25 elements. There is complete overlap between the profiles for 23 and 25 elements (i.e. the red line lies completely underneath the green line).

4.3.7.2 Inner Slope Region

The region forming the inner slope below the surface layer does not require as fine a discretisation as the surface layer to achieve mesh independence. The magnitude and rate of change of pore water pressures is far less than in the surface layer. In VADOSE/W an initial mesh can be created by defining a 'global element size', which is the maximum size, in metres, of any element within the mesh. The global element size does not apply to the thickness of elements in the surface region; only the length of them. A sensitivity analysis of the pore water pressures calculated within the inner slope region (below the surface layer) to the global element size has been carried out. Global element sizes of 2.0, 1.5 and 1.0 metre have been analysed. From the results of the surface layer sensitivity analysis, 23 vertical elements were used within the surface layer. Table 4-6 details each of the analyses carried out, including the total number of elements in the model and the total time to solve the analysis. The results

for this sensitivity analysis are shown in Figure 4-20. Sketches of each model tested in these analyses can be found in Appendix B.

Global element size	Total number of elements in model	Total number of nodes in model
2.0 m	733	783
1.5 m	1023	1082
1.0 m	1719	1797

Table 4-6: Model details for inner slope region mesh sensitivity analysis.
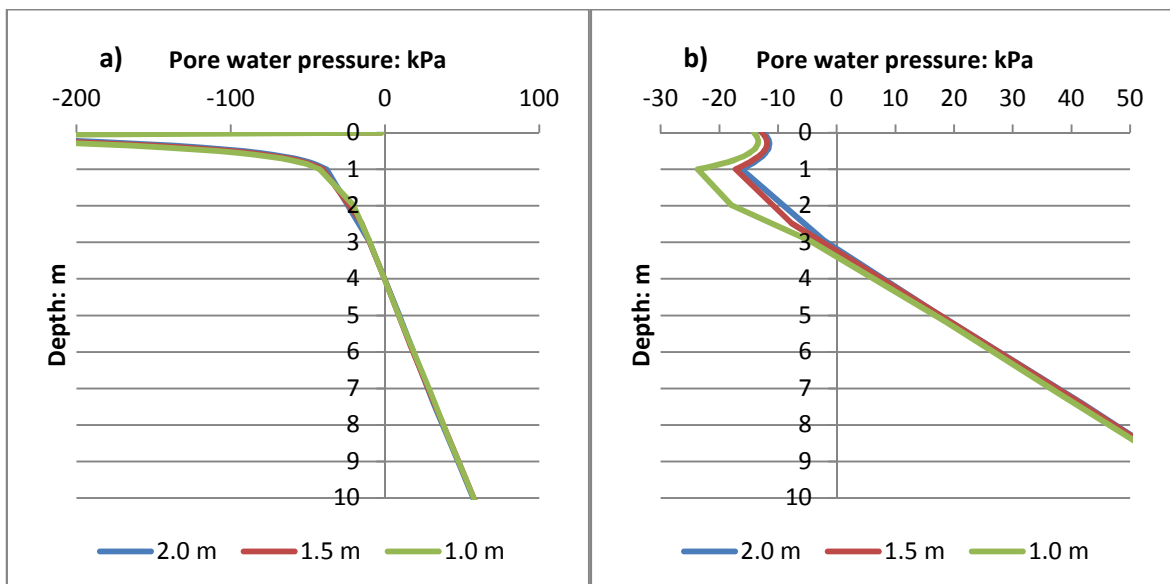
Figure 4-20: Results of inner slope region mesh sensitivity analysis; showing pore water pressure profiles, for a) end of summer, and b) winter.

Figure 4-20 a) and b) shows the pore water pressure profiles generated at the end of summer and the end of the year respectively. Changing the fineness of the mesh in the main body of the model affects the pore water pressures, but only significantly in the top 2 – 3 metres of the soil profile. Below 3 metres depth, changing the fineness of the mesh has almost no effect on the magnitude of calculated pore water pressures. This shows that a large global element size may be used in this part of the model.

Figure 4-20 b) shows that reducing the global element size from 1.5 metres to 1.0 metres is still not sufficient to result in no change to the calculated pore water pressures in the top 3 metres of the slope profile. A further model has been created

that uses a maximum element size of 0.5 metres in the region below the surface layer and a global element size of 2.0 metres in the rest of the model (Figure 4-21). This two size approach has been taken to try and keep control of the total number of elements, which could become excessive if a global element size of 0.5 metres was used.
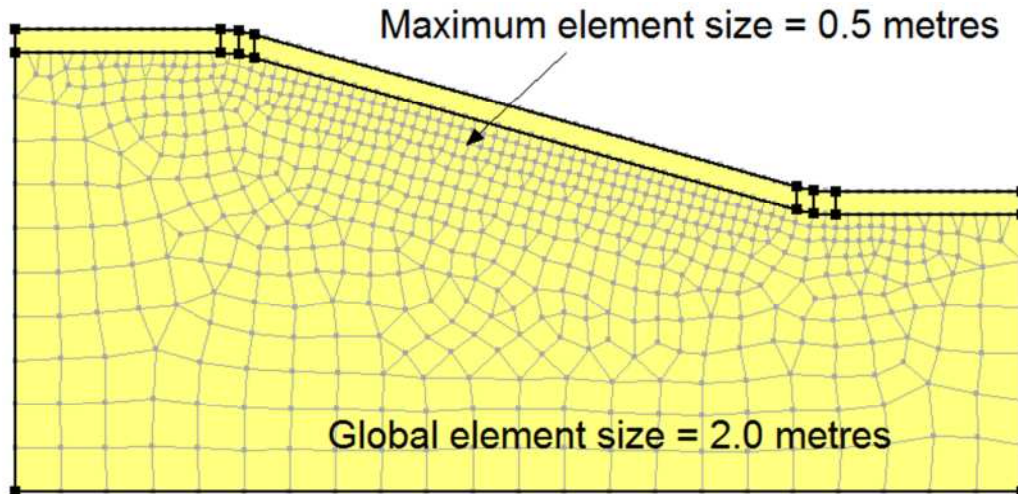
Figure 4-21: Inner slope region mesh of first order quadrilateral and triangular elements for the secondary sensitivity analysis – 2706 elements, 2753 nodes.

Figure 4-22 a) and b) show the results of this model compared to the model with a global element size of 1.0 metres.
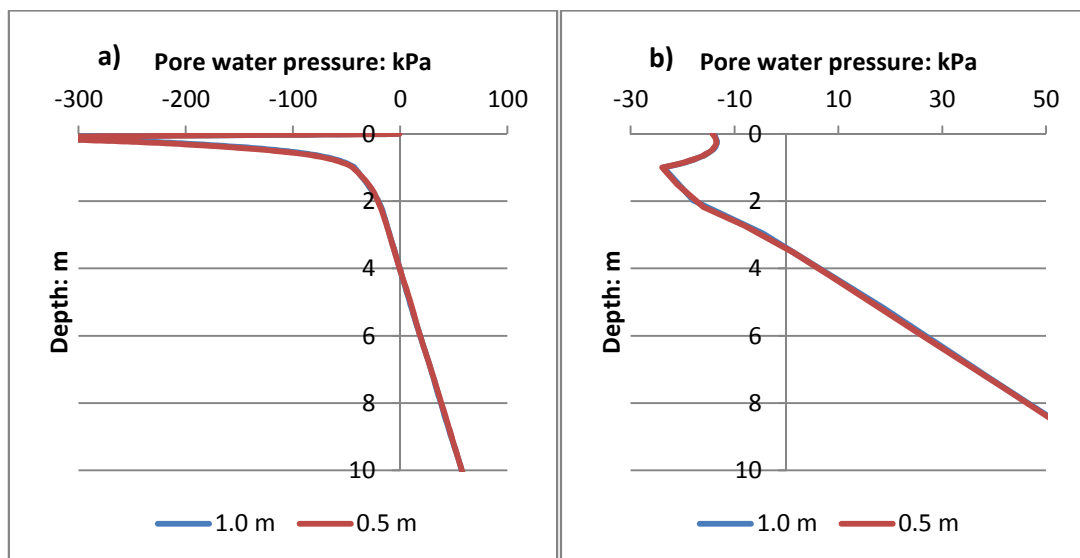
Figure 4-22: Results of secondary inner slope region sensitivity analysis; showing pore water pressure profiles, for a) end of summer, and b) winter (there is complete overlap of profiles in both plots).

Decreasing the element size from 1.0 metres to 0.5 metres has no discernable effects on the calculated pore water pressures and suctions. Using two element sizes within the model is also shown to be a suitable approach to discretisation.

4.3.7.3 Final Mesh

Details of the final mesh are shown in Figure 4-23. The first image (Figure 4-23 a)) shows the surface layer and the region below that. In these regions there are 23 elements vertically in the surface layer and a maximum element size of 1.0 metres. Figure 4-23 b) shows the remainder of the model where there is a global element size of 2.0 metres and where the surface region meshing lies in relation to this.
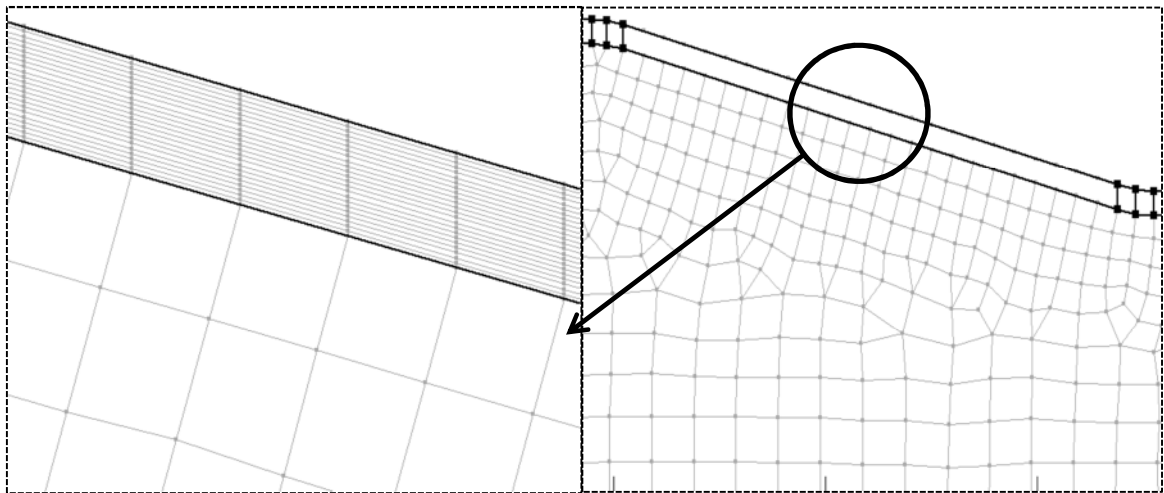
Figure 4-23: Details of the final mesh: a) surface layer and b) inner slope region.

4.4   Final Model Run

The final model (Figure 4-24) with the mesh and geometry established in the previous sections has been run with 400 days of climate data applied. An initial water table has been defined at a depth of 0.5 metres with hydrostatic pore water pressures below. Above the water table are hydrostatic suctions which extend to the slope surface. The model was run from 1 January 2003 to the end of January 2004 covering the dates for which Smethurst et al. (2006) have recorded and published pore water pressure and suction data. From studying this data it is expected the model will calculate maximum suctions at the end of September 2003 and the minimum suctions at the end of December 2003/beginning of January 2004.

In summary the model has the following features:

- Impermeable bottom and far field boundary conditions.
- Climate surface boundary condition, including weather data and vegetation data.
- Initial conditions specified by an initial water table at a depth of 0.5 metres.
- A mesh of first order quadrilateral and triangular elements, consisting of 3272 elements and 3357 nodes.
- Hydraulic material properties defined by a soil water characteristic curve and a hydraulic conductivity function.

Complete data has been published covering instrument group C at mid-slope (Smethurst et al., 2006). The data includes the pore water pressures and suctions measured by all instruments throughout 2003. Pore water pressure and suction profiles were generated for these locations to compare the measured data with the outputs from the VADOSE/W model and hence to validate the model.
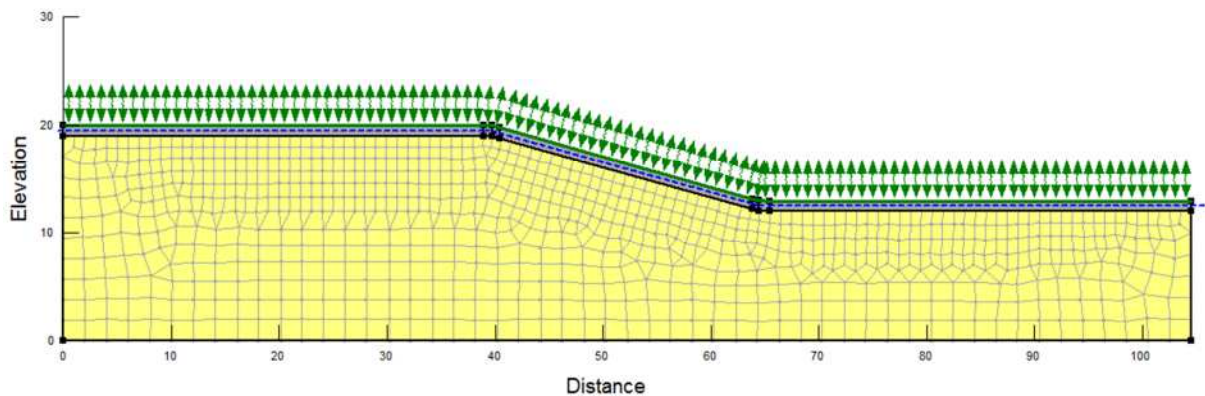
Figure 4-24: Final model set-up, with material model, boundary conditions, initial water table and discretisation applied.

4.4.1 Results

A number of pore water pressure and suction profiles have been generated from the calculated results of the VADOSE/W validation model. The profiles are for instrument group C (Figure 4-25 and Figure 4-26) September 2003 (maximum suctions) and the end of December 2003/beginning of January 2004 (minimum suctions). The profiles

are compared to the observed pore water pressures and suctions from Smethurst et al. (2006) and also compared to the modelling results of Davies et al. (2008a). Figure 4-25 shows the profiles at the end of September. The profile shows that both models have, for the most part, successfully recreated the suctions developing in the slope up to the end of summer. The magnitudes of the suctions are very close to the observed values as well as capturing the actual shape of the profile; particularly well below a depth of 0.5 metre.
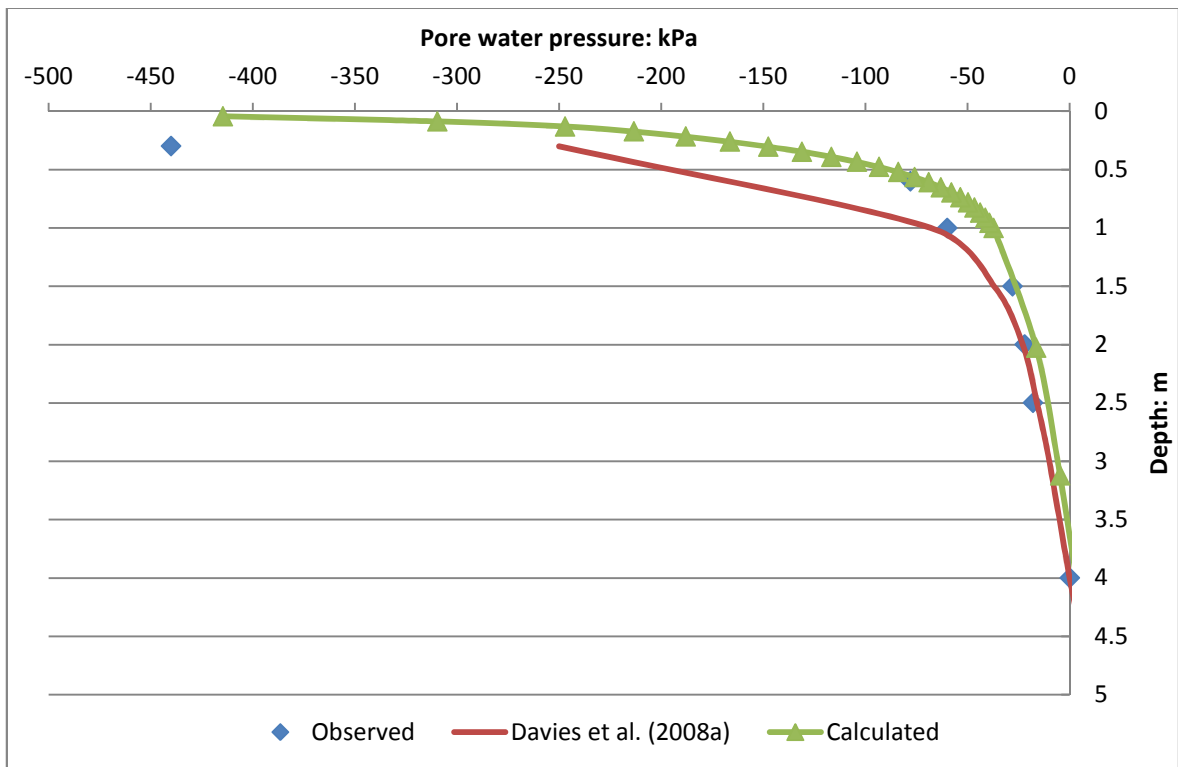
Figure 4-25: Comparison of observed and calculated suction profiles at the end of September 2003 at instrument group C (mid-slope).

Both the VADOSE/W model and the model of Davies et al. (2008a) perform less ably when modelling the very high suctions developing within the top 0.5 metres of the slope profile. Suctions of up to 440 kPa were measured by an equitensiometer at a depth of 0.3 metres Smethurst et al. (2006); at this depth the VADOSE/W model calculated a maximum suction of just 150 kPa whereas the model of Davies et al. (2008a) calculated a suction of approximately 240 kPa at a depth of 0.30 metres. It is noted by Smethurst et al. (2006) that the equitensiometer is very sensitive to the water content–suction relationship of the ceramic in the instrument and therefore data from it should be treated as indicative rather than quantitative, which could

169

explain some of the disparity between the observed and calculated magnitudes of suctions.

The second profile (Figure 4-26) shows the observed and calculated suctions at the same location at the end of December 2003. The observed profile shows that suctions in the top 1.5 metres of the profile have completely dissipated; the VADOSE/W model and the Davies et al. (2008a) model have both been unable to recreate this. However, suctions are much reduced from the summer maximum which shows the model has been able to reflect the general hydrological behaviour within the Newbury cutting.
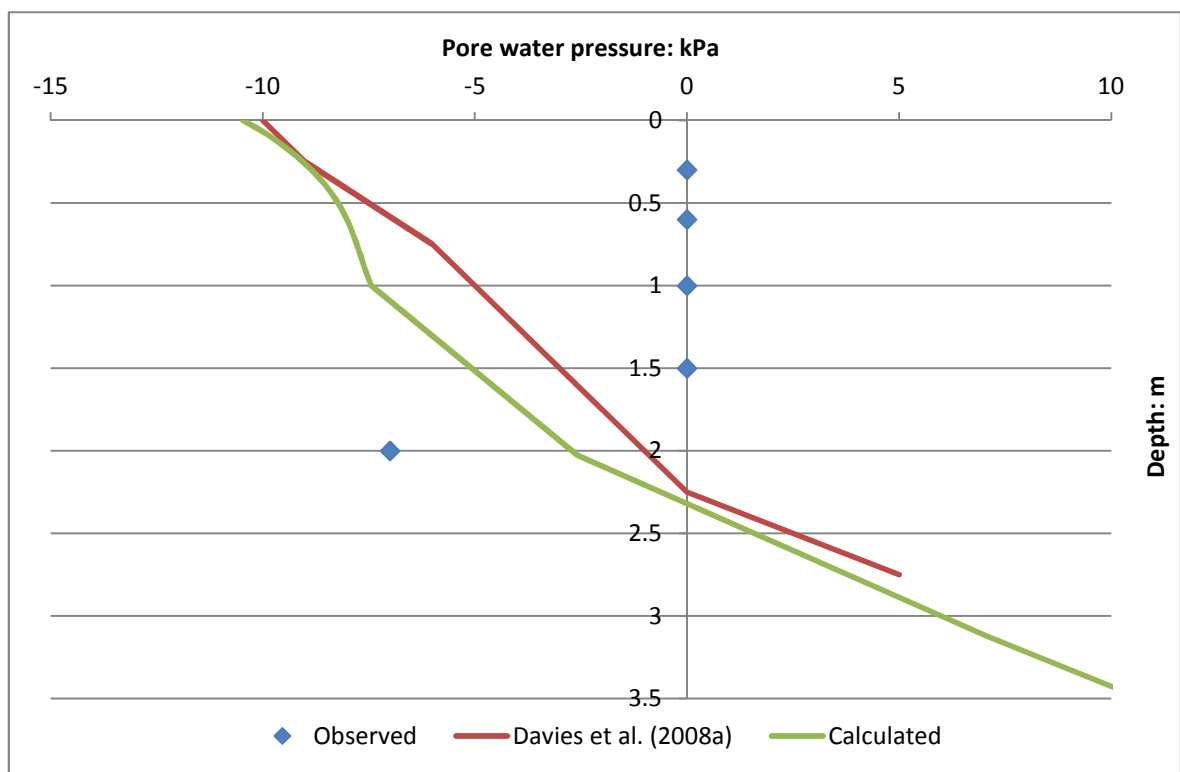
Figure 4-26: Comparison of observed and calculated suction profiles at the end December 2003 at instrument group C (mid-slope).

The results from this initial analysis show that the model is capable of modelling the general hydrological behaviour within the Newbury cutting slope just as well as the Davies et al. (2008c) model. The model has been able to identify the timing of the maximum and minimum suctions and model the magnitude and profile of the maximum summer suctions quite well. The magnitude and profile of the winter suctions are not as well modelled. In the discussion the possible reasons for this are identified and analysed.

4.5 Discussion

The model has performed relatively well, compared to the model of Davies et al. (2008a). The pore water pressure profiles generated, during the summer and winter, and the relationships between them are realistic. In the literature review measurements and observations of pore water pressure profiles and trends in embankments and cuttings in the United Kingdom were reviewed (Section 2.6). Ridley et al. (2004a) and Vaughan et al. (2004) have both presented measurements exhibiting the following features and relationships:

- Maximum suctions occur at the surface, generally at the end of summer/beginning of autumn, and decrease non-linearly with depth
- Pore water pressures become hydrostatic during winter
- Seasonal variation is the greatest near the slope surface and decreases with depth

Figure 4-27 shows the summer and winter pore water pressure profiles plotted together.
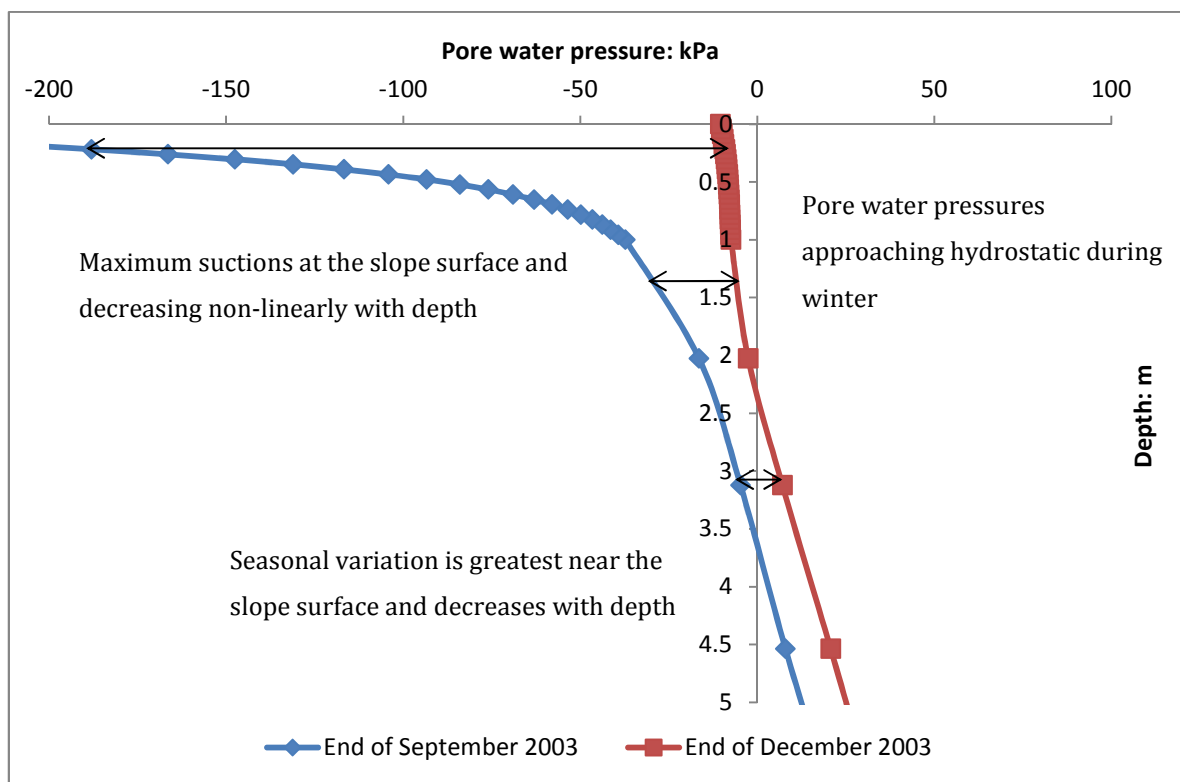
Figure 4-27: End of summer and winter pore water pressure profiles generated by the VADOSE/W model presented in Chapter 4.

4.5.1 Implications for slope stability

Delayed or progressive failure is a deep seated mode of failure that affects infrastructure slopes (Section 2.5). This type of slope failure has been linked to the size of pore water pressure cycles, with a series of large cycles expected to lead to failure in less time, due to the 'ratcheting' process (Section 2.5). The size of pore water pressure cycles is linked to seasonality in climate, with dry summers and wet winters typically leading to greater variation. 2003 was a year of extremes for the Newbury cutting; the year began following a very wet winter 2002, moving through a very dry summer 2003 and culminating in an extremely wet winter 2003. This seasonal variation has produced large pore water pressure cycles at the slope surface of around 400 kPa. However, below a depth of 2.0 metres the pore water pressure cycles are relatively small; only 13-14 kPa. This suggests that in the current climate, delayed failure brought about by large pore water pressure cycles is unlikely.

The climate in the United Kingdom is forecast to change (Section 2.11.1) with drier summers and wetter winters in the south of the country becoming far more frequent and more severe in nature. There are likely implications for the hydrology of the Newbury cutting slope, which being located in the south of England will be influenced by climate change. The expected major changes to the climate could lead to the following effects:

- Warmer and drier summers – greater summer drying of the slope, perhaps to greater depths and increased desiccation cracking.
- Wetter winters – rewetting of the slope can occur even with very high suctions developing in the summer as desiccation cracks allow water to infiltrate to greater depths.

The overall effects of this would be more deep seated progressive failure and perhaps more shallow failures as the slope rewets. There are also possible effects on vegetation, which are discussed in the following section.

The results have shown that the Newbury cutting model created in VADOSE/W can be used to investigate the effects of climate on the slope hydrology and stability. However, when considering the potential of climate change and other factors, the use

of steady-state conditions must be called into question (Dixon et al., 2006). Therefore if the model is to be used to analyse the effects of climate change, an approach that acknowledges the temporal and spatial variability of climate, material properties (specifically hydraulic conductivity) and vegetation must be used.

4.5.2 Vegetation

The vegetation present on the Newbury cutting slope is grass. The rooting depth of this grass is relatively shallow (a maximum of 1.0 metres), and therefore only directly affects the slope hydrology to this depth. This means that the vegetation does not have any effect on the size of pore water pressure cycles at depths where progressive failure could occur. In Section 4.5.2 of the literature review the role of vegetation in influencing infrastructure slopes was investigated, considering how the role may change as the climate changes. It is believed that rooting depth may increase as vegetation tries to reach moisture at greater depths during periods of drought and that the growing season may increase as average temperatures increase (Rouainia et al., 2009). These changes will influence the hydrology and the slope and also the stability, with the possibility of greater pore water pressure cycles at depth influencing progressive failure and larger volume changes affecting serviceability.

It is also worth considering the effects of other types of vegetation, such as trees. Large, mature trees can have rooting depths of up to 5.0 metres (Section 2.3.2), therefore influencing pore water pressures to a depth where progressive failure becomes an issue. There are other effects that must be considered, such as the mechanical effects mentioned in Section 2.3.2 of the literature review, which can be beneficial or detrimental. It is clear that the effects of large trees are much more complex than that of the grass located on the Newbury cutting slope.

The effects of vegetation in general (i.e. not just the grass on the Newbury cutting slope) are quite complex, especially when considering how unclear the effects that climate change may have. As the vegetation on the surface of the Newbury cutting slope only affects the top 1.0 m of the slope profile, it is relatively easy to identify the

effects of climate on the slope hydrology at greater depths. Therefore this slope and its vegetation should be ideal for studying the effects of climate change.

4.5.3 Winter pore water pressures

The performance of the VADOSE/W model is similar to that of the model of Davies et al. (2008a). Summer positive pore water pressures and suctions are replicated well. However, similar to the model of Davies et al. (2008a) this model struggles to replicate the dissipation of suctions that occurs throughout the autumn and winter. Material models that do not account for the effects of desiccation cracking on the soils hydraulic properties and lack of accounting for hysteresis are believed to be two possible causes of this. There are other reasons related to the water balance such as the effects of vegetation and evaporation and also the definition of the climate boundary condition that could also explain the difference observed. In the following sections three areas are discussed to try and understand the reasons why the model cannot model the dissipation of suctions:

1. Water balance
2. Climate boundary condition
3. Material properties

4.5.3.1 Water balance

The concept of the water balance was introduced in the literature review (Section 2.8.1). With every VADOSE/W model run, the water balance for the model domain is created and can be plotted. Figure 4-28 shows the water balance for the Newbury cutting numerical model, with cumulative precipitation, runoff, evaporation, transpiration and storage plotted for the whole year (2003). The water balance reveals that storage does not recover to anywhere near the original level at the start of the year, showing that insufficient water is infiltrating the slope to recover the high suctions that developed during the summer. By looking at the other processes it is possible to ascertain the reason for this. Precipitation is shown to be very heavy from the end of September, with over 20 m^3 falling on the slope until the end of the year and therefore it could be expected that suctions should be dissipated. However by

174

looking at the other processes it can be seen that a lot of this water is lost as runoff and evaporation.

There are a number of reasons that this could happen, falling under two categories:-

1. Model definition, including material properties and climate boundary condition.

2. Incorrect calculation of water balance variables such as runoff, evaporation etc. by VADOSE/W.
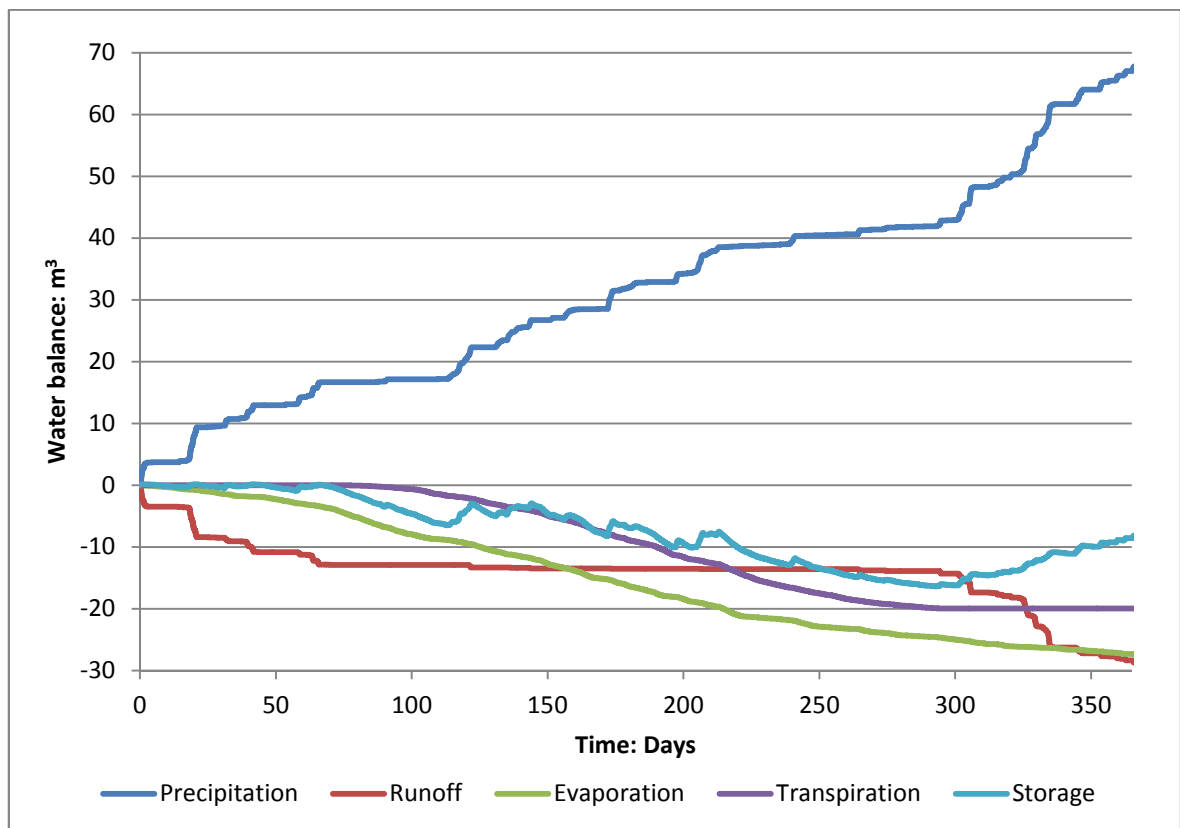
Figure 4-28: Newbury cutting water balance for 2003, calculated by the VADOSE/W model presented in Chapter 4.

Runoff, which occurs when the ground is saturated and the precipitation rate exceeds the infiltration rate, would be expected to be high due to the heavy rainfall saturating the slope. However, it may not be expected for the evaporation amounts to be as high as they are during the winter. The rate of evaporation is not much less during the winter as it is during the summer. By looking at the levels of potential evapotranspiration, which were discussed in the literature review (Section 2.8.4), it may be explained why evaporation is still significant during winter. Figure 4-29

175

shows the potential evapotranspiration (PET) throughout the year for the Newbury site. As expected, PET is the highest in the summer months and falls steadily to its minimum value in December.
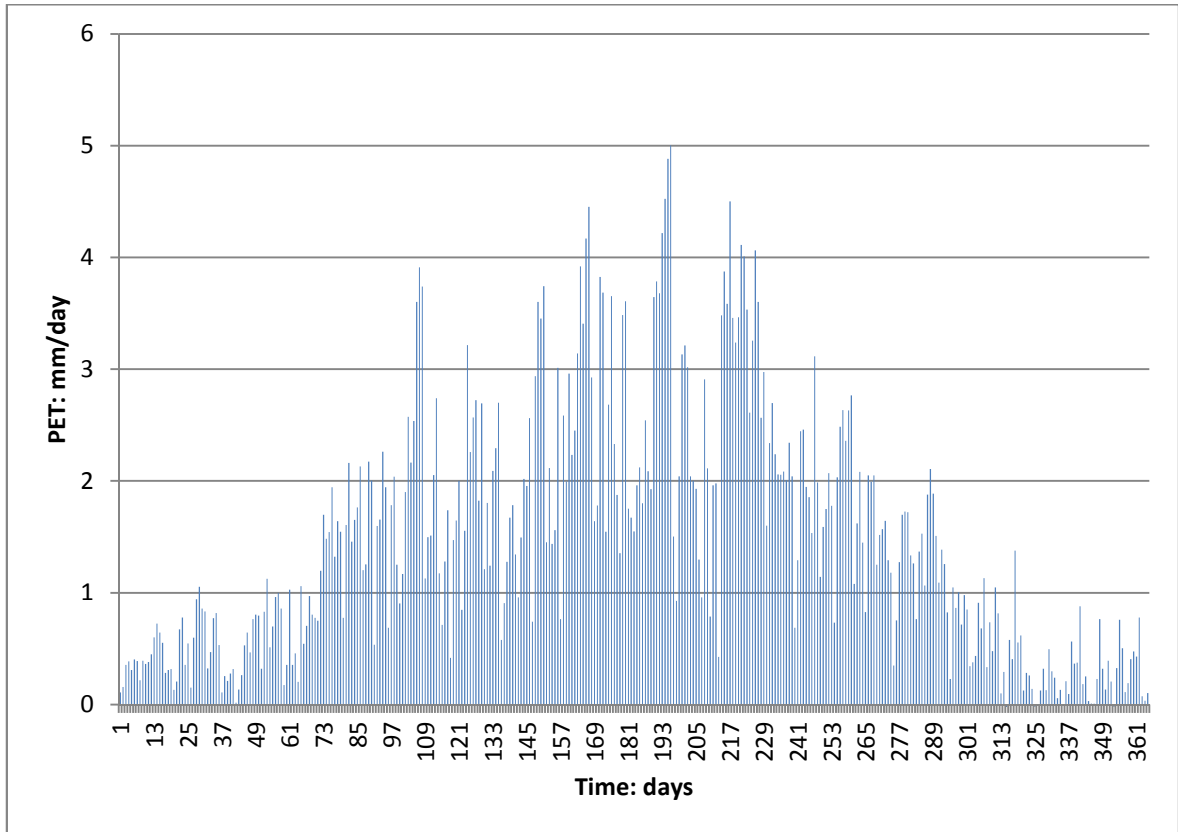
Figure 4-29: Potential evapotranspiration throughout 2003 for the Newbury cutting site.

Despite maximum summer daily PET being around 5 times greater than maximum winter daily PET, evaporation rates in the winter are not of that magnitude less than those in the summer. Figure 4-28 shows the average rate of evaporation from the beginning of March until the end of August, is 0.105 m^3/day. From the end of August until the end of the year the average evaporation rate is 0.0418 m^3/day; 2.5 times less than the summer evaporation rates. The reason for this is the lack of available water for evaporation during the summer and that vegetation stops extracting water from the soil at the end of October meaning more water is available for evaporation.

4.5.3.2 Climate boundary condition

The use of hourly or even sub-hourly precipitation data has been recommended (Fredlund et al., 2010a), particularly for the quantification of storm events where using daily precipitation data would not identify the difference between the same amounts of precipitation falling in 10 minutes or 10 hours. The model described in this chapter has used precipitation data at a daily level, due to limitations of the finite element software VADOSE/W (Section 4.3.4.1). Davies et al. (2008c) were able to implement hourly precipitation data in their Newbury cutting model. Initial results, presented in Section 4.4.1, suggest that using daily precipitation data has not adversely affected the modelling of the pore water pressures, as very similar results to Davies et al. (2008c) have been obtained. However, without knowing the intensity of rainfall events that occurred, it is hard to say whether daily precipitation data will always produce as satisfactory modelling results as hourly data. If rainfall could be applied in shorter intervals (perhaps even shorter than hourly) then modelling results could be more accurate. Runoff could be better calculated as more intense rainfall events would be more likely to saturate the slope surface; having repercussions on the calculation of infiltration and ultimately the pore water pressures.

Significant rainfall events can occur over a whole day, or a few hours, and if it is found that it is the former in the case of the Newbury site in 2003, then it cannot be said with any degree of certainty if the VADOSE/W model can provide good replication of the hydraulic response of the cutting to more intense rainfall events, perhaps occurring over only a few hours. Figure 4-30 shows the daily precipitation throughout 2003 for the Newbury site. The five heaviest rainfall days of winter and the heaviest summer rainfall day have been identified. The winter events occurred on 01/01, 19/01, 02/11, 26/11 and 01/12, the summer event occurred on 22/06. Hourly precipitation data has also been plotted for each of these days (Figure 4-31).
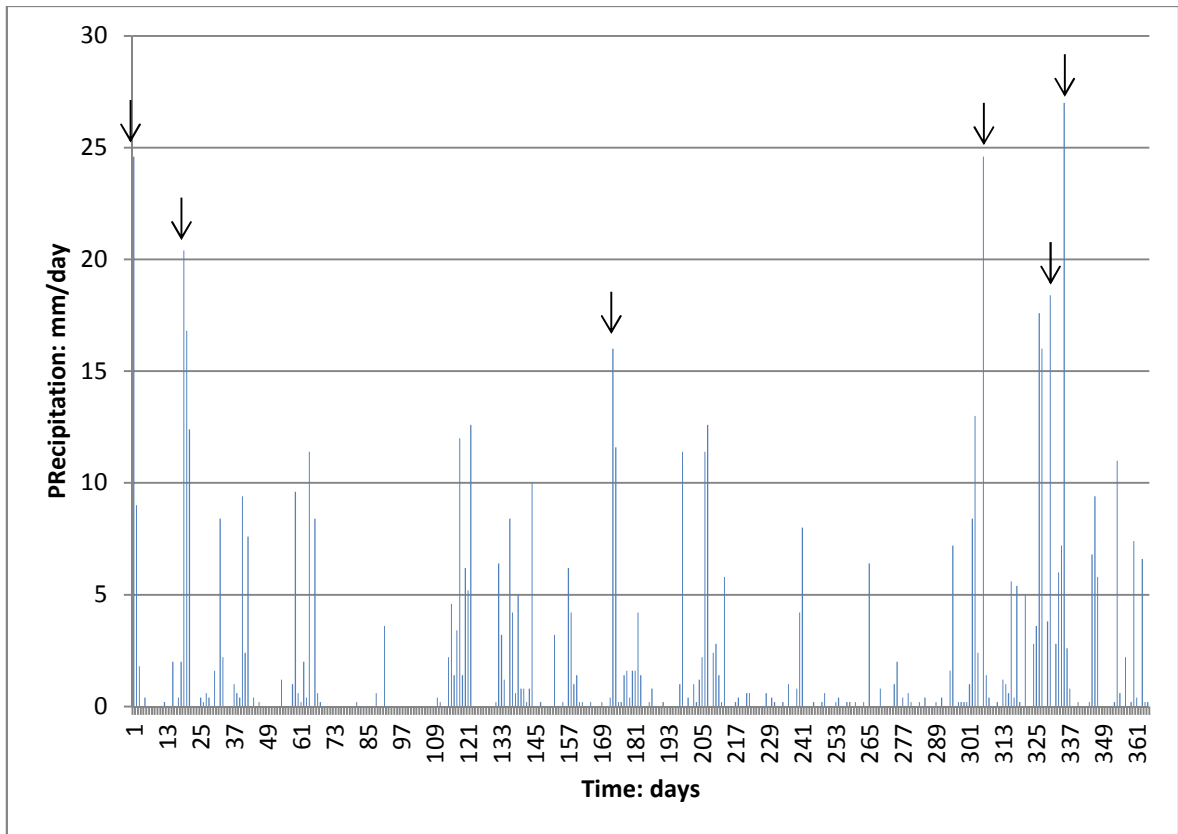
Figure 4-30: Daily precipitation amounts for the Newbury bypass cutting site throughout 2003, with arrows denoting extreme precipitation events.

Figure 4-31 shows the hourly precipitation data for each of the identified heavy rainfall days. On five of the six days the events last no longer than 10 hours, with the most intense part of the events lasting between 1 and 2 hours. The only exception to this is the rainfall event occurring on 1 December, when the event lasted for 13 hours and the rainfall intensity was fairly constant. These plots show that even when the heaviest rainfall events are short in duration the VADOSE/W model, using daily precipitation data can still replicate the hydraulic behaviour of the Newbury bypass cutting. When considering how well the results compare to those of Davies et al. (2008a), who used hourly precipitation data, this finding is further supported.

178
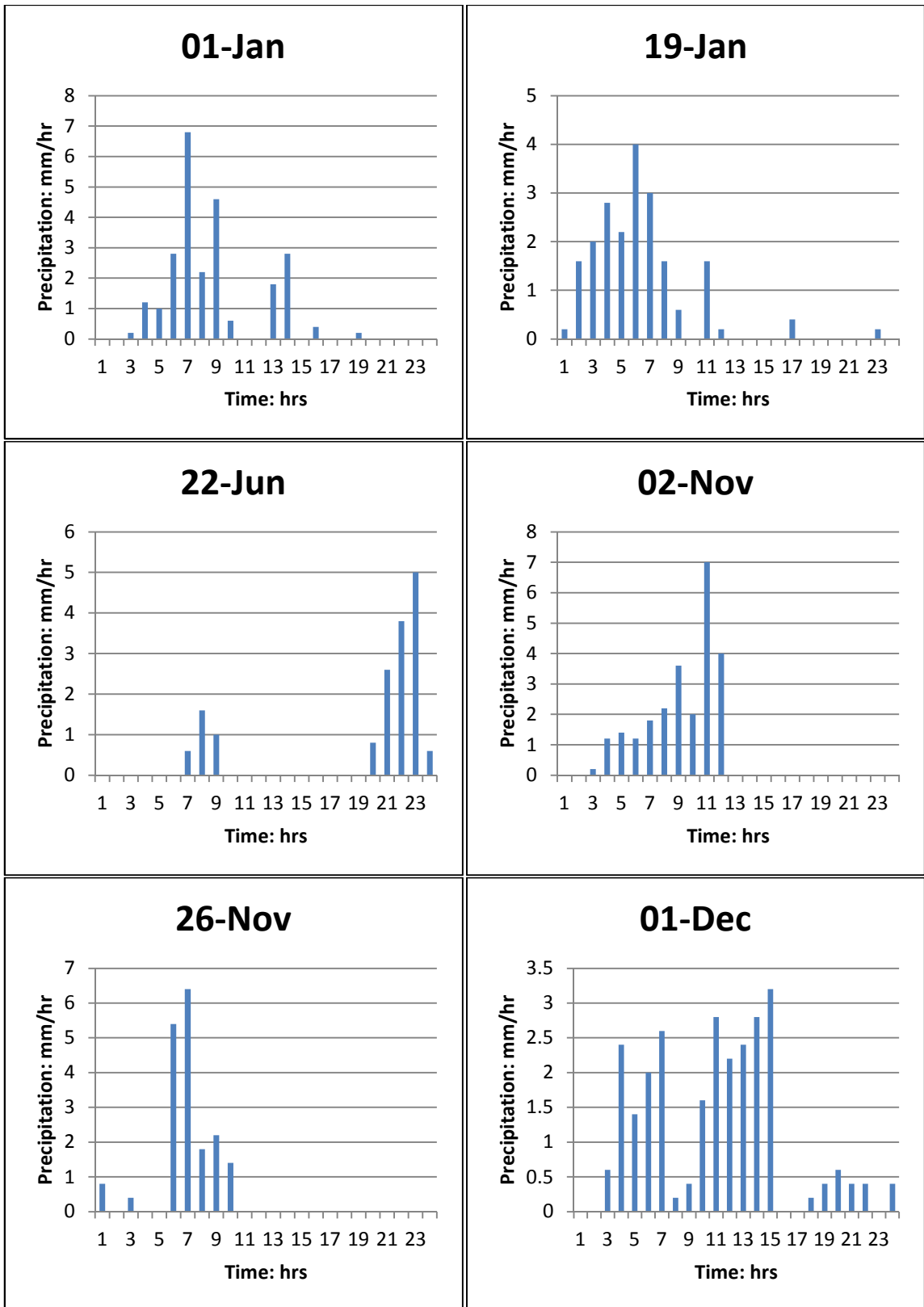
Figure 4-31: Hourly precipitation of heavy rainfall events for each of the identified days.

4.5.3.3 Material properties

In the literature review the probable effects of hysteresis (Section 2.9.3.4) and desiccation cracking (Section 2.10.2) on soil hydrology and the implications of not considering these for modelling were considered. It is thought that desiccation cracking of the soil can have a major influence on the hydraulic conductivity of soil and concurrently the magnitude of pore water pressures (Novak et al., 2000; Arnold et al., 2005; Fredlund et al., 2010a). Neither the effects of desiccation cracking or hysteresis have been included in this model.

4.5.3.3.1 Hysteresis

Hysteresis is the effect whereby a soil exhibits different suction magnitudes at the same soil moisture content depending on whether the soil is drying or wetting. Fredlund et al. (2011) suggest that for a clay soil the wetting curve may shift 100% of a log cycle laterally to the drying curve.
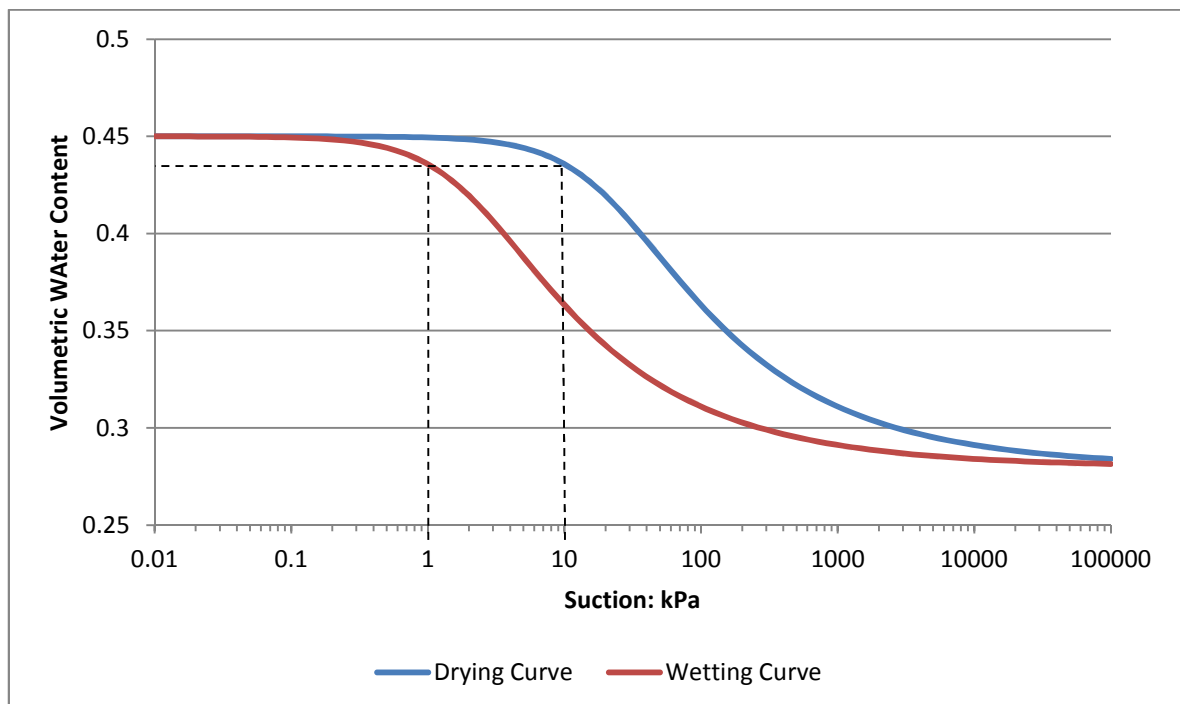
Figure 4-32: Drying and wetting curve of the London Clay SWCC generated with the parameter values shown in Table 4-1 and Equation 4-1 for the drying curve and applying a 100% log shift to obtain the wetting curve.

Figure 4-32 shows the effect of this on the London Clay SWCC used for the Newbury cutting slope model. On the drying curve at a volumetric water content of ~0.44 the suction is 10 kPa, whereas on the wetting curve it would be 1 kPa. As only the drying curve was used in the Newbury cutting model, the suctions could possibly be always being overestimated if the state of the soil is actually on the wetting curve. It should be noted that as the state moves from the drying curve to the wetting curve a wetting scanning curve would be followed. On this curve a small decrease in water content leads to much greater decreases in suction than on the drying curve and thus it is not only the representative suction at a given water content that will be different, but also the overall behaviour of the system.

It is possible that the Newbury model struggles to replicate the winter suctions due to not considering the effects of hysteresis. Throughout the summer the soil will mostly be drying, and using only the drying part of the SWCC has resulted in good replication of the end of summer suctions (Figure 4-25). After summer when the weather becomes wetter, it is more likely that soil, particularly in the top layers, will be wetting and therefore should be modelled by the wetting curve. Figure 4-33 shows the theoretical pore water pressures at the end of December 2003 obtained by applying a lateral shift the same as in Figure 4-32 to those actually calculated by the numerical model. The shift has only been applied to the pore water pressures in the top 2.0 metres of the soil profile, to reflect the section of the soil profile where the majority of wetting and drying processes occur.
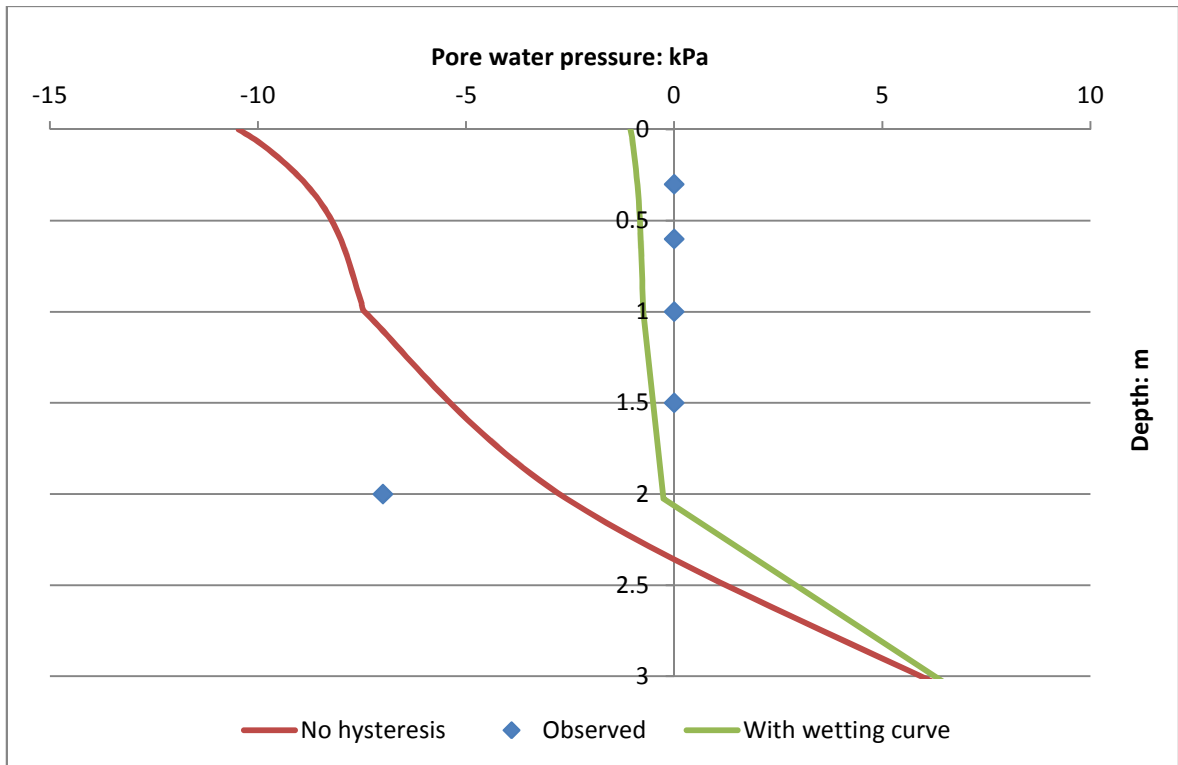
Figure 4-33: Theoretical results including the effects of hysteresis compared to the observed values and those calculated by the VADOSE/W model presented in Chapter 4.

Shifting the pore water pressures in the top 2.0 metres shows the potential for improved modelling results if the wetting curve was to be implemented. Clearly, the inclusion of the effects of hysteresis could be significant on the performance of a hydrological mode.

4.5.3.3.2   Desiccation cracking

Similar to the model of Davies et al. (2008c), desiccation cracking has not been included in this model. When desiccation cracking was investigated in the literature review (Section 2.10) a number of implications for soil hydrology and stability of slopes in the United Kingdom were found:

- Networks of desiccation cracks can directly control the soil's hydraulic properties, by allowing rapid infiltration of rainfall, giving elevated pore water pressures within the upper surface zone of the slope (Clarke and Smethurst 2010; Tang et al. 2011).

- By allowing easier infiltration of water, cracks effectively increase the hydraulic conductivity of the soil. The effects of soil cracking on hydraulic conductivity can in turn have a negative effect upon slope stability (Dijkstra and Dixon, 2010; Zhang et al., 2011); when rain falls, water will fill the cracks, softening and weakening the soil leading to possible failures in excavations, slopes, dams, and infrastructure slopes (Fang, 1994).
- The existence of cracks in a soil can lead to poor estimates of runoff and infiltration (Arnold et al., 2005), and in most soil-water-plant-atmosphere models their effects are inadequately described (Novak et al., 2000). Not accounting for the effects of desiccation cracking would lead to underestimated infiltration and overestimate of surface runoff. Indeed, tests have shown that the infiltration capacity of a cracked clay soil was more than twice that of the same soil without cracks (Novak et al., 2000).

Taking all these points into consideration it seems that the inclusion of desiccation cracking could be important for the proper modelling of temporal pore water pressures in the Newbury cutting slope. Including the effects of desiccation cracks on soil hydrology could improve modelling results especially when considering that the summer of 2003 was a particularly dry one which would result in significant crack networks potentially extending to the base of the summer drying zone (Clarke and Smethurst, 2010).

It is believed that the lack of inclusion of desiccation cracking is one of the causes of the poorer performance of the Newbury cutting VADOSE/W model when calculating the winter pore water pressure. In Chapter 5, a method for including the effects of desiccation cracking on the soil hydrology is developed.

4.6 Summary

In summary, the numerical model of the Newbury bypass cutting, developed and analysed in this chapter, has been relatively successful. By using suitable material properties, boundary conditions, including climate and vegetation, and model geometry the model was able to replicate the hydrology of the slope with some accuracy. The results compared favourably to those obtained by other authors

(Davies et al., 2008a) and the pore water pressure relationships and profiles generated for the end of summer and end of year compared well to those observed in the field (Ridley et al, 2004a; Vaughan et al., 2004).

The model performed better when calculating the high suctions developing in the slope throughout the summer, but experienced similar problems to Davies et al. (2008a) when replicating the dissipation of suctions at the end of the year. In the model, significant suctions were still present in the top 2.0 metres of the slope profile, whereas it had been observed by Smethurst et al. (2006) that these suctions had dissipated.

It was suggested that the most likely cause for the problems replicating this behaviour lies within the definition of the material properties. The inclusion of desiccation cracking or the effects of hysteresis, have both been suggested as possible ways that the model could be improved. Desiccation cracks develop throughout the summer and then act to increase the hydraulic conductivity of the soil. By including the effects of these cracks on the hydraulic properties of the soil, it is thought that the replication of winter pore water pressures could be improved. Soils display hysteretic behaviour, with separate soil water characteristics depending on whether the soil is drying or wetting. By accounting for this behaviour in the soil model it could be possible to improve the modelling results.

It was found that in the case of this model the use of daily climate data does not adversely affect the results of the model when compared to the use of hourly or even sub-hourly climate data. However it is important to stress that this may not be the case in all scenarios, particularly those with many short, extreme rainfall events whereby using daily data could easily underestimate runoff and therefore overestimate infiltration, ultimately leading to an incorrect water balance and calculation of pore water pressures.

It was decided that in the next chapter the effects of desiccation cracking would be focussed on. It is acknowledged that the effects of hysteresis can be great, but due to a lack of proper measurements of the wetting curve and the difficulty associated with

implementing hysteresis it was decided to focus efforts on establishing a method for including the effects of desiccation cracking on the slope hydrology.

5 Effects of desiccation cracks

5.1 Chapter Outline

In Chapter 5, steps are taken to improve the performance of the hydrological model that was developed in the previous chapter. Bimodal soil water characteristic curve and hydraulic conductivity functions are introduced, taking account of the effects of desiccation cracks by introducing a second pore series to the van Genuchten (1980) equation. New models have been run in Chapter 5 with the bimodal functions applied as the soil properties; the results are then compared to those obtained in Chapter 4 to judge the change in performance in predicting pore water pressures and suctions within the Newbury cutting slope achieved by the introduction of the new bimodal functions.

The structure of this chapter breaks down as follows:-

- Sections 5.2 and 5.3 – The bimodal equations are introduced and their development discussed. Results from an initial model run are presented.
- Sections 5.4.1 to 5.7 – Various sensitivity analyses on the parameters of the equations have been carried out with the intention of improving the performance of the model. The results of these analyses are then shown.
- Section 5.8 – The results are discussed in more detail.

5.2 Bimodal SWCC and HCF

In Section 2.10.2 of the literature review possible methods of including the effects of desiccation cracking into a hydrological model were investigated. It has been suggested that a bimodal soil water characteristic curve and hydraulic conductivity function could be used to represent the effects of cracking in desiccated soils

(Fredlund et al., 2010a). In this section a bimodal SWCC and complementary HCF, where cracks are implemented as a large pore series, are developed and presented. The model assumes that:

1. The soil can be separated into two distinct pore systems for the intact soil matrix and the cracks with separate hydraulic properties for each.

2. The system as a whole can be considered as a superposition of the two separate systems over the same volume – i.e. a continuum.

3. In the first development of the desiccation model cracks do not change volume as the soil wets or dries. In subsequent models the role of crack development through the year will be taken into account.

4. Cracks act as capillaries and water flows through these by capillary action. Therefore the Darcy and Richards equations for saturated and unsaturated flow in porous media can be applied.

The implications of these assumptions are investigated in the discussion at the end of this chapter (Section 5.8.1.2).

5.2.1 Developing the Bimodal SWCC Equation

Fredlund et al. (2010a) and Durner (1994) have suggested the use of bimodal equations to represent the effects of desiccation cracking in a hydrological model. This equation could be developed by combining SWCCs that are representative of the two separate parts of the desiccated soil; namely the soil matrix and the cracks themselves. Zhang and Chen (2005) suggest that any of the traditional closed-form equations could be used to form these bimodal equations; those of van Genuchten (1983) or Fredlund and Xing (1994) for example. In this work the closed-form equations of van Genuchten (1983) are used to develop the bimodal equations. These were chosen for consistency with the previous chapter.

Equation 5-1 defines the SWCC for the intact soil matrix and Equation 5-2 the SWCC for the cracks. In both equations θ_w is the volumetric water content at the suction Ψ. The parameters θ_r, θ_s, a, m, and n have the same meaning as in the VADOSE/W for of the van Genuchten equation (Equation 3-1), but with separate values for the soil part and cracks part denoted by the subscript *soil* or *crack*.

Equation 5-1

$$\theta_w = \theta_{r_{soil}} + \frac{\theta_{s_{soil}} - \theta_{r_{soil}}}{\left[1 + \left(\frac{\Psi}{a_{soil}}\right)^{n_{soil}}\right]^{m_{soil}}}$$

Equation 5-2

$$\theta_w = \theta_{r_{crack}} + \frac{\theta_{s_{crack}} - \theta_{r_{crack}}}{\left[1 + \left(\frac{\Psi}{a_{crack}}\right)^{n_{crack}}\right]^{m_{crack}}}$$

The bimodal SWCC was finally derived by combining the separate van Genuchten curves for the intact soil matrix and the cracks. Each equation is multiplied by its respective weighting factor, ϑ_{soil} for the soil matrix and ϑ_{crack} for the cracks. The meaning and derivation of these weighting factors is discussed in Section 5.2.3. The governing equation for the bimodal soil water characteristic curve is therefore:

Equation 5-3

$$\theta_w = \vartheta_{soil} \cdot \left[\theta_{r_{soil}} + \frac{\theta_{s_{soil}} - \theta_{r_{soil}}}{\left[1 + \left(\frac{\Psi}{a_{soil}}\right)^{n_{soil}}\right]^{m_{soil}}}\right]$$

$$+ \vartheta_{crack} \cdot \left[\theta_{r_{crack}} + \frac{\theta_{s_{crack}} - \theta_{r_{crack}}}{\left[1 + \left(\frac{\Psi}{a_{crack}}\right)^{n_{crack}}\right]^{m_{crack}}}\right]$$

Values for these parameters will be introduced from the literature (Section 5.2.4), and in Section 5.4 a sensitivity analysis will be carried out on parameter values to ascertain the sensitivity of the modelling results to these parameters.

5.2.2 Developing the Bimodal HCF Equation

The bimodal hydraulic conductivity function equation has been derived in the same manner as the bimodal soil water characteristic curve equation. Separate equations for each part of the desiccated soil were firstly defined; these were then combined to form the final bimodal HCF equation.

Equation 5-4 defines the HCF for the intact soil matrix and Equation 5-5 the HCF for the cracks. In both equations K_w is the hydraulic conductivity at suction Ψ. The parameters $K_s, \vartheta_r, \vartheta_s$, *a, m,* and *n* have the same meaning as in the standard van Genuchten Equation 2-23, but with separate values for the soil part and cracks part denoted by the subscript *soil* or *crack*.

Equation 5-4

$$K_w = K_{S_{soil}} \frac{\left[1 - \left(a_{soil}\Psi^{(n_{soil}-1)}\right)\left(1 + (a_{soil}\Psi^{n_{soil}})^{-m_{soil}}\right)\right]^2}{\left(((1 + a_{soil}\Psi)^{n_{soil}})^{\frac{m_{soil}}{2}}\right)}$$

Equation 5-5

$$K_W = K_{S_{crack}} \frac{\left[1 - \left(a_{crack}\Psi^{(n_{crack}-1)}\right)\left(1 + (a_{crack}\Psi^{n_{crack}})^{-m_{crack}}\right)\right]^2}{\left(((1 + a_{crack}\Psi)^{n_{crack}})^{\frac{m_{crack}}{2}}\right)}$$

The bimodal HCF equation was finally derived by combining the separate van Genuchten equations for the intact soil matrix and the cracks. Each equation is multiplied by its respective weighting factor, ϑ_{soil} for the soil matrix and ϑ_{crack} for the cracks. The governing equation for the bimodal hydraulic conductivity function is therefore given by Equation 5-6 on the following page.

Equation 5-6

$$K_w = \vartheta_{soil}.K_{S_{soil}} \frac{\left[1 - \left(a_{soil}\Psi^{(n_{soil}-1)}\right)\left(1 + \left(a_{soil}\Psi^{n_{soil}}\right)^{-m_{soil}}\right)\right]^2}{\left(\left((1 + a_{soil}\Psi)^{n_{soil}}\right)^{\frac{m_{soil}}{2}}\right)}$$

$$+ \vartheta_{crack}.K_{S_{crack}} \frac{\left[1 - \left(a_{crack}\Psi^{(n_{crack}-1)}\right)\left(1 + \left(a_{crack}\Psi^{n_{crack}}\right)^{-m_{crack}}\right)\right]^2}{\left(\left((1 + a_{crack}\Psi)^{n_{crack}}\right)^{\frac{m_{crack}}{2}}\right)}$$

5.2.3 Weighting Factors

In Section 5.2.1 and 5.2.2 it was shown that each part of the bimodal equation must be multiplied by its own weighting factor. The weighting factors determine the relative contribution of each part to the final bimodal equations. The weighting factor ϑ_{crack} is also known as the crack porosity which is simply the proportion of a unit volume of soil that is cracked (Section 2.10.1). Li and Zhang (2010) define the crack porosity by:

Equation 5-7

$$n_c = \frac{A_c}{A}$$

Where A_c is the cracked area of soil (through a 2D cross-section) and A is the total area of the soil through the section. Therefore the weighting factors used within the bimodal equations are defined as:

Equation 5-8

$$\vartheta_{crack} = n_c$$

Equation 5-9

$$\vartheta_{soil} = 1 - \vartheta_{crack}$$

5.2.4 Parameter Values

To run an initial test of the bimodal equations, values for the van Genuchten parameters of the crack part of the SWCC and the HCF were required. Values for the

hydraulic properties of a crack have been suggested by Gerke and van Genuchten (1993) for the hydraulic properties of a crack appearing in a fractured soil or rock matrix. The value for the crack porosity is a value observed by Arnold et al. (2005). This value is the maximum crack porosity observed in high plasticity clay. The values used for the intact soil part of the equation are the same used in Chapter 4 (Section 4.3.3). Table 5-1 details all the parameter values that were used in the initial model run that is detailed in Section 5.3. Following this initial test a sensitivity analysis was carried out, looking at the sensitivity of the modelling results to these parameters. This analysis is described in Section 5.4.

Parameter	Soil	Cracks
θ_r	0.28	0
θ_s	0.45	0.5
a	22.14 kPa	0.98 kPa
n	1.443	2
m	0.307	0.5
K_s	1e-7 m/s	2.3e-4 m/s
ϑ	0.982	0.018

Table 5-1: van Genuchten parameters for soil and cracks used in the bimodal model.

Figure 5-1 shows the bimodal soil water characteristic curve and hydraulic conductivity function defined by the parameter values given in Table 5-1. The effect of the cracks is clear, especially on the hydraulic conductivity function. There is an obvious bimodal shape to this curve. The maximum hydraulic conductivity of the soil, because of the inclusion of desiccation cracking, is now 3 orders of magnitude greater than that of the un-cracked soil.
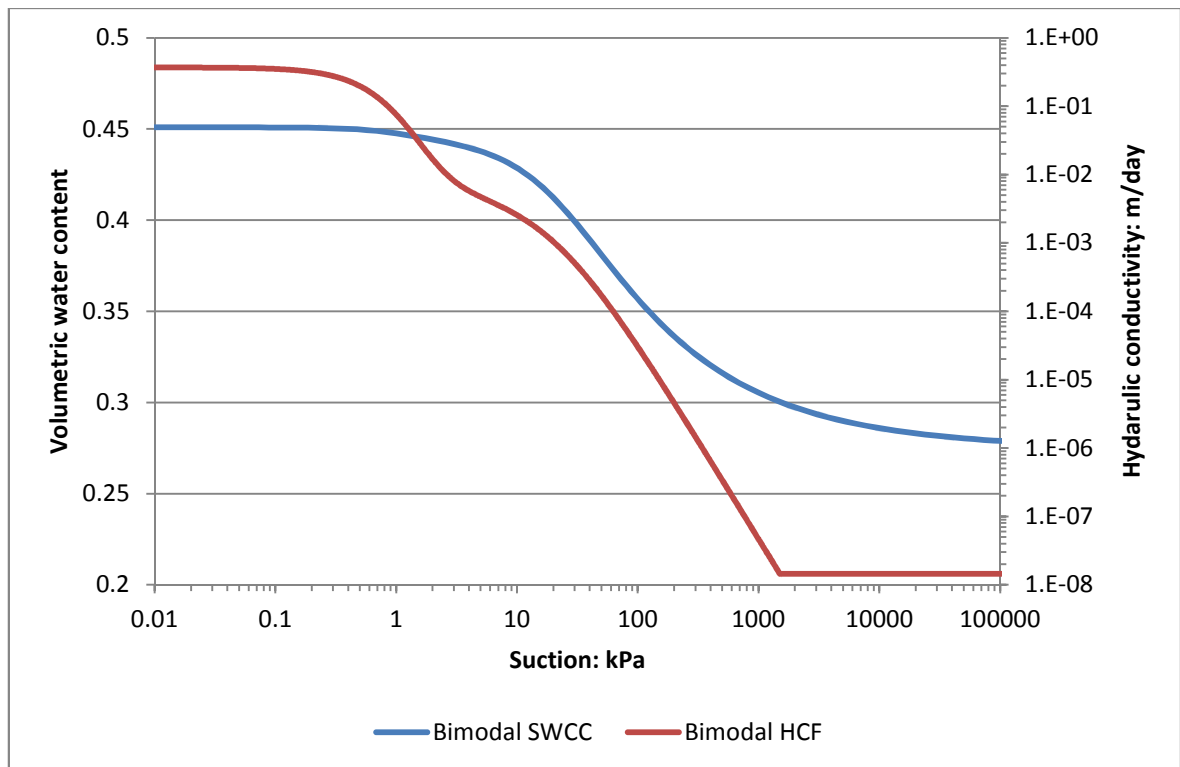
Figure 5-1: Bimodal SWCC and HCF defined with Equation 5-3 and Equation 5-6 respectively and the parameter values given in Table 5-1.

5.3   Initial Bimodal Hydrological Model

The purpose of this initial model was to gain some insight into how the bimodal equations function when implemented into a numerical hydrological model. It was not carried out with the intention of providing validation of the method; therefore it was assumed that the van Genuchten parameter values for the crack from Gerke and van Genuchten (1993) are correct (Table 5-1). Following on from the results of this model, further analyses were carried out, testing the sensitivity of the results to the van Genuchten parameters of the crack (Section 5.4.1 to 5.7). These final analyses were carried out with the objective of developing a final model, that implements the bimodal equations and that has been validated against the results of Smethurst et al. (2006).

5.3.1   Model Geometry, Boundary Conditions and Mesh

The model geometry, boundary conditions and finite element mesh used in this analysis is identical to the one used in Chapter 4. The only property of the model that

was changed was the material properties (Section 5.3.2). By using an identical model as was used in Chapter 4 the effects of the bimodal equations could be isolated. Figure 5-2 shows the model that was developed in Section 4.3. The development of each part of the model is detailed in the following sections from Chapter 4:

- Model geometry and far field boundary locations – Section 4.3.1 and 4.3.6
- Surface boundary condition – Section 4.3.4
- Initial conditions – Section 4.3.5
- Finite element mesh – 4.3.7
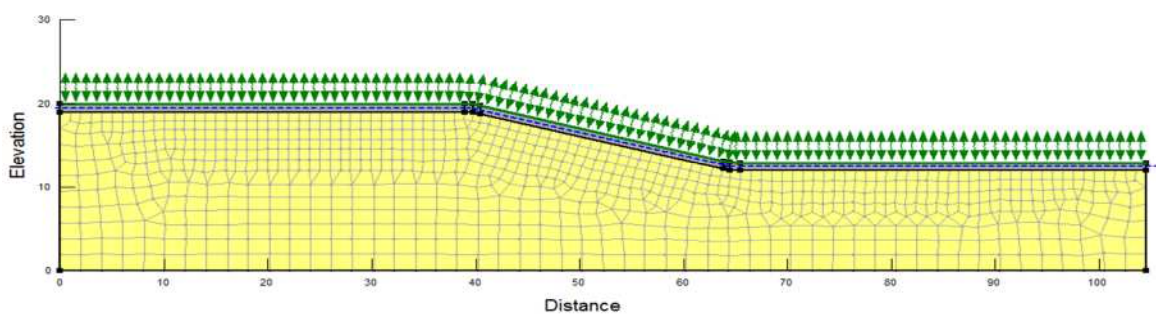
Figure 5-2: Model geometry used in this analysis, with finite element mesh and boundary conditions applied.

In summary the model has the following features:

- Impermeable bottom and far field boundary conditions.
- Climate surface boundary condition, including weather data and vegetation data.
- Initial conditions specified by an initial water table at a depth of 0.5 metres.
- A mesh of first order quadrilateral and triangular elements, consisting of 3272 elements and 3357 nodes.
- Hydraulic material properties defined by a bimodal soil water characteristic curve and a bimodal hydraulic conductivity function.

5.3.2 Material Properties

The bimodal functions shown in Figure 5-1 have been used in this initial model. The bimodal SWCC and HCF are implemented into VADOSE/W by the means of a 'data point function'. The values are copied from a spread-sheet into VADOSE/W which uses a spline function to connect the added points to complete the function for the

required suction range (Figure 5-3). The spline function is a mathematical technique used by GeoStudio to fill in gaps between adjacent data points with curved line segments (Geo-Slope, 2007).
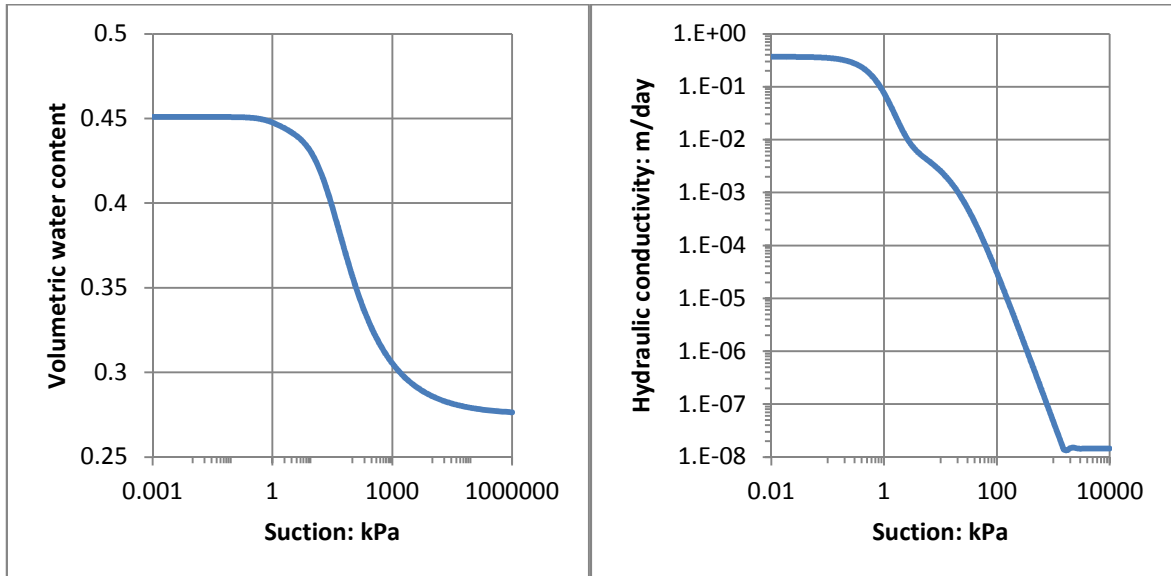
Figure 5-3: a) Bimodal SWCC and b) bimodal HCF.

The new, bimodal, material properties were applied to the surface layer of the model only. Soil properties in the rest of the model were the same as those in the model developed in Section 4.3.3. Observations of crack depths in the field are rare, but there are some recordings available. Inci (2008) stated that maximum crack depths of 1.0 metres had been observed in these types of soil whereas Arnold et al. (2005) measured that the majority of cracking (>70%) occurred in the top 1.5 metres of a clay soil profile. In this model, a crack depth of 1.0 metres was used. This value is consistent with some crack depths observed in the field (Inci, 2008) and also allowed the model from Chapter 4 to be utilised with no additional changes to the model geometry. As part of the sensitivity analyses carried out in this chapter, the effects of changing the crack depth were investigated (Section 5.7), which provides more insight into the function of the bimodal model.

Figure 5-4 shows a detail of the new bimodal model with the bimodal soil properties applied to the surface layer and the un-cracked London Clay soil properties applied to the rest of the soil profile. Initial conditions are also shown by the initial water table

(dashed line) and the surface vegetation and climate boundary condition (green arrows).
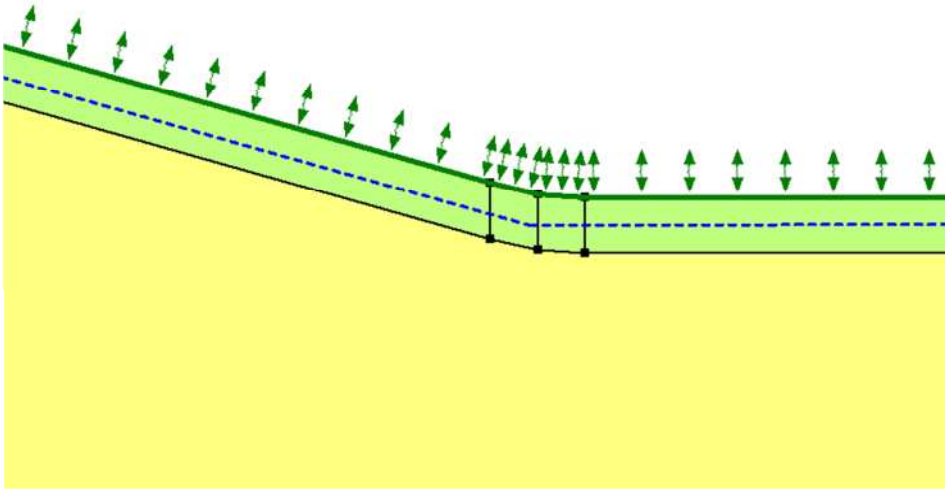
Figure 5-4: VADOSE/W model with the bimodal SWCC and HCF applied to 1 metre thick surface layer, shown in green.

5.3.3 Model Run

The model with the geometry, mesh, initial conditions, boundary conditions and material properties established in the previous sections (Section 5.3.1 and 5.3.2) has been run with 400 days of climate data applied. The model was run with the Newbury climate data (Section 4.3.4.1) from 1 January 2003 to the end of January 2004 covering the dates for which Smethurst et al. (2006) have recorded and published pore water pressure and suction data. These are also the dates which the model in Chapter 4 was run and therefore a direct comparison with the results obtained when desiccation cracking was not taken into account was possible.

5.3.4 Modelling results

Figure 5-5 and Figure 5-6 show pore water pressure and suction profiles at instrument group C. Previously, the model with no cracking included had successfully modelled these suctions and the new model, with bimodal soil functions, has modelled them with similar effectiveness. The first model struggled to calculate winter suctions, which had been observed to be completely dissipated.
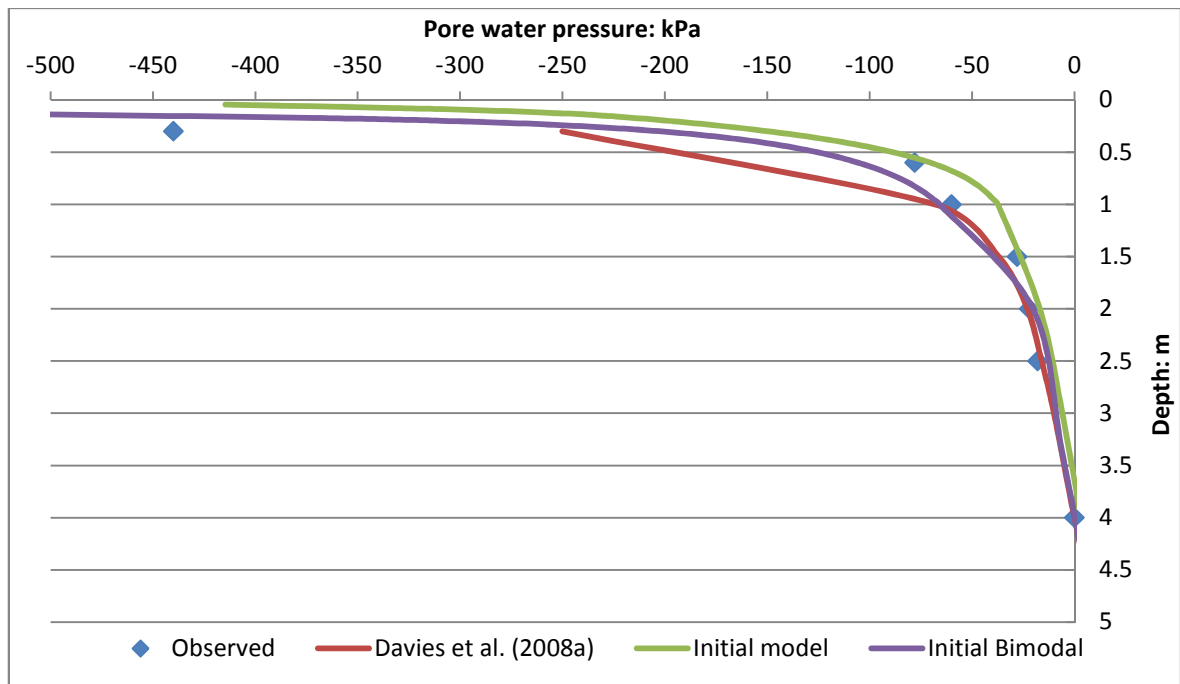
Figure 5-5: Suction profiles at the end of September 2003 at instrument group C for initial bimodal model. The results are compared to the observed values, the model of Davies et al. (2008a) and the results from Chapter 4 (referred to as initial model).

Figure 5-5 shows suction profiles at the end of September 2003 (time step: 275 days). With the bimodal functions applied in the surface layer, the model can still calculate the end of summer suctions with similar effectiveness as the initial model. In the top 0.5 metres the initial bimodal models actually performs better than the initial model. In Section 4.4.1 it was shown that the initial model did not perform as well as Davies et al.'s (2008a) when predicting the higher suctions developing in the top 0.5 metres of the slope profile.

Model	Suction at 0.3 metres
Observed	440 kPa
Davies et al. (2008a)	240 kPa
Initial model	150 kPa
Initial bimodal	200 kPa

Table 5-2: Observed and modelled suctions at a depth of 0.3 metres.

Table 5-2 shows the observed and modelled suctions at a depth of 3.0 metres. The bimodal model has improved the replication of suctions at this depth but still does not perform as well as the model of Davies et al. (2008a). It is still important to consider that Smethurst et al. (2006) recommend that the suctions measured by the equitensiometer are only indicative of the magnitudes of suctions at this depth. Figure 5-6 shows the pore water pressures in the slope at instrument group C at the end of December 2003. The initial VADOSE/W model, not including the effects of cracking, struggled to replicate the pore water pressures at this time of the year, as did that of Davies et al. (2008a).
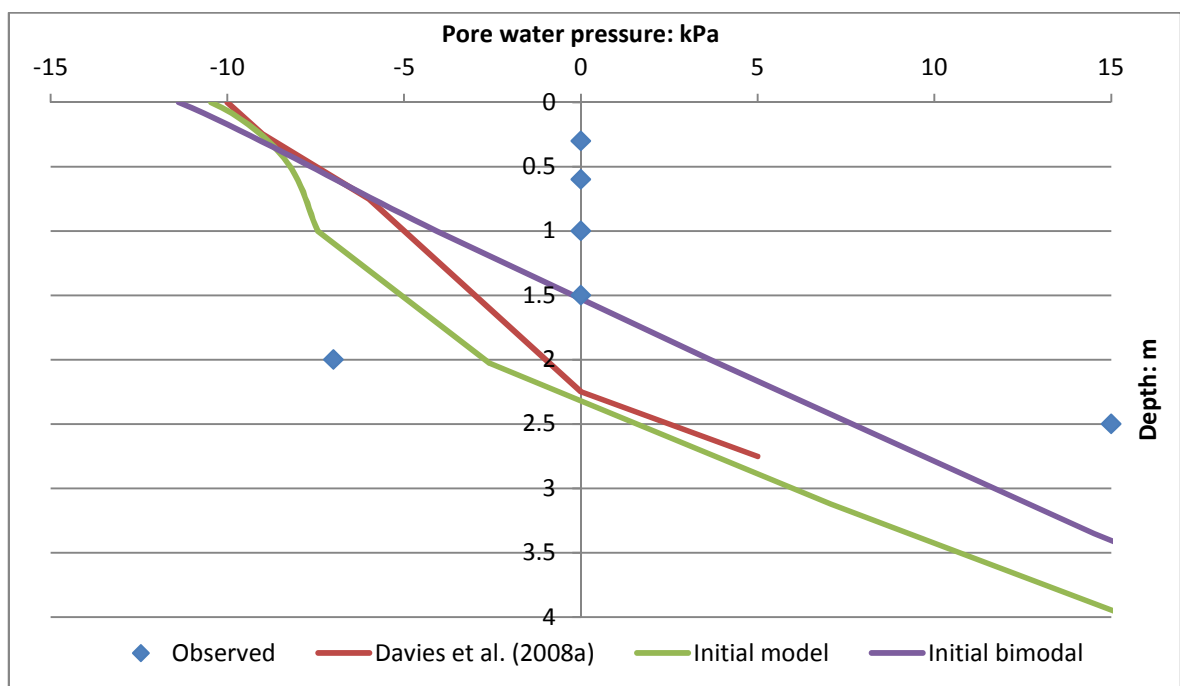
Figure 5-6: Suction profiles at the end December 2003 at instrument group C for initial bimodal model. The results are compared to the observed values, the model of Davies et al. (2008a) and the results from Chapter 4 (referred to as initial model).

Using the bimodal SWCC and HCF has affected the results at the end of December (365 days of model run time), but not significantly. Suctions of up to 11 kPa still remain in the slope, and a similar suction profile to the previous model can be observed to a depth of 0.5 metres. However, below this depth results are more promising. Below 0.5 metres depth suctions are generally 3 – 4 kPa less with the bimodal model applied. The location of the phreatic surface is also significantly higher

with the new model, at a depth of 1.5 metres, compared to 2.25 metres for the initial model and Davies et al. (2008a) model.

5.3.4.1 Long term behaviour

Figure 5-7 shows pore water pressure trends at various depths at the group C instrumentation location. In all sections (5.3.4.1 to 5.3.4.5) the model developed in Chapter 4 is referred to as the 'initial model' and the model with bimodal equations developed in Section 5.3 is referred to as the 'bimodal model'.

The pore water pressures observed by Smethurst et al. (2006), calculated by the initial model and calculated by the bimodal model are shown for time steps leading up to and after maximum suctions have occurred (240 days to 365 days). As shown by the observed suctions, there is a rapid increase in pore water pressures after maximum suctions. In the literature review (Section 2.10.2) it was discussed that this kind of behaviour could be caused by desiccation cracking in the soil. A very dry summer, such as the one that occurred in 2003 at Newbury (the year modelled here), results in significant desiccation cracking occurring in the soil slope. When followed by a very wet winter, as 2003 at Newbury was, the desiccation crack network can act as a preferential pathway for infiltrating water essentially increasing the permeability of the soil where it is cracked. The combination of heavy rainfall and increased permeability can result in sudden increases of pore water pressure and the dissipation of suctions. This can reduce short term stability as well as resulting in large pore water pressure cycles. Any hydrological model hoping to capture the effects of desiccation cracking on pore water pressure and suction trends should be able to recreate this behaviour. Therefore, analysing the results at the chosen time of the year should give a good indication of the relative performance of each model at capturing the effects of cracking.

Figure 5-7 reveals that neither model can actually fully replicate the pore water pressure and suction trends that occur within the Newbury cutting slope. However, by studying the graphs more thoroughly it can be shown that when including the bimodal functions, there is a better agreement between the observed and calculated

values and the general behaviour is replicated with much more precision. By considering magnitude, timing and rates it can be shown that the bimodal model is superior. Magnitude refers to the size of maximum and minimum suctions, timing refers to the point when maximum and minimum suctions occur and rate refers to the rate at which the pore water pressures increase after summer.
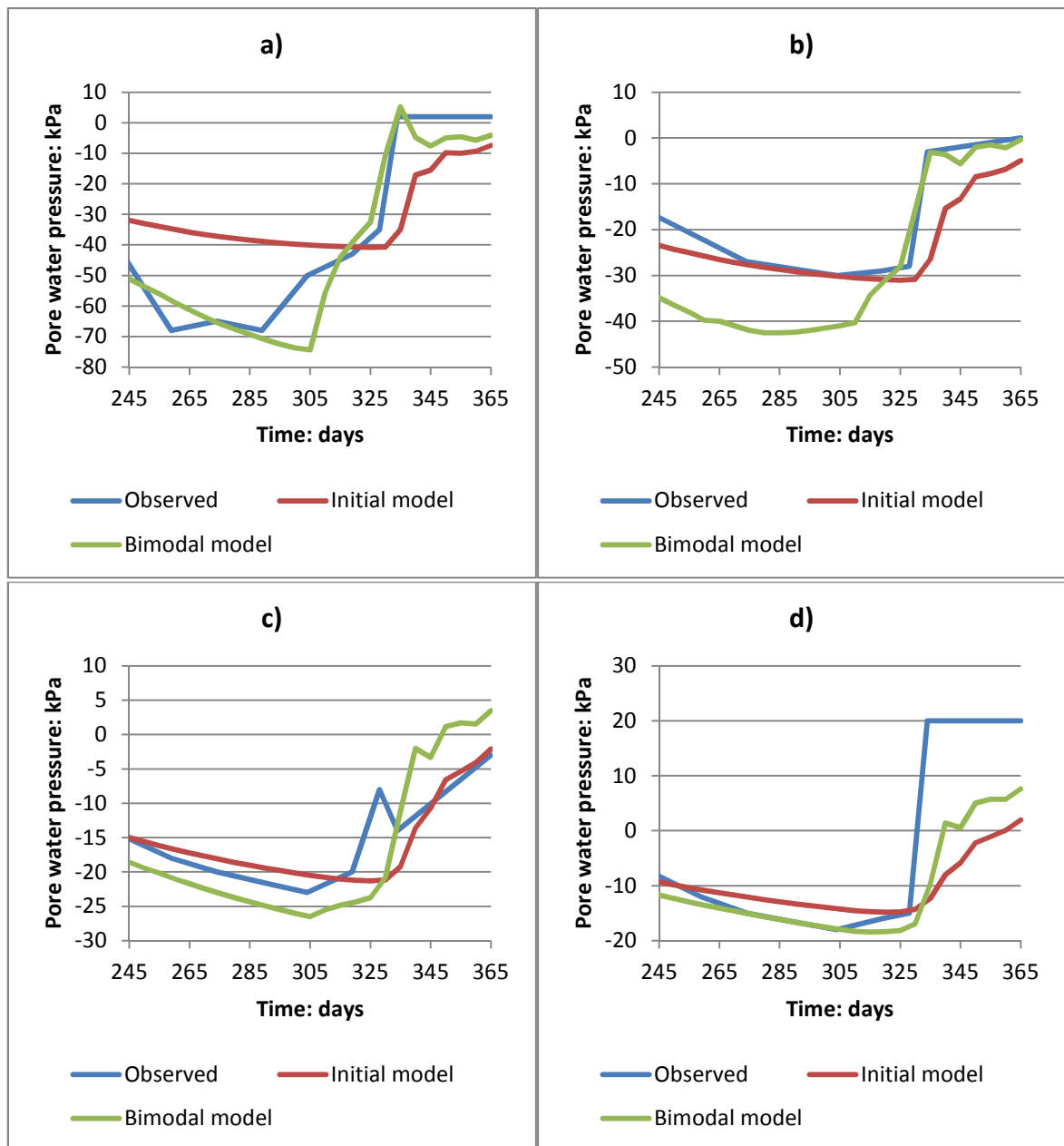
Figure 5-7: Temporal pore water pressures for observed, initial model (from Chapter 4, no cracks) and the bimodal model at a) 1.0 metres, b) 1.5 metres, c) 2.0 metres and d) 2.5 metres. The results are compared to the observed values and the results from Chapter 4 (referred to as initial model).

5.3.4.2 Magnitude

Table 5-3 shows the maximum and minimum suctions observed by Smethurst et al. (2006), calculated by the initial model (with no cracks present) and calculated by the bimodal at all four depths within the slope at the instrument group C location.

Depth		Observed	Initial	Bimodal
1.0 m	Maximum	-68 kPa	-40 kPa	-74 kPa
	Minimum	2 kPa	-7 kPa	5 kPa
1.5 m	Maximum	-30 kPa	-31 kPa	-42 kPa
	Minimum	0 kPa	-5 kPa	0 kPa
2.0 m	Maximum	-23 kPa	-21 kPa	-26 kPa
	Minimum	-3 kPa	-2 kPa	3 kPa
2.5 m	Maximum	-18 kPa	-14 kPa	-18 kPa
	Minimum	20 kPa	2 kPa	8 kPa

Table 5-3: Comparison of the magnitude of maximum and minimum suctions of the observed, un-cracked soil model and cracked soil model.

The models perform similarly well when predicting the magnitude of maximum suctions. The initial model significantly underpredicts the value at 1.0 metre depth but is accurate at the deeper locations. The bimodal model overpredicts by 10 kPa at a depth of 1.5 metres but again is accurate at all other depths. It is when predicting the magnitude of minimum suctions that the superiority of the bimodal model becomes more apparent. There is only one location where the initial model has predicted the minimum suctions better than the bimodal model. The bimodal model predicts minimum suctions more accurately at three of the four depths. At a depth of 1.0 metre the difference between observed and calculated falls by 66 %, at 1.5 metres by 100 % and at 2.5 metres by 33 %.

The bimodal model, despite its improved performance over the initial model, is not infallible. With the intention of improving the bimodal model, further sensitivity analyses have been carried out on the parameter values used for the bimodal

functions and also the crack depth. These analyses are described in proceeding sections (5.4.1 to 5.7).

5.3.4.3 Timing

This section looks at the timing of the occurrence of maximum and minimum suctions at each of the four depths. Results from the initial model with no cracks present and the bimodal model are compared with the observed values (Smethurst et al., 2006). Table 5-4 on the following page shows the results of this analysis.

Depth		Observed	Initial	Bimodal
1.0 m	Maximum	289 days	330 days	305 days
	Minimum	334 days	365 days	335 days
1.5 m	Maximum	304 days	325 days	280 days
	Minimum	365 days	365 days	365 days
2.0 m	Maximum	304 days	325 days	305 days
	Minimum	365 days	365 days	365 days
2.5 m	Maximum	304 days	325 days	310 days
	Minimum	334 days	365 days	365 days

Table 5-4: Comparison of the timing of maximum and minimum suctions of the observed, un-cracked soil model and cracked soil model.

The bimodal model predicts the timing of the occurrence of maximum and minimum suctions at all depths either as well or better than the initial model. When predicting maximum suctions the initial model lags behind the observed behaviour, generally occurring 20 days after the observed and up to 40 days (depth of 1.0 metres). The bimodal model predicts the occurrence of maximum suctions within 15 days at all depths, and within 1 day and 6 days at depths of 2.0 metres and 2.5 metres respectively. In percentage terms, the difference between the calculated occurrence and observed occurrence decreases by 60 % at 1.0 metre, 95 % at 2.0 metres and 70 % at 2.5 metres.

When considering the occurrence of minimum suctions the bimodal model performs better than the initial model. The initial model again lags behind at a depth of 1.0 m, predicting the minimum suctions to occur 31 days after they were actually observed to, whereas the bimodal model predicts within 1 day. At depths of 1.5 and 2.0 metres the suctions are still decreasing so it is difficult to say how well the timing is predicted; there is no observed data past 365 days. At 2.5 metres both the initial and bimodal models have struggled to match the observed behaviour with minimum suctions not actually being reached within the 365 days whereas they were observed to first occur at 335 days. In percentage terms, the difference between the calculated occurrence and observed occurrence decreases by 97 % at 1.0 metre, but offers no improvement at the other depths.

5.3.4.4 Rate

From Figure 5-7 it is shown that in the observed behaviour, after maximum suctions have occurred, there is initially a slow increase in pore water pressures which then becomes very rapid as the suctions fall to a minimum value. This behaviour is most clear at depths of 1.5 metres and 2.5 metres. The bimodal model is far better at replicating this behaviour. The maximum rate at which suctions are falling is matched at depths of 1.0, 1.5 and 2.0 metres by the bimodal model and is closer at 2.5 metres than the initial model. By including the effects of desiccation cracking on the hydraulic properties of the soil, water is able to infiltrate to greater depths quicker, increasing the rate at which suctions are dissipated. By looking at the precipitation data used in this model it can be seen that this sudden increase in pore water pressures corresponds with heavy rainfall events (Figure 5-8). The initial model has clearly been unable to replicate the effects of this; there is a significant lag between the first heavy rainfall events (around day 300) and pore water pressures beginning to increase (day 330), and when they do increase the rate is not as high as would be expected. Conversely, when desiccation cracking has been taken into account the lag between the rainfall events and pore water pressures increasing is ~5 days and the trends follow the observed much more closely.
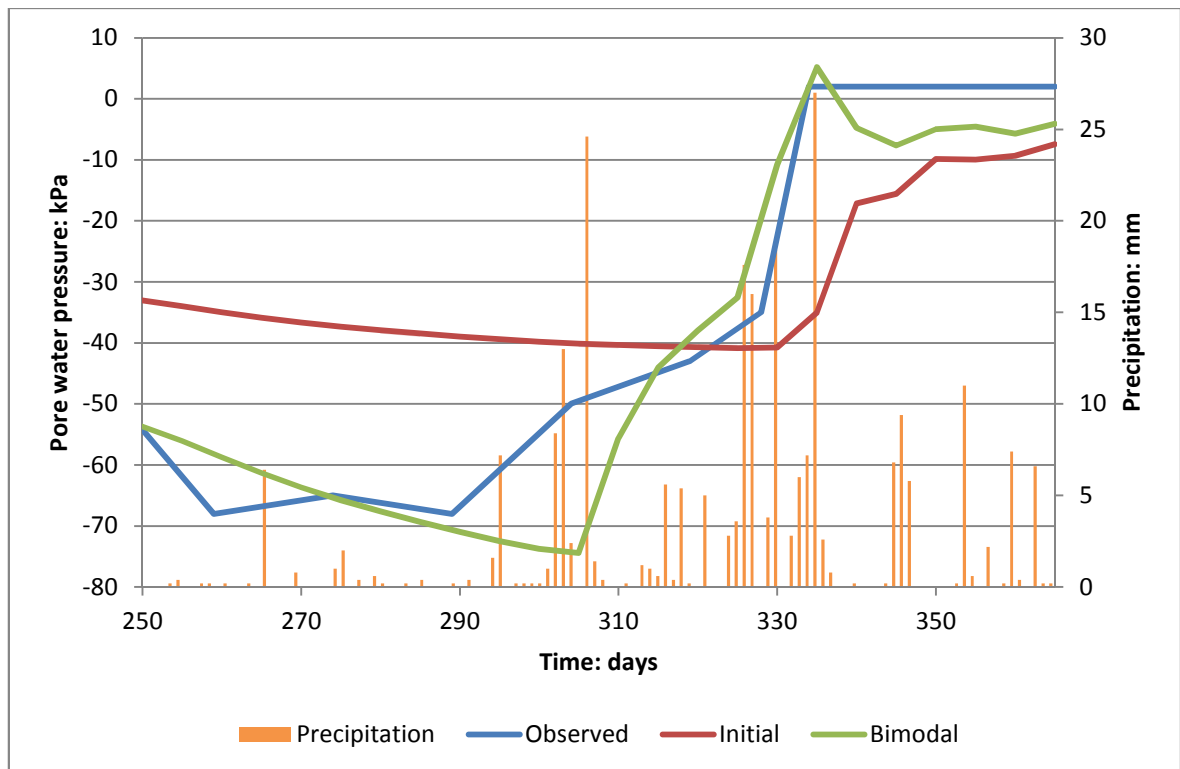
Figure 5-8: Temporal pore water pressures for observed, initial model (from Chapter 4, no cracks) and the bimodal model at a) 1.0 metres compared to recorded precipitation events.

5.3.4.5 Summary

The initial results of the bimodal model are promising, particularly when considering the pore water pressure trends. The use of a bimodal soil water characteristic curve and hydraulic conductivity function has improved the finite elements model's ability to replicate the pore water pressure and suction trends within the Newbury bypass cutting. However, there are still some deficiencies; the model, with the parameters defined in Table 5-1, has still not been able to fully match the observed minimum suction profile (Figure 5-6), with suctions of up to 11 kPa still present.

There may be a multitude of reasons why the model still struggles with the winter pore water pressures. For example the crack depth used was only 1.0 m, but observations in other high plasticity clays have shown cracks in these types of soil can extend to much greater depths than this (Arnold et al., 2005; Nahlawi and Kodikara et al., 2006). Similarly, the crack porosity and other parameters used to define the bimodal functions may be representative of a soil with 'small cracks'. Both of these

factors could influence the ability of water to infiltrate the slope with greater ease, leading to the dissipation of suctions that was observed in the Newbury bypass cutting at the end of December 2003.

In the following sections further development of the model shall be explored, beginning with sensitivty analyses of the crack porosity (Section 5.4.1) and also the van Genuchten parameters used to define the bimodal soil water characteristic curve and hydraulic conductivity function (Section 5.4.3. and Section 5.4.4). The effects of increasing the crack are also investigated in the crack depth analysis which is described in Section 5.7.

5.4 Sensitivity Analyses

In the sensitivity analyses presented in this section the influence of the crack porosity and the van Genuchten parameters a and n on the modelling results are investigated. The physical meaning of each parameter is considered and their respective effects on the bimodal functions is described.

5.4.1 Crack Porosity Sensitivity Analysis

In the bimodal model a crack porosity value of 0.018 was used. This value was reported in the literature (Arnold et al., 2005). Compared to other values that have been found (Table 5-5) this is relatively low and therefore may represent a comparatively low crack volume soil. This low crack porosity may explain why suctions were not fully dissipated, as sufficient water was still not able to infiltrate into the slope. By increasing the crack porosity this problem could be negated, by creating more pathways for water to infiltrate from the slope surface.

In the literature review a number of observed crack porosities were identified. A number of these have been chosen to carry out a senstivity analysis of the calculated pore water pressures to the magnitude of the crack porosity. In Table 5-5 the crack porosities used in this analysis are shown. Section 5.2.3 describes how crack porosity is calculated using Equation 5-7.

Crack Porosity	Soil Type	Reference Source
0.025	Silty Clay	Li and Zhang (2010)
0.046	Clay	Novak et al. (2000)
0.0658	Clay	Novak (1999)
0.078	Clay	Novak (1999)

Table 5-5: Crack porosity values used in crack porosity sensitivity analysis.

5.4.1.1 Crack Porosity Sensitivity Analysis Results

The bimodal model has been re-run with each of the crack porosities detailed in Table 5-5, with all other parameters, boundary conditions and time stepping the same as in the initial run and the bimodal run. End of summer (maximum suctions) and end of year (minimum suctions) profiles have been created (Figure 5-9 and Figure 5-10 respectively). The results of the model with a crack porosity of 0.078 are compared to the observed values and to the results from the initial bimodal model run.
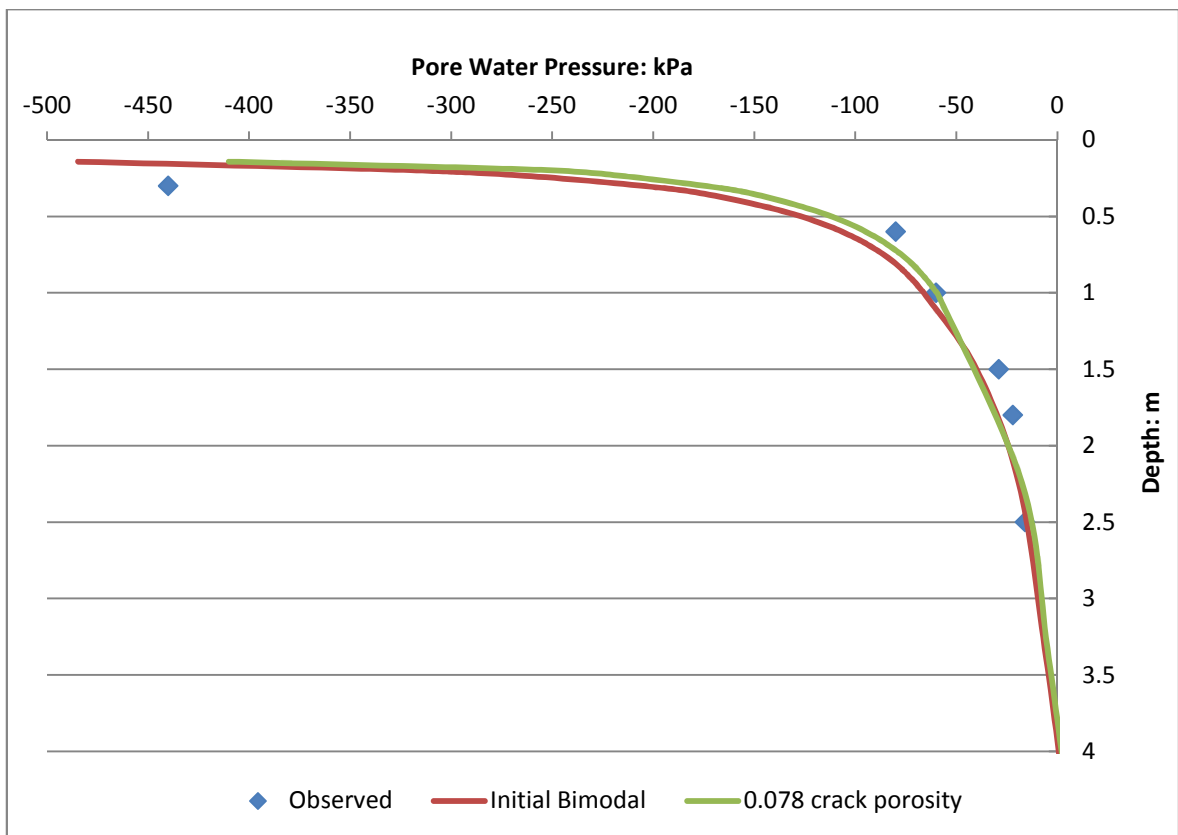
Figure 5-9: Results of the crack porosity sensitivity analysis; 275 days suctions profile. The results of the first bimodal model (Section 5.3.4) are represented by the red line.

205

Increasing the crack porosity does not unduly affect the calculated suctions at the end of summer (275 days). The observed values are still acceptably modelled and at some points better than the initial bimodal model (between depths 0.5 metres and 1.0 metres). The results from the other porosities were very similar to the above and have therefore been omitted to maintain clarity of the graph.
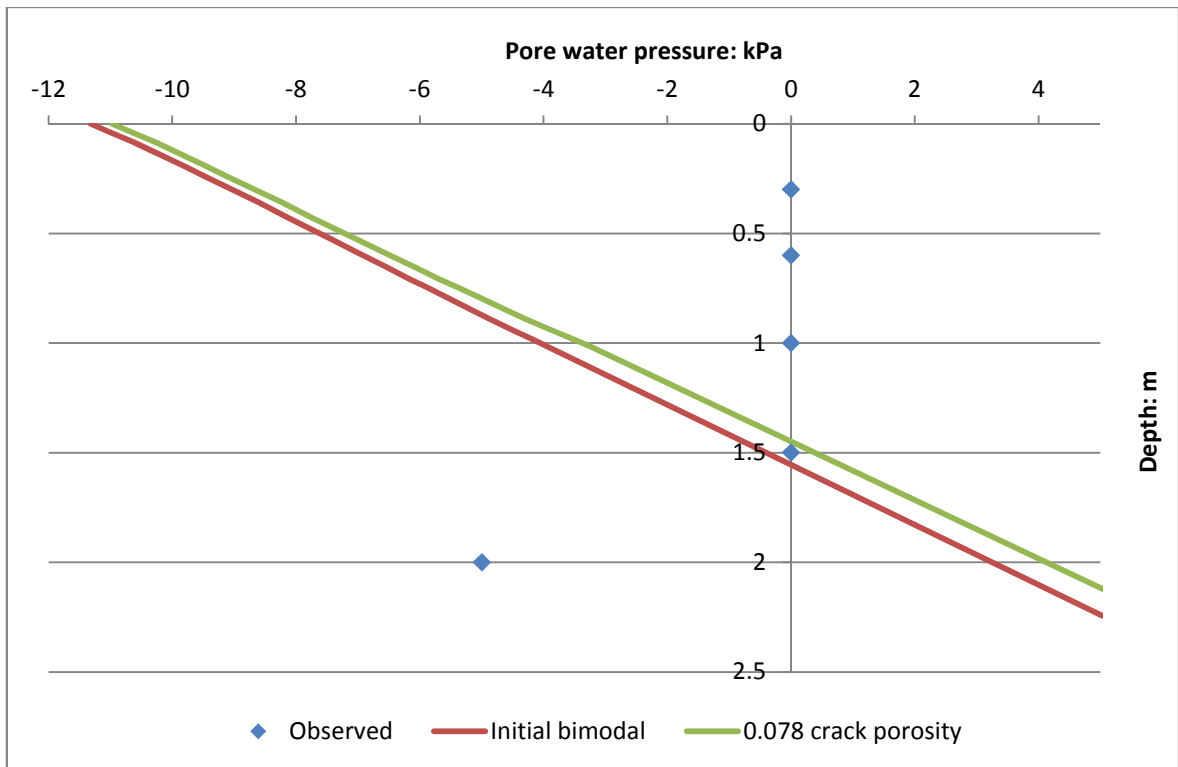
Figure 5-10: Results of the crack porosity sensitivity analysis; 365 days suctions profile. The results of the first bimodal model (Section 5.3.4) are represented by the red line.

In Figure 5-10 only the model with a crack porosity of 0.078 is shown for the end of year suctions because the effects of increasing the crack porosity were so small. There has been a very small decrease in suctions, by 0.4 kPa at the slope surface increasing with depth to 0.9 kPa at 1.5 metres.

5.4.2 Van Genuchten Parameters Sensitivity

It has been shown in the crack porosity sensitivity analysis (Section 5.4.1) that simply increasing the crack porosity has no significant effect on the calculated suctions within the slope profile. In the first bimodal model and the crack porosity sensitivity

analysis the van Genuchten parameters used in the bimodal equations have been the same (Table 5-1). However, when the physical meaning of increased crack porosity is considered it would seem erroneous that these parameters would be constant.

As the size and number of cracks in a given area of soil increases, the crack porosity must also increase. The implications this has on the van Genuchten parameters used to define the bimodal functions can be explained by considering how the parameters vary for different soil types, with differing grain size distributions. In the literature review (Section 2.9.3) it has been explained how soils with larger pore sizes drain more freely, with steeper water retention curves a consequence of this. Figure 5-11 illustrates how water retention curves can change as the ability for a soil to drain water quickly increases. Three separate soil water characteristic curves have been created, each representing soils of differing drainage properties. Table 5-6 details the parameter values used to generate each of the curves.
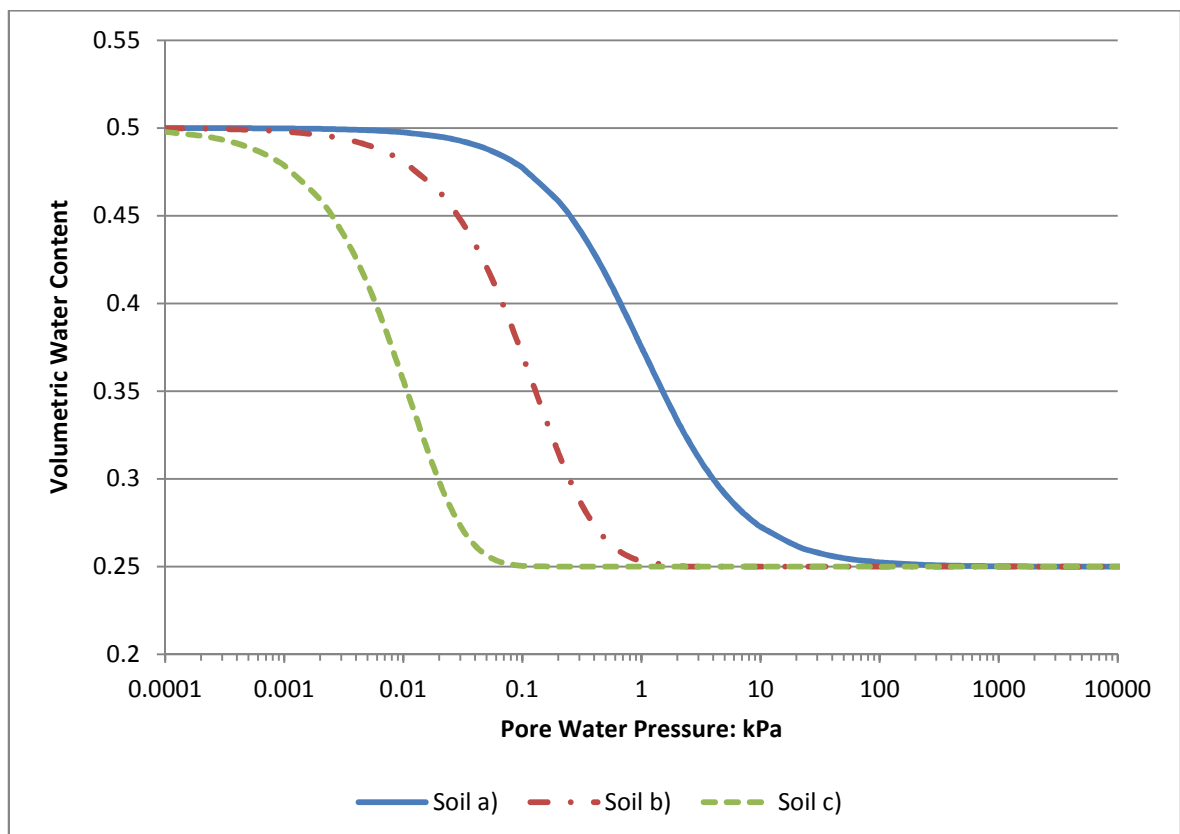
Figure 5-11: Comparison of SWCCs for three soils of differing drainage properties, defined with Equation 4-1 and the parameter values givin in Table 5-6.

Parameter	Soil a)	Soil b)	Soil c)
θ_r	0.5	0.5	0.5
θ_s	0.25	0.25	0.25
a	1	0.5	0.1
n	2	5	10
m	0.5	0.8	0.9

Table 5-6: van Genuchten parameters used to define the representative soil water characteristic curves shown in Figure 5-11.

Soil c) is a soil that drains very easily compared to the other soils, a) and b). The parameters that have changed to result in this water retention curve are 'a' and 'n'. The parameter 'a' defines a pivot point about which 'n' changes the slope of the function; therefore a soil with a low value of 'a' will start to fall from saturated water content before one with a high value. If this concept is extended to the crack system developing in a desiccated soil it would seem logical that when applying the bimodal van Genuchten model a system with greater crack size and crack density should have different van Genuchten parameters that reflect this hydraulic behaviour.

In the next sections (Section 5.4.3 and 5.4.4) the sensitivity analyses of the 'a' and 'n' van Genuchten parameters that were carried out are described.

5.4.3 'a' Parameter Sensitivity Analysis

An analysis of the van Genuchten parameter 'a' was carried out to investigate the effects of altering this parameter on the calculated pore water pressures and suctions in the bimodal model. As discussed in Section 5.4.2 the value of 'a' should be reduced when crack porosity is increased, and therefore the following values were considered:

1. a = 0.75
2. a = 0.5
3. a = 0.25

These values of 'a' were applied to the bimodal van Genuchten equations (Equation 5-3 and Equation 5-6), other parameters, including those for the intact soil part of the bimodal equations, are unchanged from those in Table 5-1. Figure 5-12 shows the

effects on the soil water characteristic curve of reducing the 'a' parameter. The dotted line shows the model with the lowest value of 'a'; the effect of reducing this parameter is clear, the soil starts draining at lower suctions. The functions are shown in the suction range 0.01 kPa to 100 kPa (outside this range the functions are identical).
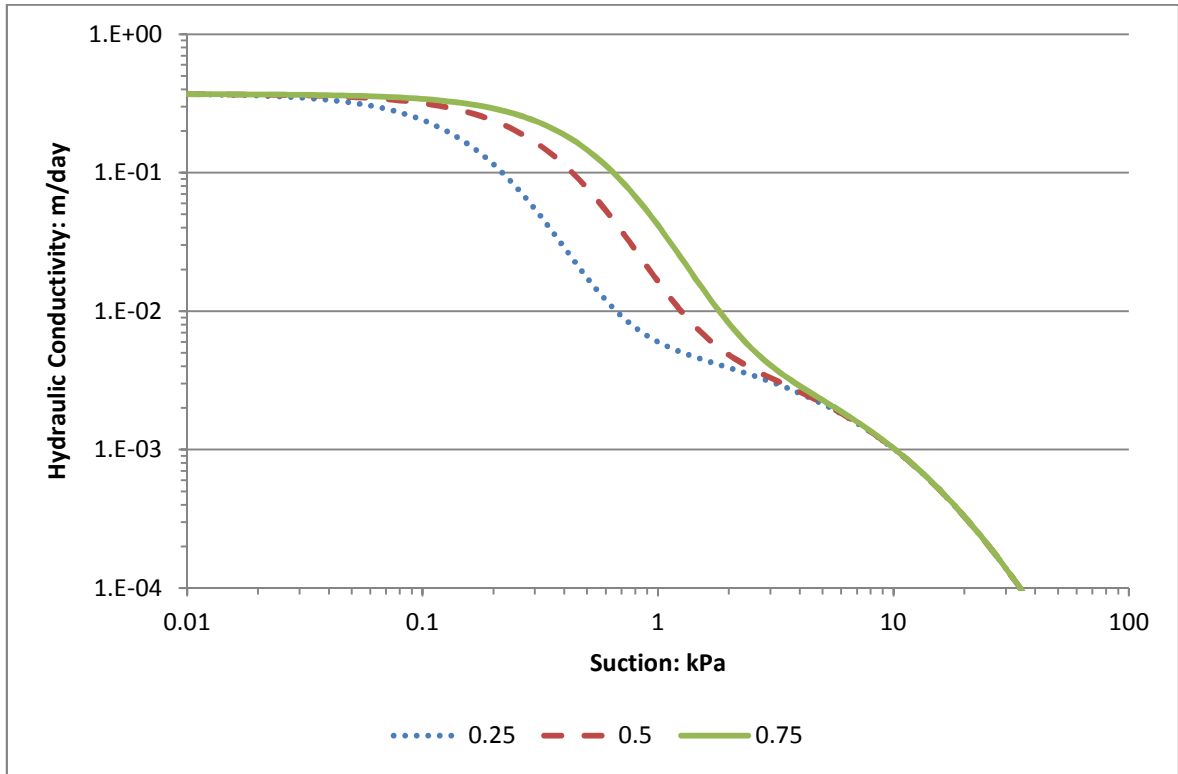
Figure 5-12: Effects of 'a' van Genuchten parameter on the shape of the bimodal HCF. Curves are produced with Equation 5-6.

The model was run with each of these bimodal functions applied, again for 400 days of climate. The same climate and vegetation surface boundary condition was applied and the model geometry and mesh density was kept the same.

5.4.3.1 'a' Parameter Sensitivity Analysis Results

Figure 5-13 shows the suction profiles at instrument group C at 275 days and 365 days respectively for each of the sensitivity analysis models compared against the first bimodal model results (Section 5.3.4) and the observed suctions.
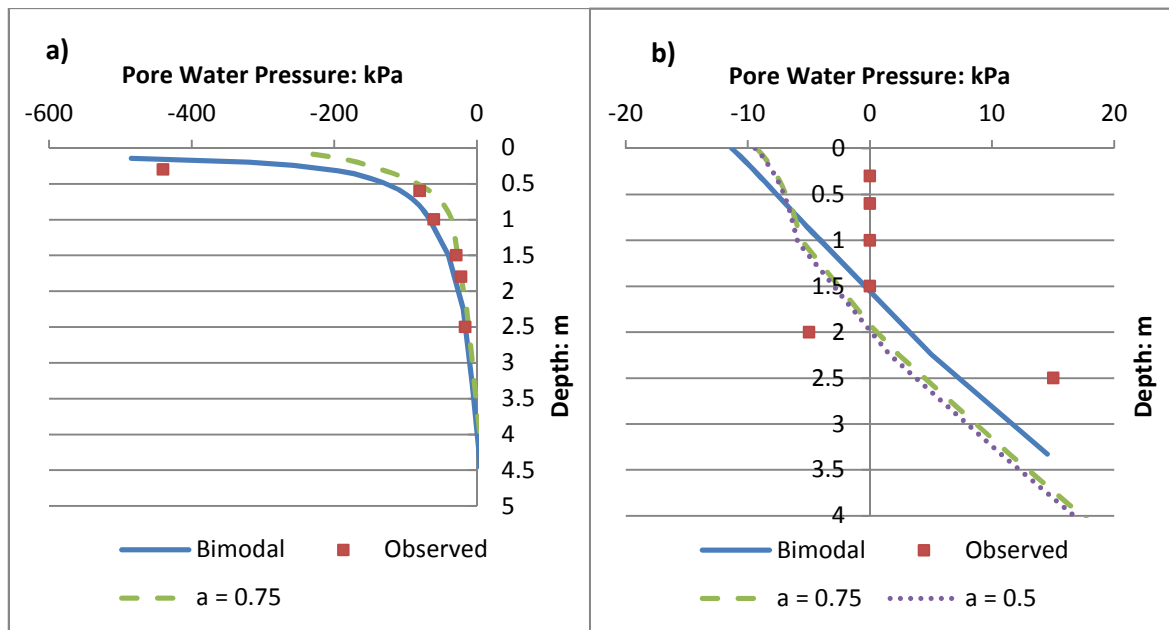
Figure 5-13: Results of the 'a' sensitivity analysis; showing pore water pressure profiles at mid-slope, at a) 275 days and b) 365 days. Results are compared to the first bimodal results (Section 5.3.4) and the observed results.

Figure 5-13 a) shows the profile at 275 days. Reducing the 'a' parameter is shown to have a negative impact on the ability of the model to predict the suctions at this time of the year. The shape of the profile is not as well predicted and the maximum suctions are not matched. This result highlights the problem of assuming no change of volume of the cracks throughout the year. By prescribing a lower 'a' parameter it assumes that the soil, as a whole, can drain water quicker, and by extension there is a greater crack density with larger cracks present. At the start of the year this may not be realistic as cracks will have shrunk from their maximum size as water infiltrates after maximum suctions have occurred. A possible solution to this problem would be the inclusion of separate bimodal models to represent the evolution of cracks throughout the year; an idea that is investigated further in Section 5.7.

The profile at 365 days (Figure 5-13 b)), shows that suctions in the slope profile are sensitive to the value of 'a' used in the cracking part of the bimodal equations. The effect is not large but is noticeable; by reducing the value of 'a' suctions at the slope surface are of a lesser magnitude than using higher values. The maximum suction (at the slope surface) has reduced from 11 kPa to 9.1 kPa. It is noted that the effects of reducing the value of 'a' below 0.75 are negligible (results for the 'a' = 0.25 test have been omitted from Figure 5-13 a) and b) for this reason.

Reducing the value of 'a' also affects suctions in the deeper part of the slope; below a depth of approximately 0.75 metres the suctions are greater than the initial bimodal model. This sensitivity analysis has not fully considered the effects of greater crack size on the van Genuchten parameters; the value of the 'n' parameter should also be tested. Therefore a sensitivity analysis of the magnitude of the 'n' parameter was also carried out. This analysis is described in Section 5.4.4.

5.4.4 'n' Parameter Sensitivity Analysis

In the van Genuchten equation for the SWCC (Equation 5-1) the 'n' parameter governs the steepness of the curve as it falls from saturated water content to residual water content. Similarly to the 'a' parameter, 'n' has different values for different types of soil. Soils with large pores that drain well have larger values of 'n' and hence a large crack should also have a larger value.

Three values of 'n' are tested in this analysis:
1. n = 3
2. n = 5
3. n = 7

Figure 5-14 shows the hydraulic conductivity functions created for each of these tests, in the suction range 0.1 kPa to 10 kPa (outside this range the functions are identical). Higher values of 'n' result in steeper curves. Steep SWCCs are synonymous with well-draining soils. The model is run with each of these bimodal functions applied, again for 400 days of climate. The same climate and vegetation surface boundary condition is applied and the model geometry and mesh density is kept the same.
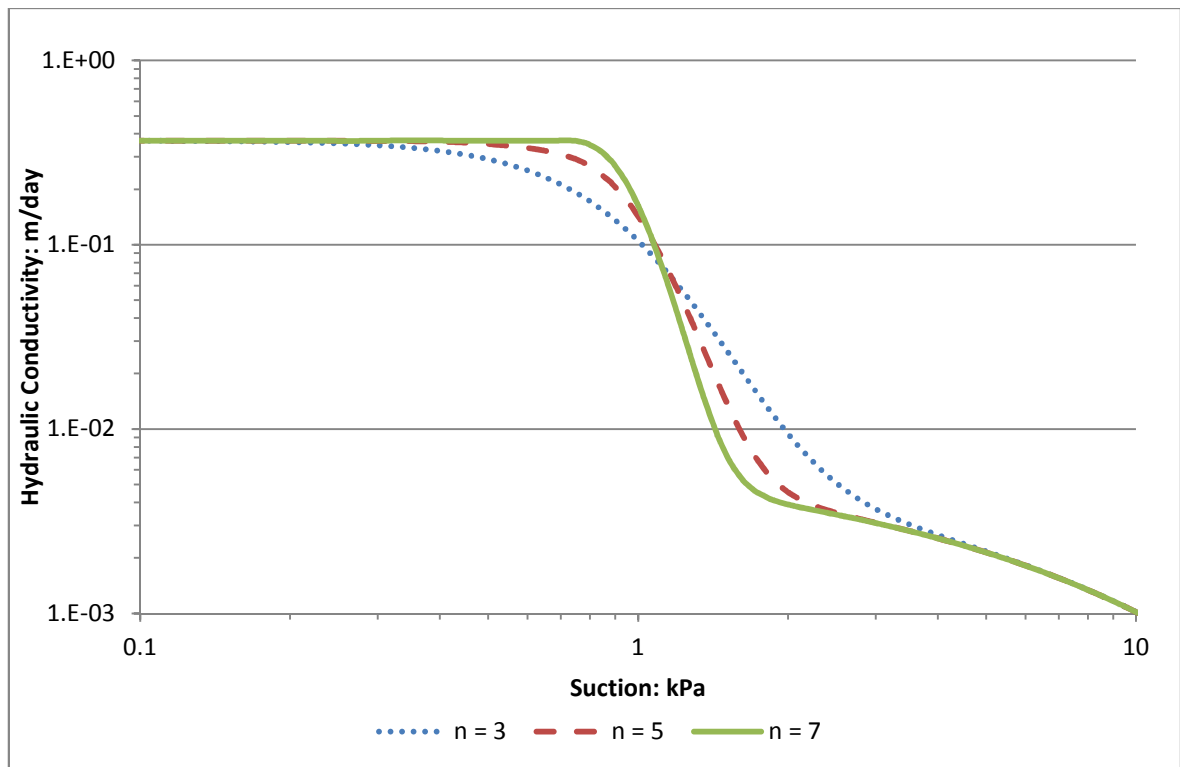
Figure 5-14: Effects of 'n' van Genuchten parameter on the shape of the bimodal HCF. Curves are produced with Equation 5-6.

5.4.4.1 'n' Parameter Sensitivity Analysis Results

Figure 5-15 a) and b) show the suction profiles at instrument group C at 275 days and 365 days respectively for each of the sensitivity analysis models compared against the first bimodal model results and the observed suctions. Increasing the 'n' parameter has similar effects to decreasing the 'a' parameter. Once the parameter is increased beyond a value of 5 the effects are negligible, and therefore the results for the analysis of 'n = 7' have been omitted for clarity. The magnitude of suctions is affected, generally decreasing as 'n' increases in the top 1.0 metres of the slope compared to the initial bimodal model. Below 1.0 metres suctions have increased compared to the initial model, a similar effect was found to occur in the 'a' sensitivity analysis.
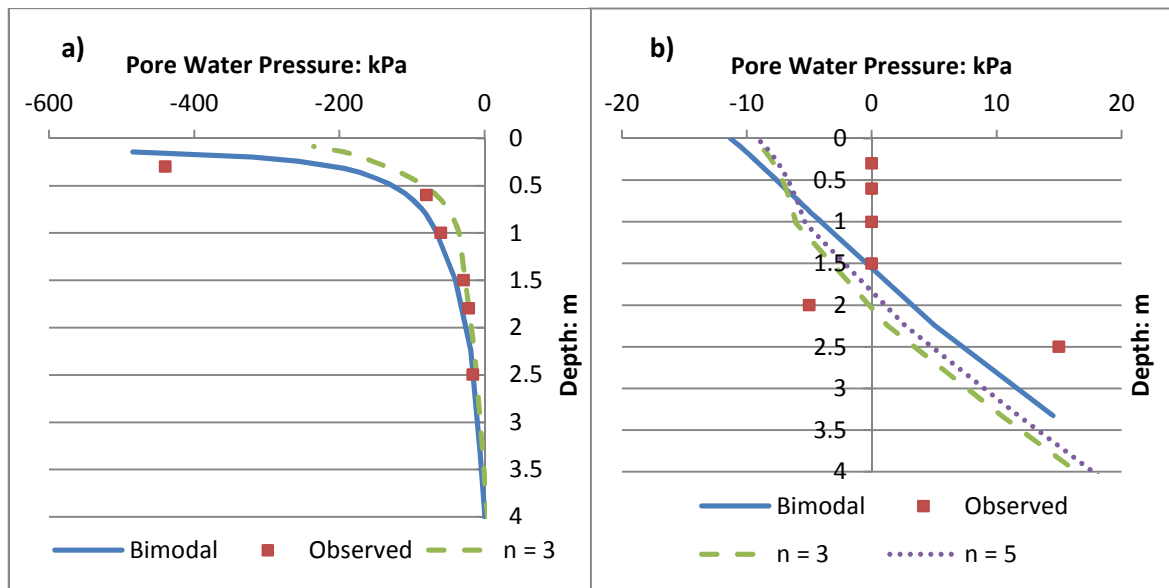
Figure 5-15: Results of the 'n' sensitivity analysis; sowing pore water pressure profiles at mid-slope, at a) 275 days and b) 365 days. Results are compared to the first bimodal results (Section 5.3.4) and the observed results.

Changing the van Genuchten parameters of the crack part of the bimodal equations does affect the calculated suctions and pore water pressures. Reducing 'a' and increasing 'n' was intended to replicate larger cracks that drain quickly. In the sensitivity analyses when one was changed the other was kept constant, however it is more realistic that both would change as crack size varies. In Section 5.5 a new SWCC and HCF is introduced that are built upon the results of the three sensitivity analyses; crack porosity, 'a' parameter and 'n' parameter.

The results of the sensitivity analyses carried out here are discussed in more detail in a later section (Section 5.8.1.3).

5.5 Further Development of the Bimodal Model

In the sensitivity analysis of the crack porosity (Section 5.4.1) it was established that increasing the crack porosity alone will not significantly affect the magnitude of calculated suctions. With reason, it was recognised that the values of some of the van Genuchten parameters in the bimodal equations also required different values to account for this greater crack porosity, which relates to the size of the cracks and also the density of cracking.

213

It was found in the 'a' and 'n' parameters sensitivity analyses (Section 5.4.3 and Section 5.4.4 respectively) that by decreasing 'a' and increasing 'n', calculated suctions are affected. In this model new bimodal SWCCs and HCFs are presented that use the parameters as given in Table 5-7. Another finding of the sensitivity analyses was that the use of the same crack properties throughout the year will result in poor representation of suctions at some point within the analysis. When the parameters 'a' and 'n' were changed to reflect the greater crack size and density synonymous with increased crack porosity, maximum suctions during summer were not calculated to the same degree of accuracy as the initial bimodal model could manage (Figure 5-13 a and Figure 5-15 a).

5.5.1 Material Properties

In the model described in this section, two bimodal material property models were used. The first represents a soil with low crack porosity, with small cracks and a low crack density. The second material model represents a soil with large crack porosity, with larger cracks and a greater crack density. These material properties are applied to the Newbury cutting model at different times of the year to reflect the different magnitudes of cracking occurring on the slope, due to the variability of the climate throughout the year.

The material models are referred to as low porosity and high porosity to reflect the effects of crack size and crack density on this parameter. The parameter values used in the cracking part of the bimodal SWCC (Equation 5-3) and the bimodal HCF (Equation 5-6) for each of the material models are shown in Table 5-7. The low porosity material has the parameter values used in the initial bimodal model (Section 5.3), as suggested by Gerke and van Genuchten (1993); these parameter values were shown to achieve good representation of the suctions developing at the end of summer (Figure 5-5). The results of the sensitivity analyses (Section 5.4) have been used to develop the high porosity material model; it was found that decreasing 'a' and increasing 'n' had a positive effect on modelling of the end of year suctions. Therefore, the high porosity material model uses parameter values that have been adjusted accordingly, in conjunction with an increased crack porosity value.

The aim of using this methodology was to attempt to replicate more realistic field conditions. A small network of cracks will be present at the beginning of the year when the soil is most likely to be saturated. The crack network will expand as the soil dries, resulting in larger cracks with a greater crack density. Therefore at the end of summer when suctions are of the greatest magnitude the crack network will be at its greatest extent. To reflect this process the two material models in Table 5-7 were applied at different times of the year. The low porosity material was applied from the beginning of the year until the end of the summer, when maximum suctions are usually attained. The high porosity material was then applied to the Newbury cutting until the end of the year.

Parameter	Low Porosity	High Porosity
θ_r	0	0
θ_s	0.5	0.5
a	0.98 kPa	0.5 kPa
n	2	7
m	0.5	0.857
K_s	2.3e-4 m/s	2.3e-4 m/s
ϑ	0.018	0.078

Table 5-7: van Genuchten parameters for soil and cracks of new bimodal model

Figure 5-16 compares the soil water characteristic curves and hydraulic conductivity functions for the two cracked soil material models used in this analysis. The low porosity SWCC and HCF are plotted with solid lines and the high porosity SWCC and HCF are plotted with dashed lines.
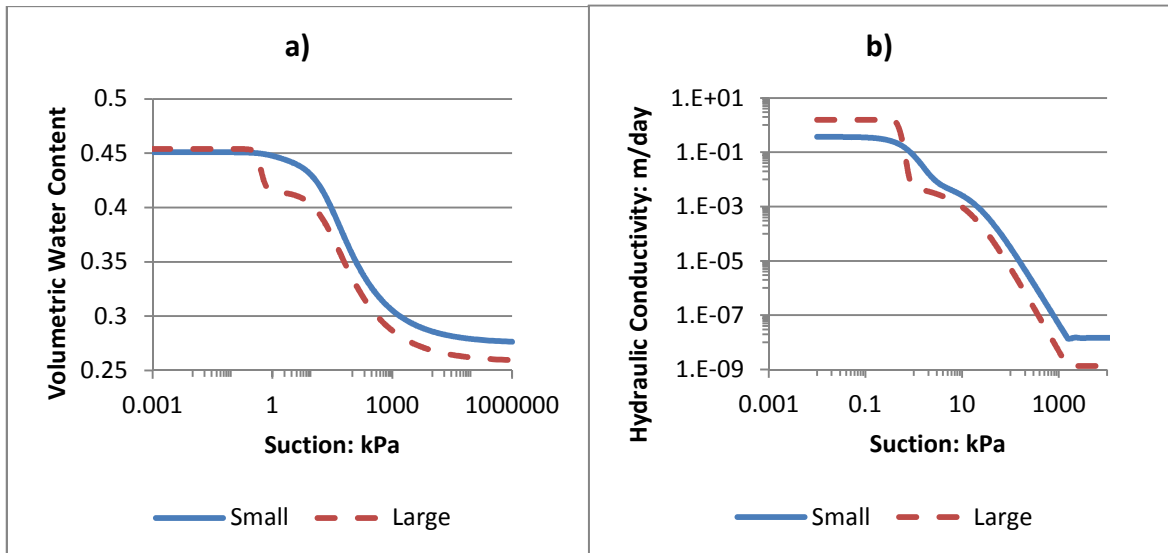
Figure 5-16: a) Low porosity SWCC and high porosity SWCC, and b) small porosity HCF and high porosity HCF. Both defined with Equation 5-3 and Equation 5-6 and the parameter values given in Table 5-7.

There is a clear difference between the bimodal curves representing low porosity and high porosity soils. The difference is most prominent in the part of the curves dominated by the crack parameters, between suctions of 0.001 kPa and 10 kPa. Firstly, considering the SWCCs it can be seen that water can drain from the soil much quicker and at lower suctions for the high porosity, exhibited by the steepness of the curve and the lower value of suction at which the curve falls from the saturated water content. Regarding the HCFs, the large crack function possesses a significantly higher saturated hydraulic conductivity of 1.57 m/day compared to 0.37 m/day for the small cracks function. The combination of high saturated hydraulic conductivity and steeper curves results in a soil through which water may infiltrate and drain at a quicker rate than the soil with low porosity parameters.

5.5.2 Model Run

The model was run with the low porosity material properties applied to the surface layer for the first 275 days and the high porosity material properties applied to the surface layer for the next 90 days Figure 5-17. Model geometry, boundary conditions, initial conditions and the finite element mesh are identical to those used in the initial bimodal hydrological model described in Section 5.3.

216
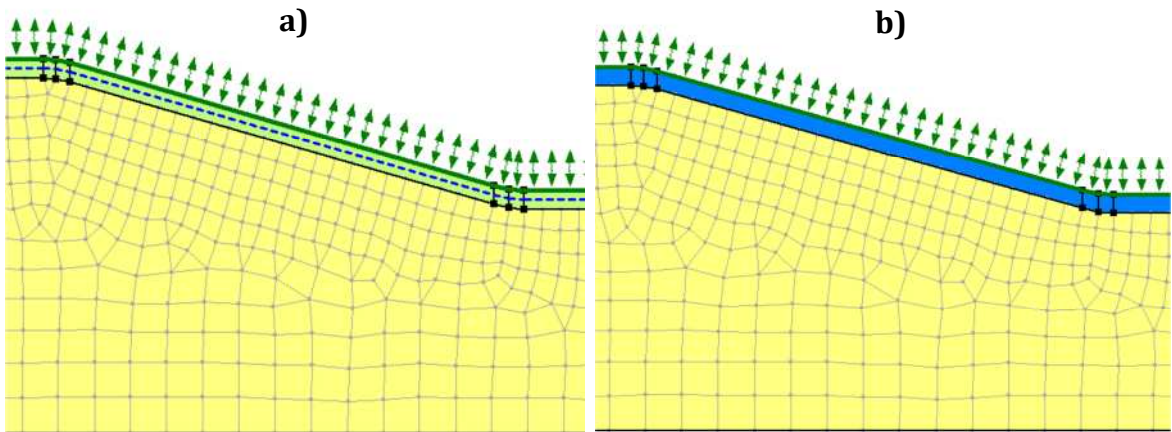
Figure 5-17: VADOSE/W model with a) low porosity material properties (green region) applied for the first 275 days and b) high porosity material properties (blue region) applied for the final 90 days.

5.5.3 Further Development Results

Figure 5-18 shows the results from the post sensitivity analyses model.
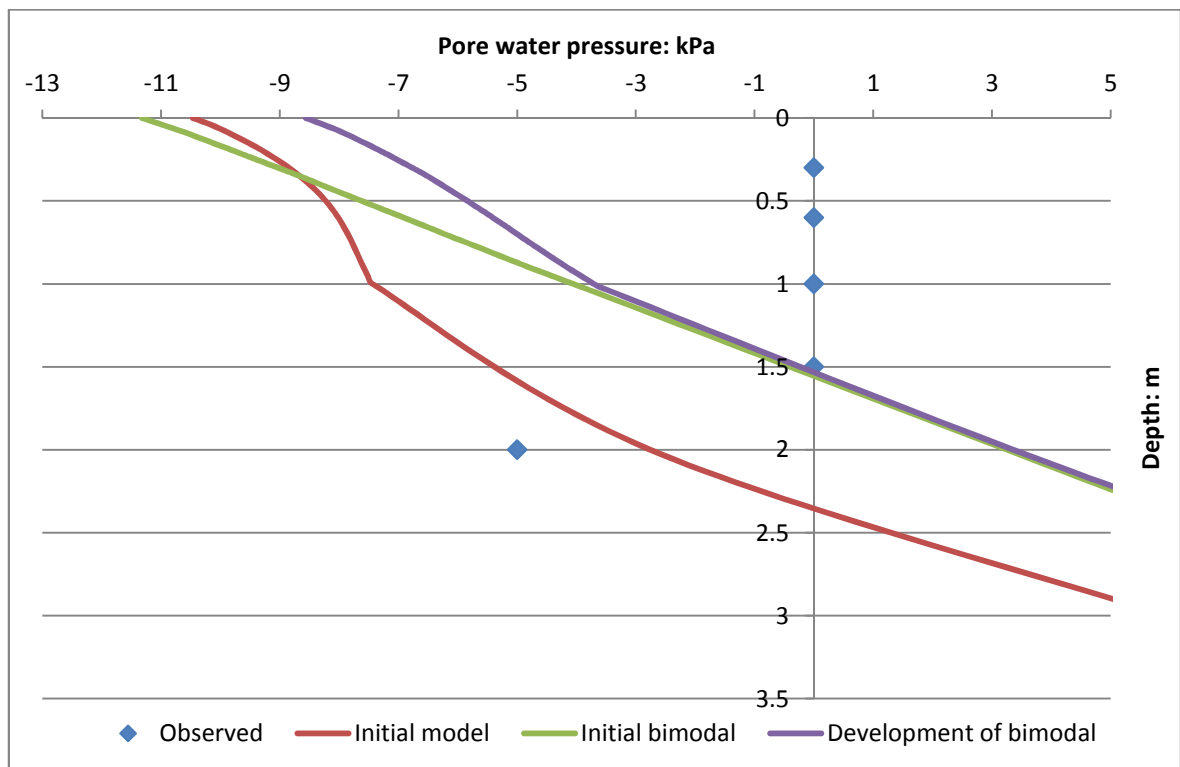
Figure 5-18: Results of the post sensitivity analysis model, showing minimum suctions at 365 days. The results are compared to those from the model developed in Chapter 4 (red line) with no desiccation cracking, and the first bimodal model (green line) from Section 5.3.4.

The profiles show the minimum suctions at 365 days, with the results from the initial model with no cracking accounted for (Section 4.4.1), the initial bimodal model (Section 5.3) and the model developed in this section. The observed values (Smethurst et al., 2006) are also presented.

Figure 5-18 shows that the combination of new van Genuchten parameters established in the sensitivity analyses does affect the magnitude of the minimum suctions calculated by the VADOSE/W model. The maximum suction at this time step (365) is reduced from 11.3 kPa to 8.5 kPa and all suctions within the top 1.0 m of the slope profile are lower than the initial bimodal model was able to achieve. Below 1.0 m suctions and pore water pressures are essentially unaffected.

Despite better performance of the model there is still room for improvement. There is a fundamental flaw in the definition of parameters, or the model geometry, that is adversely influencing the models' ability to dissipate the suctions developing throughout the summer. For example, the depth of cracking applied to the model is likely to be influencing the results. Secondly, the value of the saturated water content (θ_s) of the cracks part of the bimodal equations has thus far been kept constant. A value of 0.5 has been used for the saturated water content (θ_s) of the cracks. This value, suggested by Gerke and van Genuchten (1993), specifies that cracks cannot fill with water, but are limited to being 'half-full'. This is not consistent with what has been observed in the field or the lab (Greve et al., 2010; Kuna et al., 2013). Cracks can be 'full', which would be the same as designating the value of θ_s as 1.0.

Further models have been created in the next two sections (Section 5.6 and 5.7) that analyse the effects of changing the saturated water content of the cracks (Section 5.6), and the effects of changing the depth of cracking (Section 5.7).

5.6 Effects of the Crack Saturated Volumetric Water Content

In this section a further development of the bimodal model is made. It has been established that the value of the saturated VWC of cracks used in previous sections is almost certainly erroneous. Saturated VWC of the cracks does not affect the shape of

HCF and therefore the maximum hydraulic conductivity; it does however affect the amount of water retained by the cracked soil at low suctions. Figure 5-19 shows the bimodal SWCC when $\theta_{s\,crack} = 1.0$ and the initial bimodal SWCC from Section 5.2.4.
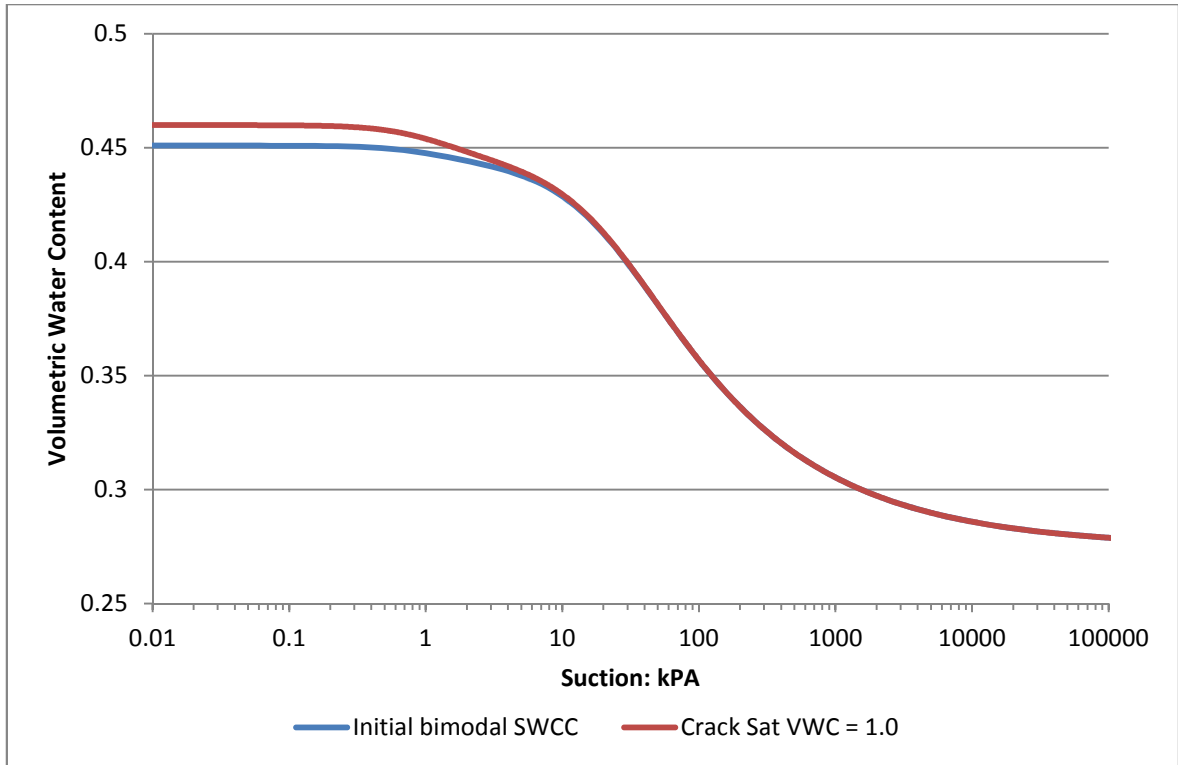
Figure 5-19: Comparison of initial bimodal SWCC (and bimodal SWCC generated when θ_s of the crack = 1.0, both generated with Equation 5-3 and the other parameter values in Table 5-1 .

5.6.1 Crack Saturated Volumetric Water Content Analysis Results

Figure 5-20 shows the results from the analysis considering the saturated VWC of the cracks. The profile shows the minimum suctions at 365 days, with the results from the initial model with no cracking accounted for (Section 4.4.1), the previous development of the bimodal model (Section 5.3) and the model developed in this section. The observed values (Smethurst et al., 2006) are also presented.
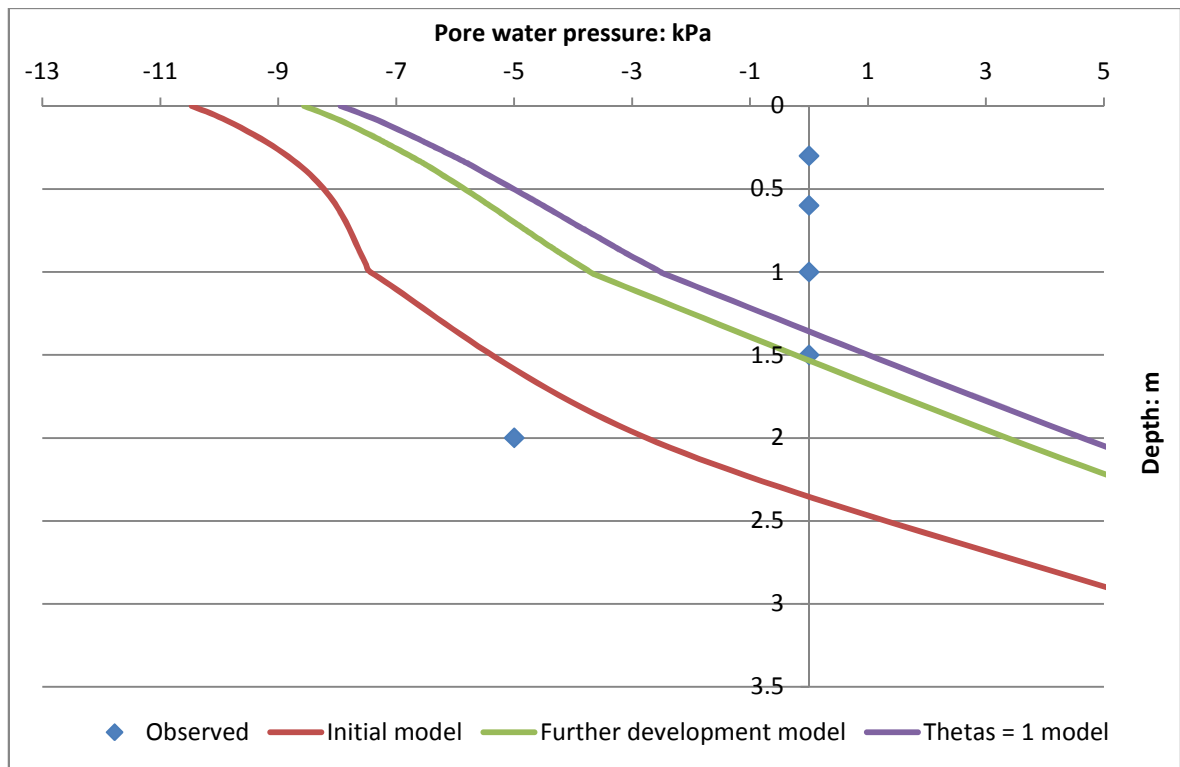
Figure 5-20: Results of the crack saturated volumetric water content analysis, showing minimum suctions at 365 days (purple line). The results are compared to those from the model developed in Chapter 4 (red line) with no desiccation cracking, and the previous bimodal model (green line) from Section 5.5.3.

Figure 5-20 shows that the suctions are affected by the value of the crack's saturated VWC, reducing by up to 1.2 kPa at a depth of 1.0 m when compared to the previous development of the bimodal model (Section 5.5). However the improvement is quite marginal, and there are still possible developments in the model that could further increase its ability to calculate winter pore water pressures. There are now no more parameters within the bimodal equation that can be altered to influence the results, and therefore to further improve performance of the model, some other factor must be changed. In the following analysis (Section 5.7) the effect of increasing crack depth is analysed.

5.7   Crack Depth Analysis

In all previous analyses a crack depth of 1.0 m has been utilised. This value was assumed for ease of modelling, and because it was also consistent with some observed measurements of maximum crack depths in clay soils (Inci, 2008). However,

this value of crack depth has not resulted in adequate modelling of winter pore water pressures. Therefore the effects of increasing the crack depth were investigated.

Arnold et al. (2005) measured that the majority of cracking (>70%) occurred in the top 1.5 metres of a clay soil profile. This is consistent with observations of the effects of desiccation cracking on pore water pressures made by Smethurst et al. (2006) at the Newbury bypass cutting site. When considering the sudden changes in pore water pressures at the beginning of December 2003 Smethurst et al. (2006) state that "the sudden large changes of pore pressure at 1.0 m and 1.5 m depth are the result of rain filling tension cracks close to the instrument". This comment suggests that cracking at this location has reached a depth of 1.5 metres.

The model used in previous sections has been modified to allow a cracking depth of 1.5 metres. This is simply achieved by increasing the thickness of the surface layer to 1.5 metres and applying the cracked soil material properties in the same manner as previously. Similarly to the models from Section 5.5 onwards, two types of cracked material properties have been used; one representing low crack porosity applied from the beginning of the year until end of summer and one that represents high crack porosity, applied from the end of summer to the end of the year.

5.7.1 Model Geometry and Boundary Conditions

To account for different levels of cracking throughout the year the surface layer was split into two separate parts (Figure 5-21) of 1.0 m and 0.5 m to give a total surface layer thickness of 1.5 metres. It is possible to split the surface layer into as many separate parts as desired allowing the user to define many different material properties throughout the whole surface layer. For the first part of the model run, to the end of summer, bimodal material properties were applied to the top 1.0 metres of the surface layer only. This was done to account for the lower depth of cracking present at the end of winter, and as it has already been shown that this setup results in a good calculation of the maximum suctions present in the slope at the end of summer (see Figure 5-5 in Section 5.3.4).
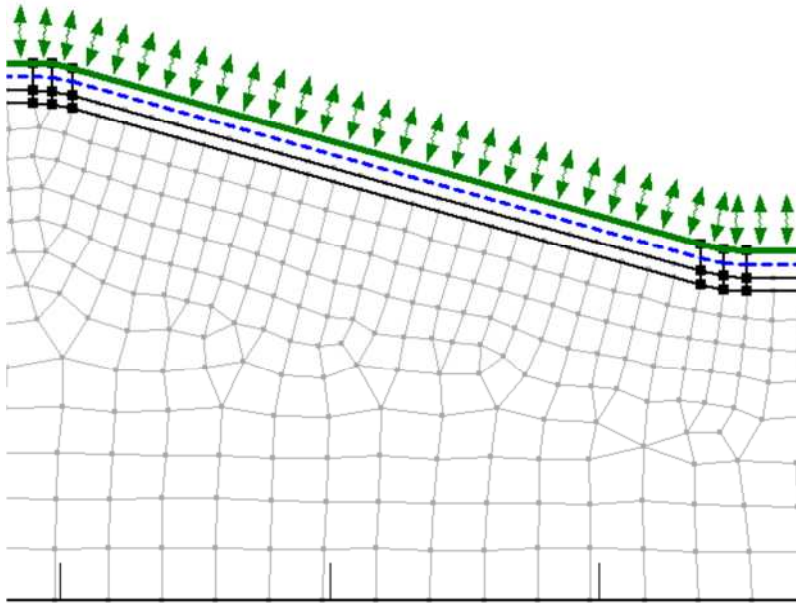
Figure 5-21: Model showing split surface layer, initial mesh, initial water table and surface climate boundary condition.

Figure 5-22 shows the model with the relevant material properties applied. For the first part of the model run from the beginning of the year to end of summer. To establish maximum suctions, the bimodal low crack porosity material properties were applied to the top 1.0 metres of the surface layer (green region in Figure 5-22 a)). After maximum suctions are achieved material properties for high crack porosity were applied to the whole 1.5 metres of surface layer (blue region in Figure 5-22 b)) and the model was then run to the end of the year. Normal London Clay material properties are applied to the rest of the model (yellow regions).
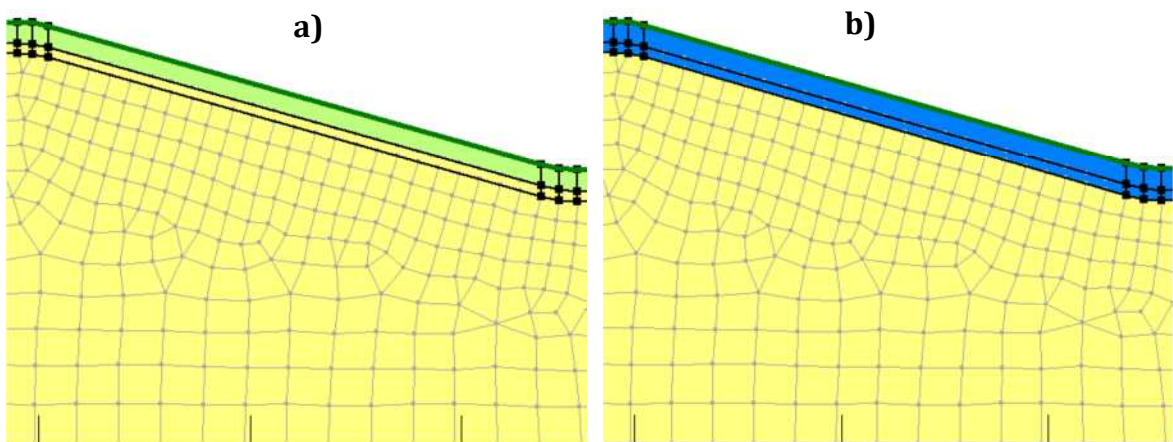
Figure 5-22: Model with bimodal materials applied. a) Model setup from beginning year to end of summer (0 - 275 days, b) model setup from end of summer to end of year (275 - 365 days).

Once the model was generated, with the correct geometry, material properties and boundary conditions applied, the finite element mesh was created. As the model geometry has changed, with a thicker surface layer defined; a new mesh is required in this region. In Section 5.7.2 the development of the new surface layer mesh is shown.

5.7.2 Meshing

A new mesh was required for the increased thickness of surface layer. The ratio of element thickness to surface layer thickness is kept constant. With a surface layer of 1.0 m, 23 elements were required, 1 element every 4.35 centimetres of surface layer. Therefore with the surface layer increased to 1.5 meters thickness the number of elements required is:

150/4.35 = 34.48

The new surface layer will be 35 elements thick, as shown in Figure 5-23. This new surface layer mesh results in the entire model mesh with a total of 4481 elements. For such a large mesh it is very important to select the appropriate equation solver to solve the problem within a reasonable time. Geo-Slope (2007) recommends the use of the parallel direct equation solver for large meshes such as this one.

35 elements
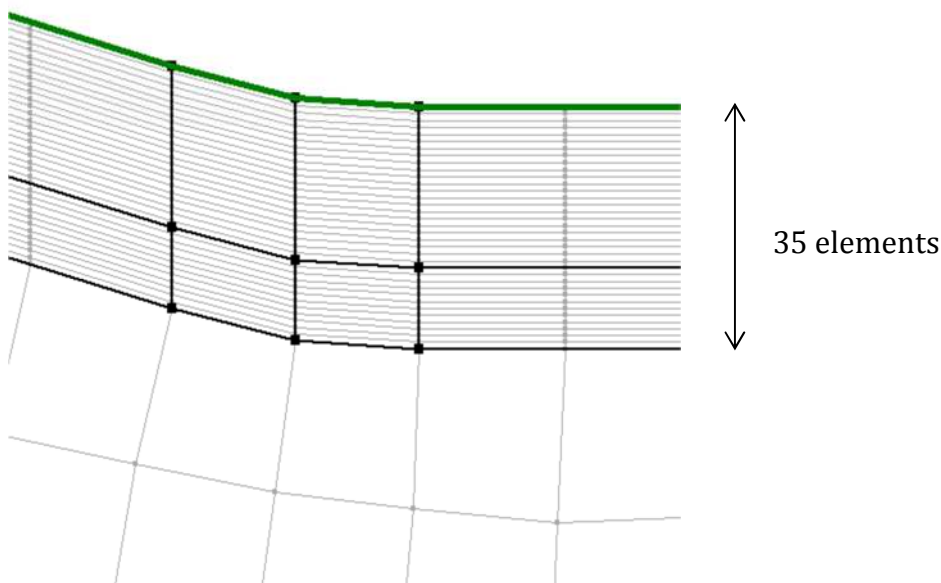
Figure 5-23: Detail of the new model mesh focussing on the toe of the slope.

Once the new mesh was generated, the model could be run. The model was run for 365 days of the Newbury climate. In Section 5.7.3 the results obtained from this run are presented and compared to the results from previous model runs. By looking at the profiles and suction and pore water pressure trends it is shown that this model, with an increased maximum crack depth, can replicate the slope hydrology behaviour better than any of the previous models.

5.7.3 Crack Depth Analysis Results

In this section the results of the crack depth analysis are presented. The first set of graphs (Figure 5-24 and Figure 5-25) show the pore water pressure profiles generated at instrument group C location at maximum suctions (275 days) and the end of the year (365 days). Following these profiles are Figure 5-26 to Figure 5-29 that show the trend of suctions and pore water pressures at depths of 1.0, 1.5, 2.0 and 2.5 metres below instrument group C. In these figures four sets of results are compared; the observed trends, those calculate by the initial model with no cracks, those calculated by the first model with cracks included and the final model presented in this section.

5.7.3.1 Maximum and Minimum Suction Profiles

Figure 5-24 shows the suction profile generated at instrument group C at 275 days showing the maximum suctions in the slope. The profile shows that this iteration of the bimodal model, with increased crack depth, can predict maximum suctions as well as previous versions of the bimodal model; and at some depths with more precision. Between depths of 1.0 and 2.5 metres this version of the bimodal model predicted the magnitudes of suctions better. The new version of the model has over-predicted the maximum suction; 523 kPa, compared to 490 kPa by the first bimodal model and the observed value of 440 kPa.

224
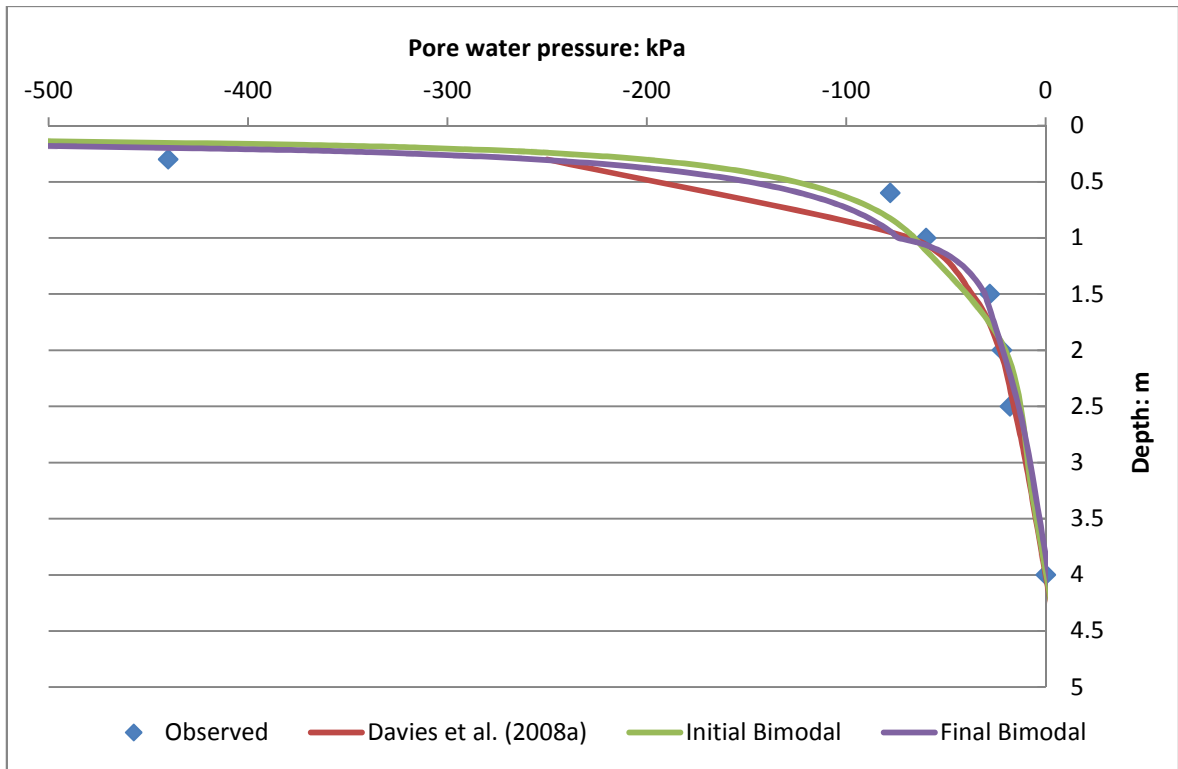
Figure 5-24: Results of crack depth analysis model, showing maximum suction profiles at 275 days. Results are compared to the observed values, the results of Davies et al. (2008a) and the initial bimodal model from Section 5.3.4.

Figure 5-25 shows the suction profile generated at instrument group C at 365 days showing the minimum suctions in the slope. The profile shows that the model created for the crack depth analysis performs similarly to the initial bimodal model when calculating the suctions at this time step. Performance is somewhat reduced when comparing each model to the observed values. Minimum suctions are slightly greater than those calculated by the initial bimodal model. If this is taken as the only indication of model performance then it may seem reasonable to suggest that the crack depth analysis model does not improve the overall ability to model the hydrological behaviour in the slope over the whole year.
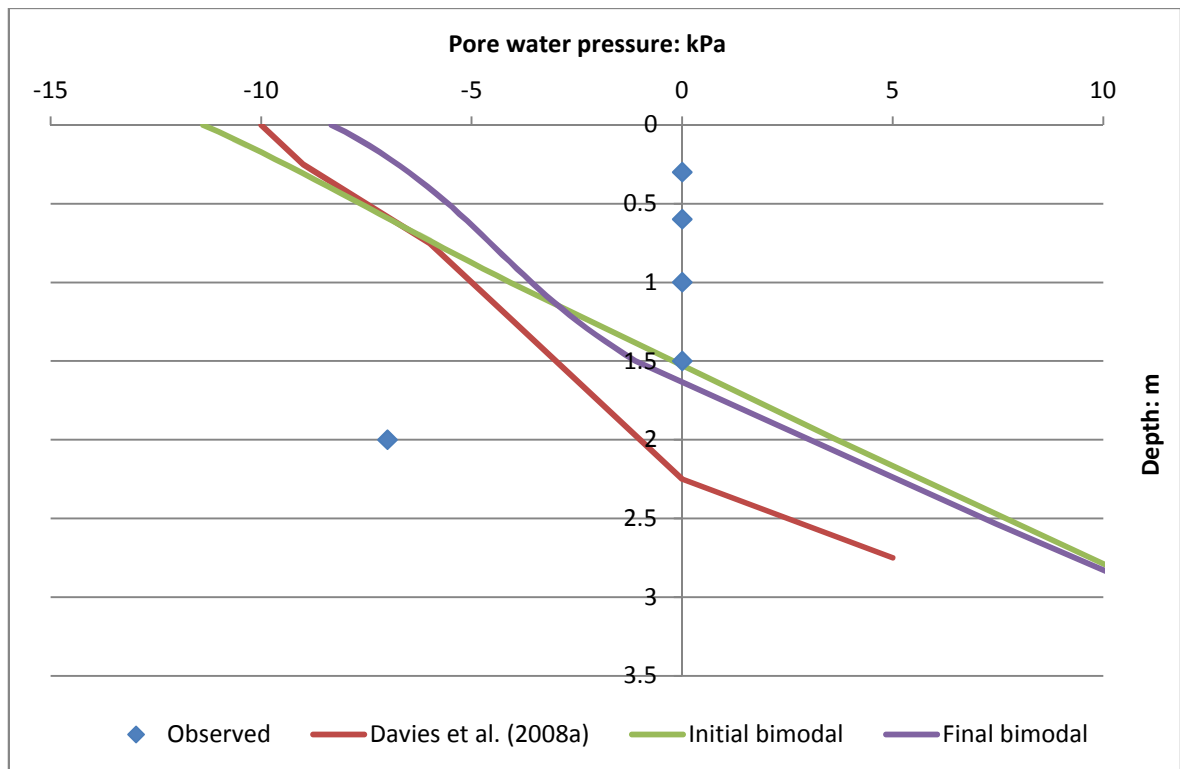
Figure 5-25: Results of crack depth analysis model, showing minimum suction profiles at 365 days. Results are compared to the observed values, the results of Davies et al. (2008a) and the initial bimodal model from Section 5.3.4.

In Section 5.7.3.2 the results are analysed in more detail by looking at suction and pore water pressure trends throughout the year. By looking at these trends it is shown that the model developed for the crack depth analysis is actually superior to any other iteration of the bimodal models at predicting suction magnitudes and trends throughout the whole year.

Further observed data is available for the years 2004 – 2008 (Smethurst et al., 2012). To provide further validation of the model two more years were run, concurrently after 2003. Years 2004 and 2005 were modelled, by applying the same bimodal material properties to the same depth (1.5 metres). Initial conditions for each model were defined by the pore water pressure conditions at the end of the previous year. Minimum and maximum pore water pressures have been recorded and compared to the observed values; these profiles can be found in Appendix B. The results for these years show good replication of the observed pore water pressure magnitudes, particularly in 2005.

5.7.3.2 Suction and Pore Water Pressure Trends

A single 'snapshot' of suctions at one time step, such as those presented in Section 5.7.3.1, cannot give a full understanding of the performance of the model. Judging from Figure 5-25 it would appear that the latest version of the model is actually inferior to the previous. However, by investigating further it can be shown that this iteration of the model actually out-performs the first bimodal model. Figure 5-26 to Figure 5-29 show suction and pore water pressure trends at depths below instrument group C. These graphs compare the results obtained in the crack depth analysis model to those obtained by the initial bimodal model (Section 5.3). The graphs show obvious improvements in the calculation of the trends through the various model iterations. Graphs have been produced for depths of 1.0 metre (Figure 5-26), 1.5 metres (Figure 5-27), 2.0 metres (Figure 5-28) and 2.5 metres (Figure 5-29).
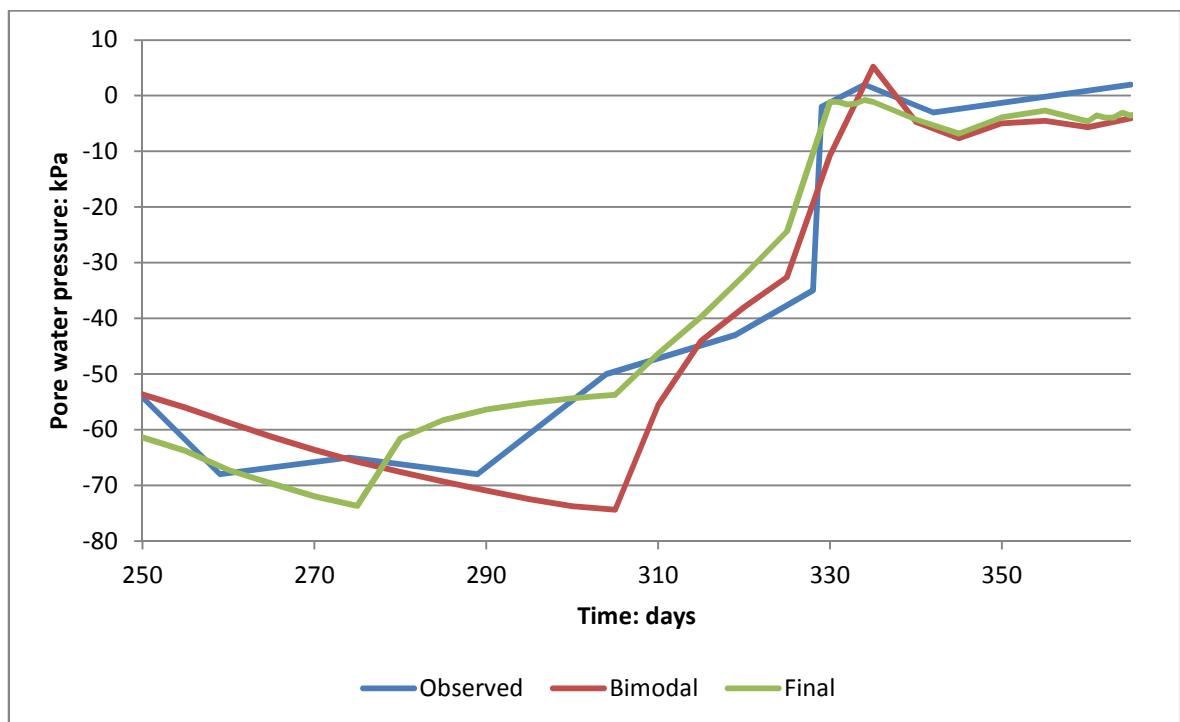
Figure 5-26: Pore water pressure trends at 1.0 metre depth. Results are compared to the observed values and the initial bimodal model from Section 5.3.4 (red line).

Figure 5-26 shows the results at a depth of 1.0 m. Both bimodal models match the trends of the observed pore water pressures better than the initial un-cracked model. The latest version of the cracked model performs better than the initial bimodal

227

model between days 250 and 310, but from days 310 to 365 the performance is similar. Maximum suctions are well estimated by each bimodal model and the rate at which suctions fall from maximum to minimum is also well predicted by both. Both models perform similarly at predicting minimum suctions; both predicting within 3 kPa.
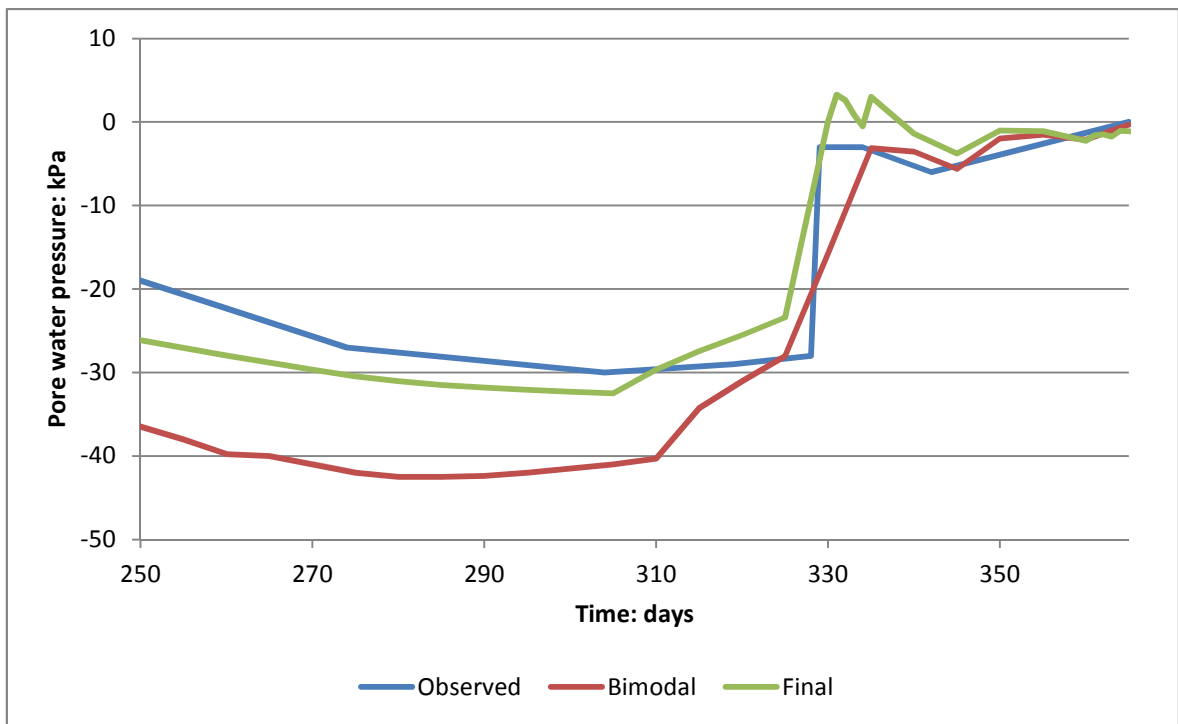
Figure 5-27: Pore water pressure trends at 1.5 metres depth. Results are compared to the observed values and the initial bimodal model from Section 5.3.4 (red line).

Figure 5-27 shows the results at a depth of 1.5 metres. The performance of the model has been much improved over that of the initial un-cracked model and the first bimodal model. The final bimodal model has predicted a maximum suction of 32 kPa at this depth, whereas the initial bimodal model predicted 42 kPa. When both results are compared to the observed value of 30 kPa the final model clearly outperforms the initial.
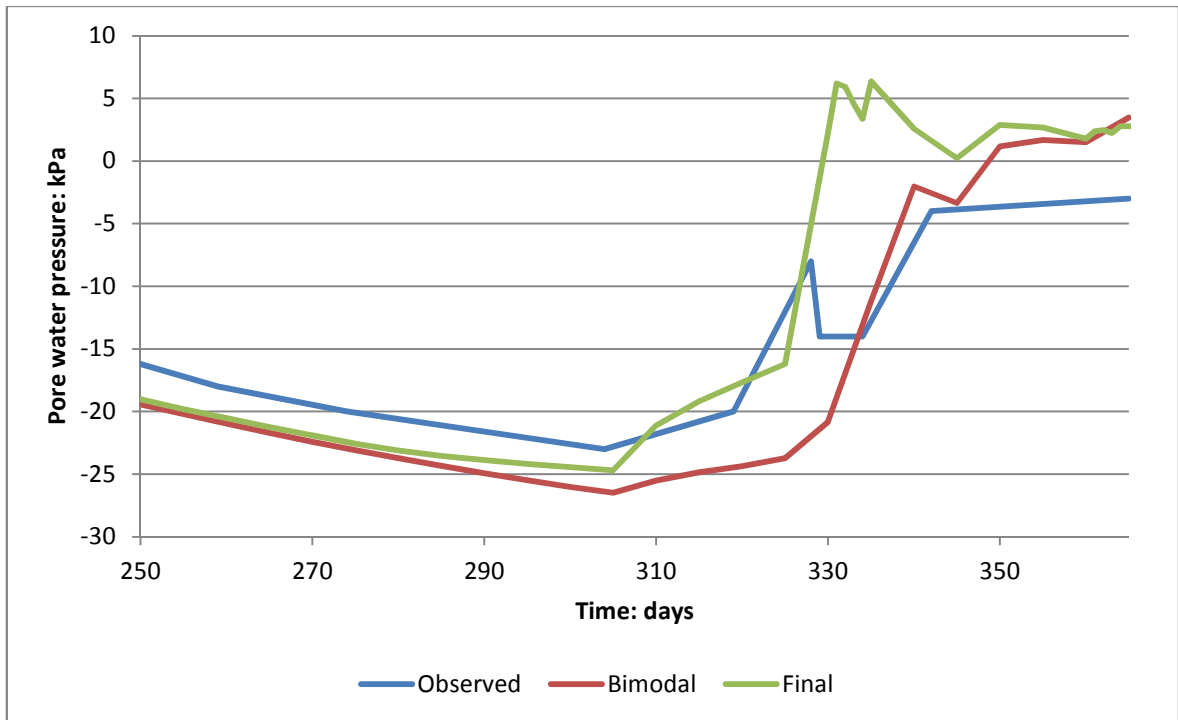
Figure 5-28: Pore water pressure trends at 2.0 metres depth. Results are compared to the observed values and the initial bimodal model from Section 5.3.4 (red line).

Figure 5-28 shows the results at a depth of 2.0 metres. The first bimodal model struggled to model the trends at this depth and the last version has similar difficulty. The latest version predicts the magnitudes, rate of change and the timing with good accuracy, and better than the first bimodal model, up to day 330 but after this up to day 365 does not match the trends well at all.
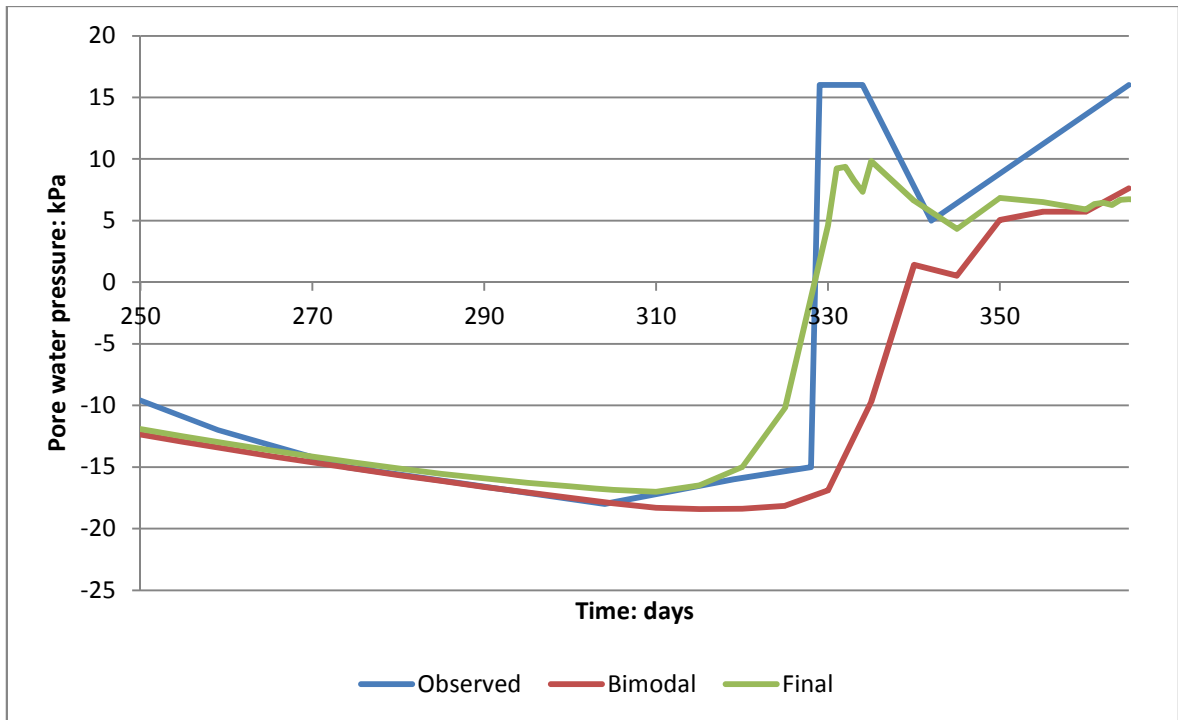
Figure 5-29: Pore water pressure trends at 2.5 metres depth. Results are compared to the observed values and the initial bimodal model from Section 5.3.4 (red line).

Figure 5-29 shows the suction and pore water pressure trends at a depth of 2.5 metres. Again the latest version of the bimodal model is superior to both the un-cracked model and the first bimodal model. This version of the bimodal model follows the trends up to day 330 very well, matching the very fast rate of decline in suctions. The model cannot match the value of minimum suctions but it does better than either the initial un-cracked model or the initial bimodal model.

5.8 Discussion

The approach taken in this model was shown to improve the outputs of the model when compared to the observed behaviour. By using two different cracked soil material properties and by varying the depth of cracking, performance of the model was significantly improved over the initial bimodal models and the model that does not include the effects of desiccation cracking.

5.8.1 Bimodal material properties

An initial bimodal model was developed in Section 5.3 and results presented in Section 5.3.4. The initial results showed that the bimodal model was promising; improving the replication of pore water pressure behaviour in the Newbury cutting slope, particularly when considering the temporal behaviour. The bimodal model could be improved further, achieved through a number of sensitivity analyses, described in Section 5.4 and 5.6. The influence of the temporal nature of desiccating cracking was also included in Section 5.7, which led to the final bimodal model. This version of the model is able to match the trends, including the magnitude and timing of maximum and minimum suctions and also the rate at which they change (Section 5.7.3).

In the following sections of the discussion, the development of the bimodal model is considered, including the implications of any assumptions made, with the intention of identifying why this model improves the replication of the hydraulic behaviour of the Newbury cutting slope throughout the year. The initial development of the bimodal model is discussed first.

5.8.1.1 Initial bimodal model water balance

In the discussion of Chapter 4 the water balance was used to explore the results obtained, and try to ascertain the reasoning behind certain behaviours of the Newbury cutting slope model. Figure 5-30 shows the water balance of the initial bimodal model, including the storage from the model presented in Chapter 4 for comparison.

The results obtained for the initial bimodal model showed improvement for all aspects of the replication of the hydraulic behaviour of the slope, including; maximum suction profile (Figure 5-5), minimum suction profile (Figure 5-6) and the pore water pressure trends (Figure 5-7 a) to d)). The maximum suctions modelled at the end of summer are greater than were calculated by the un-cracked model, exhibiting lower soil moisture content which can be explained by looking at the water balance (Figure

231

5-30). On this graph the storage for the initial model (Chapter 4) has been plotted alongside the storage for the initial bimodal model.

5.8.1.1.1 End of summer water balance

The graph shows that by the end of summer more water is removed from the slope for the bimodal model than the initial model. The magnitudes are -15.3 m³ for the initial model and -19.3m³ for the initial bimodal model, showing that the bimodal model has caused an extra 4 m³ of water to be removed from the slope, a 26 % increase.
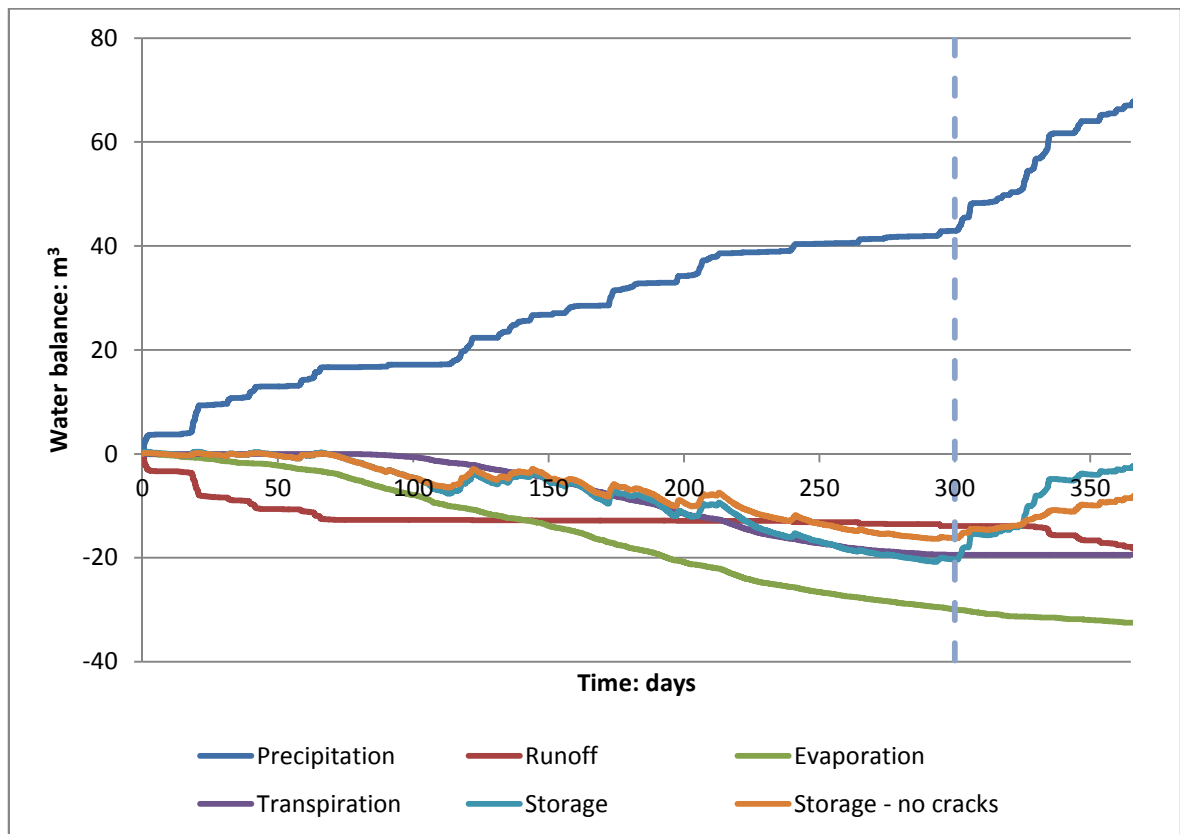
Figure 5-30: Newbury cutting water balance for 2003, calculated by the initial bimodal VADOSE/W model.

By studying the other fluxes it can be seen that the extra water being removed from the slope is solely due to increased evaporation. When compared to the water balance from the previous model (Figure 5-32) it can be seen that there is an increase from 23.9 m³ to 28.3m³ in total evaporation from the slope at the end of summer, which is

an 18 % increase. It is worth considering how this increase in evaporation is brought about.

There must be some cause that means it is easier for more water to be evaporated from the surface. Initially it may be thought that there is simply more water available due to increased infiltration, but when it is considered that precipitation and runoff are identical to the previous model up until the end of summer this can be ruled out. Therefore the only other source of water is from the ground water already present, and there must be some procedure that means it is easier for water to be extracted from the slope. By looking at the material properties at a point just below the slope surface this mechanism is identified. Figure 5-31 shows the temporal hydraulic conductivity of the soil at a point 0.5 metre below the slope surface at instrument group C for the initial model and the initial bimodal model.
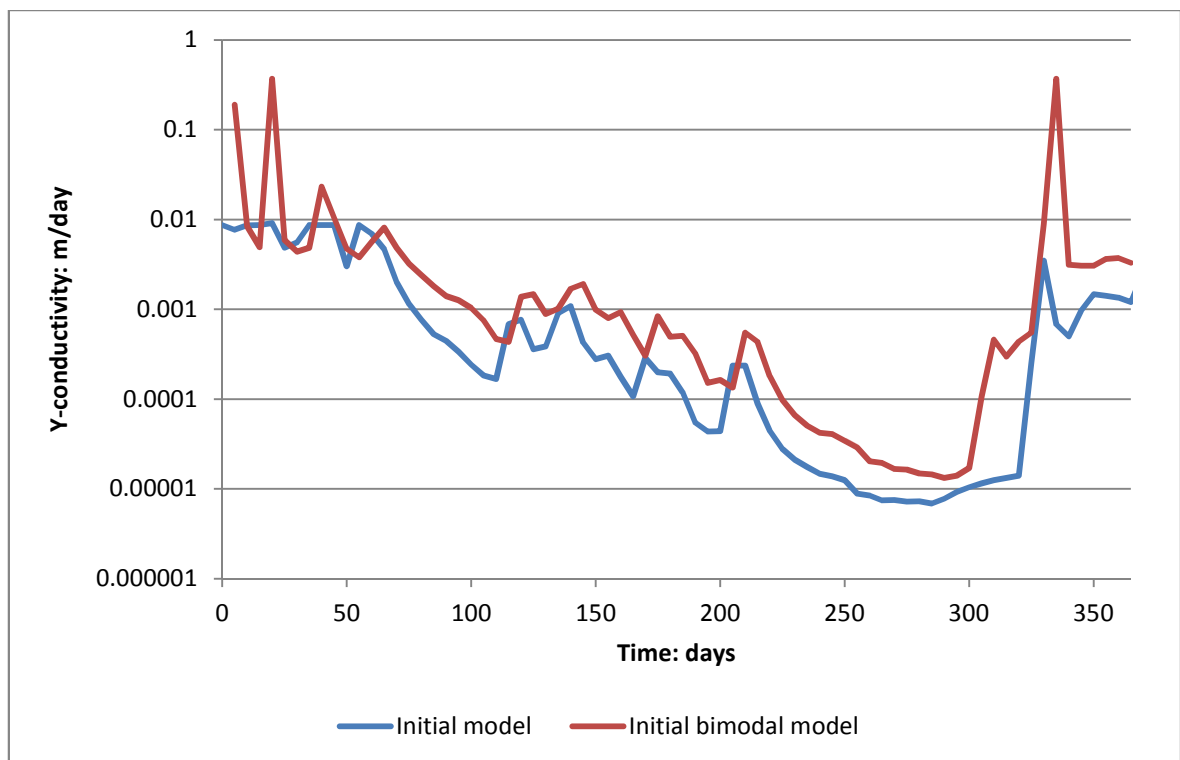
Figure 5-31: Hydraulic conductivity of the soil 0.5 metre below the slope surface. Values from the initial bimodal model are compared to those from the model developed in Chapter 4 when desiccation cracking was not included.

The graph reveals that when the bimodal material properties are introduced to the model, the hydraulic conductivity at this point is generally up to 1 order of magnitude

greater until the end of summer. The increased vertical conductivity means that water is drawn upwards easier, which means more water shall be available for evaporation, resulting in the lower volumetric water content and better replication of pore water pressures at the end of summer.
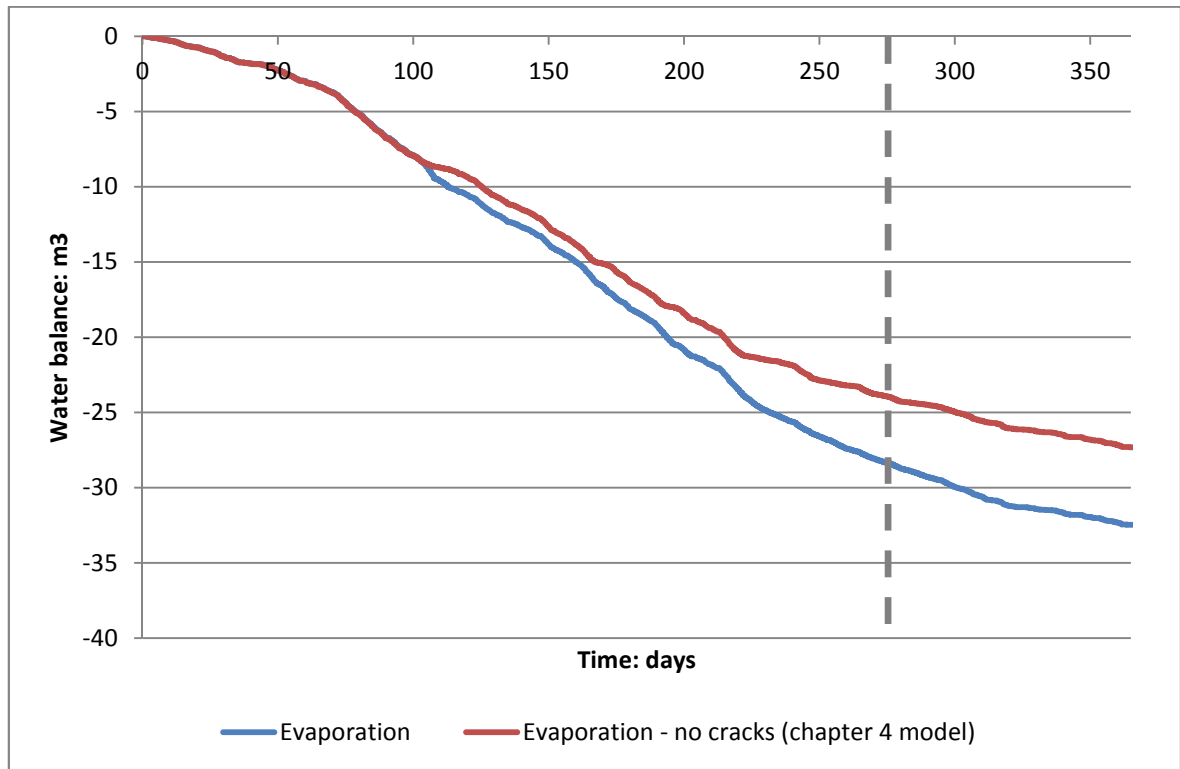
Figure 5-32: Comparison of evaporation for 2003 for the initial bimodal model (blue) and the model from chapter 4 (red). The dashed line represents the end of summer.

5.8.1.1.2   End of year water balance

The effects of the bimodal soil properties on the trends of the hydraulic conductivity can explain why the end of year pore water pressure trends and magnitudes are also replicated better. Starting from around day 300 there is a sharp increase in hydraulic conductivity and by day 335, for the bimodal model the hydraulic conductivity has increased from 1.7×10^{-5} m/day to 0.36 m/day whereas for the initial model the increase from day 300 to day 335 is from 9.2×10^{-6} m/day to 0.0035m/day. With vertical hydraulic conductivity 2 orders of magnitude greater water is able to infiltrate at a greater rate, replicating the preferential pathways that cracks form in a desiccated soil.

The magnitude of runoff is much less when the bimodal properties are introduced. In initial un-cracked model developed in Chapter 4 the total runoff was 28.0 m³ at the end of the year but in the initial bimodal model it was only 18.0 m³, a reduction of 36 %. Many authors have made the point that not accounting for desiccation cracks can lead to an overestimation in runoff and an underestimation of infiltration (Novak et al., 2000; Arnold et al., 2005; Fredlund et al., 2010a). The results presented here corroborate this, showing much improvement in the replicated pore water pressure behaviour when desiccation cracks are included in the slope hydrology model.

5.8.1.2 Implications of assumptions

When the bimodal equations, material properties and initial VADOSE/W model were developed in Sections 5.2 and 5.3, a number of assumptions regarding the implementation of the equations and properties of desiccation cracks were made. These are:

1. The soil can be separated into two distinct pore systems for the intact soil matrix and the cracks with separate hydraulic properties for each.
2. The system as a whole can be considered as a superposition of the two separate systems over the same volume – i.e. a continuum.
3. Cracks do not change volume as the soil wets or dries unless the user prescribes new soil or cracked soil properties.
4. Cracks act as capillaries and water flows through these by capillary action. Therefore the Darcy and Richards equations for saturated and unsaturated flow in porous media can be applied.

In this section the implications of each of these assumptions on the validity of the model and the impact that they will have had on the modelling results are discussed.

The first assumption applies to the development of the equations and how the crack part is integrated. By giving one distinct set of hydraulic parameter values to the cracks it implies that all cracks within the soil have the same hydraulic properties, whereas in reality at any given point in time there will likely be many cracks of differing size exhibiting different hydraulic properties. Results in the sensitivity analyses have shown that using different parameter values to represent different

sized cracks can influence the results positively, showing that different sized cracks do possess different parameter values. Modelling work done in Section 5.7 has shown that by using different hydraulic properties at different times of the year, the effect of the temporal nature of desiccation crack sizes can be accounted for.

The second assumption means that the effects of the desiccation cracks on the hydraulic properties of the whole cracked soil are essentially averaged over the whole volume that the soil occupies. In reality the cracks allow infiltration at distinct locations on the slope surface and through distinct pathways into the slope profile. By averaging the cracks over the volume it assumes that the effects of cracks occur over the whole slope surface and through the whole profile.

The third assumption assumes that cracks do not change size (i.e. width) or depth throughout the year. This is not actually realistic, as crack size and depth is related to water content of the soil, which changes constantly (Novak et al., 2000). This has been partially dealt with by the application of different crack properties and depths at different times of the year, depending on antecedent pore water pressures. At the start of the year pore water pressures are mostly positive, and therefore cracks are assumed to be small and shallow, whereas at the end of summer when high negative pore water pressures are present, the cracks are assumed to be large and deep (Section 5.7). This method considers the evolution of cracking on a macro time scale, where cracks change over a matter of seasons. Small changes, on a micro time scale, where the cracks may be changing minutely over matters of hours or even minutes are ignored.

The models using bimodal soil properties presented in this work essentially still consider the soil properties to be static, spatially and temporally, which was initially identified in the literature review as a major weakness of the existing slope hydrology models. In reality the approach has not changed, but the definition of the likely soil properties has improved, which has undeniably led to improved replication of the pore water pressure magnitudes and trends in the Newbury cutting slope.

An improvement to the model would be one that could recognise the spatial and temporal variability of desiccation cracking. This model would have to take into account the variability of the parameters, such as the porosity and the van Genuchten parameters *a*, *n* and *m,* which would become functions of the volumetric water content. Crack depth will also become a function of the water content; in the next chapter a method for estimating crack depth from pore water pressure profiles is introduced.

The final assumption is that flow in the cracks is governed by the capillary law. This assumption holds until a certain crack width is exceeded. This crack width, according to Li et al. (2011) is 11.8 mm (Section 2.10.2.4), and once the crack aperture is greater than this water would actually drain freely under the effect of gravity, exceeding the rate of infiltration that the bimodal functions allow. There is a scarcity of crack observations in the United Kingdom which would allow better judgement of the likelihood of the crack aperture for the capillary law being exceeded. What does exist is inconclusive and field evidence is wide ranging, generally incomplete and sometimes conflicting (Nahlawi and Kodikara, 2006). These kinds of measurements of crack width are very important to ascertain in which cases the bimodal equations are wholly applicable.

Even if some cracks do exceed the critical crack aperture then the bimodal functions could still provide good replication of the pore water pressures. When a soil cracks, different sizes of crack appear within the volume as the soil dries. Therefore even if some cracks are greater than the maximum width it could be possible that the majority of crack apertures are still below this value. Furthermore, crack width decreases with depth, tapering out at depth (Greve et al., 2010), meaning that even if the capillary law does not apply to some cracks at shallower depths, as the depth increases capillary flow becomes pervasive.

5.8.1.3 Effect of the bimodal van Genuchten parameters

In the development of the bimodal functions sensitivity analyses of the van Genuchten parameters for the crack part were carried out. Analyses of the crack porosity (Section 5.4.1), the '*a*' parameter (Section 5.4.3) the '*n*' parameter (Section

5.4.4) were presented. It was found that for each parameter, adjusting its value would only influence the results to a certain value, after which altering the value any more had no effects.

By increasing crack porosity, decreasing a and increasing n it was intended to replicate the influence of larger cracks present in the soil. This only worked until certain values. It is postulated by this author that these values could represent the point at which capillary flow no longer applies to fluid flow in the cracks and gravity flow takes over. This theory ties in with what was discussed in the previous section where it was noted that capillary flow only applies up to a maximum crack aperture, at which point water cannot bridge the sides of the crack and gravity flow takes over. Therefore, no matter what values are used for the cracked part of the bimodal functions the full hydrological behaviour of the cracks may never be captured.

This has not adversely affected the modelling results presented in this chapter, implying that cracking on the Newbury slope in 2003 was not that severe and capillary flow still dominated in the crack network. However, there could be implications if cracking in the slope was to be more significant. For example, if larger cracks do develop it could mean that gravity flow becomes more prominent and the bimodal functions may not be wholly applicable.

5.8.2 Final bimodal model

The final bimodal model, presented in Section 5.7.3 resulted in the best replication of the hydrology of the Newbury cutting throughout 2003. Pore water pressure profiles at instrument group C at the end of summer (Figure 5-24) and the end of the year (Figure 5-25) and the pore water pressure trends (Figure 5-26 to Figure 5-29) showed the best agreement with the observed pore water pressures for any of the models.

By increasing the crack depth to 1.5 metres, the pore water pressure trends at depths greater than this were affected. At a depth of 25 metres (Figure 5-29) particularly the very sudden increase in pore water pressures after day 310 are replicated with much

more accuracy than the initial bimodal model. By increasing the crack depth, moisture is able to infiltrate with greater ease to greater depths. These results show the importance of properly defining the depth of cracking.
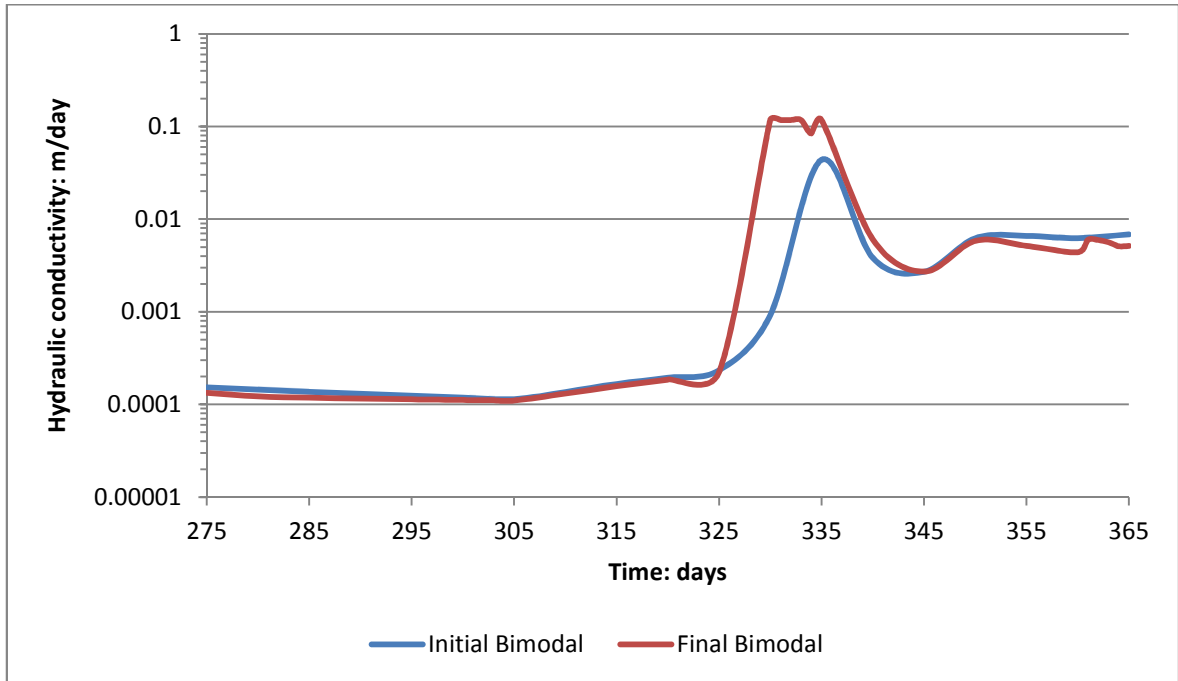
Figure 5-33: Comparison of temporal hydraulic conductivity at a depth of 1.5 metres for the initial bimodal and final bimodal models.

Figure 5-33 shows the hydraulic conductivity at a depth of 1.5 metres for the initial bimodal and final bimodal models. The maximum hydraulic conductivity reached for the final bimodal model is around one order of magnitude greater (0.12 m/day compared to 0.044 m/day). This maximum is also reached at a greater rate than the initial bimodal model; increasing at a steady rate from day 325 to the maximum at day 330, whereas the initial bimodal model increases from day 325 to a maximum at day 335.

The proper definition of the spatial and temporal variability of material properties has been identified as one of the critical factors for future modelling of the effects of climate on the hydrology of infrastructure slopes. The development of the bimodal model and the results presented show that using bimodal functions to represent the effects of desiccation cracking on the slope hydrology are a suitable way of achieving this. This method shows improved replication of pore water pressure magnitudes and

trends over methods that have not included the effects of desiccation cracking; including that of Davies et al. (2008a) and that presented in Chapter 4 of this work.

Improvements to the model may still be required, particularly definition of crack properties and cracking depth, which were both shown to be very important factors. The model is also based on a number of assumptions which may not always be realistic, meaning that the model could not actually be applicable. For example the model was developed assuming that flow in the cracks obeyed the capillary law, which may not be true if cracks exceed a certain width (Section 2.10.2.3).

5.8.2.1 Dissipation of suctions

The aim of this chapter was to develop the soil property model to improve the modelling of the temporal pore water pressures in the Newbury cutting slope. The major issue with initial models has been dissipating suctions by the end of the year. The observed values (Smethurst et al., 2006) showed that by the end of 2003 suctions in the slope had been dissipated. The model of Davies et al. (2008a) and the model presented in Chapter 4 of this thesis could not replicate this this.

By introducing the effects of desiccation, the dissipation of suctions has been captured with more success. Figure 5-34 shows a comparison between the end of year temporal pore water pressures for the observed, initial model with no cracks and final bimodal model values at a depth of 1.0m. The improvement in this facet of the modelling are clear; the initial model does not come close to dissipating suctions, whereas in the bimodal model the suctions are dissipated by 330 days.
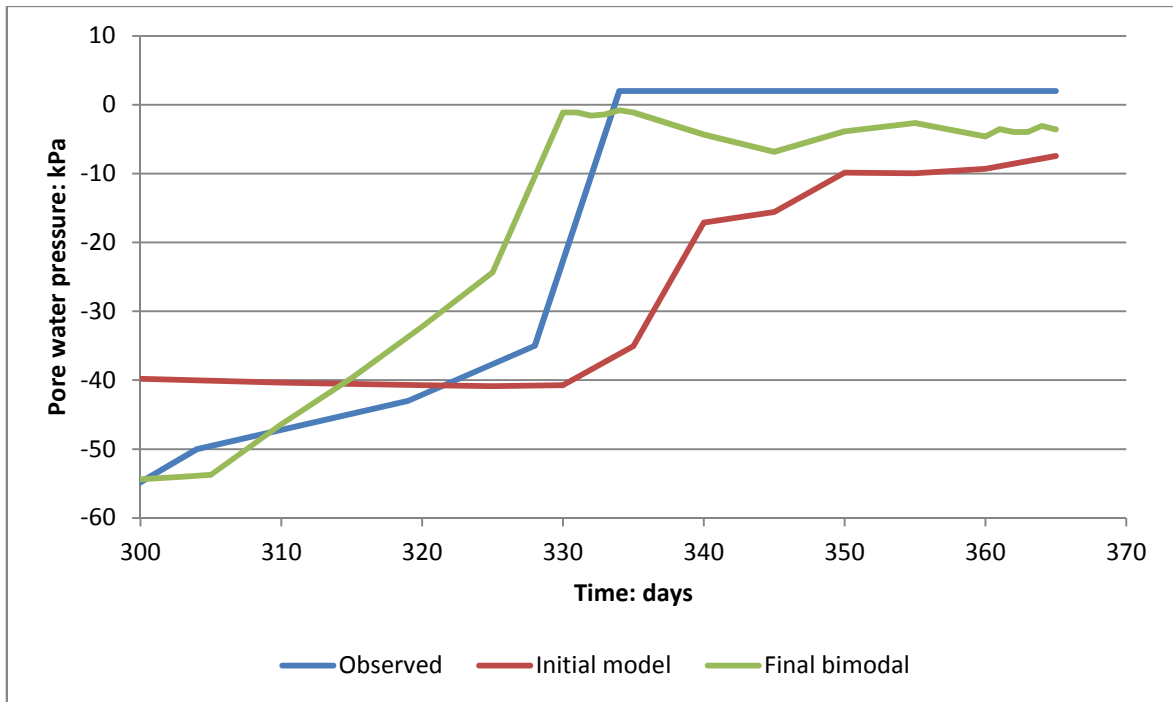
Figure 5-34: Comparison of the end of year temporal pore water pressures between observed values, the initial un-cracked model and the final bimodal model at a depth of 1.0 m.

There are still some discrepancies in the modelled results of the final bimodal model. After suctions in the final bimodal model have dissipated, they do reoccur; this does not happen in the observed values. A maximum suction of 6.8 kPa is recorded after dissipation. This suggests that in the numerical model sufficient water is unable to infiltrate the slope, or too much water is being removed, to prevent suctions from redeveloping. Considering the water balance, two possible explanations arise; excessive evapotranspiration from the soil or excessive runoff at the surface. Figure 5-35 shows the water balance for the final bimodal model, from the end of September 2003 to the end of December 2003. Transpiration is negligible and it has already been explained that evaporation is at expected magnitudes (Section 4.5.3.1). It therefore only remains that the runoff could be excessive. By comparing the calculated runoff to that measured by Smethurst et al. (2006) it can be shown whether this explains why suctions redevelop in the numerical model.
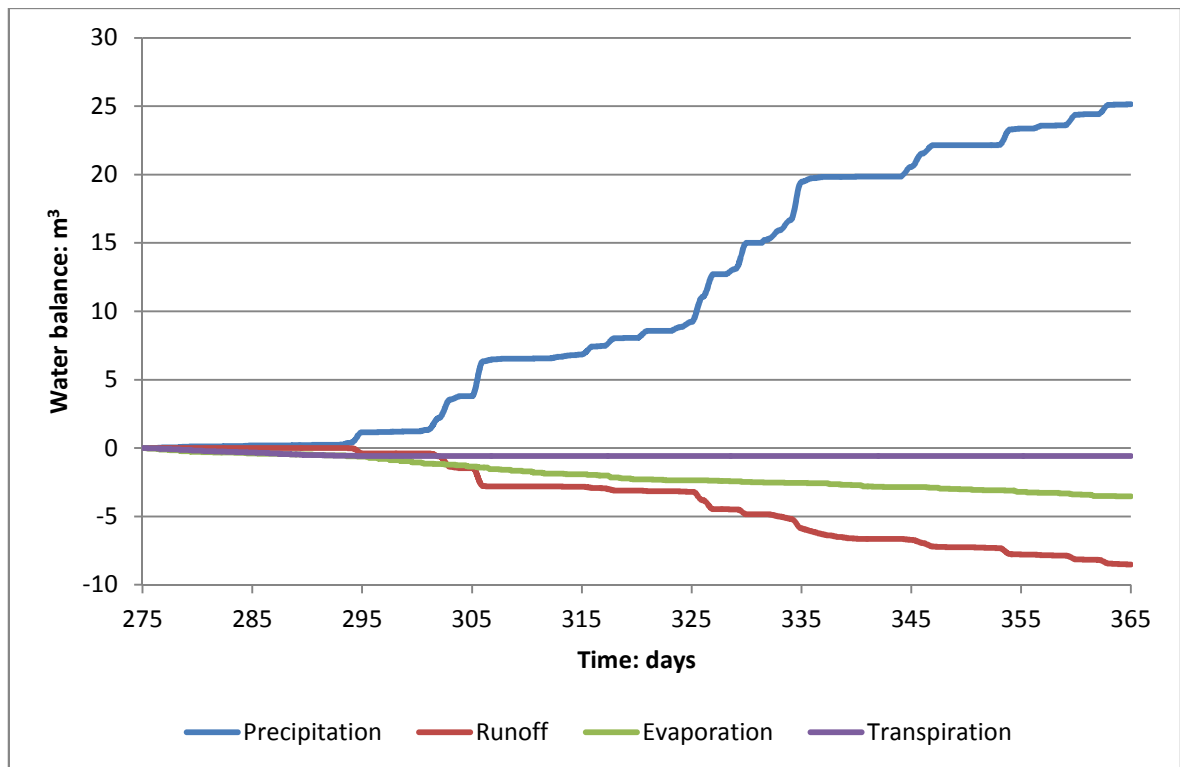
Figure 5-35: Water balance for final bimodal model; from the end of September 2003 to the end of December 2003.

Smethurst et al. (2006) recorded precipitation events and runoff at the Newbury cutting site. Runoff was recorded for all measured rainfall events greater than 1 mm. Figure 5-36 shows all recorded events, greater than 1 mm in magnitude, occurring in December 2003, and the proportion of the rainfall lost as runoff. From these values it is possible to calculate a total of 100 mm of precipitation and 43 mm of runoff, giving the cumulative proportion of precipitation lost as runoff as 43 %. During the same period in the numerical model 8.5 m^3 of precipitation fell, of which 3.5 m^3 was lost as runoff, giving a cumulative proportion of precipitation lost as runoff of 41 %.

These results suggest that the numerical model has correctly calculated the runoff from the Newbury cutting slope during December 2003. It seems that this cannot explain why suctions redevelop in the slope after they have dissipated (Figure 5-34). The problem may lie elsewhere with the model. The potential importance of hysteresis and its effects on soil hydrology have already been identified in the previous chapter and they will be considered further in the following section. It is also worth noting that the VADOSE/W model used precipitation data from a weather

station located 20 miles from the Newbury cutting site and therefore could introduce some error.
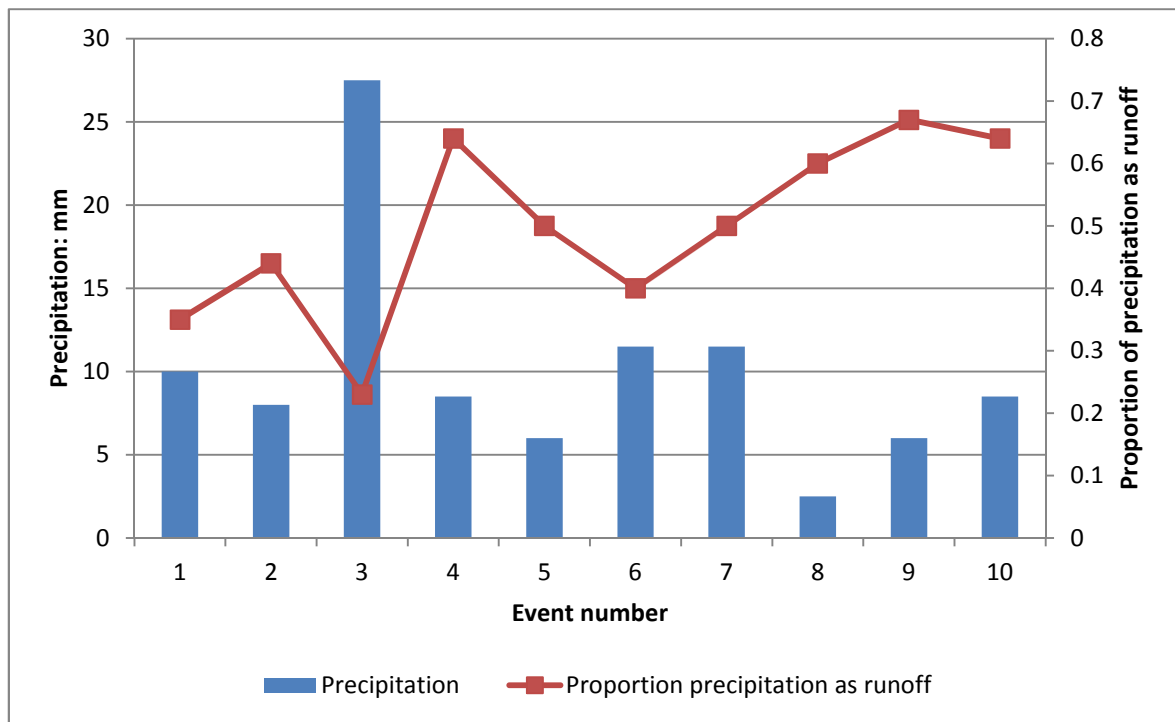
Figure 5-36: Precipitation events > 1mm and the proportion lost as runoff in December 2003. After Smethurst et al. (2006).

5.8.2.2 Hysteresis and crack development

The effects of hysteresis have not been considered in the models presented in this chapter. In Sections 2.9.3.4 and 4.5.3.3.1 the possible effects of hysteresis on the hydrology of soils and the modelling results have been discussed. It is believed that by not including the effects of hysteresis a major influence, perhaps as important as desiccation cracking, is ignored. The results in this chapter suggest that this is the case. By including desiccation cracking in the form of the bimodal SWCC and HCF the performance of the model has improved, particularly when modelling the trends of pore water pressure. However, the problems of dissipating suctions near the slope surface still exist. Figure 4-32 showed that when a soil such as the London Clay present at the Newbury site is wetting, at the same volumetric water content suctions could be up to 90% lower than when the soil is drying due to hysteresis.

The bimodal model cannot replicate these effects. The bimodal equations have allowed more water to infiltrate quicker to deeper depths but there is still a fundamental misrepresentation of the hydraulic behaviour of the soil. It shall therefore be recommended that hysteresis be considered in further research on this topic. It is however out of the scope of this project. It is also recommended that crack development be better represented. Once suctions were dissipated cracks were still present in the model; however it is probable that this has adversely affected the performance of the model. By leaving cracks present water was still bypassing the top layer of the slope meaning that even once suctions were dissipated they could increase again. Figure 5-37 shows this problem. In this plot suctions are shown to have dissipated in the model around 325 days, at this time the large crack porosity model should have been changed to the low porosity model.
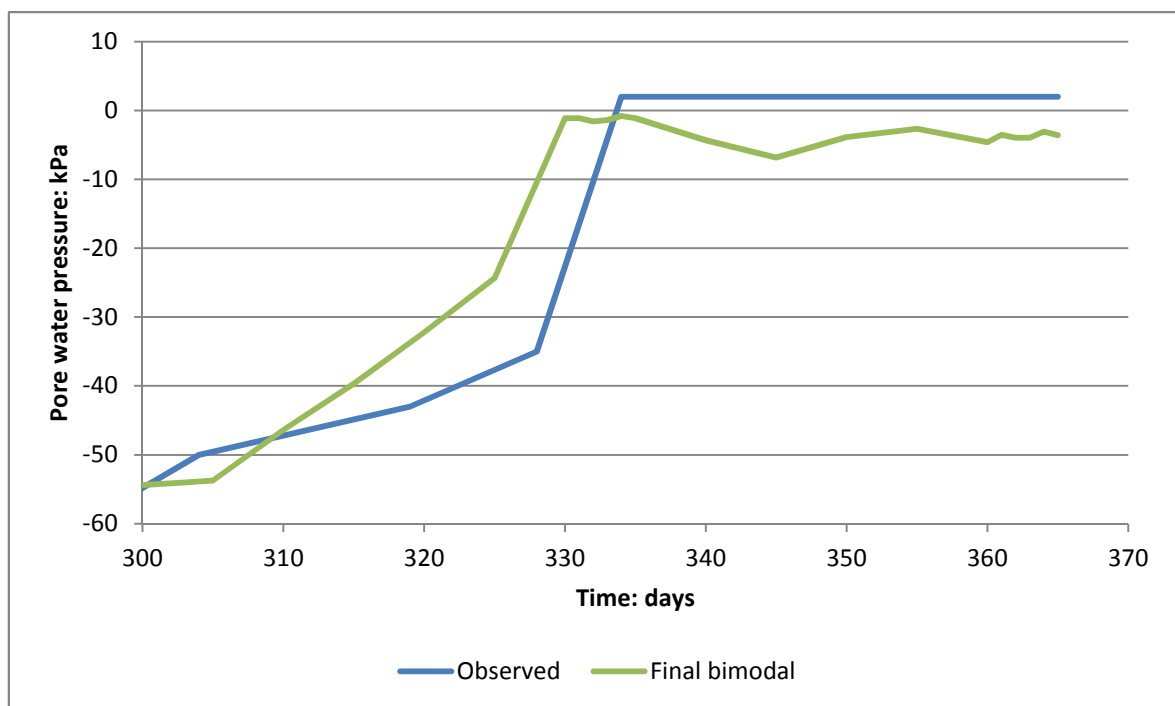
Figure 5-37: Observed and modelled temporal pore water pressures from the end of summer 2003 until the end of the year.

5.8.3 Implications for slope stability modelling

The use of static pore water pressure data to conduct slope stability analyses has been identified as poor practice in the literature review (Dijkstra and Dixon, 2010). This is due to the temporal nature of pore water pressures, which react to a seasonal

climate such as that in the United Kingdom. Temporal and spatial variability of material properties also play an important role. In the following section, it is aimed to reveal the importance of considering the role of temporal and spatial variability of climate and material properties.

5.9 Summary

In this chapter the numerical model created in Chapter 4 was improved by further development of the material model. This was achieved by accounting for the effects of desiccation cracking on the hydraulic properties of the soil. A bimodal, continuum approach was taken. Bimodal functions for the soil water characteristic curve and hydraulic conductivity function were developed by combining separate van Genuchten equations for the cracks and the intact soil each with its own set of distinct parameters.

The bimodal functions were implemented in the Newbury cutting numerical hydrology model and run with the same boundary conditions applied to the initial model in Chapter 4. The results obtained from this model run were promising; with improvements particularly noticeable in the temporal pore water pressures after the end of September. By including cracks in the model the maximum hydraulic conductivity was increased by 3 orders of magnitude, allowing water to more easily infiltrate the slope, reducing suctions to values more in line with what was observed by Smethurst et al. (2006).

It was noted that the model still struggled to dissipate suctions from the top 1.5 metres of the slope profile. Therefore, it was decided to develop the bimodal functions even further. This was accomplished by carrying out a number of sensitivity analyses on the van Genuchten parameters and also looking at the effects of changing crack depth. The results were found to be sensitive to the van Genuchten parameters a and n as well as the value of the saturated volumetric water content of the crack. By increasing the depth of cracking more in line with those observed in the field the results were improved even further. The result of these analyses was the 'final bimodal model'. This model gave the most significant improvements to the pore

water pressure replication, in terms of the profiles at the end of summer and winter, when suctions were dissipated, and also the temporal behaviour from the end of September 2003, until the end of the year.

There were still some discrepancies between the modelled results and the observed trends. For example after suctions were dissipated in the model, small suctions were able to redevelop, which was not observed in the field. This was most likely due to one of the assumptions that were made when developing the bimodal functions and the numerical model and also some misrepresentation of soil hydrology behaviour. By assuming that the cracks are of constant size with respect to water content the dissipation of suctions does not affect the hydraulic conductivity of the soil in the way that it would in the field. This may have been avoided by changing the material model to un-cracked once suctions had dissipated, mirroring the closing of cracks as the soil re-saturates. This would be an improvement in the model and should be considered for any future work on developing this method. The effects of hysteresis must also be considered, especially in clay soils where the difference between suctions on the wetting and drying curves could be as much as 90% (Fredlund et al., 2011).

6 Modelling the effects of climate change on the Newbury cutting

6.1 Chapter Outline

An improved model for predicting the temporal pore water pressures within an infrastructure cutting was developed in Chapter 5. The model includes the effects of desiccation cracking on the water retention and hydraulic conductivity properties of a clay soil. The model was shown to be particularly capable of capturing the sudden increase of pore water pressures that can occur at the end of summer when the rainfall events become more intense in nature.

In this chapter the new bimodal soil water characteristic curve and hydraulic conductivity function have been utilised to analyse the effects of climate change on the hydrology of the Newbury bypass cutting. Control and future climate boundary conditions were created using the UKCP09 weather generator (Section 6.4.1). The weather generator can create sets of temporal future climate data that can be adapted such that it can be applied as a VADOSE/W climate boundary condition.

Results from previous works identified in the literature review suggest that in the future, slope hydrology in man-made slopes will change, with larger suctions being prevalent at the end of summer which are not dissipated in the winter, slopes will become more stable (Section 2.11.3). However, none of these analyses have properly included the effects of desiccation cracking, and by doing so here, with the use of the bimodal functions, it was anticipated that a better understanding of the impact of climate change on slope hydrology would be established.

247

The aim of this chapter was to provide a better understanding of the potential effects of climate change on slope hydrology of man-made slopes. This aim was achieved by completing the following objectives:

- Identifying the type of seasonal variance, in terms of rainfall, that has the greatest effect on the magnitude of pore water pressure cycles in the Newbury cutting.
- Using the UKCP09 weather generator to create future temporal climate data series for the Newbury bypass cutting site and manipulating the data such that it could be used as a climate boundary condition in VADOSE/W.
- Applying the future climate boundary conditions exhibiting the identified seasonal variance to the Newbury cutting VADOSE/W model and run the model with bimodal material properties to calculate pore water pressures and suctions.
- Comparing the future hydrological behaviour to results from the previous sections so that conclusions on the effects of climate change on slope hydrology could be made.

The chapter is split into the following main sections:-

- A method for estimating the depth of desiccation cracks is introduced and validated against the Newbury cutting data – Section 6.2.
- Seasonal climate variance is investigated and the type most likely to affect progressive failure is identified – Section 6.3.
- The methodology for using the weather generator and applying the appropriate climate boundary conditions is developed – Section 6.4.
- The model results and analysis are presented. The statistical analysis methods used are also described – Section 6.5.
- The results are discussed in detail – Section 6.6.

6.2 Crack depth estimating

In Chapter 5 (Section 5.3 to 5.7) crack depths were based on field observations taken from the literature (Arnold et al., 2005; Inci, 2008). This approach was shown to be

reasonable when modelling just one year of climate data, showing good agreement between the calculated pore water pressure and suction trends and those observed by Smethurst et al. (2006).

In this chapter, multiple years of climate data, some based on future climate predictions, were modelled, each with different characteristics of temperature and precipitation. This led to different trends and magnitudes of soil moisture content and suctions and therefore the development of different cracking depths. When considering that future climate predictions for the United Kingdom suggest that warmer, drier summers shall become more prevalent, it is reasonable to think that in the future there will be more severe desiccation cracking in soil slopes (Section 2.11.2), with cracks extending to a greater depth. Therefore, it was decided to investigate the suitability of a method of estimating the maximum depth of desiccation cracking, suggested by Fredlund and Rahardjo (1993).

6.2.1 Crack depth estimation method

Fredlund and Rahardjo (1993) suggested the following equation for estimating the maximum crack depth:

Equation 6-1

$$y_c = \frac{D}{1 + \frac{\upsilon \rho H_s}{f_w \rho_w E_e}}$$

This equation allows the crack depth, y_c, to be calculated from the depth of water table D, the suction profile and the soil properties ρ, H_s and E_e, which are described in more detail in Section 2.10.2.6 of the literature review. The variable f_w is the ratio of actual suctions to hydrostatic suctions and is used to account for the effects of higher suctions on depth of cracking. The equation calculates the crack depth on a steady state situation where the growth of the cracks is in equilibrium with the suctions and therefore represents an upper limit on the possible crack depth. The calculated crack depth is therefore independent of the history of suctions. The implications of this are discussed in Section 6.6.1.3.

The following example shows how Equation 5-1 can be used to estimate the maximum depth of cracks developing within the Newbury cutting at the end of summer. Figure 6-1 shows two typical end of summer suction profiles (Profile 1 and Profile 2) compared to the hydrostatic profile with the phreatic surface located at a depth of 4.0 metres. The example calculations detailed below show how the depth of cracking is calculated for each suction profile, also explaining how larger magnitudes of suctions result in a greater depth of cracking (Table 6-1 and Table 6-2).
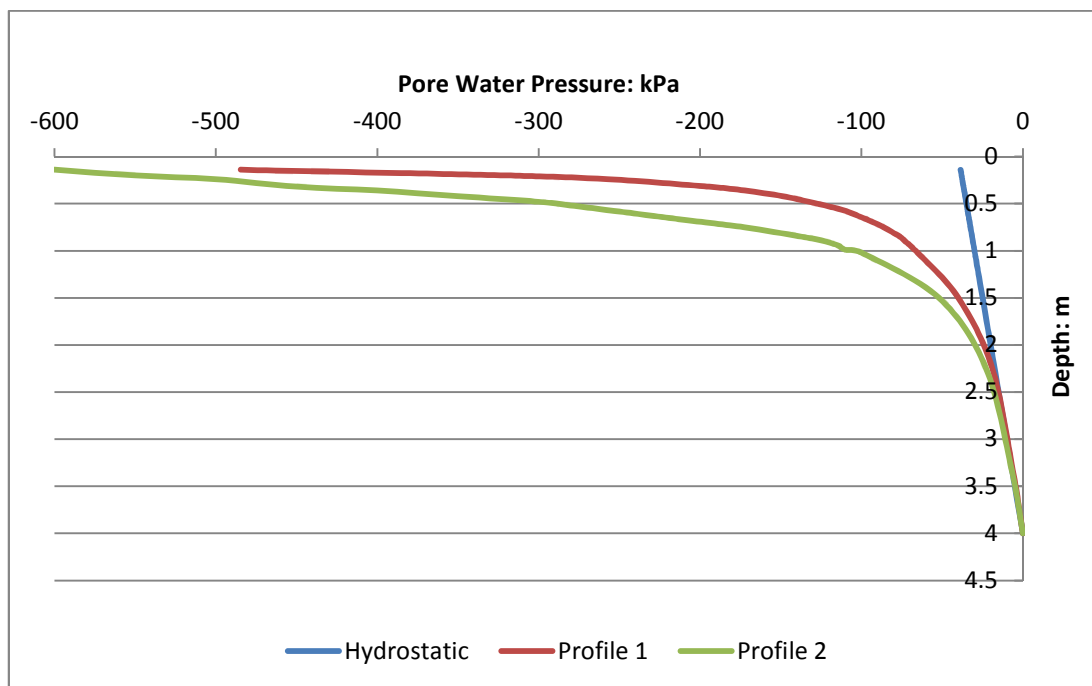
Figure 6-1: Two typical end of summer suctions profiles compared to hydrostatic suctions.

For each suction profile a value of f_w is required for Equation 5-1. To find the relevant value, an average value of f_w through each profile is calculated. This is achieved by comparing values of suction between the actual suction profile and the hydrostatic profile at many depths. Table 6-1 shows suction values at depths for each profile compared to the hydrostatic value at that depth and also the value of f_w corresponding to each depth.

Depth: m	Hydrostatic suctions: kPa	Profile 1 suctions: kPa	Profile 1 f_w	Profile 2 suctions: kPa	Profile 2 f_w
4.00	0.0	0.0	**1.0**	0.0	**1.0**
3.33	6.7	6.2	**1.0**	6.9	**1.0**

2.24	17.6	19.1	**1.1**	23.0	**1.3**
1.50	25.0	40.0	**1.6**	52.0	**2.1**
1.02	29.8	65.2	**2.2**	100.0	**3.4**
0.99	30.1	67.1	**2.2**	110.0	**3.6**
0.94	30.6	70.1	**2.3**	115.0	**3.8**
0.89	31.1	73.5	**2.4**	124.9	**4.0**
0.85	31.5	76.2	**2.4**	137.1	**4.4**
0.80	32.0	81.2	**2.5**	154.3	**4.8**
0.75	32.5	86.3	**2.7**	172.7	**5.3**
0.71	32.9	91.1	**2.8**	191.2	**5.8**
0.66	33.4	97.8	**2.9**	215.1	**6.4**
0.58	34.2	109.5	**3.2**	251.7	**7.4**
0.53	34.7	120.0	**3.5**	275.0	**7.9**
0.48	35.2	132.4	**3.8**	300.0	**8.5**
0.42	35.8	149.0	**4.2**	350.0	**9.8**
0.36	36.4	172.4	**4.7**	400.0	**11.0**
0.32	36.8	194.5	**5.3**	450.0	**12.2**
0.24	37.6	257.0	**6.8**	500.0	**13.3**
0.20	38.0	320.1	**8.4**	550.0	**14.5**
0.14	38.6	484.6	**12.6**	600.0	**15.6**

Table 6-1: Calculation of average value of fᵥᵥ.

The mean value of f_w is now calculated for each profile: 3.61 for profile 1 and 6.68 for profile 2. These values can be used in conjunction with the material property values and input into Equation 5-1 to calculate the maximum cracking depth. Table 6-2 shows the material property values used in this example and the resulting crack depth for each profile. The values of v, ρ and E_e/H_s were identified by Fredlund and Rahrdjo (1993) as suitable for a clay soil.

Parameter	**Profile 1**	**Profile 2**
D	4.0 m	4.0 m
v	0.2	0.2
ρ	1880 kg/m³	1880 kg/m³
ρ_w	1000 kg/m³	1000 kg/m³
E_e/H_s	0.17	0.17
f_w	3.61	6.68
y_c	2.48 m	3.00 m

Table 6-2: Results of crack depth estimation for two typical end of summer suction profiles.

The equation has calculated maximum cracking depths for Profile 1 and Profile 2 of 2.48 metres and 3.00 metres respectively. These results highlight the effects that high suctions have on the potential extent of desiccation cracking within slopes. The equation however needs to be validated, to show that the crack depths estimated are actually realistic for the conditions present in the soil.

6.2.2 Crack Depth Estimation Method Validation

In Section 5.7 a maximum crack depth of 1.5 metres was applied to the Newbury cutting following the end of summer. When this value, based on observations by Arnold et al. (2005), was used, the observed pore water pressure and suction trends were replicated reasonably well. However, there were still some inconsistencies in the results, and by using this equation, which is based on actual material properties and field conditions, it was believed that the performance of the model could be improved further. In this section, Equation 5-1 has been used with two intentions:

1. Validating the crack depth estimation method.
2. Improving the performance of the VADOSE/W model.

The Newbury cutting model used in Section 5.7 was run with the 2003 climate data applied until the end of summer, when suctions were at a maximum. From the end of summer, the suction profile calculated by VADOSE/W (Table 6-3), in conjunction with the material properties given in Table 6-4 was used, and a maximum crack depth was calculated using Equation 5-1.

Depth: m	Hydrostatic suctions: kPa	End of summer suctions: kPa	f_w
3.86	0.0	0.0	**1.0**
3.75	-1.1	-1.0	**1.0**
3.63	-2.3	-2.2	**1.0**
3.50	-3.6	-3.4	**1.0**
3.38	-4.8	-4.6	**1.0**
3.25	-6.1	-5.9	**1.0**
3.13	-7.3	-7.1	**1.0**
3.00	-8.6	-8.3	**1.0**
2.75	-11.1	-10.9	**1.0**

2.63	-12.3	-12.3	**1.0**
2.50	-13.6	-13.7	**1.0**
2.38	-14.8	-15.2	**1.0**
2.25	-16.1	-16.7	**1.0**
2.13	-17.3	-18.5	**1.1**
2.00	-18.6	-20.3	**1.1**
1.88	-19.8	-22.4	**1.1**
1.75	-21.1	-24.8	**1.2**
1.63	-22.3	-27.6	**1.2**
1.50	-23.6	-31.1	**1.3**
1.38	-24.8	-35.5	**1.4**
1.25	-26.1	-41.6	**1.6**
1.13	-27.3	-51.0	**1.9**
1.00	-28.6	-69.5	**2.4**
0.96	-29.0	-72.0	**2.5**
0.91	-29.5	-74.9	**2.5**
0.87	-29.9	-78.0	**2.6**
0.83	-30.3	-81.4	**2.7**
0.78	-30.8	-85.3	**2.8**
0.74	-31.2	-89.7	**2.9**
0.70	-31.6	-94.7	**3.0**
0.65	-32.1	-100.5	**3.1**
0.61	-32.5	-107.2	**3.3**
0.57	-32.9	-115.0	**3.5**
0.52	-33.4	-124.3	**3.7**
0.48	-33.8	-135.6	**4.0**
0.43	-34.2	-149.4	**4.4**
0.39	-34.7	-166.8	**4.8**
0.35	-35.1	-189.5	**5.4**
0.30	-35.5	-220.4	**6.2**
0.26	-36.0	-265.4	**7.4**
0.22	-36.4	-338.1	**9.3**
0.17	-36.9	-458.7	**12.4**

Table 6-3: Calculation of f_w *for crack depth estimation method validation model.*

Table 6-3 shows the end of summer suctions, hydrostatic suctions and the calculated values of f_w. The phreatic surface was found to be at a depth of 3.86 metres; hydrostatic suctions were calculated from this giving an average f_w value of **2.67**. Equation 5-1 was used to calculate the maximum depth of cracking. Table 6-4 shows the parameter values used in this calculation. A maximum crack depth of **2.10 metres** was calculated using the equation.

Parameter	Values
D	3.86 m
ν	0.2
ρ	1880 kg/m^3
ρ_w	1000 kg/m^3
E_e/H_s	0.17
f_w	2.67
y_c	2.10 m

Table 6-4: Parameter values used for crack depth estimation method validation model.

6.2.2.1 Model Geometry and Material Properties

Cracked soil material properties were applied to the model to a depth of 2.10 metres and the model run until the end of the year. Validity of the crack depth estimation method was tested by comparing the calculated results to the observed values (Smethurst et al., 2006) and also to the results calculated in the previous chapter (Section 5.7).

Figure 6-2 shows the model with the high porosity material properties applied to a depth of 1.5 metres and the low porosity material applied for 0.6 metres below. This splitting has been done to account for the reduction in cracking that is observed with depth. Arnold et al. (2005) observed that the majority of cracking (> 70%) occurred in the top 1.5 metres of a soil's profile, which is consistent with observations made by Smethurst et al. (2006) at the Newbury cutting site. Smethurst et al. (2006) observed sudden changes in pore water pressure occurring at depths of 1.0 and 1.5 metres in December 2003. They remark that this was due to rain filling desiccation cracks close to the measuring instruments.
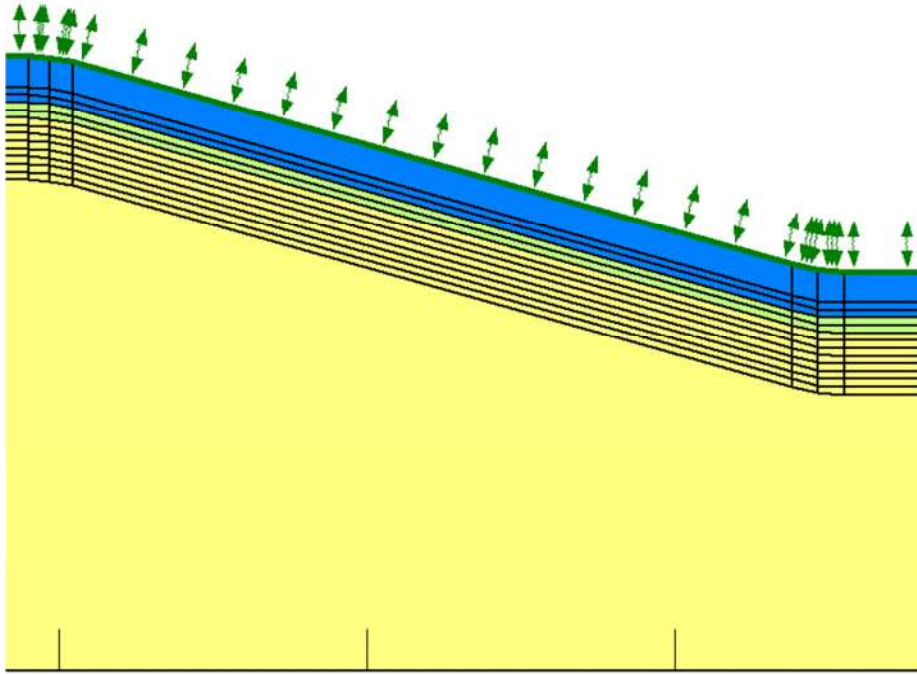
Figure 6-2: Newbury cutting slope model with high porosity (blue) and low porosity (green) bimodal material properties.

The model was run until the end of the year. Pore water pressure profiles and trends are generated which are compared to previous model runs (presented in the following section).

6.2.2.2 Results

Figure 6-3 shows the results of the crack depth method validation analysis. Pore water pressure and suction trends have been plotted from the end of summer until the end of the year. Results are compared with the observed values (Smethurst et al., 2006). In these plots 'validation' refers to the results obtained from the model run in this section and 'final' to the model run in the previous chapter (Section 5.7). The profiles show the results obtained from four depths below the location of instrument group C; 1.0, 1.5, 2.0 and 2.5 metres.
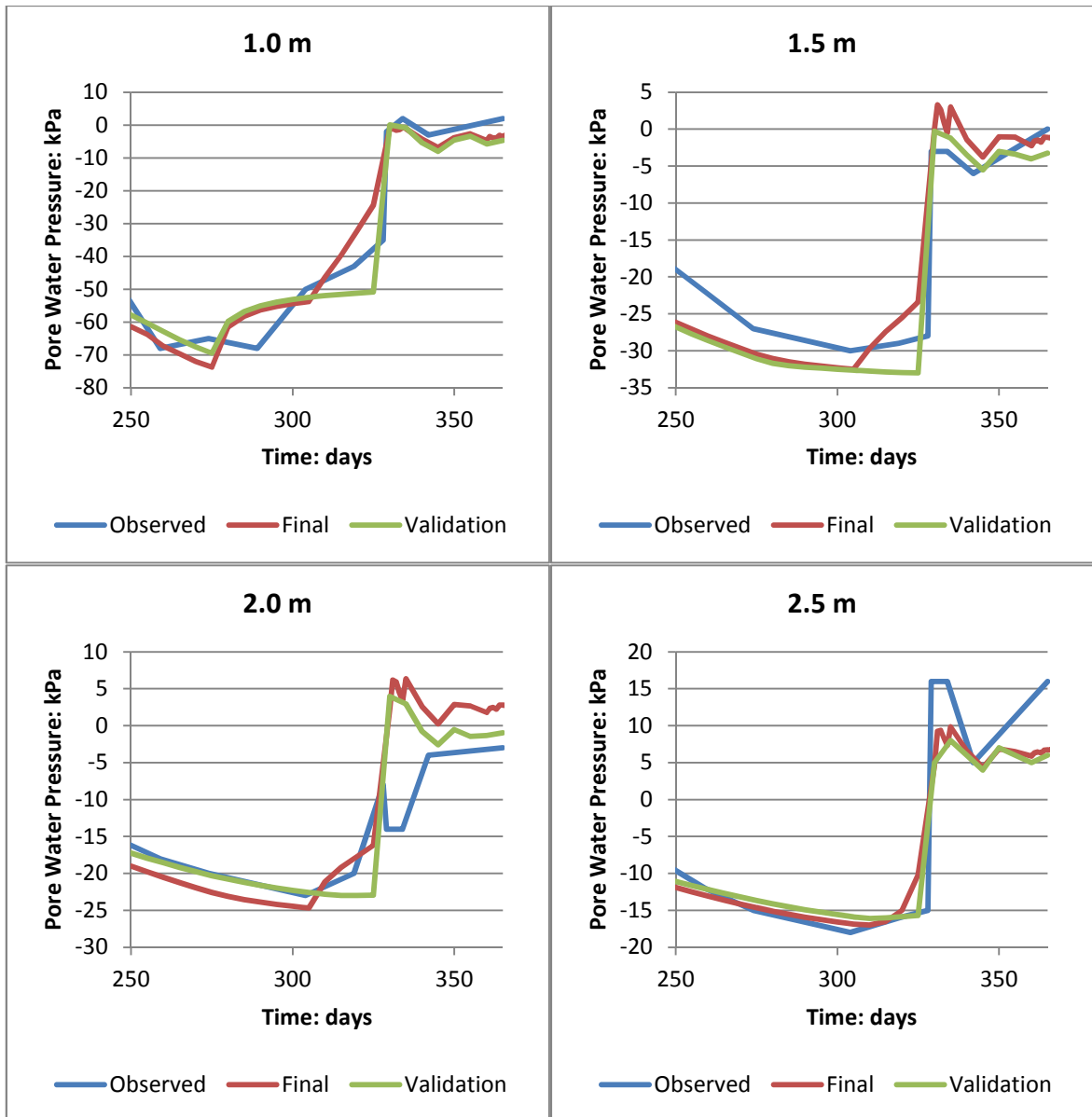
Figure 6-3: Results of crack depth estimation method validation at various depths below mid-slope. Results are compared to the observed values and the results from the final bimodal model from Section 5.7.3.

An increase in crack depth from 1.5 metres to 2.1 metres has shown some improvement in the results. In terms of the calculated minimum and maximum suctions the model performs similarly to the previous model, not significantly affecting the timing of the occurrence or the magnitude of maximum and minimum suctions. The main improvements are seen when considering the rate of decrease of suctions and the point at which this decrease begins. Previously the model had not quite matched the steepness of the gradient of falling suctions, however the latest model sees suction decrease at a much greater rate. At depths of 1.0, 1,5 and 2.0

metres this is most noticeable; the model with deeper cracks has replicated the very steep gradient of suction decrease and also the time that this decrease begins (325 – 330 days). The model has a similar performance to the previous version at a depth of 2.0 metres, but the magnitude of maximum and minimum suctions are somewhat improved.

The results of this analysis have shown that Equation 6-1 can be used to give reasonable estimates of maximum crack depth occurring in desiccated soils. By using end of summer suctions and available soil properties, a maximum crack depth can be calculated with the equation, which can then be used within the VADOSE/W model. In Section 6.3 and Section 6.4 this method is utilised.

6.3 Effects of seasonal variance

In Section 2.3 of the literature review the effects of seasonal climate variance on the magnitude of pore water pressure and suction cycles was investigated. The implications of large pore water pressure cycles on the long term stability of soil slopes has been recognised (Section 2.5). With a changing climate, including warmer and drier summers, in the United Kingdom, there is expected to be an effect on the magnitude of these cycles. Warmer, drier summers will lead to high suctions developing which contribute to the large cycles (Section 2.11.2). The purpose of the work in this section was to identify what kinds of seasonal climate variance lead to the development of such large pore water pressure cycles.

In Chapters 4 and 5 the Newbury bypass cutting model was run with only the year 2003 climate data applied. The winter of 2002/2003 was extremely wet, and was subsequently followed by a very dry summer in 2003 and another wet winter in 2003. This WET-DRY-WET seasonal variance resulted in a high magnitude cycle of pore water pressures. It could be assumed that a WET-DRY-WET year is the worst case scenario for producing the largest cycles of pore water pressures. However it may be possible that other seasonal variances may be worse; for example a DRY-DRY-WET year may develop much greater suctions in the summer. To test this theory all the available years of climate data for the Newbury site (2003-2006) were applied to the

model in order to observe pore water pressure trends over a longer term and analyse the effects of other types of seasonal variances.

Figure 6-4 shows the monthly total rainfall for each of the years of available Newbury climate data compared against the 30 year long term monthly averages (1961-1990) for the site. The long term average has been plotted as a column chart to provide some clarity, and each of the years has been plotted as a line.
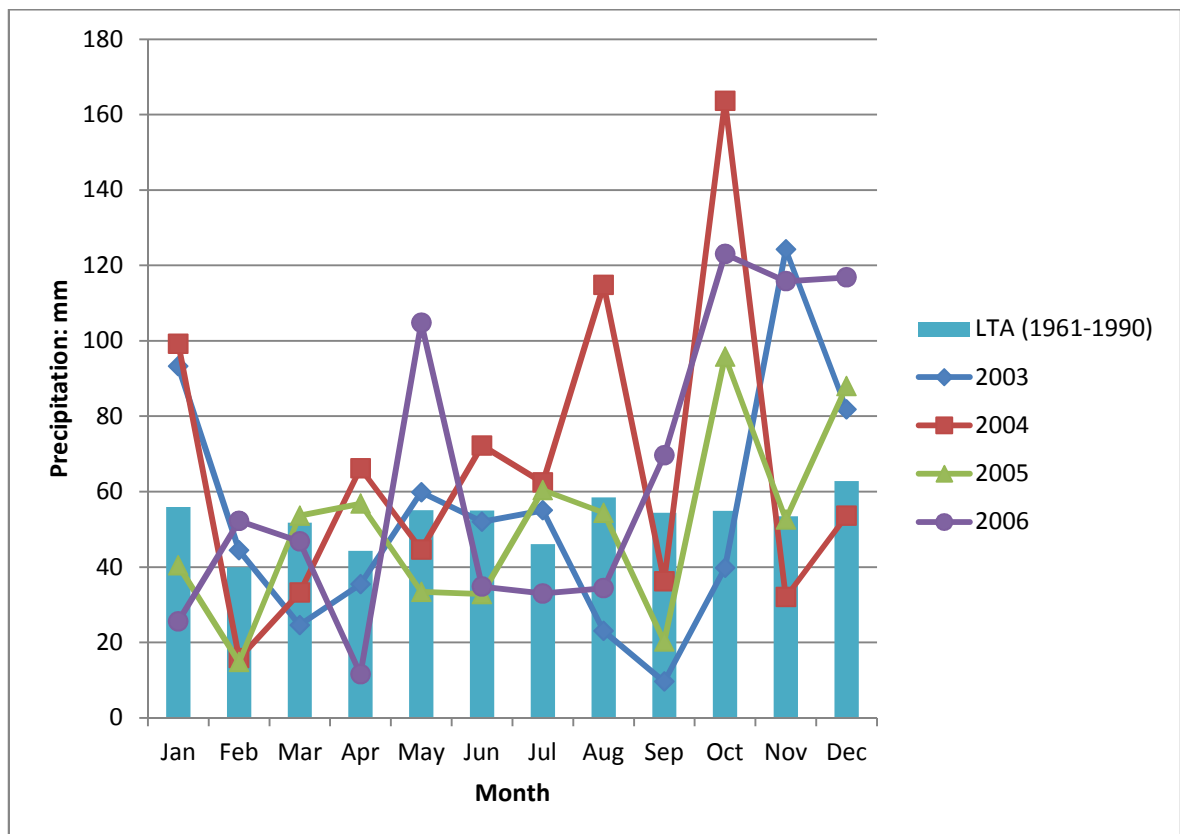
Figure 6-4: Newbury monthly total rainfall for 2003 - 2006 compared to the long term average.

From this graph it is possible to determine the seasonal variance throughout each of the years. The very dry months of August and September 2003 can be seen with precipitation shown to be well below the long term average for these months. The next year, 2004, is shown to be very wet throughout most of the year. Rainfall is above average in 6 months and the total annual rainfall is 793.8 mm, much greater than the long term average of 659.7 mm.

2004 could be described as a DRY-WET-WET year. It starts with a wet January but then moves through a dry February, March and May. Following this the summer is very wet, with the monthly average exceeded in June, July and August. October is extremely wet; with the total rainfall more than double the long term average for that month.

2005 is just on the dry side of average, with the majority of months not being extremely dry or wet. A definition of DRY-DRY-WET would seem the most appropriate for this year. Total rainfall in January and February is below average, as it is in May, June, August and September. For the winter months the total rainfall is above average in October and December.

2006 can be described as DRY/WET-DRY-WET. Total monthly rainfall in October, November and December is much greater than the long term averages resulting in a very wet winter. Total monthly rainfall in the summer months of June, July and August is below the long term average. For the first part of the year it is difficult to judge the classification. The total rainfall in January and April total is well below long term average but in May the total precipitation is significantly greater than the long term average.

6.3.1 Model Geometry, Meshing and Material Properties

To analyse the effects of each of the types of identified seasonal climate variance, the Newbury cutting model was run with all four years of climate data applied sequentially. The model was set up in such a way that the initial conditions for each year were generated from the final conditions of the year previous and thus the effects of antecedent conditions were captured.

A similar approach is taken to the final model produced in Chapter 5 with multiple crack depths and bimodal material properties being utilised throughout the model run. This is achieved by applying the low porosity material properties to the top 1.0 metre of the profile from the beginning of each year until the point that maximum suctions were reached, after which the high porosity material properties were applied until the end of the year to the depth calculated by Equation 6-1 using the

method developed in Section 6.2. Table 6-5 details the crack depths, material models and the time steps which each is applied to for the four years modelled.

There are a total of 8 models created for this analysis; 2 for each year, including low porosity and high porosity. Figure 6-5 shows how each analysis is related to the previous in VADOSE/W model.

Figure 6-5: Analyses tree, showing the relationship between analyses in the climate seasonality analysis.

Initial conditions for each model after the first (2003_to end Sept in Figure 6-5) are defined by transferring the pore water pressures calculated at the last time step of the previous model. Initial conditions of the first model will be defined by the initial water table, as they were in all the previous model runs.

Table 6-5 shows the depths of cracking calculated using Equation 6-1 at the end of summer of each year, when maximum suctions occur, the table also shows the time steps at which the cracks are applied and then deactivated. Each of these maximum crack depths is independent; i.e. the crack depth for the end of summer 2004 does not directly impact the crack depth at the end of summer 2005. The greatest crack depth was calculated at the end of summer 2003, followed by 2005 both of which have dry summers. 2004, which has a relatively wet summer, records the shallowest crack depth, of only 1.0 m.

Year	Low porosity depth	Time steps active	High porosity depth	Time steps active
2003	1.0 m	0 - 275	2.1 m	275 - 365
2004	1.0 m	365 - 641	1.0 m	641 - 731
2005	1.0 m	731 – 1006	2.0 m	1006 - 1096
2006	1.0 m	1096 - 1371	1.7 m	1371 - 1461

Table 6-5: Material models, crack depths and applied time steps.

6.3.2 No cracks model

To gain further understanding of the effects of desiccation cracking on the slope hydrology the same model without the bimodal soil models was run. This model was also run for all 4 years of climate data but with only London Clay un-cracked material properties used throughout.

6.3.3 Results of seasonal variance analysis

Results of the full model runs are now shown. Pore water pressure and suction trends have been plotted at various depths below the location of instrument group C. Several depths are chosen so as to ascertain the effects of different seasonal variance throughout the slope in soil at different states, ranging from always un-cracked at a depth of 4.0 metres to constantly within the cracked zone at 0.5 metres. Graphs have been produced for the following depths:

1. 0.5 metres - Figure 6-6 a)
2. 1.0 metres - Figure 6-6 b)
3. 1.5 metres - Figure 6-7 a)
4. 2.0 metres - Figure 6-7 b)
5. 4.0 metres - Figure 6-8

Each of the graphs shows seasonal pore water pressure and suction trends from the beginning of 2003 through to the end of 2006. Pore water pressure cycles have been calculated at each depth. The magnitude of a pore water pressure cycle is defined as the difference between the minimum suctions present during the winter and

261

maximum suctions present during the summer, whether this be when suctions are increasing or decreasing. Table 6-6 summarises the magnitude of the cycles at each of the depths for all years taken from both the model including desiccation cracking and that without desiccation cracking.
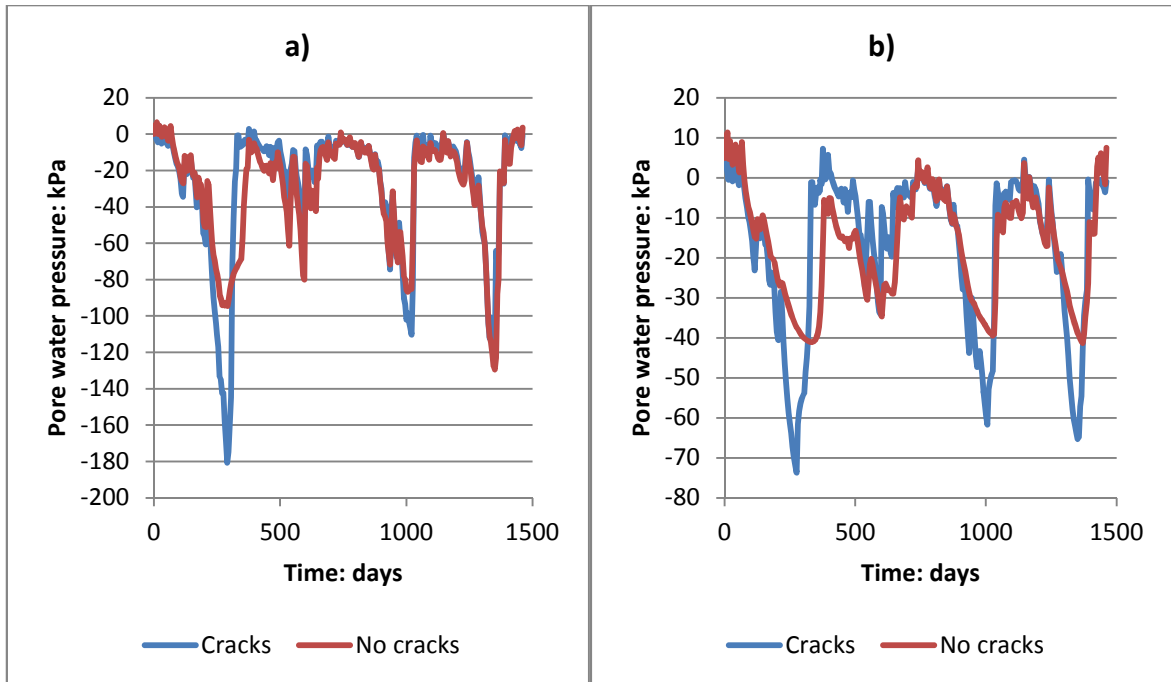
Figure 6-6: Pore water pressure and suction trends at a depth of a) 0.5 metres and b) 1.0 metre, showing the difference between a model with desiccation cracking and one without.

Figure 6-6 a) shows the pore water pressure and suction trends at a depth of 0.5 metres. This is within the zone of soil that is always cracked and also within the rooting zone of the present slope vegetation. The effect of the very dry summer of 2003 is evident; suctions are extremely high, reaching a maximum of 205 kPa at the end of summer. This value is significantly greater than at any other year; the wet summer of 2004 yields suctions reaching a maximum of only 54 kPa. The following year sees larger suctions developing once more; a dry start to 2005 and a dry summer leads to a maximum suction of 109 kPa at this depth. 2006, which also has a dry summer, following an average winter again results in high suctions of almost 120 kPa developing at a depth of 0.5 metres.

Figure 6-6 b) shows the pore water pressure and suction trends at a depth of 1.0 m. At this depth the difference in magnitude of maximum suctions for each year is less

apparent. 2003 still experiences the greatest suctions of 72 kPa at the end of summer. 2005 and 2006 which both had dry summers also experience high suctions at this depth of 60 kPa and 65 kPa respectively. The year 2004, which had the wettest summer of the four years, experiences significantly lower suctions of 35 kPa at a depth of 1.0 m.
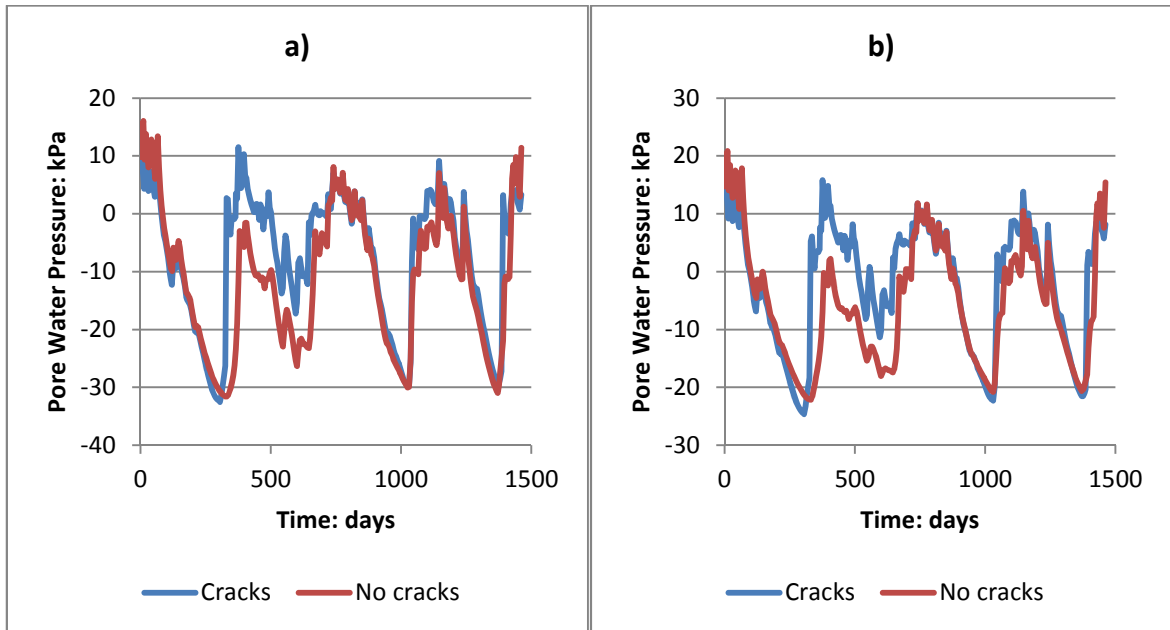
Figure 6-7: Pore water pressure and suction trends at a depth of a) 1.5 metres and b) 2.0 metres, showing the difference between a model with desiccation cracking and one without.

Figure 6-7 a) and b) shows the pore water pressure trends at depths of 1.5 and 2.0 metres respectively. At these depths the differences between maximum suctions during each of the years experiencing dry summers are reduced. During 2003 the maximum suctions are 33 kPa and 24 kPa, during 2005 they are 30kPa and 22 kPa and during 2006 they are 30 kPa and 22 kPa. Suctions are still significantly lower during 2004, only 17 kPa at 1.5 metres and 11 kPa at 2.0 metres.
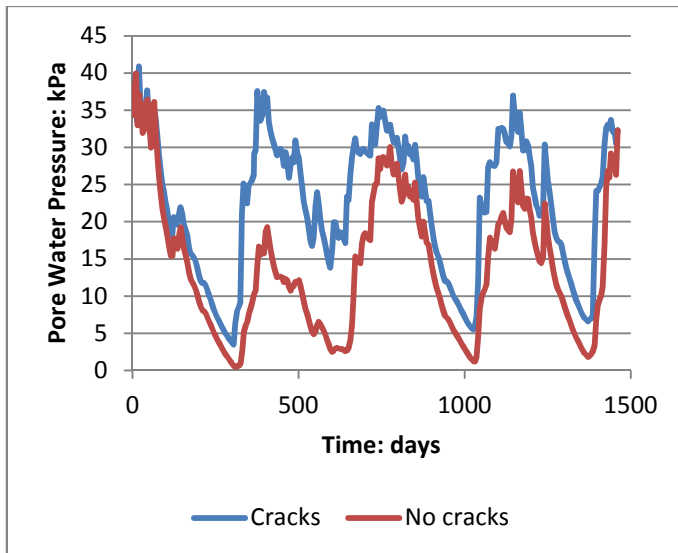
Figure 6-8: Pore water pressure trends at a depth of 4.0 metres, showing the difference between a model with desiccation cracking and one without.

Figure 6-8 shows the pore water pressure trends at a depth of 4.0 metres. At this depth no suctions have developed during any year; therefore positive pore water pressures are considered. The difference between the smallest pore water pressures is small between the years with dry summers; 2003 has the lowest of 4 kPa, 2005's and 2006's are 5 kPa and 7 kPa respectively. The minimum pore water pressures during 2004 are significantly greater; 15 kPa.

| Depth | Year | | | |
| | 2003 | | 2004 | |
	Cracks	*No cracks*	*Cracks*	*No Cracks*
0.5 m	185 kPa	98 kPa	54 kPa	74 kPa
1.0 m	83 kPa	42 kPa	41 kPa	38 kPa
1.5 m	46 kPa	47 kPa	29 kPa	34 kPa
2.0 m	32 kPa	42 kPa	27 kPa	30 kPa
4.0 m	37 kPa	39 kPa	24 kPa	27 kPa

Depth	Year			
	2005		2006	
	Cracks	*No Cracks*	*Cracks*	*No Cracks*
0.5 m	109 kPa	87 kPa	117 kPa	130 kPa
1.0 m	64 kPa	43 kPa	70 kPa	48 kPa
1.5 m	36 kPa	38 kPa	38 kPa	42 kPa
2.0 m	24 kPa	32 kPa	35 kPa	35 kPa
4.0 m	30 kPa	28 kPa	30 kPa	30 kPa

Table 6-6: Magnitude of pore water pressure cycles for the models including and not including cracks for every year.

At all depths the slope experiences the greatest pore water pressure cycles during the year of 2003. The very dry summer results in large suctions generating through the top 2 metres of the soil profile which are recovered in the following wet winter. The results from the other years show that a dry summer is paramount to developing these large cycles. 2004, with its relatively wet summer, had the lowest cycles at all depths, whereas 2005 and 2006 which also exhibit dry summer months experience larger cycles, but not of the magnitude of 2003.

As the depth increases, the effect of the seasonal variance decreases. At a depth of 4.0 metres the difference between the minimum cycle and the maximum cycle is 54 % whereas at a depth of 0.5 metres the difference is 243 %. This difference can be due to the negligible effects of evapotranspiration at greater depths within the slope and also less water infiltrating from the surface. During dry summers demand for moisture by the vegetation increases leading to the high suctions seen in the top 1.0 metres of the profile. This effect however is not seen at greater depths, within this slope, as the roots do not extend any deeper. Desiccation cracks also have a role to play in the smaller cycles seen at greater depths; the small cracks in the slope from the beginning of the year and the larger cracks prevalent at the end of summer means that moisture can more readily infiltrate the slope, 'bypassing' the upper profile. This

effect also means that during a wet winter, as in each of the years in this analysis, suctions are generally recovered to their beginning of year level very rapidly.

Now considering the same model run with no desiccation cracking included, there is a significant difference between the results, including the magnitude of maximum and minimum suctions each year and also the size of pore water pressure cycles. Assuming that the model with cracks is more representative of the field conditions, it is clear that not considering its impact on soil hydrology can result in wildly erroneous predictions of pore water pressure magnitudes and trends, particularly in the top of the slope profile.

6.4   Outcome and Proceeding Methodology

Following the analysis of the results the decision was taken to further analyse the effects of WET-DRY-WET seasonal climate variance on the hydrology within the Newbury cutting when subjected to future climate scenarios. This was achieved by following a number of steps which are each described in their respective section:

1. Using the UKCP09 weather generator to create series of baseline and future climate scenarios for the Newbury bypass cutting location (Section 6.4.1).

2. Within each of the generated sets of data identify a year that exhibits WET-DRY-WET variance through the year, specifically focussing on very dry summers (Section 6.4.2).

3. Applying each identified year to the VADOSE/W Newbury bypass cutting model as a climate boundary condition and run the model to the end of summer (Section 6.5).

4. Analyse the results from the baseline climate series and future climate series and compare the magnitude of suctions developing at the end of summer. By utilising the developed suction profiles, the extent of desiccation cracking can be estimated.

5. Run each model until the end of the year with cracking included to the depth estimated in the previous step.

6. Analyse the final model runs, looking at the magnitude of the pore water pressure cycles and the magnitude of the pore water pressures or suctions in the slope at the end of the year (Section 6.5.1).

By carrying out these analyses it was possible to develop a better understanding of the effects that climate change will have on hydrology of infrastructure slopes in the UK, including the role that desiccation cracking will have on the magnitude of pore water pressure cycles in the future and the frequency with which the large cycles synonymous with progressive failure will occur.

In Section 6.4.1 the method of creating a VADOSE/W climate boundary condition is explained and in Section 6.4.2 the extraction of climate data from the weather generator. Sections 6.4.3 to 6.5 describe the models, including geometry, material properties and initial conditions.

6.4.1 Creating a VADOSE/W climate boundary condition with the UKCP09 weather generator data

The UKCP09 weather generator was used to generate the climate boundary conditions. The weather generator produces sets of future (referred to as scenario) and present (referred to as control) temporal climate data that can be used in conjunction with VADOSE/W to evaluate the effects of climate on infrastructure slopes in the United Kingdom. The weather generator procedure is explained in greater detail in section 2.11.4 of the literature review and a simplified process is given in Appendix A.

The weather generator allows the user to produce probabilistic series of climate variables for 5km squares at any point in the United Kingdom, for one of three emissions scenarios, over one of seven 30-year time periods. Figure 6-9 shows the 5 km grid layer over the location of the Newbury bypass cutting with the relevant square selected.
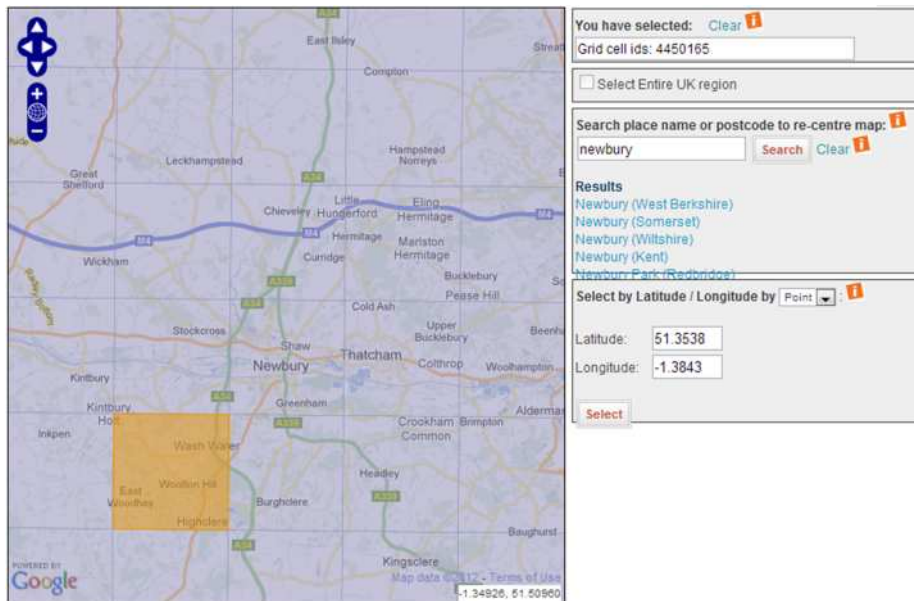
Figure 6-9: Selecting the relevant 5 km square in the weather generator setup (UKCIP, 2012).

The worst case 'High' emissions scenario was chosen to be used in this analysis. This scenario was chosen to maximise the likelihood that changes in the climate would be observed and the hydraulic behaviour of the cutting slope would be influenced. UKCP09 (2012) suggest that the high emissions scenario results in the greatest modelled climate change. In Appendix C graphs have been produced that show the effects of selecting each emissions scenario on the levels of some of the projected climate change at the Newbury cutting site. It can be seen that for all variables the high emissions scenario results in the greatest change by the 2050s.

The weather generator allows the selection of 30 year time slices centred on the 2020s, 2030s, 2040s, 2050s, 2060s, 2070s and 2080s. For this work the 2050s time slice was chosen, covering the years 2040 to 2069.

The next step was to choose the number of sets of climate data that are required, the minimum number being 100 for statistical viability. 100 have been used in this case, to keep the number of numerical model runs to the minimum necessary. Finally, the time frequency of the outputs and the number of years in each climate data set was chosen.

Emissions scenario	High
Time period	2050s (2040-2069)
Number of samples	100
Time frequency	Daily
Duration of each run	30 years

Table 6-7: Summary of the weather generator configuration.

The weather generator produces climate data sets at daily and hourly time frequencies. The models described in this section use a daily time frequency. A daily time frequency was chosen because the time frame over which the 100 models are being considered is so long that if hourly climate data was to be used then the amount of time for the numerical models to run would be unreasonable; the finite element programme VADOSE/W is also only capable of using daily climate data. In the models run in Chapters 4 and 5 it has been shown that using daily climate data can still lead to good predictions of suctions and pore water pressures in the slope and therefore it is not expected to lead to erroneous results in this set of analyses.

6.4.1.1 Weather Generator Output

For each output the weather generator produces one control climate series and one future climate series. Therefore in this analysis 200 sets of climate data were produced, each with its own unique file name. Each file will either be suffixed with _cntr or _scen, if it is a control series or future series. Therefore the file r_0050_cntr refers to the control output of the fiftieth sample and r_0050_scen is the scenario (or future) output of the same sample.

Each weather generator output is provided in a Microsoft Excel .csv format. To create a climate boundary condition VADOSE/W requires climate variables to be input in a prescribed order which differs from that in which the weather generator data is provided. In Section 6.4.1.2 the method of editing, then applying the weather generator output is described.

6.4.1.2 Turning the weather generator outputs into VADOSE/W climate boundary conditions

The raw data from weather generator output is provided in Microsoft Excel files in the .csv format (Figure 6-10). So that the data is usable in VADOSE/W, the required climate variables must be firstly identified and a new .csv file created with the variables placed in columns in the correct order. The example of a raw data file shown below gives daily future climate data; from left to right the columns are; year counter, month counter, day counter, cumulative days (of that year), transition, daily precipitation, minimum temperature, maximum temperature, vapour pressure, relative humidity, sunshine hours, diffracted radiation, direct radiation and PET. Figure 6-10 shows the first month of control climate data of the first output from the weather generator (r_0001_cntr_dly).

	A	B	C	D	E	F	G	H	I	J	K	L	M	N
1	3001	1	1	1	1	0	1.77	8.1	8.67	1	1.02	0.51	0.08	0.11
2	3001	1	2	2	5	0	4.55	11.75	8.41	0.78	6.19	0.47	0.75	0.24
3	3001	1	3	3	5	0	-0.22	3.49	6.87	1	4.03	0.56	0.4	0.2
4	3001	1	4	4	5	0	-1.43	0.95	4.54	0.76	0.35	0.48	0.04	0.57
5	3001	1	5	5	5	0	-1.18	4.74	6.81	0.98	0.81	0.51	0.07	0.05
6	3001	1	6	6	5	0	-0.3	5.92	7.47	1	0	0.29	0	0.1
7	3001	1	7	7	5	0	2.65	8.16	8.05	0.9	0.22	0.49	0.03	0.37
8	3001	1	8	8	3	14.4	-2.66	10.67	4.84	0.6	0	0.29	0	2.26
9	3001	1	9	9	2	7	4.21	9.91	8.01	0.8	0	0.3	0	1.07
10	3001	1	10	10	4	0	4.16	10.15	8.97	0.89	0.11	0.49	0.03	0.72
11	3001	1	11	11	1	0	7.88	14.31	9.12	0.69	0.83	0.55	0.07	0.96
12	3001	1	12	12	5	0	15.03	20.24	10.38	0.52	0.18	0.51	0.03	1.37
13	3001	1	13	13	5	0	9.2	12.45	10.31	0.8	0.13	0.51	0.03	1.21
14	3001	1	14	14	5	0	8.09	12.3	9.3	0.75	0	0.32	0	0.47
15	3001	1	15	15	3	3.7	5.93	12.78	10.37	0.88	0.52	0.56	0.05	0.6
16	3001	1	16	16	2	3.6	8.15	11.99	9.32	0.76	0.11	0.53	0.04	0.83
17	3001	1	17	17	2	5.2	5.58	10.84	10.39	0.96	0	0.33	0	0.44
18	3001	1	18	18	2	1.8	1	5.1	6.29	0.83	2.58	0.67	0.24	0.77
19	3001	1	19	19	4	0	-0.91	5.65	7.17	0.99	0.46	0.59	0.05	0.2
20	3001	1	20	20	1	0	-1.37	0.15	5.81	1	4.07	0.7	0.45	0.12
21	3001	1	21	21	5	0	-7.12	0.25	4.25	0.93	1.07	0.64	0.1	0.34
22	3001	1	22	22	5	0	-9.19	-3.21	2.42	0.67	0	0.36	0	0.53
23	3001	1	23	23	5	0	-8.26	-4.07	2.21	0.61	7.82	0.52	1.22	0.05
24	3001	1	24	24	3	4.9	-5.94	0.49	4.35	0.89	0.52	0.64	0.06	0.29
25	3001	1	25	25	2	1.2	0.47	5.79	6.65	0.87	0.46	0.65	0.06	0.38
26	3001	1	26	26	4	0	-1.54	3.45	5.78	0.88	0.43	0.65	0.05	0.52
27	3001	1	27	27	1	0	-2.36	0.37	4.52	0.8	1.75	0.75	0.17	0.63
28	3001	1	28	28	5	0	-2.88	-0.78	3.23	0.62	0.25	0.66	0.04	0.94
29	3001	1	29	29	3	4.8	-1.01	4.38	6.09	0.88	2.62	0.8	0.28	0.35
30	3001	1	30	30	2	6.5	-3.19	5.54	6.65	1	0	0.41	0	0.23
31	3001	1	31	31	2	2.5	-1.14	2.94	5.51	0.85	0.62	0.73	0.07	0.58

Figure 6-10: Initial output of the weather generator in the .csv format.

In this format the climate data cannot be easily applied within VADOSE/W as a climate boundary condition. It was therefore necessary to identify the climate variables relevant to VADOSE/W, extract them from the .csv file and create a new file from which the data could be more readily used to create a VADOSE/W climate boundary condition. The following variables were extracted from the initial weather generator output:

- Maximum temperature

- Minimum temperature
- Relative humidity
- Precipitation
- Potential evapotranspiration

A new excel spread-sheet was created that identifies these variables from the initial output and places them in the correct column order so as to be ready to copy into the VADOSE/W climate boundary condition. Figure 6-11 shows the first month of climate data in the edited file with the same data from Figure 6-10 extracted and placed in relevant columns to allow implementation into VADOSE/W. To apply this climate data as a VADOSE/W climate boundary condition it was simply a case of selecting all the data and copy/pasting it into the climate data sets sub-menu (Figure 6-12).

All 30 years of each climate series were copied into VADOSE/W meaning that any year or multiple years could be selected as the climate boundary condition for that model run. So that the model ran with the chosen year applied as the boundary condition the correct starting time step has to be chosen. Therefore if the 5th year is to be run the model must be started on the day of the end of the 4th year, or day 1460.

	A	B	C	D	E	F	G	H	I	J
1	Day	Temp Max	Temp Min	RH max	RH min	Wind	Precipitation	Precip start	Precip end	PET
2	1	8.1	1.77	100	100	0	0	0	24	0.11
3	2	11.75	4.55	78	78	0	0	0	24	0.24
4	3	3.49	-0.22	100	100	0	0	0	24	0.2
5	4	0.95	-1.43	76	76	0	0	0	24	0.57
6	5	4.74	-1.18	98	98	0	0	0	24	0.05
7	6	5.92	-0.3	100	100	0	0	0	24	0.1
8	7	8.16	2.65	90	90	0	0	0	24	0.37
9	8	10.67	-2.66	60	60	0	14.4	0	24	2.26
10	9	9.91	4.21	80	80	0	7	0	24	1.07
11	10	10.15	4.16	89	89	0	0	0	24	0.72
12	11	14.31	7.88	69	69	0	0	0	24	0.96
13	12	20.24	15.03	52	52	0	0	0	24	1.37
14	13	12.45	9.2	80	80	0	0	0	24	1.21
15	14	12.3	8.09	75	75	0	0	0	24	0.47
16	15	12.78	5.93	88	88	0	3.7	0	24	0.6
17	16	11.99	8.15	76	76	0	3.6	0	24	0.83
18	17	10.84	5.58	96	96	0	5.2	0	24	0.44
19	18	5.1	1	83	83	0	1.8	0	24	0.77
20	19	5.65	-0.91	99	99	0	0	0	24	0.2
21	20	0.15	-1.37	100	100	0	0	0	24	0.12
22	21	0.25	-7.12	93	93	0	0	0	24	0.34
23	22	-3.21	-9.19	67	67	0	0	0	24	0.53
24	23	-4.07	-8.26	61	61	0	0	0	24	0.05
25	24	0.49	-5.94	89	89	0	4.9	0	24	0.29
26	25	5.79	0.47	87	87	0	1.2	0	24	0.38
27	26	3.45	-1.54	88	88	0	0	0	24	0.52
28	27	0.37	-2.36	80	80	0	0	0	24	0.63
29	28	-0.78	-2.88	62	62	0	0	0	24	0.94
30	29	4.38	-1.01	88	88	0	4.8	0	24	0.35
31	30	5.54	-3.19	100	100	0	6.5	0	24	0.23
32	31	2.94	-1.14	85	85	0	2.5	0	24	0.58

Figure 6-11: The edited weather generator output.

Some assumptions and simplifications have had to be made for the climate data sets. Firstly it is noticed that there are no values for the wind speed, as this variable is not

271

provided as part of the UKCP09 weather generator output. Therefore for both the control and future climate boundary conditions there is no wind speed defined. When the PET values used as the energy data source are calculated by the weather generator wind speed is not used and therefore there should be no discrepancy in the calculated results because of this (UK Climate Projections, 2012).

A simplification that has had to be made regards the values of relative humidity that were provided by the weather generator. Relative humidity is only provided as an average figure by the weather generator, therefore this figure is used for both the maximum and the minimum value throughout each day.

The final assumption is the length of rainfall events. The weather generator has been used to create daily climate data, therefore it is not known in what period of time the precipitation has fallen. For these models it is assumed that rainfall events last the whole day, with a sinusoidal distribution pattern. It was shown in the validation model (Chapter 4) that this approach still provides good precision in the calculation of pore water pressure and suction trends occurring in the Newbury cutting slope throughout the year.
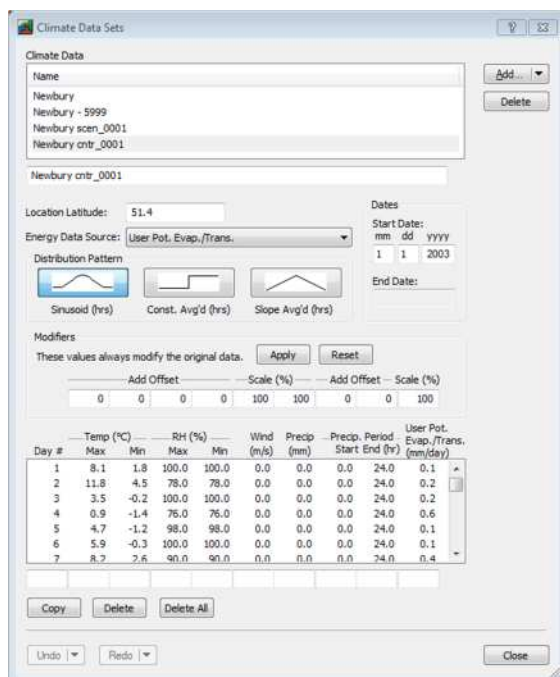
Figure 6-12: VADOSE/W climate boundary condition with weather generator data applied.

Figure 6-12 shows the final VADOSE/W climate boundary condition that was created from the weather generator output r_0001_cntr for the Newbury bypass location. Settings from previous runs are kept the same; location latitude is 51.4 degrees, a sinusoidal precipitation distribution pattern is used and the energy data source is the user input potential evapotranspiration data.

6.4.2 Extraction of extreme years from weather generator data

From each 30 year series of climate data produced by the weather generator, one year was applied to the Newbury cutting model to analyse the effects of a baseline (control) and future (scenario) WET-DRY-WET seasonal variance on the hydrology of the slope. By analysing each output of the weather generator a suitable year from each control series was selected and then the same year from the scenario series could also be selected from the equivalent file. The implications of this method are analysed and discussed in Section 6.6.3 of the discussion.

To identify a suitable year for the analysis from each control output, the total monthly precipitation for each year within the sample is compiled and conditional formatting is used to identify years where a particularly dry summer is preceded and also followed by wet winters (Figure 6-13).

Year	Jan	Feb	Mar	Apr	May	Jun	Jul	Aug	Sep	Oct	Nov	Dec
1	55.6	46.2	35.6	93.5	61	61.2	8.5	48.7	50.6	52.7	36.4	142.7
2	42.6	87.6	69.2	105.8	55.4	61.4	78.2	27.8	37.8	63.8	121.7	116.6
3	62.3	32.2	49.4	61.9	84.9	96.2	27.4	22.2	68.4	75.5	86.2	75.6
4	103.3	124.8	66.5	100.4	59.7	42.8	23.2	63.6	97.4	15.7	37.7	119.8
5	79.6	72.3	120.9	108.9	57.6	53.7	75.6	28.9	110.2	101.8	91.6	143
6	165.1	59.8	87	59.6	41.1	74.8	39.6	75.4	120.6	90.9	59.4	94.7
7	54.8	20.5	47.4	44.2	47.3	51.9	18.9	83.2	30.4	97.4	82.8	38.5
8	126.7	22.7	70.4	17.2	77.7	71.1	47.6	30.7	46.3	66.4	110.9	48.8
9	35.4	75.2	48.1	53.3	76	85	22.7	52.5	55.7	22.8	102.6	174.4
10	73.3	56.9	94.2	43.1	90.6	35.7	70.5	63.4	121	102.4	42.1	90.6
11	79.3	48.7	84.9	54	31.6	42.9	21.3	33.6	17.7	36.2	30.5	86.4
12	77.2	49.6	77.1	77.5	61	108.4	29.2	49.2	49.7	82.1	59	153.3
13	127.4	38.7	100.4	44.1	62.3	49.6	32.9	51.5	28.5	164.9	193.5	62.4
14	57.9	75.8	80.7	57.3	67.3	23.1	46.5	89.8	70.4	115.9	121.5	93.4
15	164.4	75.9	50.1	53.8	114.5	28.4	88	41.9	56.4	86.4	48.6	73.9
16	121.9	62.2	56.1	85.4	43.5	37.1	35.7	88.6	78.8	114.3	92.7	74.6
17	56.4	98.8	39.1	93.6	45.9	106.3	77.3	38.7	111	120	158.8	89.3
18	51.6	21.3	64.7	40	41	72.1	66.8	69.2	1.9	81.6	109.6	73.5
19	106.1	62	42.3	40.9	85.7	77.2	25.1	113.2	30.4	50	95.9	85
20	52.9	87.5	50.5	44.8	42.5	63.9	30.1	74.5	59.7	91.8	32.2	58.2
21	105.4	70.1	70.2	73.9	17.9	45	5.8	61.5	101.2	67.3	157.8	118.5
22	76.2	42.9	27.8	43.7	101.5	95.8	96	43.7	94.8	170.3	98.3	105.3
23	49.2	68.5	39	81.5	54.7	35.5	43.1	30	20.8	109.9	61.7	60.7
24	94.1	37.5	46.2	53.6	71.2	105.1	18	26.6	48.4	51	40.8	104.9
25	57.6	25.2	90.8	131.5	52.8	59.2	49.3	47.9	54.9	98.3	56.3	117.7
26	100.7	54.7	56.3	68.9	30.1	92.5	67.8	54.8	43.8	69.1	73.8	85.4
27	121.4	58.3	34.3	61.1	37.3	49.1	64.3	20.4	78.6	97.4	15.9	128.8
28	72.3	45.4	70	22.9	22.7	13.7	71.7	39.5	67.4	47.3	97.4	79
29	67.6	96.2	120	98	59.5	9.4	33.2	69.6	32.7	81.4	102.8	125.4
30	114.6	32.3	56.4	54.5	41.1	90.8	103.5	30.2	72.9	122.3	113.7	129.7
1961-1990	55.9	40	51.8	44.3	55.1	55	46.1	58.5	54.4	54.9	53.5	62.8

Figure 6-13: Conditional formatting to identify dry summers and wet winters in the cntr_0001 weather generator output.

In Figure 6-13 the yellow highlighted cells show the months where total precipitation is above the long term average (1961 – 1990 baseline) and the red highlighted cells show the months where total precipitation is below the long term average. In this example the 23rd year from this output (cntr_0001) was chosen to be used in the analysis. The conditional formatting has shown that from May to September the total precipitation is below the long term average in every month, significantly so in August and September, as it was in the year 2003. This is followed by a winter (October to December) where the first two month's total precipitation is above the long term average and December's is only a small quantity below. January through April are not so significantly different to the long term averages, with two of the months showing total precipitation above average and two showing total precipitation below average. It was shown in the seasonal variance analysis (Section 6.3.3) that a very wet start of the year was not so critical to the large pore water pressure cycle in the year 2003; this was because the previous winter had been very wet, resulting in a high water table. By using this water table as the initial conditions in the analyses to follow, a preceding very wet winter can be represented. Figure 6-14 shows a plot of the total monthly precipitation from the selected year, compared

against the long term average, the year 2003 Newbury data and the corresponding future year from the weather generator output.
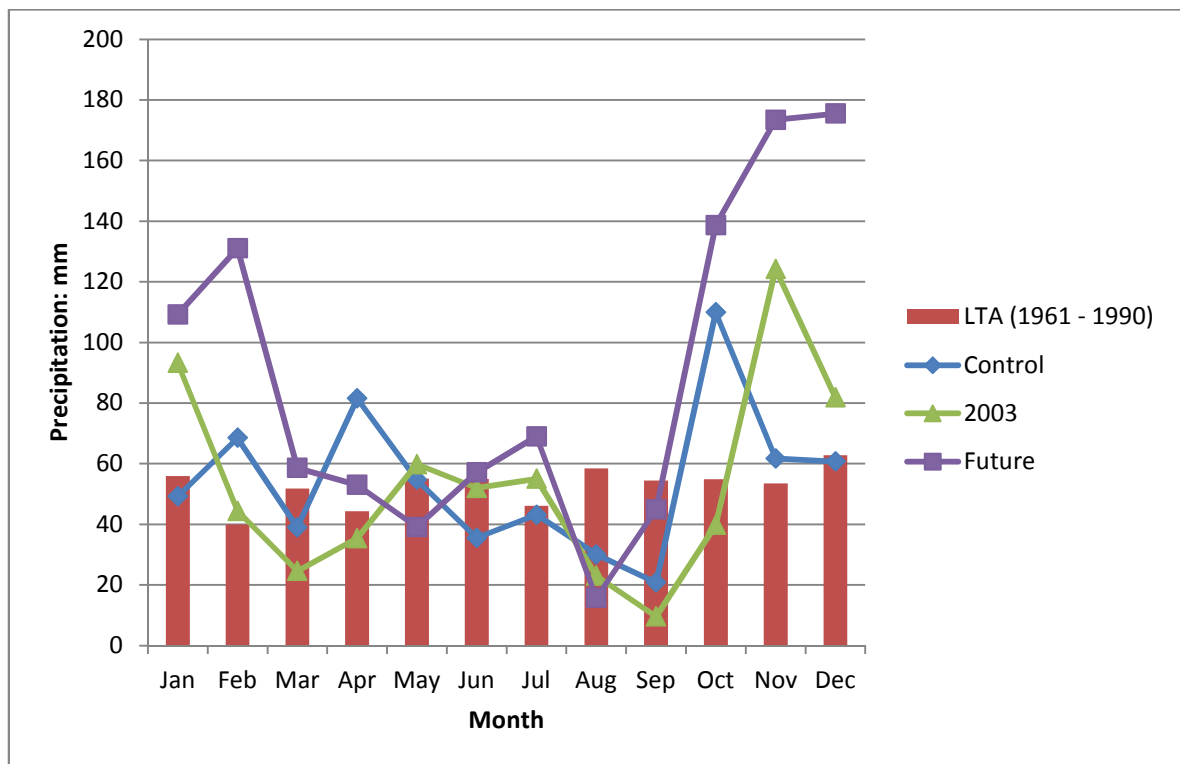
Figure 6-14: Total monthly precipitation summary for weather generator output 0001, compared to the long term average and the year 2003.

In Figure 6-14 the similarity between the control output and the year 2003 is clear, showing that the selection of this year from the weather generator output is reasonable to generate the large pore water pressure cycles observed when a WET-DRY-WET year is experienced by the Newbury bypass cutting. The corresponding year from the future output has also been plotted, showing a substantial difference in some month's total precipitation, most notably in the winter months of January, February, October, November and December when total precipitation exceeds the long term average by over 100%.

This process of choosing a year to extract from each 30 year series was repeated for each of the 100 weather generator control outputs. Each of the control and scenario series were then modified so that they can be used as VADOSE/W climate boundary conditions using the method described in Section 6.4.1. The implications of this process and methodology are discussed in Section 6.6.3.

6.4.3 Model Geometry and Initial Conditions

The same geometry used in previous models was used in these analyses (Figure 6-15), with the same location of side and bottom boundaries. For each model run the relevant boundary conditions were applied to the surface layer, namely the control and scenario climates generated from each output of the weather generator. Initial conditions for each analysis are again defined by an initial water table at 0.5 metre depth, which is shown by the dashed line in Figure 6-15. This water table is the same as that used in the preceding analyses and is used here to be representative of the conditions prevalent in the slope at the beginning of the year when the previous winter has been very wet.
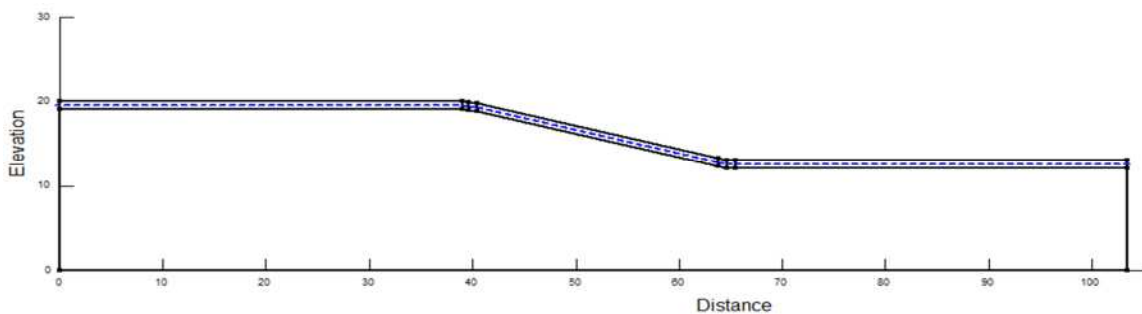
Figure 6-15: Model geometry, before the application of material properties, boundary conditions and meshing.

The surface layer in these analyses was 1.0 m thick. This depth allowed for the maximum rooting depth of the vegetation to be accounted for and cracking to be applied throughout the year. In each analysis, once maximum suctions were reached a different depth of cracking was applied. To account for the possible different depths of cracking, further regions were added to the model below the surface layer such that the bimodal soil properties could be applied to the depth of cracking that was estimated. The development of these regions is explained in Section 6.4.6.

6.4.4 Material Properties

Three material models were used in these analyses. Each of these material models includes a soil water characteristic curve (SWCC) and hydraulic conductivity function (HCF) generated either by the van Genuchten (1980) equations or the bimodal van

Genuchten equations developed in Chapter 5 (Section 5.2). Material properties are defined for each of the following:

1. Un-cracked London Clay
2. Low Porosity Cracked London Clay
3. High Porosity London Clay

In Chapter 5 bimodal models representing low porosity cracked soil and high porosity cracked soil were developed. These bimodal material properties were used for the material properties in the models described in this chapter. Table 6-8 details the parameters and values used to define the SWCC and HCF for each of the materials. The bimodal functions are formed by combining the un-cracked van Genuchten parameters with the relevant crack parameters in the bimodal equations.

Parameter	Un-cracked	Low Porosity	High Porosity
θ_r	0.28	0	0
θ_s	0.45	0.5	1.0
a	22.14 kPa	0.98 kPa	0.5 kPa
n	1.443	2	7
m	0.307	0.5	0.857
K_s	1e-7 m/s	2.3e-4 m/s	2.3e-4 m/s
ϑ	0.922	0.078	0.078

Table 6-8: van Genuchten parameters for the three material properties to be implemented.

6.4.5 Vegetation

It has been suggested that in the future the role that vegetation has in influencing slope hydrology will change. It is thought that rooting depth could change with the potential for volume changes at greater depths (Rouainia et al., 2009) and that a small change of temperature could result in different types of vegetation, water use and rooting characteristics (Glendinning et al., 2006).

In the models described in this chapter vegetation has been assumed to remain unchanged from the characteristics laid out in Section 4.3.4.2. Despite the possible

effects of climate change on vegetation mentioned above, there is no work available that quantifies what the magnitude of these effects may actually be. By ignoring any possible changes to vegetation characteristics, a possible source of error is removed and the effects of climate change on the slope hydrology can be isolated.

6.4.6 Meshing

The mesh in these models was based upon that developed in previous chapters, but with some alterations made to account for the need to be able to include cracking to the estimated depth. The following areas of the mesh are considered:

- Surface layer
- Main body
- Added regions for increased crack depth

The surface layer in these models was defined as 1.0 m thick, which is the maximum root depth of the vegetation and the crack depth from the beginning of the year until the point when maximum suctions are reached. In Chapter 4 it was found that the minimum number of elements required in a surface layer of this thickness was 23.

The added regions for increasing the crack depth were included by creating regions below the surface layer. Each of these regions had a depth of 0.25 metres. 0.25 metres thickness was chosen for two reasons:-

1. This depth allowed reasonable approximations of the crack depth to be included; greater depths, such as 0.5 metres could too often result in two differing crack depth estimates being defined in the model to the same depth. For example, if the crack depths for a control and scenario were estimated to be 2.76 m and 3.24 m respectively these would both be defined to 3.0 m within the model. However, by reducing the layer depth to 0.25 m much better definition could be made of 2.75 m and 3.25 m respectively.

2. Clearly even thinner regions would result in even better crack depth definition. However, this would result in increasingly great number of finite elements in the mesh, and experience has shown that very high mesh densities result in very long run times. As 200 models were run, such long run times are deemed as unacceptable. Therefore 0.25 m is considered a good compromise between

being able to approximate the depth of cracking well and having reasonable model run times.
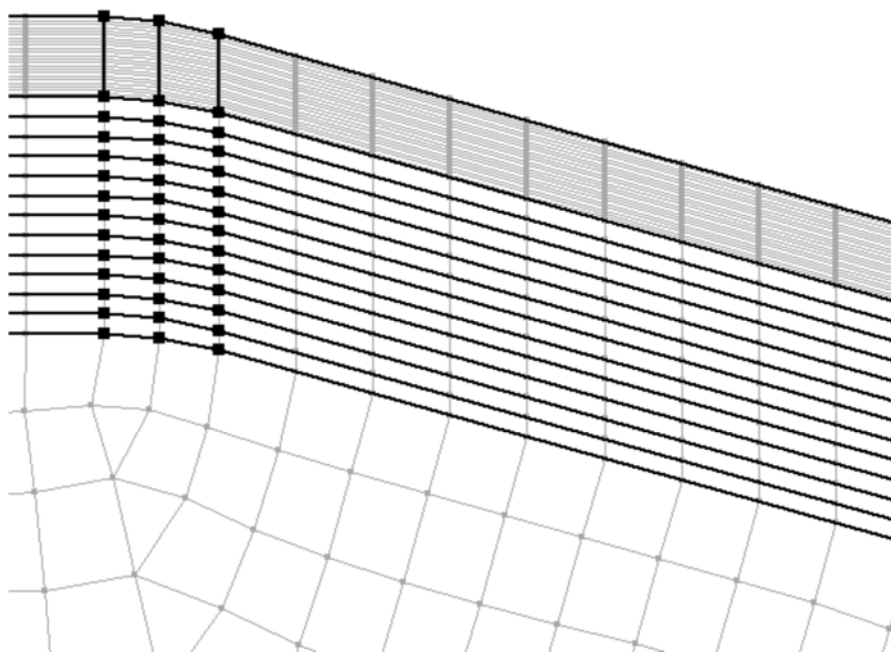
Figure 6-16: New mesh, developed to allow application of cracks to greater depths.

Figure 6-16 shows the initial mesh. There are 23 vertical elements in the top surface layer and 1 in each of the layers below this. The added regions were applied to a depth of 4.0 metres, meaning that cracking could be applied to this depth. In previous analyses observations of the phreatic surface were made and the maximum depth it reached was 4.0 metres, which is therefore the theoretical maximum depth of cracking.

6.4.6.1 Surface Layer Mesh Sensitivity Analysis

The initial mesh in Figure 6-16 has one vertical element per added region. To produce the correct pore water pressure and suction calculations a finer mesh may be required. A sensitivity analysis was carried out to ascertain the actual number of elements required so that any increase in the number would not change the calculated results of the model. The Newbury cutting model with the new mesh was run with one year of Newbury climate data applied. By using the 2003 year the

results from these sensitivity analyses could be compared to the results from the validated model so that the new model geometry was validated.

6.4.6.1.1   Surface Layer Mesh Sensitivity Analysis Results

Temporal pore water pressures and suctions at depths of 1.0, 2.0, 3.0 and 4.0 metres are shown in Figure 6-17 a), b), c) and d) respectively, for each sensitivity analysis compared to the original bimodal model results.
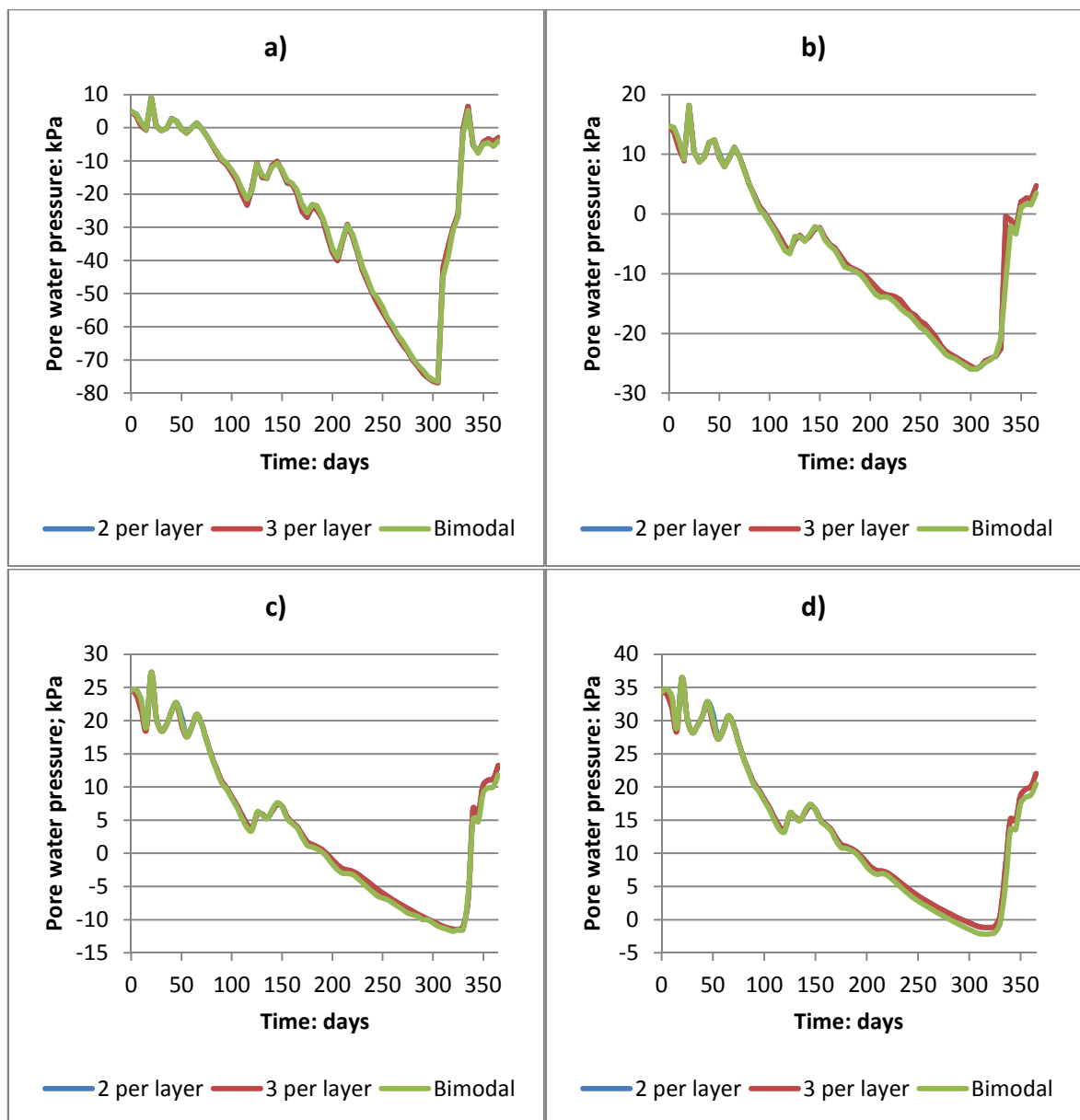
Figure 6-17: Surface layer mesh sensitivity analysis results at a) 1.0 metres depth, b) 2.0 metres depth, c) 3.0 metres depth and d) 4.0 metres depth.

Each of the graphs show that by increasing the number of vertical elements in each supplemental surface layer from 2 to 3 there is no effect on the modelling of the pore water pressures at any depth. There is also little difference between these results and that of the initial bimodal model, showing that the introduction of the extra surface layers does not adversely affect the models' ability to replicate pore water pressures in the Newbury cutting. In the models used in the proceeding analyses 2 vertical elements were used in each of the supplementary surface layers (Figure 6-18).
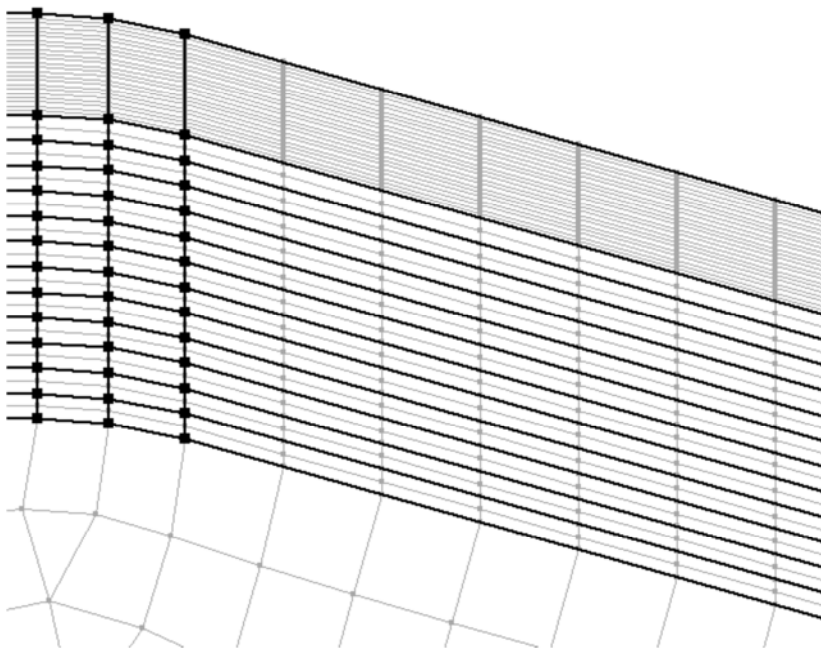
Figure 6-18: Final finite element mesh in surface layers.

6.4.7 Time Steps

Initially, each model was run for 275 days of climate data. This calculates the pore water pressures and suctions until the end of September when the suctions are expected to be at their maximum. Once the model is run until this point the actual timing of the occurrence of maximum suctions is identified and the model run was then continued from this point with the increased crack depth applied.
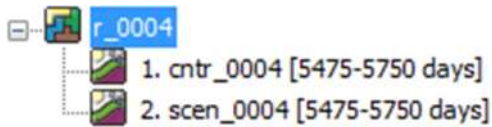
Figure 6-19: Analyses tree with initial runs (first 275 days) shown.

Figure 6-19 shows the initial time steps set up for the 4th output of the weather generator. For these series the 16th year was chosen and therefore the analysis begins at the start of this year. Once these model runs were completed the crack depth was estimated from the maximum suctions and Equation 6-1; finally, the remaining climate data is run, so that pore water pressures and suctions are calculated until the end of the year.
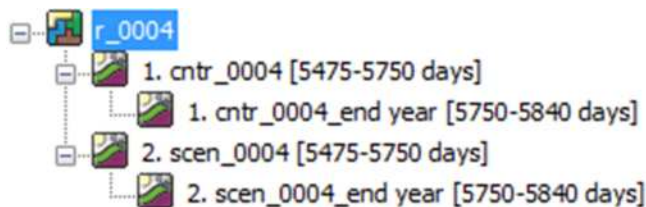
Figure 6-20: Analyses tree with secondary runs (until 365 days) added.

Figure 6-20 shows the time steps for the final analysis with the final 90 days of climate data applied taking the total run time to 365 days. The initial conditions for this part of the analysis are defined as the pore water pressure and suction conditions in the cutting model at the end of the first analysis.

For a number of the model runs it was observed that the maximum suctions did occur before the end of September and therefore for some models the second analysis had to begin before this point. This was accomplished in VADOSE/W by choosing the earlier saved time step at which maximum suctions were observed from the first part of the analysis to act as the initial conditions of the second part of the model run.

6.5 Final Model Runs

Once the model geometry, mesh, material properties and boundary conditions had been established the models were ready to be run. Figure 6-21 shows an initial model with the relevant boundary condition applied to the surface layer, the final mesh

applied to all regions and material properties applied. This initial setup was used for both control and scenario runs. The low porosity crack model has been applied to the top 1.0 metre of the slope profile. This is applied for the duration of the run until maximum suctions are reached and the high porosity material property is applied. This approach was shown to be successful when implemented in Chapter 5 (Section 5.7).
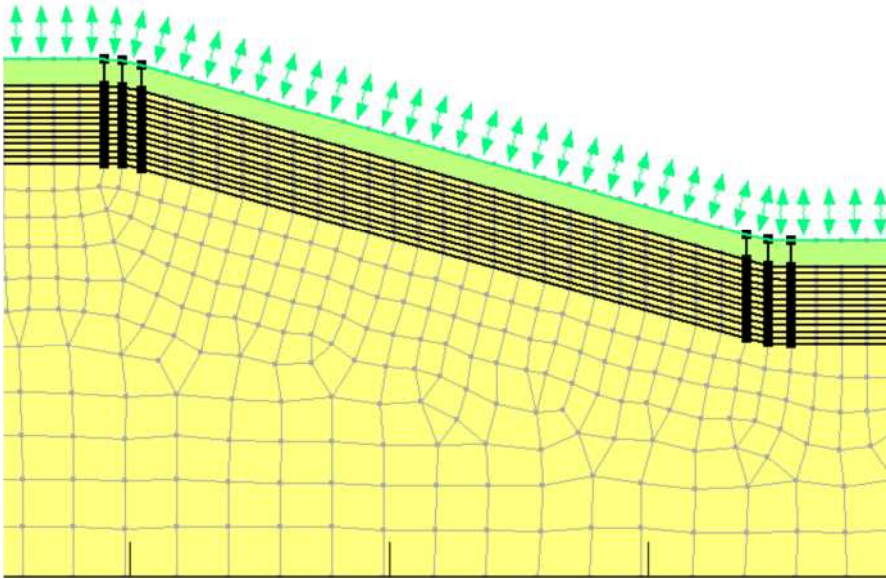
Figure 6-21: Initial model setup for control and scenario model runs.

The model setup in Figure 6-21 was run until the end of September for each climate boundary condition. Maximum suctions were then identified and the crack depth estimated from Equation 6-1. The calculated crack depth was then applied to the model by defining new material properties in the added regions. The models were then finally run until the end of the year. Figure 6-22 shows the control and scenario model setups for the 33rd output after deeper cracks have been added.
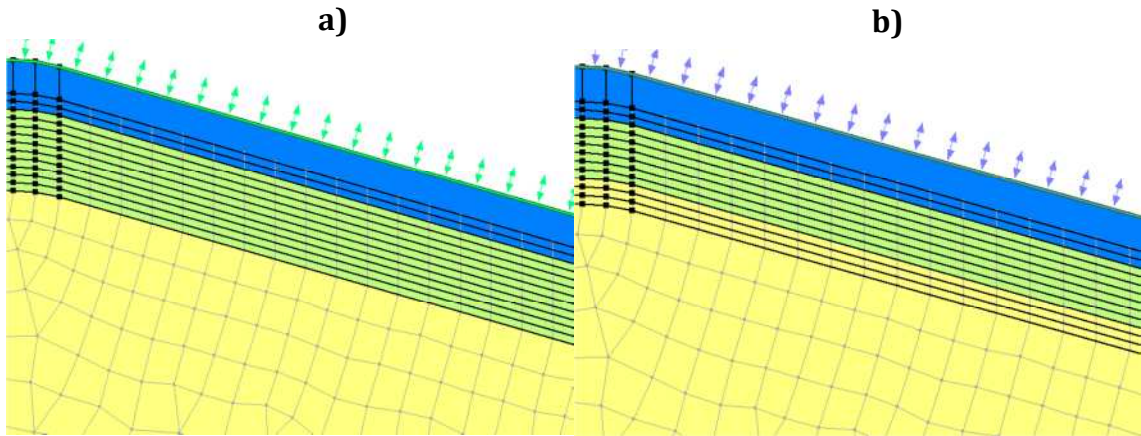
Figure 6-22: a) Control and b) scenario model geometries with cracks applied to deeper depths for the 33ʳᵈ output.

In these models crack depth was applied to depths of 4.0 metres and 3.25 metres for the control and scenario models respectively.

6.5.1 Results and Analysis

For each model there are two sets of results; the control results and the scenario results. There are therefore 200 years of data to compare and analyse. Due to the large amounts of data it was deemed necessary to run a statistical analysis of the results. The statistical analysis software IBM SPSS Statistics 20 was used to carry out these analyses. This software package was used to discover if climate change will have statistically significant effects on the hydrology of the Newbury bypass cutting. Statistical Product and Service Solutions or SPSS statistics is one of the most widely used programmes for statistical analysis. It is a comprehensive, easy-to-use set of data and predictive analytics tools for business users, analysts and statistical programmers (IBM, 2013).

The effects of climate change on the slope hydrology were investigated by considering the following results from each of the models:

1. Cumulative evapotranspiration at the end of summer
2. Maximum summer suctions.
3. Maximum depth of desiccation cracking.
4. Dissipation of suctions by the end of the year.

5. Size of pore water pressure cycle.

Due to an increase in evapotranspiration, climate change is expected to increase the magnitude of suctions occurring in the summer. The maximum summer suctions at 0.5, 1.0, and 3.0 metres were analysed. By analysing multiple depths the changing effects of transpiration by vegetation and evaporation could be identified. The extent and severity of desiccation cracking is expected to increase as an outcome of the increased suctions prevalent in the slope, by analysing the maximum depth of cracking that occurs in the slope this hypothesis was tested. Dissipation of suctions signifies whether the slope profile has rewetted by the end of the year. If suctions are dissipated it shows that a significant amount of precipitation has infiltrated the slope. By analysing whether this occurs more often in the scenario models the aim was to reveal more about how climate change was influencing the hydrology of the slope.

The size of the pore water pressure cycle is linked to progressive failure. Large cycles, caused by greater variation in the climate from summer to winter are thought to be conducive to this kind of failure (Nyambayo et al., 2004; Rouainia et al., 2009). The size of pore water pressure cycles in the control and scenario models were therefore calculated and compared to ascertain whether climate change was influencing them. The pore water pressure cycle is calculated by the difference between the maximum suctions at the end of the summer and the maximum positive pore water pressures at the end of the year. This method does have some implications for the results. In reality, maximum pore water pressures are often reached in January (for example see the full Newbury run in Section 6.3.3), therefore with this method the size of pore water pressure cycles could be underestimated slightly. This point is addressed in more detail in the discussion section (Section 6.6.2.2).

A summary of all the statistical analyses and the results from the model runs, including pore water pressure magnitudes, upon which these analyses are based, can be found in Appendix C.

6.5.1.1 Statistical Analysis

The data obtained through these analyses was analysed by comparing means. This allowed the differences between the two groups (control models and scenario models)

to be identified, and to ascertain whether the differences were significant. It also meant that the large amount of data produced by these analyses was easier to handle. In this research the climate boundary condition has been manipulated and is therefore known as the 'independent variable', the outcomes that are measured, such as maximum suctions, crack depth etc. are known as the 'dependent variables'. The purpose of the statistical analysis performed in this section was to determine if differences in the outcome of the dependent variables is caused by the manipulation of the independent variable.

6.5.1.1.1 Dependent t-test for Parametric Data

The t-test has been specifically designed to analyse this kind of experimental data (Field, 2005a). In this research the dependent t-test was used. This test was chosen because the same models, with constant material properties, initial conditions and vegetation conditions are subjected to each climate condition.

The dependent means t-test assumes that:-
- The data is from normally distributed populations.
- The data is measured at least at the interval level meaning that data is measured on a scale along which all intervals are equal.

Once it has been established that each of the assumptions has been met the t-test can be carried out within SPSS. To discover if an effect is substantive the effect size, or r-value, can be calculated. Effect sizes provide an objective measure of the importance of an effect. Regardless of what the effect is or the variables that have been measured it is known that an effect size of 0 means that there is no effect whereas an effect size of 1 means there is a perfect (or 100%) effect (Field, 2005b). The effect size can be calculated by:-

Equation 6-2

$$r = \sqrt{\frac{t^2}{t^2 + dof}}$$

Where t is the t-statistic calculated by SPSS and *dof* is the degrees of freedom.

Some selected r-values have the following meanings (Field, 2005b):-

- r = 0.10 (small effect): in this case the effect explains 1% of the total variance.
- r = 0.30 (medium effect): in this case the effect accounts for 9% of the total variance.
- r = 0.50 (large effect): in this case the effect accounts for 25% of the total variance.

6.5.1.1.2   Tests for non-parametric data

If the data sets to be analysed do not meet one of the assumptions (in the case of these analyses it will only be that the data is not normally distributed) then other tests exist that can be used to analyse differences between means. The Wilcoxon signed-rank test (Field, 2005a) for dependent data works in a similar way to the t-test described in Section 6.5.1.1.1.

An effect size can also be calculated from this test. For the Wilcoxon signed-rank test this is given by:-

Equation 6-3

$$r = \frac{Z}{\sqrt{N}}$$

Where Z is the z-score that SPSS produces and N is the size of the study, or the total number of observations. The z-score is the value of an observation expressed in standard deviation units.

6.5.1.1.3   Testing normality of data

Normality of data can be tested by using the Kolmogorov-Smirnov test (Field, 2005a). This test works by comparing the data in the sample to a normally distributed set of data with the same mean and standard deviation. If the significance p is >0.05 it means that the distribution of the data is not significantly different from the normal distribution and meets the assumption of normally distributed data.

6.5.1.2 End of summer results

The results of the statistical analyses have been split into end of summer and end of year. To recap, the following results from the control and scenario runs are tested for statistical significance between the mean values, for the end of summer:-

1. End of summer evaporation
2. End of summer transpiration
3. Max summer suctions at 0.5 metre depth
4. Max summer suctions at 1.0 metre depth
5. Max summer suctions at 3.0 metres depth
6. Depth of water table at end of summer
7. Maximum crack depth at end of summer.

The approach is to first establish whether the data is parametric by applying the Kolmogorov-Smirnov test. Once this is established, either the dependent means t-test or the Wilcoxon signed ranks test are used for parametric and non-parametric data respectively to test whether climate change has had a statistically significant effect on the values of the means. Table 6-9 shows a summary of the results of the end of summer statistical analyses; showing the mean values tested, whether the data was parametric, the test used and the significance of the results. From this data it can be said that:-

1. At the end of summer, mean cumulative evaporation was significantly higher for the scenario climate (M = 29.80.) than for the control climate (M = 25.79), $t(99) = -9.725$, $p < .05$, r = 0.70.

2. At the end of summer, mean cumulative transpiration was significantly higher for the scenario climate (M = 21.32.) than for the control climate (M = 19.34), $t(99) = -7.052$, $p < .05$, r = 0.58.

3. At a depth of 0.5 metres, maximum suctions were significantly higher for the scenario climate (Mdn = 284.0) than for the control climate (Mdn = 201.5), z = -5.378, $p < .05$, r = -0.38.

4. At a depth of 1.0 metre, maximum suctions were significantly higher for the scenario climate (Mdn = 94.0) than the control climate (Mdn = 86.0), z = -3.199, $p < .05$, r = -0.23.

5. At a depth of 3.0 metres, maximum suctions were not significantly different for the scenario climate (Mdn = 10.5) compared to the control climate (Mdn = 10.0), z = -1.182, $p > .05$, r = -0.08.

6. The depth of the water table at the end of summer for the scenario models (Mdn = 4.025 metres) is not significantly greater than the depth of water table at the end of summer for the control models (Mdn = 4.000 metres), z = -0.037, $p > .05$, r = 0.00.

7. The maximum depth of cracking was not significantly greater for the scenario models (M = 3.25) compared to the control models (M = 3.21), z = -1.095, $p > .05$, r = - 0.08.

Where p is the significance and r is the effect size. The implications of these results are discussed further in Section 6.6.1.

Results tested	Control results mean	Scenario results mean	Parametric data	Test used	Significance, p	Significant difference?
1. End of summer evaporation	25.79 m³	29.80 m³	Yes	Dependent means t-test	0.000	Yes
2. End of summer transpiration	19.34 m³	21.32 m³	Yes	Dependent means t-test	0.000	Yes
3. Max summer suctions at 0.5 m depth	209 kPa	352 kPa	No	Wilcoxon signed ranks test	0.000	Yes
4. Max summer suctions at 1.0 m depth	85.7 kPa	91.4 kPa	No	Wilcoxon signed ranks test	0.001	Yes
5. Max summer suctions at 3.0 m depth	9.8 kPa	9.9 kPa	No	Wilcoxon signed ranks test	0.237	No
6. Depth of water table	3.98 m	3.95 m	No	Wilcoxon signed ranks test	0.970	No
7. Maximum crack depth	3.21 m	3.25 m	No	Wilcoxon signed ranks test	0.274	No

Table 6-9: Results of SPSS statistical analyses of end of summer results.

6.5.1.3 End of year results and analysis

In this section the results of the statistical analyses for the end of year are presented. Analyses of the size of pore water pressure cycles and dissipation of suctions are shown. The implications of the results are discussed in Section 6.6.2.

6.5.1.3.1   Pore water pressure cycles

The size of pore water pressure cycles at 3.0 metres have been analysed in this section. Table 6-10 shows the results of the analyses.

Results tested	Pore water pressure cycle at 3.0 m depth
Control results mean	13.8 kPa
Scenario results mean	10.2 kPa
Parametric data	No
Test used	Wilcoxon signed ranks test
Significance, *p*	0.043
Significant difference	-0.14

Table 6-10: Results of statistical analyses for size of pore water pressure cycles.

From these results it can be said that at a depth of 3.0 metres, suction cycles were significantly less for the scenario climate (Mdn = 12.00) than for the control climate (Mdn = 16.00), z = -2.025, $p < .05$, r = -0.14

6.5.1.3.2   Dissipation of suctions

Dissipation of suctions was determined by looking at pore water pressure profiles generated by VADOSE/W. Dissipation was adjudged to have occurred when pore water pressures in the top 1.0 m were consistently greater than -10.0 kPa. Figure 6-23 shows pore water pressure profiles of the model scen_0002 for the time steps 300, 310, 320, 330, 340, 350 and 360. The suctions in this example were determined to be dissipated.
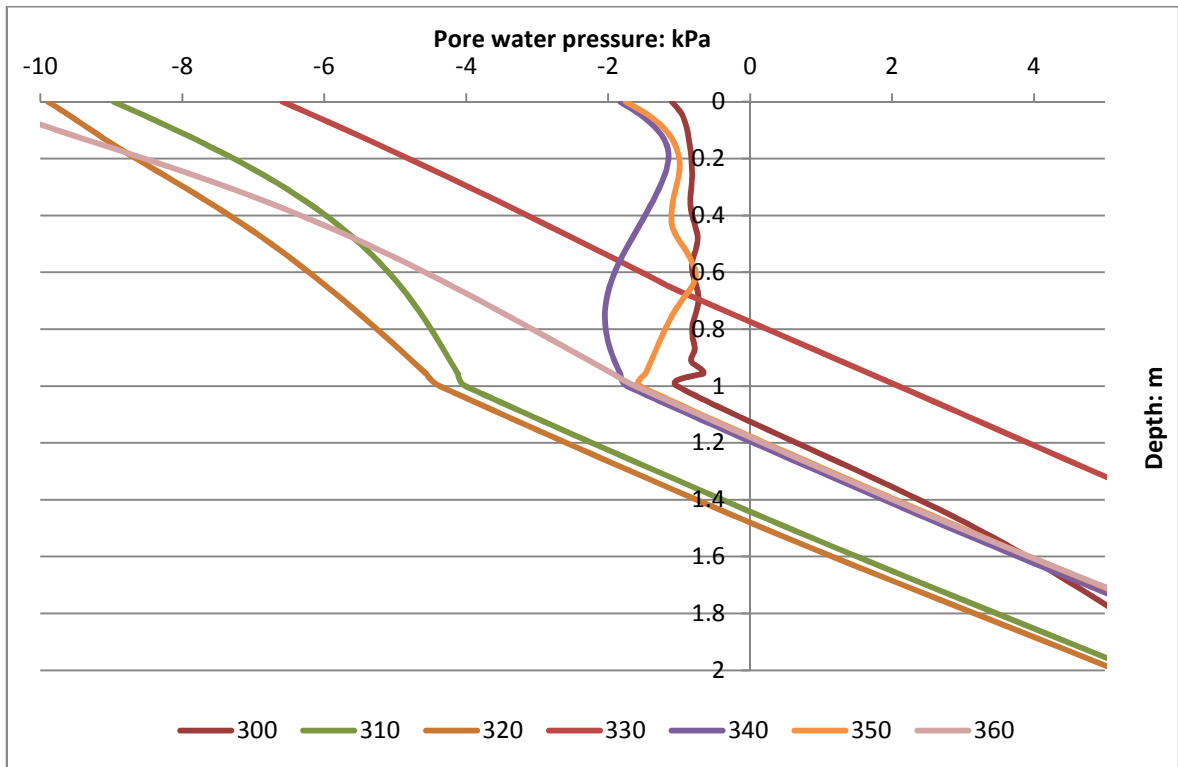
Figure 6-23: Pore water pressure profiles for the model scen_0002; from the end of the summer (300 days) until the end of the year (360 days).

In the SPSS file the dissipation of suctions was simply signified by stating 'Yes' or 'No'; meaning that the data is categorical. Therefore to determine whether the introduction of climate change influences the likelihood of suctions being dissipated, a test that can deal with categorical data must be used, namely the chi-square test.

		Model type		
		Control	**Scenario**	**Total**
Suctions	**Yes**	64	52	116
dissipated?	**No**	36	48	84
	Total	100	100	200

Table 6-11: Contingency table showing effects of climate change on likelihood of suctions dissipating.

Table 6-11 shows the contingency table showing the frequency of models where suctions were dissipated for each model type. Initially it would seem that climate change has had a negative effect on the likelihood of suctions being dissipated

suggesting that suctions are more likely to be retained through the winter and the slope generally being in a more stable condition. The chi-square test was run to test whether the difference is statistically significant.

Table 6-12 shows the results of the chi-square test. The significance of the finding is 0.115, which by being > 0.05 shows that climate change does not have a statistically significant effect on the likelihood of suctions being dissipated.

Chi-Square Tests

	Value	df	Asymp. Sig. (2-sided)	Exact Sig. (2-sided)	Exact Sig. (1-sided)
Pearson Chi-Square	2.956[a]	1	.086	.115	.057
Continuity Correction[b]	2.484	1	.115		
Likelihood Ratio	2.964	1	.085	.115	.057
Fisher's Exact Test				.115	.057
N of Valid Cases	200				

Table 6-12: Results of Chi-Square test for suction dissipation analysis.

Therefore there was not a significant association between the type of model tested and the likelihood of suctions being dissipated at the end of the year $\chi^2(1) = 2.956$, $p > 0.05$.

6.6 Discussion

In the following sections the results and statistical analyses are discussed. The discussion is split into end of summer (Section 6.6.1) and end of year (Section 6.6.2).

6.6.1 End of summer results

In the following sections the results and statistical analysis of the end of summer features are discussed. Evapotranspiration (Section 6.6.1.1), magnitude of suctions (Section 6.6.1.2) and the depth of desiccation cracking (Section 6.6.1.3) results and analyses are discussed. It will be found that climate change has had an influence on the hydrology of the slope at the end of the year the implications of which are discussed in Section 6.6.1.4.

6.6.1.1 Evapotranspiration

Statistical analyses were carried out on the cumulative evaporation and transpiration occurring at the end of summer for all the models; control and scenario. This was carried out with the intention of establishing the effect of climate change on these two processes which have significant effects on the slope hydrology.

The analysis has shown that there was a statistically significant increase in both the cumulative evaporation and cumulative transpiration occurring by the end of summer within the future slopes compared to the control slopes. The effect of climate change on these increases was large. The increase in both of these processes has affected the slope hydrology, increasing the magnitude of suctions occurring at the end of summer.

These results are based on the assumption that the vegetation present on the Newbury cutting slope will exhibit the same properties in the future as it currently does (Section 6.4.5).

6.6.1.2 End of summer suctions

The magnitude of suctions occurring at the end of summer was recorded for each model; control and scenario. Statistical analyses were then carried out to identify whether the differences were statistically significant. In the following sections the findings are discussed and the implications for the Newbury cutting slope stability are considered.

6.6.1.2.1   0.5 metres

The models and statistical analysis carried out on the magnitude of suctions occurring at a depth of 0.5 metres at the end of summer have shown that climate change has had a statistically significant affect. Due to the increased evaporation and transpiration the suctions occurring at this depth are much greater when the future climate boundary conditions are applied. The statistical analysis revealed that the effect size that climate change had on the magnitude of these suctions was medium to

large, meaning that climate change could account for between 9% and 25% of the total variance (see Section 6.5.1.1.1).

6.6.1.2.2   1.0 metre

The models and statistical analysis have shown that climate change has had a statistically significant effect on the magnitude of suctions occurring at a depth of 1.0 metre at the end of summer. The size of the effect of climate change is small to medium (climate change can only account for between 1% and 9% of the total variance), showing that as the depth increases the effect of climate change on the slope hydrology decreases.

The results show that more moisture is generally being removed from the soil profiles when the future climate scenario is applied, due to the increased effects of evaporation and transpiration. The effect is not as great as it is at a depth of 0.5 metres as the amount of moisture that is removed by evapotranspiration decreases with depth. At 1.0 metre the effect of vegetation is at its minimum as this is the maximum extent of the rooting zone.

6.6.1.2.3   3.0 metres

The models and subsequent statistical analysis have shown no significant difference in the maximum suctions occurring in the slope at a depth of 3.0 metres at the end of summer. Despite the increased evaporation brought about by climate change, the hydrology at this depth is relatively unaffected. The effects of evaporation and transpiration from vegetation are focussed on the top 1.0 metre of the slope profile.

However the possible effects of a changing climate on the vegetation have not been considered, which at this time are unclear. In the future it is thought that rooting depths of some vegetation may increase in periods of drought to access sufficient moisture (Rouainia et al., 2009), possibly influencing the hydrology more significantly at greater depths. Also, trees have a much greater rooting depth than the grass present on the Newbury slope; mature trees can extend their roots between 3 and 5

metres deep (Glendinning et al., 2009b; Briggs, 2011). Slopes with large, mature trees are likely to be more affected by climate change, even to depths of greater than 3 metres.

6.6.1.3 Depth of desiccation cracking

Desiccation cracks were implemented in these models. The equation suggested by Fredlund and Rahardjo (1993) was used to calculate the maximum crack depth occurring at the end of summer. Crack depths are calculated as a function of suctions, water table depth and various material properties. A statistical analysis of the crack depths calculated for each model was carried out. It was expected that as a result of greater summer drying due to greater evapotranspiration the crack depths calculated for the future models would be significantly greater than those calculated for the control models.

The statistical analysis showed that the maximum depth of cracking for the future climate models was not statistically significantly higher than the depth of cracking calculated for the control models, this despite the maximum suctions being significantly greater at depths of 0.5 m and 1.0 m. The reason for this is explained by looking at the equation and how it takes into account the suctions and also the depth of water table. Figure 2-38 (Section 2.10.2.6) shows how the depth of the water table and the value of f_w influence the estimated crack depth. It can be seen that for a given depth of water table the rate of increase in calculated crack depth decreases significantly above an f_w value of around 10. As the depth of cracking is also a function of the water table depth (which were not significantly different between the control and scenario models) deeper cracks for the future models would be reliant on the values of f_w generally being greater than 10 for the scenario models and less than 10 for the control models. The average values of f_w for the control and scenario models are 17 and 30 respectively. It is now clear why the depth of desiccation cracking is not significantly different between the models; despite significantly greater suctions (reflected in the higher average value of f_w) in the scenario models, the effect of similar water table depth means that, due to the nature of the Fredlund and Rahardjo

(1993) equation, crack depths cannot be calculated to be much greater than the control models'.

It was mentioned that the crack depth equation calculates the depth of cracking based on a steady state assumption and does not take into account the history of pore water pressures. History of pore water pressures includes the rate at which the suctions develop and fluctuations in the magnitude. It is reasonable to assume that if the development of suctions occurs at a very quick rate or that there are many fluctuations in the magnitude as they develop then the maximum crack depth is actually unlikely to occur. This has implications for the results presented in this chapter as maximum crack depths may be overestimated.
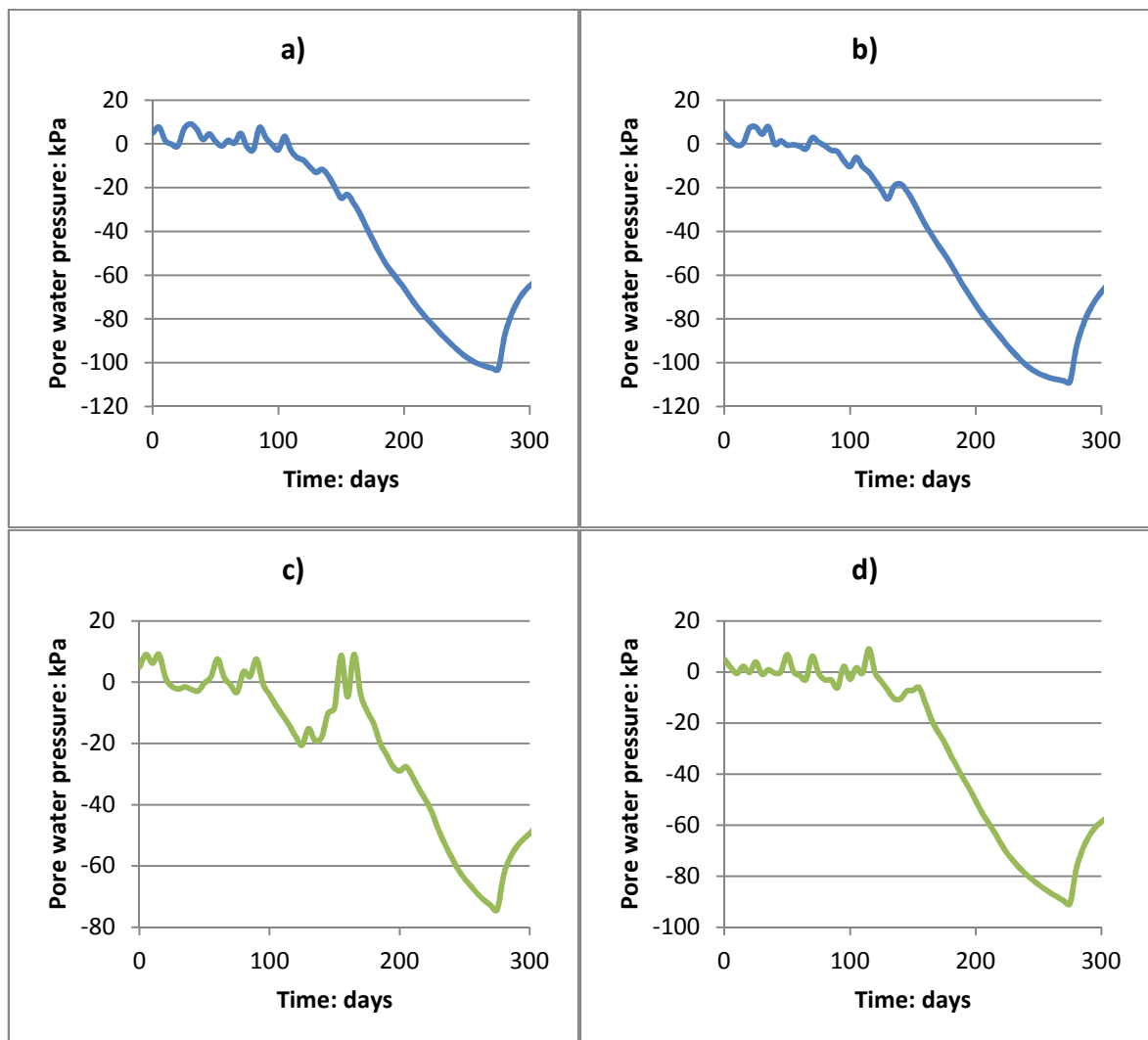
Figure 6-24: Development of suctions in models a) scen_0008 b) scen_0013 c) scen_0057 and d) scen_0094.

Figure 6-24 shows the development of suctions until the end of summer for four models; a) cntr_0008, b) cntr_0013, c) scen_0057 and d) scen_0094. These plots show for the majority of models the development of suctions occurs at quite a slow rate and fluctuations, especially once the main fall begins, are essentially negligible. This suggests that crack development could closely follow suction development and crack depths could reach the maximum estimated by the equation suggested by Fredlund and Rahardjo (1993). The profile of scen_0057 is an exception to this, showing large fluctuations in suctions, suggesting that perhaps the equation should not have been applied here. However, this kind of behaviour was actually observed to be very rare and therefore will not have influenced the overall results, analysis and discussion. In these models the climate was generally dry over summer, meaning that suctions could develop with little fluctuation, however if the summers had had particularly wet periods then this may not have been the case. If modelling climates with varying weather in the summer months then the equation should be applied with caution.

6.6.1.4 Implications and summary

Climate change has affected the hydrology of the Newbury cutting slope at the end of summer. The increased evapotranspiration at the soil surface and in the top 1.0 metre of the slope profile have resulted in significantly greater suctions occurring in this region of the slope when the future climate scenarios are applied. These increased suctions will lead to greater resistance to shallow slope failures throughout the summer as higher suctions are linked to increased shear strength of the soil (Section 2.9.1).

Loss of water throughout summer leads to shrinkage at the slope surface. As more water is removed from the slope when the future climate boundary condition is applied it can be anticipated that there shall be more shrinkage of the slope, leading to more serviceability problems.

The effects of climate change decrease with depth, and by 3.0 metres there is not a significant difference between the size of suctions at this depth between the control and scenario models. This is because the effects of evapotranspiration are focussed in

the top 1.0 metre. The vegetation roots to a maximum depth of 1.0 metre and will therefore not remove moisture from the soil below this. The direct effects of climate change on vegetation have not been considered in this work. It is postulated that rooting depths in the future may increase as moisture availability decreases. Also large, mature trees, which have not been considered in this work, can have rooting depths of up to 5 metres and therefore could influence the hydrology at greater depths.

Climate change has not effected on the depth of the water table, or the maximum estimated depth of desiccation cracking. As the effect of climate change is focussed on the top 1.0 metre of the slope the effect on the water table is negligible. Again, however, if other types of vegetation were present, or if rooting depths were to increase there could be an effect.

Generally, the results shown here could apply to other slopes in temperate climate zones, which experience the same levels of climate change as the United Kingdom. However, these implications only apply with certainty for the climate change scenario used (high emissions by the 2050s) and for this location (Newbury bypass cutting). Other climate change scenarios and different seasonal variations may result in different effects on the slope hydrology. Also slopes of different geometry and material property could be influenced otherwise.

6.6.2 End of year results

In the following sections the results and statistical analysis of the end of the year features are discussed. Dissipation of suctions (Section 6.6.2.1 and, pore water pressure cycle (Section 6.6.2.2) results and analyses are discussed. It will be found that climate change has had an influence on the hydrology of the slope at the end of the year, which is linked to the changing temporal variability of precipitation events (discussed in Section 6.6.2.3) and the antecedent pore water pressures at the end of summer (discussed in Section 6.6.2.4). Implications of the findings are then discussed in Section 6.6.2.6.

6.6.2.1 Dissipation of suctions

The dissipation of suctions was studied and analysed to give an initial idea of whether more water is likely to infiltrate the Newbury cutting in the future when winter precipitation is projected to be greater in magnitude, in terms of total amounts and intensity of events. The method for determining whether suctions are dissipated, the results and subsequent statistical analysis are presented in Section 6.5.1.3.2.

The results showed that the suctions were dissipated more often for the control models than the scenario models (64% and 52% respectively). Although the statistical analysis did show that the difference was not statistically significant, it was close to being so ($p = 0.115$ 2-tailed). It can still be inferred that there is a difference between the probabilities of suctions dissipating (Field, 2005a). It can also be shown that climate change has had measureable effects by looking at the strengths of association. Table 6-13 shows the strength of association measures created from the chi-square test, including Cramer's V which can be interpreted as the effect size. The value for this test is 0.122 showing that climate change has had a small effect on the likelihood of suctions being dissipated by the end of the year.

Symmetric Measures

		Value	Approx. Sig.	Exact Sig.
Nominal by Nominal	Phi	-.122	.086	.115
	Cramer's V	.122	.086	.115
N of Valid Cases		200		

Table 6-13: Measures of strength of association for dissipation of suctions chi-square test.

6.6.2.2 Pore water pressure cycle

The magnitude of pore water pressure cycles has been linked to progressive failure, with larger cycles thought to bring about failure sooner (Nyambayo et al., 2004; Rouainia et al., 2009). The size of the pore water pressure cycle at a depth of 3.0 metres was established for each model and a statistical analysis carried out to ascertain whether there was a statistically significant difference between the mean values for the control and scenario models. The depth of 3.0 metres was chosen as

this falls with the zone of where delayed failures typically occur. It has been suggested that the predicted future climate, with drier summers followed by wetter winters would lead to greater cycles occurring. However, the analysis presented in Section 6.5.1.3.1 has shown that for this slope, for the applied climate change conditions it has generally not been the case.

The statistical analysis revealed that the pore water pressure cycles at a depth of 3.0 metres were significantly less for the scenario models than the control models. The results suggest that less moisture is infiltrating the slope to this depth for the scenario models, this being despite cracks generally extending to the same depths as the control models and there generally being more precipitation falling on the slope after summer for the scenario models. It is believed that the temporal distribution and antecedent pore water pressure conditions have a major influence upon the hydrology of the slope after summer, and these two factors are investigated and discussed in greater detail in following sections (Section 6.6.2.3 and Section 6.6.2.4).

Statistics

		Size of suction cycle at 3.0 metres depth cntr	Size of suction cycle at 3.0 metres scen
N	Valid	100	100
	Missing	0	0
Mean		13.7670	10.1500
Std. Deviation		11.10325	15.00059
Minimum		-7.00	-8.00
Maximum		32.00	37.00

Table 6-14: Statistics summary of pore water pressure cycle analysis.

Table 6-14 shows the minimum, maximum and standard deviation of the pore water pressure cycle for the control and scenario models. It can be seen that despite on average having significantly smaller pore water pressure cycles, the maximum cycle for the scenario models is considerably greater than the maximum for the control models. Therefore it is possible that when the conditions allow, the worst case in the future may be more severe than the worst case for the current climate. It is suggested that successive, large pore water pressure cycles are required to bring about

301

progressive failure (Nyambayo et al., 2004; Rouainia et al., 2009). Despite the 'worst case' being greater in the future there is nothing in the results to suggest that under the analysed conditions these large cycles will become more frequent. Therefore, based on these results it is unlikely that progressive failure will become more frequent due to climate change.

It was mentioned in Section 6.5.1 that the method of calculating the pore water pressure cycles could lead to a slight underestimation of the magnitude of pore water pressure cycles. This issue arises due to the nature of the models, where only one year of weather data is used, thus missing the most likely time when pore water pressure are at a maximum; January. Overcoming this could be achieved by running a further year of climate after the first, although this raises further questions of what criteria the second year would need to meet.

6.6.2.3 Effect of temporal variability of precipitation

In the preceding discussion sections the temporal variability of precipitation events was identified as one of the sources of the changing hydraulic behaviour of the Newbury cutting slope when the future climate scenario boundary conditions were applied. To investigate the effect of the temporal distribution of precipitation, a number of models have been chosen and the precipitation patterns analysed. The models chosen are as follows and have been chosen because the observed results are of particular interest.

- 0004 – The end of summer suctions for the scenario model were very high, but were still dissipated by the end of the year. This behaviour was an infrequent occurrence for the scenario models.
- 0006 – End of summer suctions for both the control and scenario model were high and neither were dissipated by the end of the year.
- 0086 – This model run resulted in high pore water pressures at the end of the year.
- 0087 – The end of summer suctions for the scenario model are high and suctions have been dissipated by the end of the year.

Scen_0004

The model scen_0004 produced some of the largest suctions developing in the slope at the end of summer. These suctions were then subsequently dissipated, which was a relatively uncommon occurrence. Figure 6-25 shows the total monthly precipitation compared to the LTA (1961 – 1990) for scen_0004. The summer months are generally dry with three months where the precipitation total is significantly below the LTA (May, July and August but a very wet June). The autumn and winter that follows is very wet; a total of 350 mm of precipitation falls from September to December, which is 55% greater than the LTA total for these months.
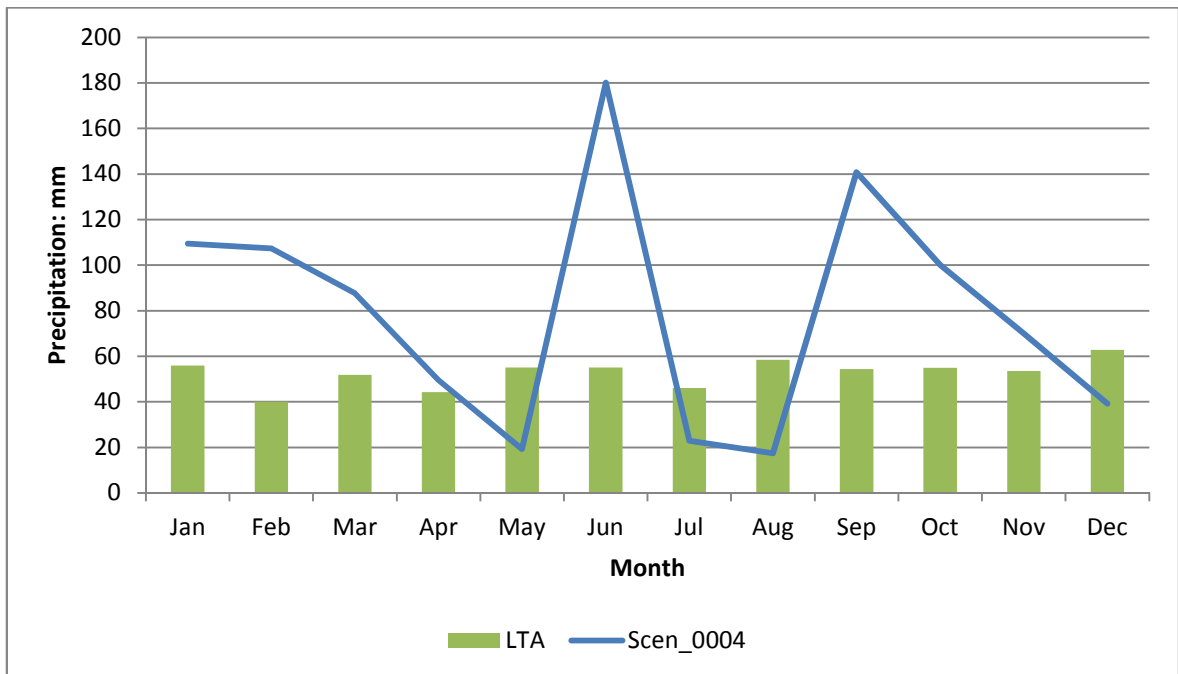
Figure 6-25: Total monthly precipitation for scen_0004.

Figure 6-26 shows the daily precipitation totals throughout the year for scen_0004. Precipitation events are fairly evenly spread through September to December (Day 240 onwards, with there being no particularly exceptional precipitation events. This suggests that for dissipation of suctions to occur, the requisite is for a large amount of precipitation over a long period rather than a smaller number of high magnitude precipitation events. This idea is further supported by observation and analysis of further model results and precipitation distribution in this section.
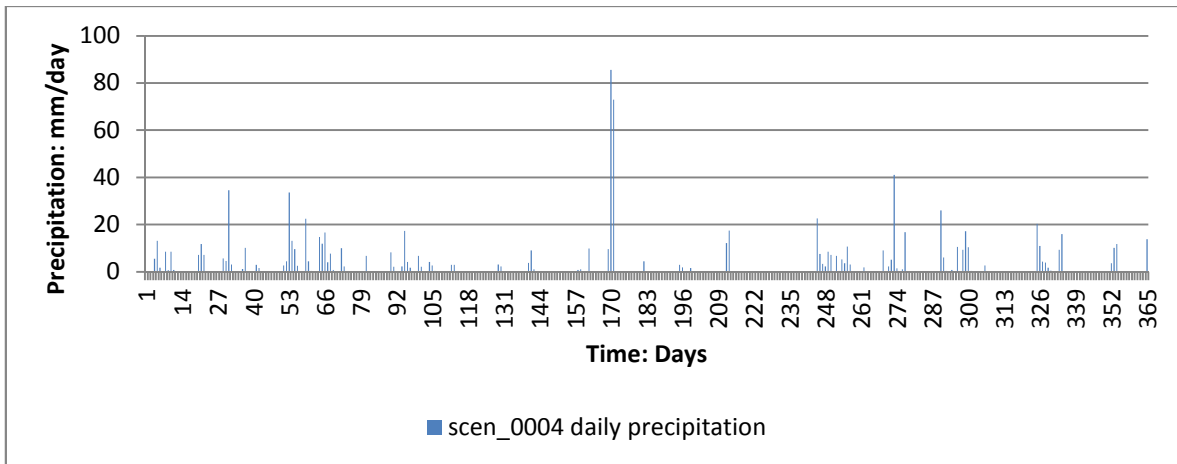
Figure 6-26: Daily precipitation totals for scen_0004.

Cntr_0006 and Scen_0006

Cntr_0006 and scen_0006 both resulted in high suctions at the end of summer, especially scen_0006 which was followed by no dissipation of suctions at the end of the year. As shown by Figure 6-27 both the cntr and scen models have dry summer/autumn months (both have 4 months of below average precipitation between May and September), followed by winter months that are wetter than average but not extremely so, such as in some of the other examples presented in this section.
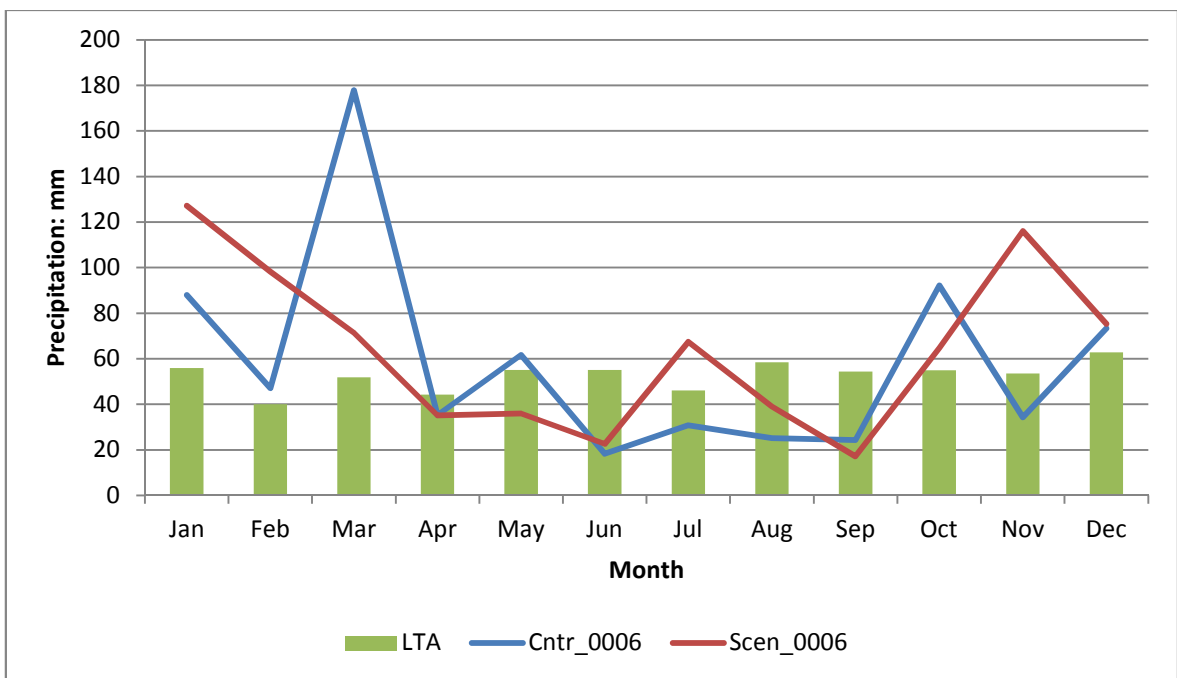
Figure 6-27: Total monthly precipitation for cntr_0006 and scen_0006.

304

Figure 6-28 a) and b) show the daily precipitation totals from the beginning of September until the end of the year for cntr_0006 and scen_0006 respectively. Neither model exhibits any extraordinarily wet days. Precipitation events are relatively evenly spread throughout October, November and December. These observations coupled with those made of scen_0004 support the theory that the hydrology of the slope is more affected by the total magnitude of precipitation falling in the winter rather than the actual temporal distribution and magnitude of the precipitation events.
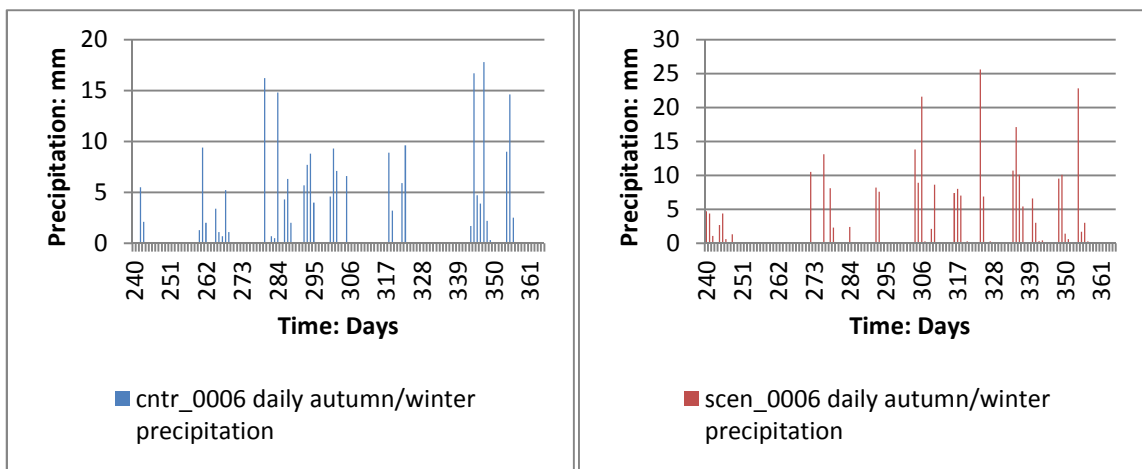
Figure 6-28: Daily winter precipitation totals for a) cntr_0006 and b) scen_0006.

Scen_0086

The model scen_0086 resulted in very high pore water pressures at the end of the year. Figure 6-29 shows the monthly total precipitation for this model compared to the LTA. The graph shows that precipitation during this year was very high, with 1089 mm falling, compared to the LTA yearly total of 633 mm. Precipitation is only below the LTA for three months of the year; March, August and October. For some months, namely January, February, July, September and November the precipitation was significantly greater than the LTA; by between 70 and 370 %.
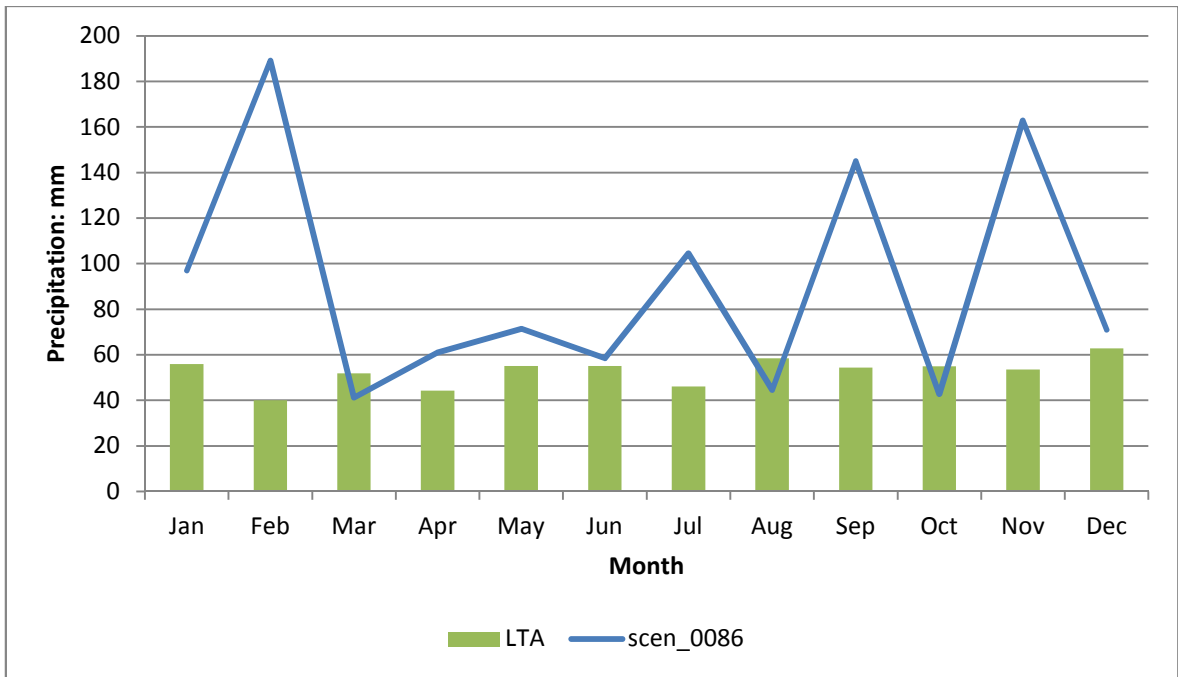
Figure 6-29: Total monthly precipitation for scen_0086.

Figure 6-30 shows the daily precipitation for scen_0086. It can be seen that precipitation is spread throughout the year with heavier events occurring in all seasons. This suggests that to attain such high pore water pressures for the Newbury slope, heavy rain throughout the year is required. This keeps the pore water pressures relatively high through summer so that in the winter, when the precipitation is at its greatest, suctions are easily dissipated.
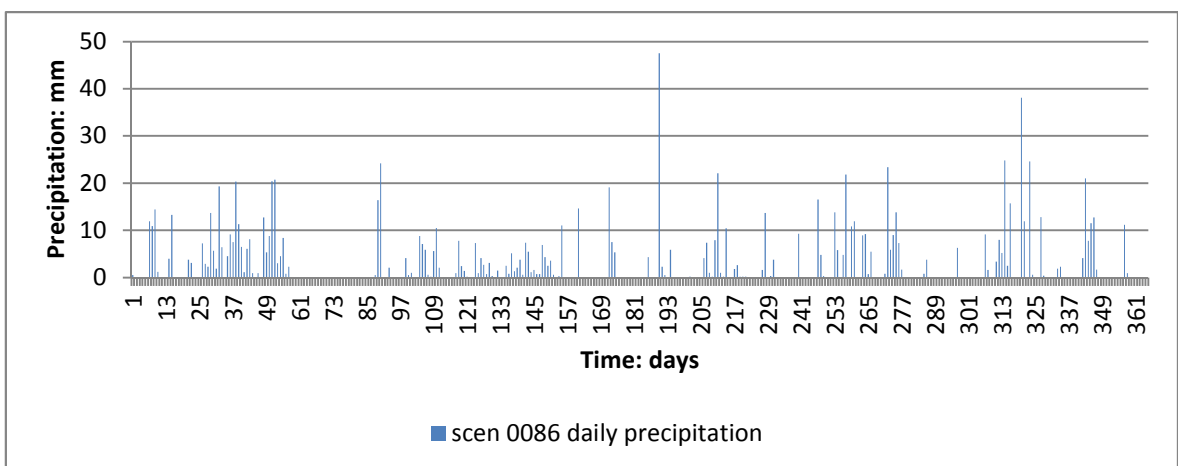
Figure 6-30: Daily precipitation totals for scen_0086.

Scen_0087

Scen_0087 resulted in dissipation of suctions and the largest pore water pressure cycle at a depth of 3.0 metres of 37 kPa (for cntr or scen models). The summer consisted of two months (May and June) of precipitation significantly below LTA followed by July being just below and a very wet August where nearly 100 % more precipitation than the LTA fell (Figure 6-31). This summer is followed by a winter with more very heavy rainfall. In October a total of 259 mm of precipitation fell, with 82 mm on one day alone (Figure 6-32). September and December were also very wet with total precipitation for these months being 84 mm and 104 mm respectively. This meant that a total of 601 mm of precipitation fell between the months of August and December, not much less than the LTA for a whole year (632 mm).
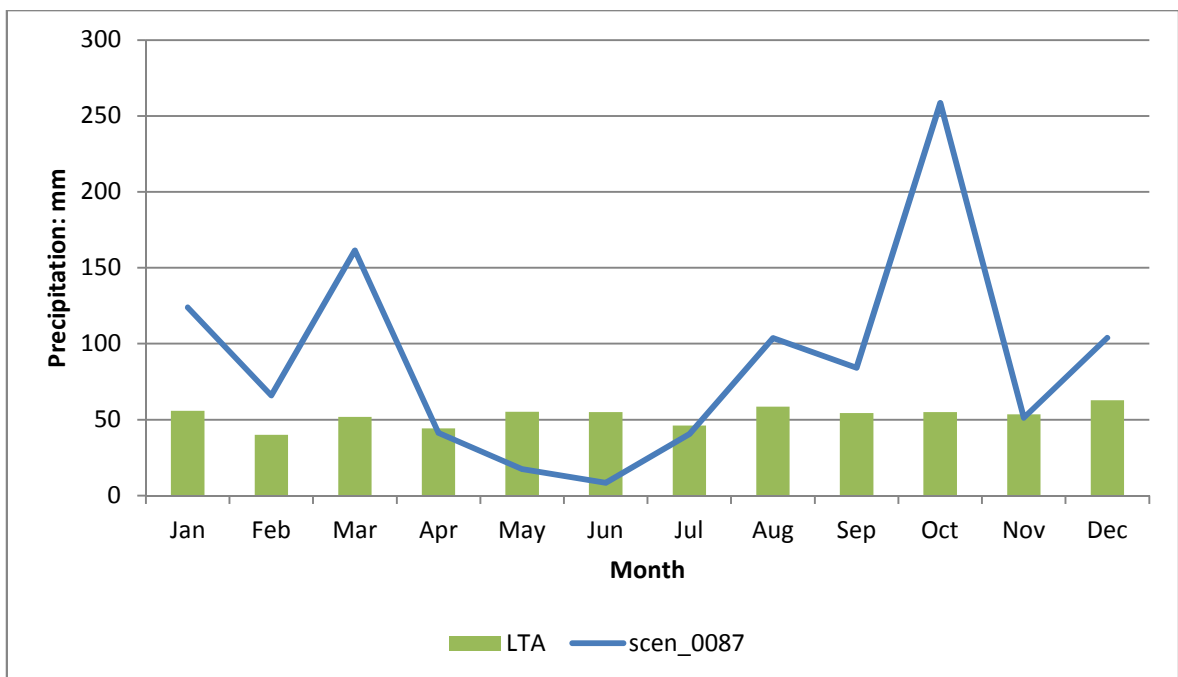
Figure 6-31: Total monthly precipitation for scen_0087.
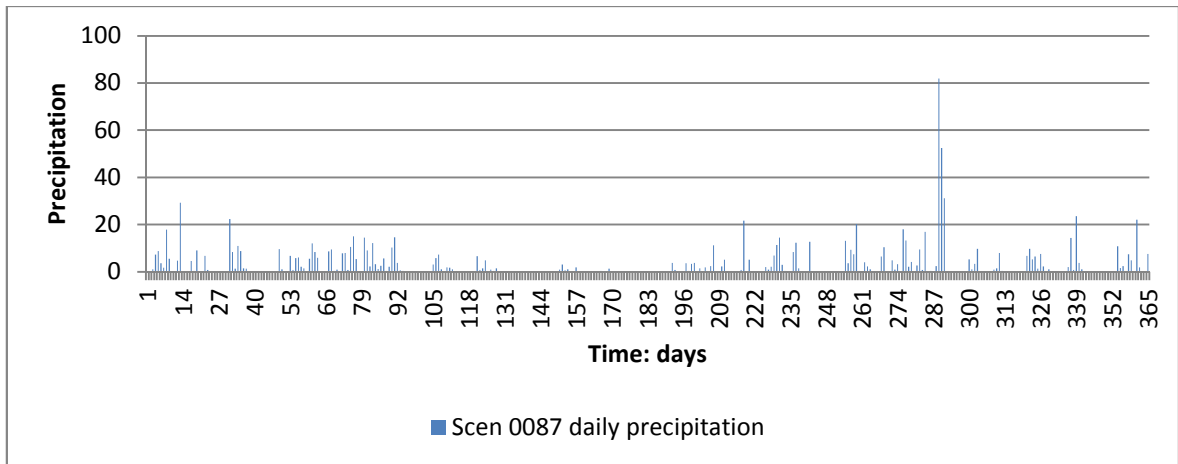
Figure 6-32: Daily precipitation totals for scen_0087.

The end of summer suctions were approximately average for scenario models. The resulting extremely high pore water pressure cycle seems to have resulted from the significant precipitation during October. It is postulated that a combination of high, but not extremely high end of summer suctions, combined with a significant rainfall month have led to this large cycle. In the next section the influence of antecedent pore water pressures (end of summer suctions) on the proceeding behaviour is investigated.

6.6.2.4 Effect of antecedent pore water pressure conditions

It has been observed that suctions dissipate in the scenario models less often (Section 6.5.1.3.2) and the size of pore water pressure cycles at a depth of 3.0 metres are on average significantly less (Section 6.5.1.3.1). This suggests that despite similar cracking depths and the use of the same material properties water infiltrates the scenario models with less ease than the control models. In the previous section it was established that the magnitude of precipitation in the winter months is one of the major factors determining the hydrological behaviour of the slope. There must, however be other factors influencing this as there are a number of models with high magnitudes of winter precipitation where suctions are still not dissipated and suctions cycles are low.

As shown in the Richards equation below the vertical flow of water is directly controlled by the magnitude of hydraulic gradients ($\frac{\delta h_\psi}{\delta x}$ and $\frac{\delta h_\psi}{\delta y}$) and the hydraulic conductivity ($K_{(\psi)}$).

$$\frac{\delta}{\delta x}\left[K_{(\psi)}\frac{\delta h_\psi}{\delta x}\right] + \frac{\delta}{\delta y}\left[K_{(\psi)}\left(\frac{\delta h_\psi}{\delta y}+1\right)\right] = \frac{\delta \theta}{\delta t}$$

Antecedent pore water pressures in the slope at the end of summer affect both the hydraulic gradients and the hydraulic conductivity. Very dry soil near the surface will result in high negative hydraulic gradients and low hydraulic conductivity, both of which are conducive to low flow rates in the downward vertical direction. In this section the influence of antecedent pore water pressures on the hydraulic gradients and the hydraulic conductivity and the resulting hydraulic behaviour is examined.

Figure 6-33 shows the high porosity bimodal hydraulic conductivity function developed in Section 5.5.1. In this graph it is clear how the antecedent pore water pressures in the slope can influence the hydraulic conductivity and the ability of water to quickly infiltrate the slope. At very low suctions (<1.0 kPa) hydraulic conductivity is dominated by the crack network and at suctions greater than this it is dominated by the intact soil (Figure 6-33). Due to the capillary law that the model is founded on cracks do not impact the value of K_w until suctions are small; this is because water enters the larger pores at these lower suctions. The change between the influence of intact soil and cracks is also very sudden; the hydraulic conductivity reduces by 2 orders of magnitude when the suction increases from 0.3 kPa to 1.0 kPa.
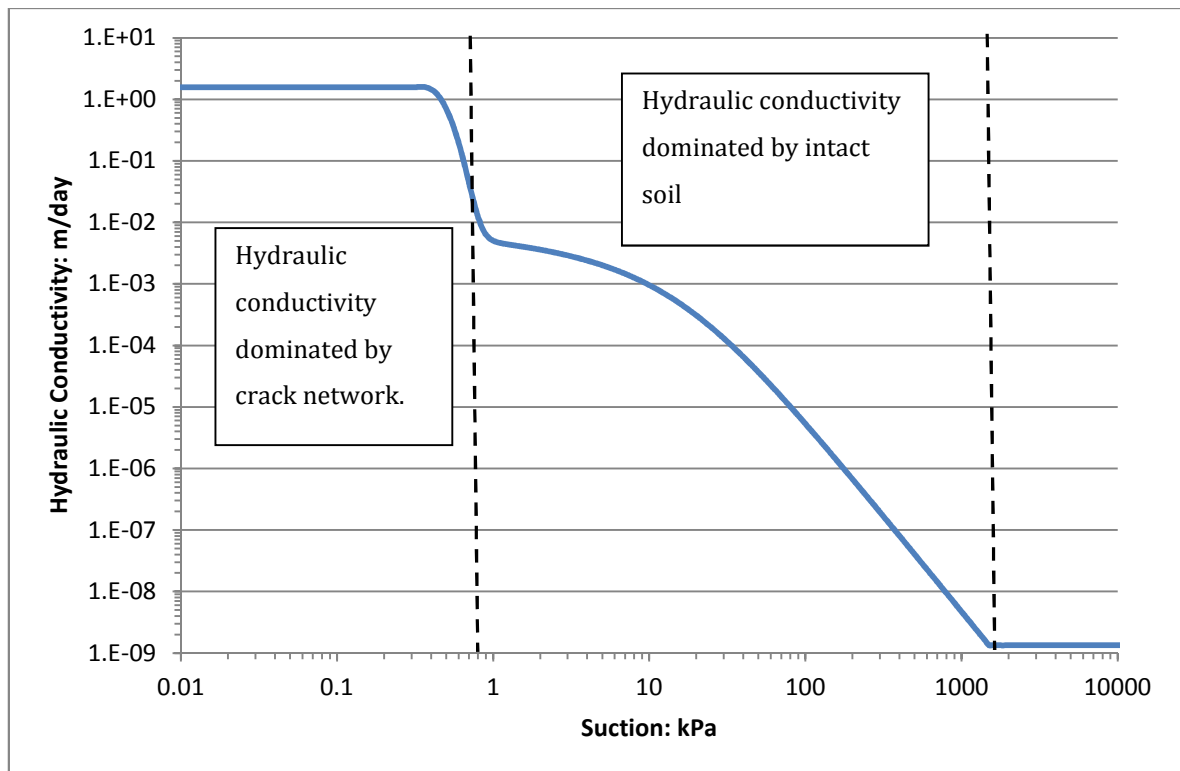
Figure 6-33: Bimodal hydraulic conductivity function.

Clearly this will have repercussions on subsequent hydraulic behaviour of the slope. The scenario models have significantly greater suctions at the end of summer than the control models suggesting significantly lower values of hydraulic conductivity, and more moisture being required to infiltrate the slope before the suctions fall to a level where the crack portion of the soil dominates the value of K_w.

In the literature review the performance of bimodal SWCCs and HCFs to represent cracked soil was investigated (Section 2.10.2.5). The type of behaviour discussed above has been observed by Fredlund et al. (2010a) who modelled infiltration into a cracked soil at several different pore water pressure initial conditions. They observed that when suctions were initially high less water infiltrated the soil and suctions did not significantly decrease (see Section 2.10.3 of literature review for more detail).

In this section a number of models have been selected and analysed to illustrate the effects of antecedent pore water pressures at the end of summer on the hydraulic behaviour throughout the remainder of the year. The models that have been chosen for this analysis are:-

- 0008 – End of summer suctions for the scenario model were high. By the end of the year, suctions had not been dissipated.
- 0013 – End of summer suctions for the scenario model were very high. These suctions were dissipated though at the end of the year and the pore water pressure cycle was high.
- 0057 – Low end of summer suctions in the scenario model that were dissipated at the end of the year.
- 0094 – In the scenario model suctions at the end of summer are around the median value for scenario models.

Scen_0008

Figure 6-34 shows the pore water pressures at a depth of 1.0 metre and the daily precipitation data for the model scen_0008. Maximum suctions at this depth were high for this model (103 kPa) and were not dissipated by the end of the year. The summer was very dry and was followed by a not exceptionally wet winter. This will have resulted in large negative hydraulic gradients and low hydraulic conductivity at the end of the summer.
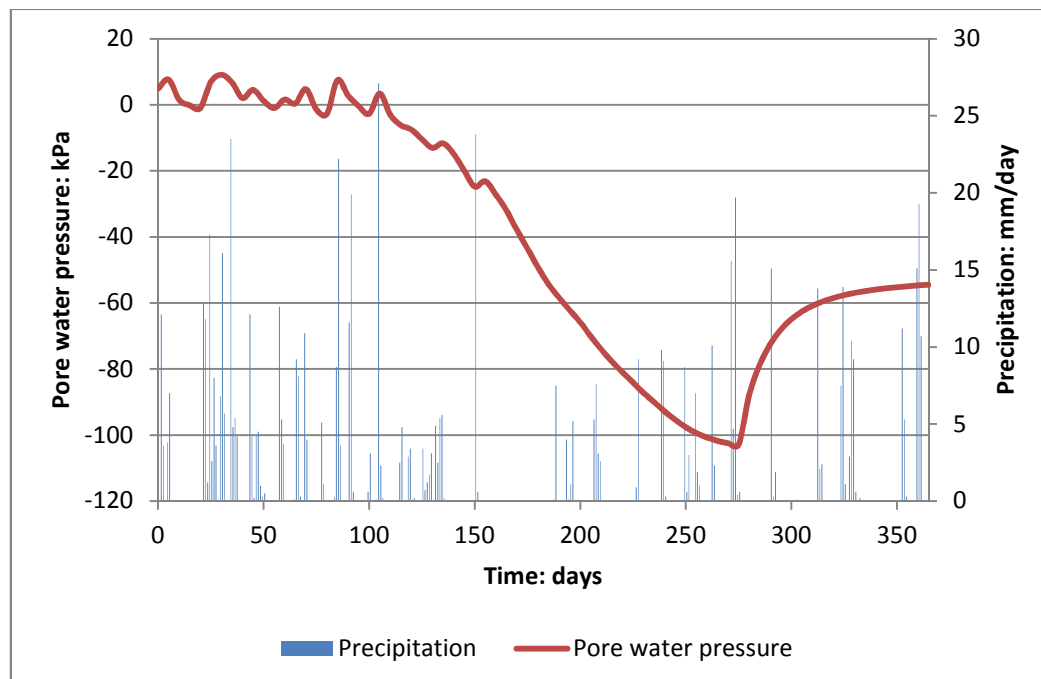
Figure 6-34: Temporal pore water pressures and daily precipitation distribution for scen_0008.

Figure 6-35 shows the same temporal pore water pressures plotted with the temporal hydraulic conductivity at the same point in the slope. The relationship between the two is clear; high pore water pressures at the start of the year result in a high hydraulic conductivity and as the water pressure decreases so does the conductivity of the soil. The graph shows that pore water pressures do start to recover after day 275, resulting in an increase in the hydraulic conductivity but never reach a magnitude where the crack part of the HCF becomes dominant (denoted by the dashed, grey line where $K_w = 0.005$ m/day). The effect of this is that the cracks do not come into play and bypass flow cannot occur through the cracked portion of the soil when winter precipitation occurs. The combination of high negative hydraulic gradients and low hydraulic conductivity has resulted in the suctions not being dissipated by the end of the year.
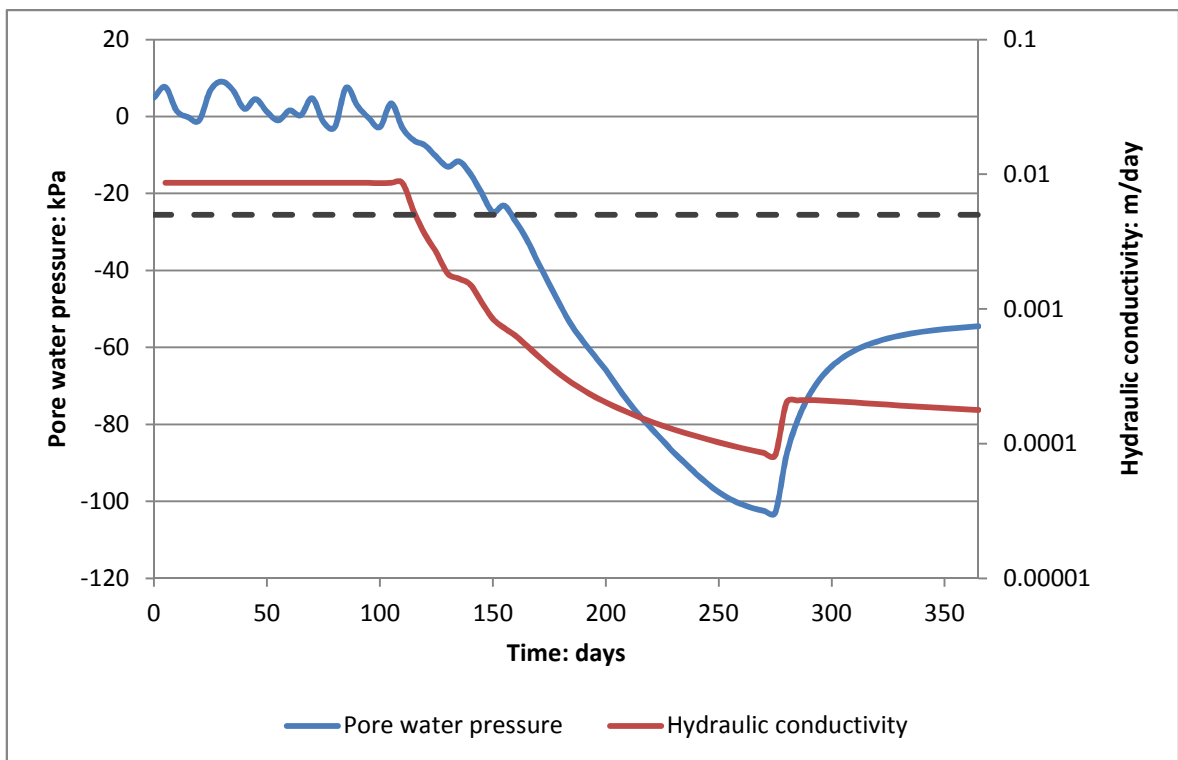
Figure 6-35: Temporal pore water pressures and hydraulic conductivity for scen_0008.

Scen_0013

Figure 6-36 shows the temporal pore water pressures at a depth of 1.0 metre and the daily distribution of precipitation for the model scen_0013. This model exhibits the WET-DRY-WET seasonal variance very well; precipitation between June and September is significantly below the long term average, followed by a winter where there is an extremely large amount of precipitation (390 mm in October, November and December). In this model maximum pore water pressures were very high (108 kPa) and were recovered by the end of the year. This model also exhibited one of the larger pore water pressure cycles at a depth of 3.0 metres of 26 kPa. Negative hydraulic gradients at the end of the summer were very high and the hydraulic conductivity was very low which would suggest, as in scen_0008, that suctions would not be dissipated.
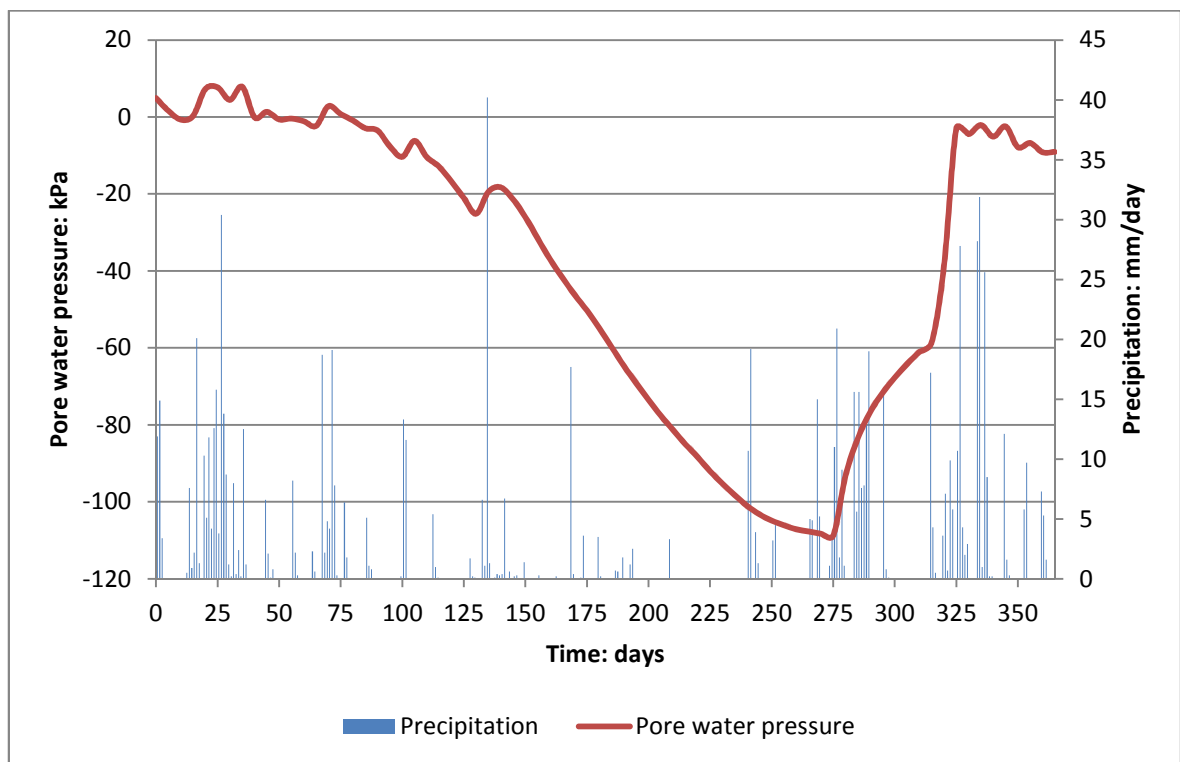
Figure 6-36: Temporal pore water pressures and daily precipitation distribution for scen_0013.

Figure 6-37 shows the temporal pore water pressures and hydraulic conductivity at the same point. The grey dashed line represents the value of hydraulic conductivity above which the cracks become dominant (K_w = 0.005 m/day). In this graph, the

effects that the cracks have on the hydraulic conductivity are clear. Maximum suctions occur at day 275 and decrease steadily until day 310 when a rapid decrease begins which is accompanied by a rapid increase in hydraulic conductivity to a maximum value of 0.028 m/day meaning that cracks have become dominant in the hydraulic conductivity function and bypass flow is possible. This is likely to have had an influence on the large pore water pressure cycle that was observed at 3.0 metres. This model has shown that a combination of significant desiccation cracking and heavy precipitation events can overcome the effects of the large negative hydraulic gradients and low hydraulic conductivity and allow the slope to rewet.
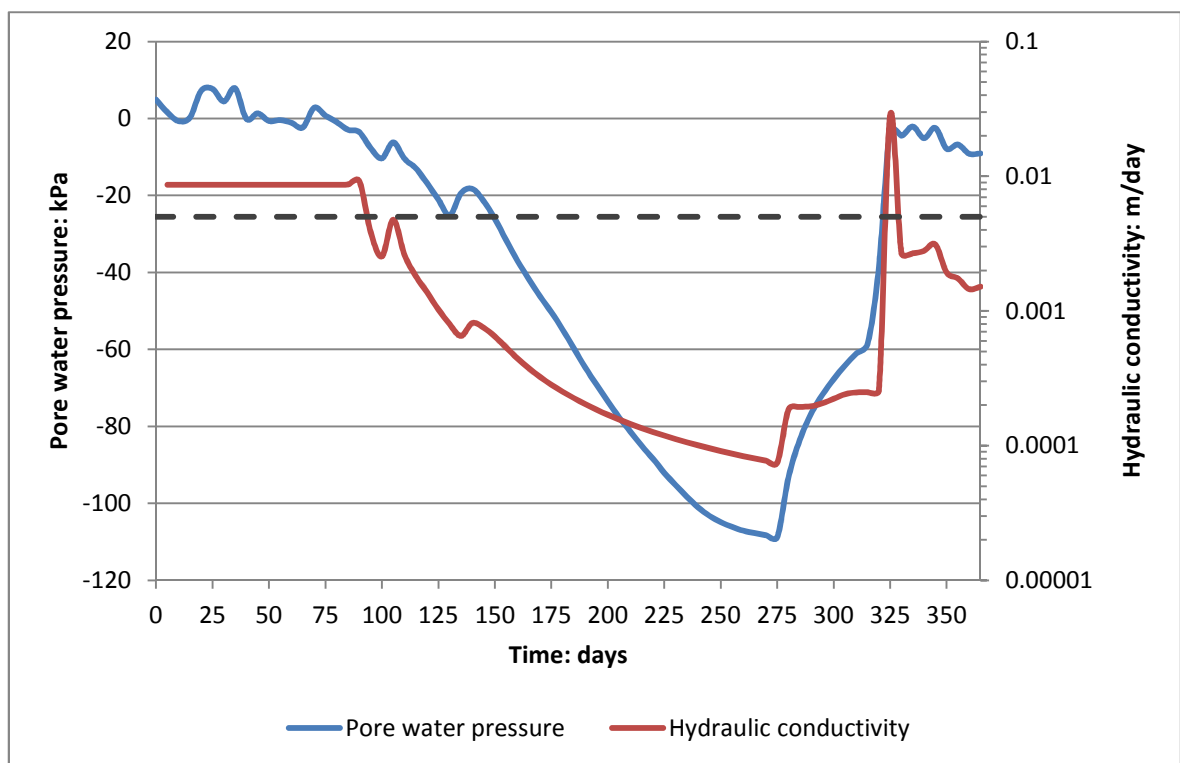
Figure 6-37: Temporal pore water pressures and hydraulic conductivity for scen_0013.

Scen_0057

Figure 6-38 shows the temporal pore water pressures at a depth of 1.0 metre and the distribution of daily precipitation for the model scen_0057. Maximum suctions for this model were relatively small; only 74 kPa (compared to the average of 91 kPa and median of 94 kPa). These suctions were dissipated by the end of the year. Summer for this model was not particularly dry with precipitation being above the LTA in May,

June and August, which explains why the maximum end of summer suctions were not very large. Winter precipitation was above the long term average but not excessively so; 217 mm of precipitation fell in October, November and December, compared to the LTA of 171 mm (the average for scenario models was 289 mm).
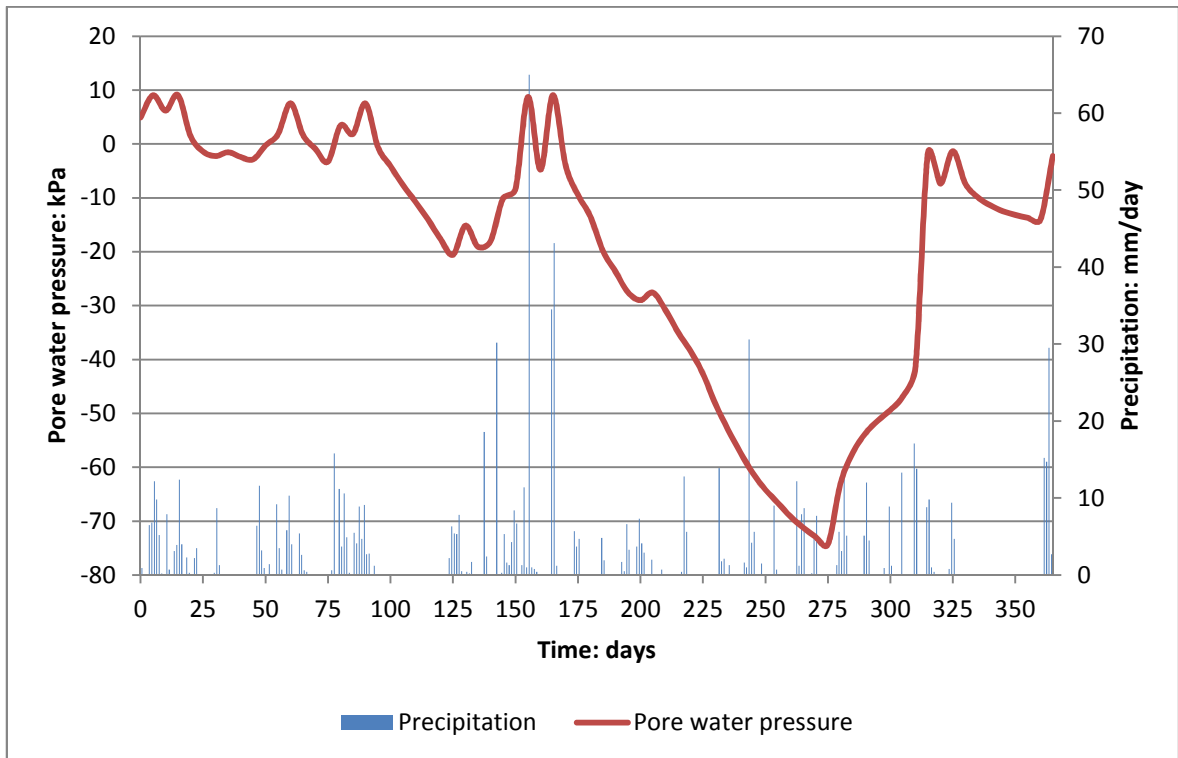
Figure 6-38: Temporal pore water pressures and daily precipitation distribution for scen_0057.

Figure 6-39 shows the temporal pore water pressures and hydraulic conductivity at 1.0 metres depth. In this plot the relationship between pore water pressures and hydraulic conductivity is again very clear particularly after 300 days. At day 315 the pore water pressure is at a value of 1.7 kPa, shortly afterward the hydraulic conductivity increases sharply to its maximum value of 1.01 m/day. The crack part of the HCF is clearly dominant at this point, with an increase in K_w of 3 orders of magnitude in only 5 days. Hydraulic conductivity then falls sharply again; at 330 days K_w has fallen back to a value of 0.0024 m/day. Figure 6-38 shows that this coincides with the occurrence of an extended period of no precipitation between 325 and 360 days.
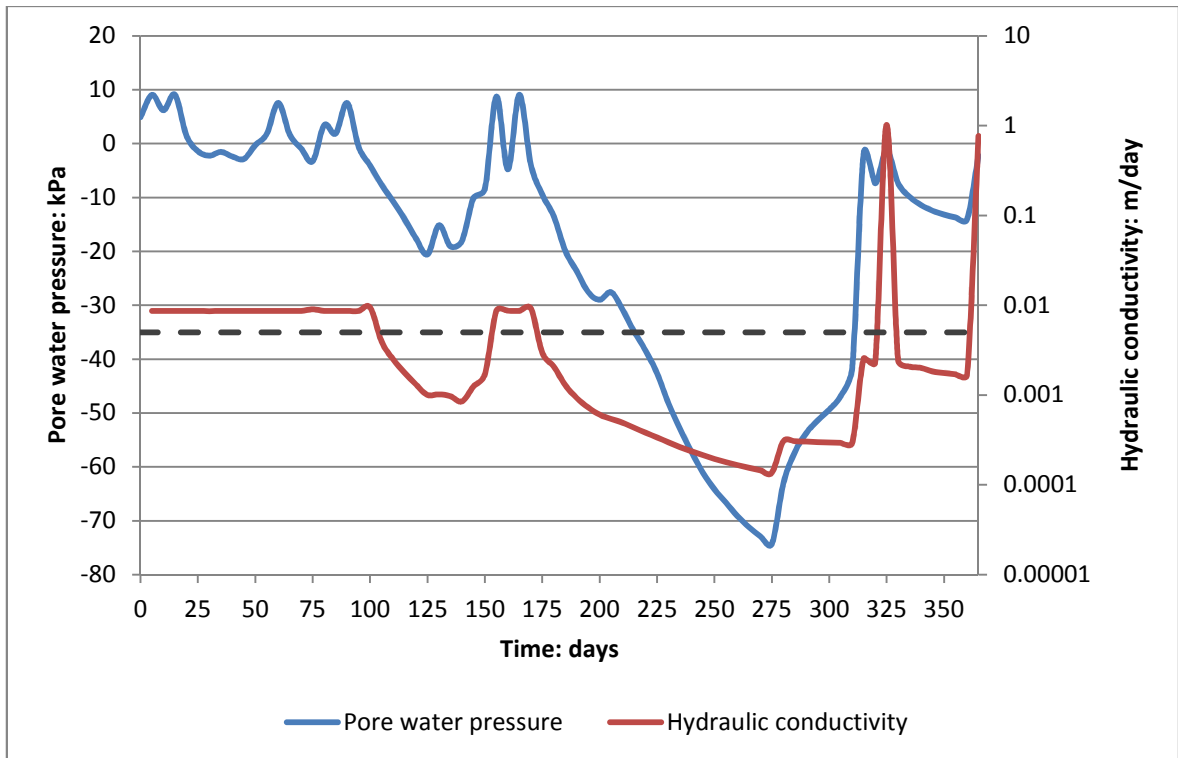
Figure 6-39: Temporal pore water pressures and hydraulic conductivity for scen_0057.

Scen_0094

In this model the maximum end of summer suctions were 90 kPa, just less than the mean and median (91.4 kPa and 94.0 kPa respectively), meaning that around average negative hydraulic gradients were present. These suctions are not dissipated at the end of the year. Figure 6-40 shows that despite considerable precipitation in the winter months suctions only decrease by 40 kPa. This has the expected effect on hydraulic conductivity. Figure 6-41 shows the temporal pore water pressures and hydraulic conductivity, a similar trend in hydraulic conductivity is exhibited to scen_0008's. The coupled/cyclical relationship between infiltration, pore water pressure and hydraulic conductivity is clear. If insufficient water is infiltrating the slope then the suctions will not decrease which in turn means that, the negative hydraulic gradients will not decrease and the hydraulic conductivity will not increase, both of which control the rate at which water can infiltrate.
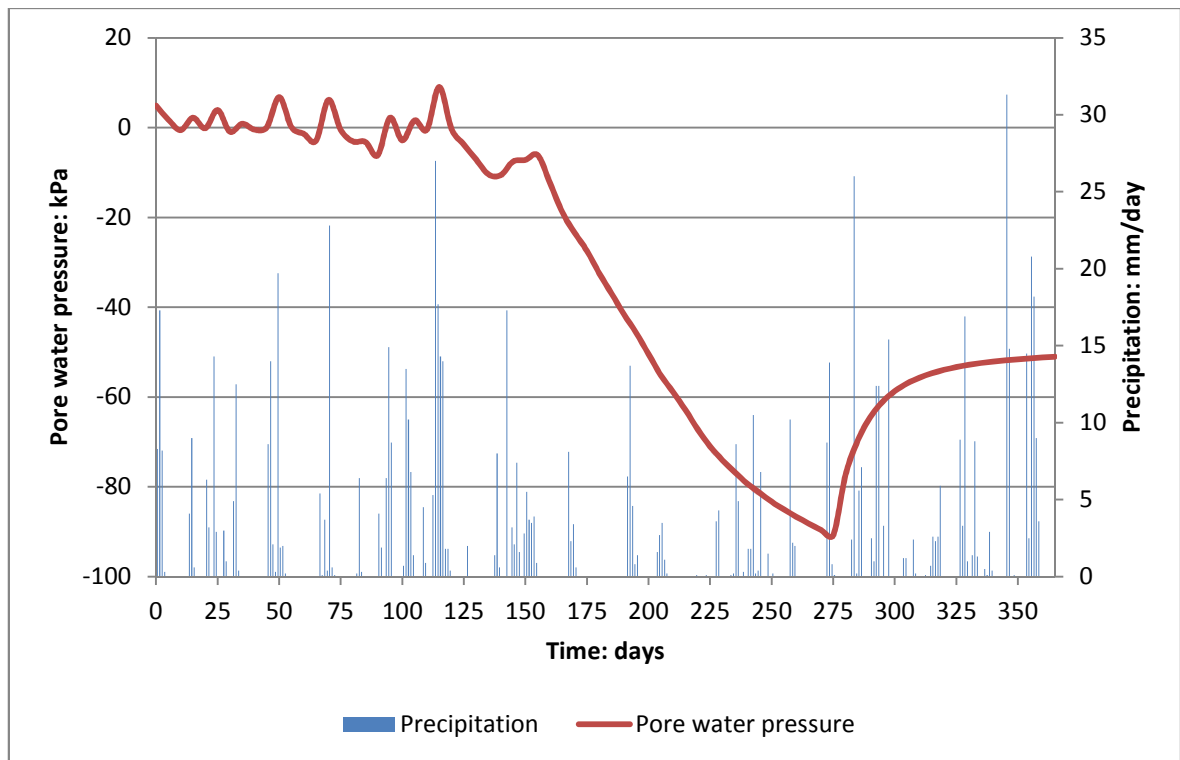
Figure 6-40: Temporal pore water pressures and daily precipitation distribution for scen_0094.

For the scen_0094 model winter precipitation is actually quite high, in the months of October, November and December 269 mm of precipitation fall, which is way above the LTA of 171 mm. In a lot of cases a model exhibiting these magnitudes of end of summer suctions and this magnitude of winter precipitation would result in suctions being dissipated and larger suction cycles. There is a link between magnitude of winter precipitation and likelihood of suctions dissipating but results such as scen_0094 suggest there are other factors that can influence the hydrology. For example the amount of runoff; this is directly related to the quantity of precipitation infiltrating the slope. If the proportion of precipitation lost as runoff is high then less water will be infiltrating the slope. In a following section the effect of the quantity of precipitation lost as runoff is analysed and discussed (Section 6.6.2.5).
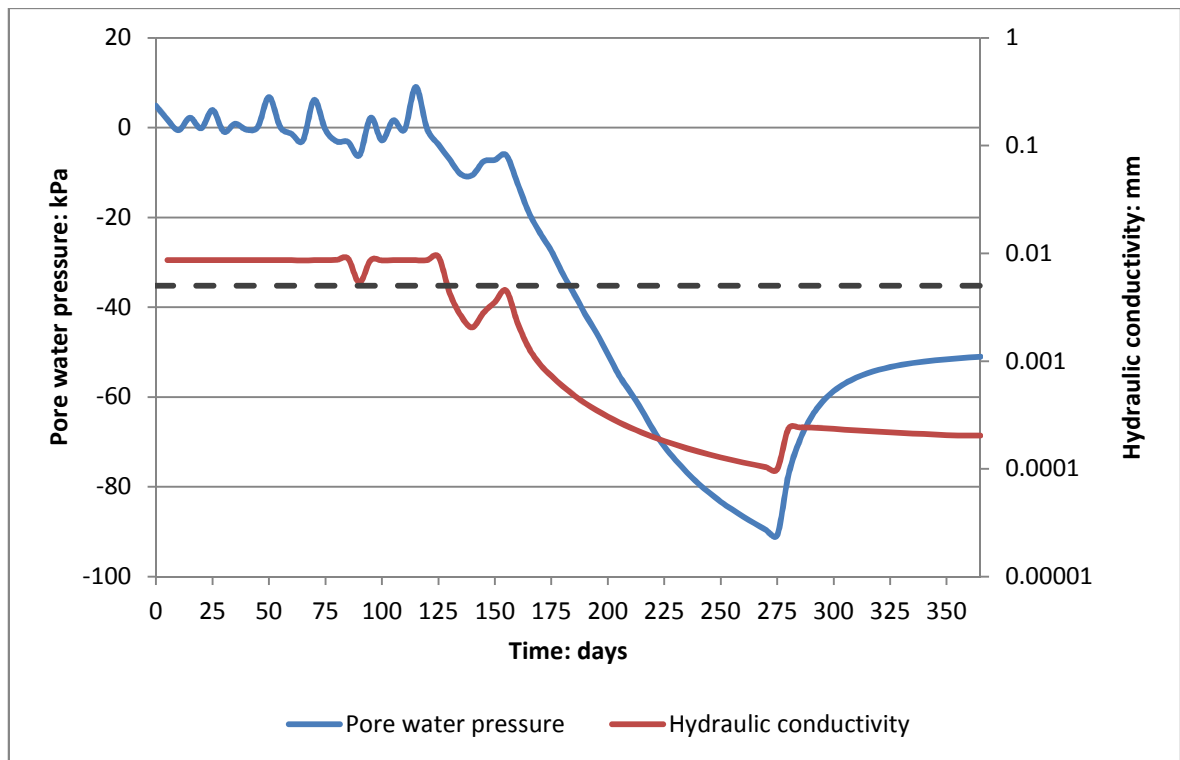
Figure 6-41: Temporal pore water pressures and hydraulic conductivity for scen_0094.

6.6.2.4.1   Summary of antecedent pore water pressure discussion

In summary the analysis of these models' results has shown that:-

1. High antecedent suctions in the slope at the end of summer have an effect on the subsequent slope hydrology throughout the rest of the year. These high suctions mean that negative hydraulic gradients are high and the hydraulic conductivity is low. Significant moisture is therefore required to infiltrate the slope before the negative gradients decrease and hydraulic conductivity increases to a level where the cracks become dominant in the HCF.

2. The magnitude of winter rainfall is also important. If the antecedent suctions are high, but rainfall throughout winter is also high then there is a good chance that suctions will be dissipated and the pore water pressure cycles will be high.

3. There are some exceptions to the previous point. It is believed that runoff may be significant in these cases; this shall be analysed in a proceeding section.

4. There is a strong relationship between suctions being dissipated and the size of the suction cycle at 3.0 metres (Figure 6-42). This shows how the cracked

soil properties influence the slope's hydrology. If suctions are dissipated, it indicates that the hydraulic conductivity will be dominated by the crack part of the bimodal equation meaning that K_w can increase by 2 orders of magnitude. This allows for easier infiltration of moisture to deeper parts of the slope increasing the pore water pressures at these locations leading to larger pore water pressure cycles.
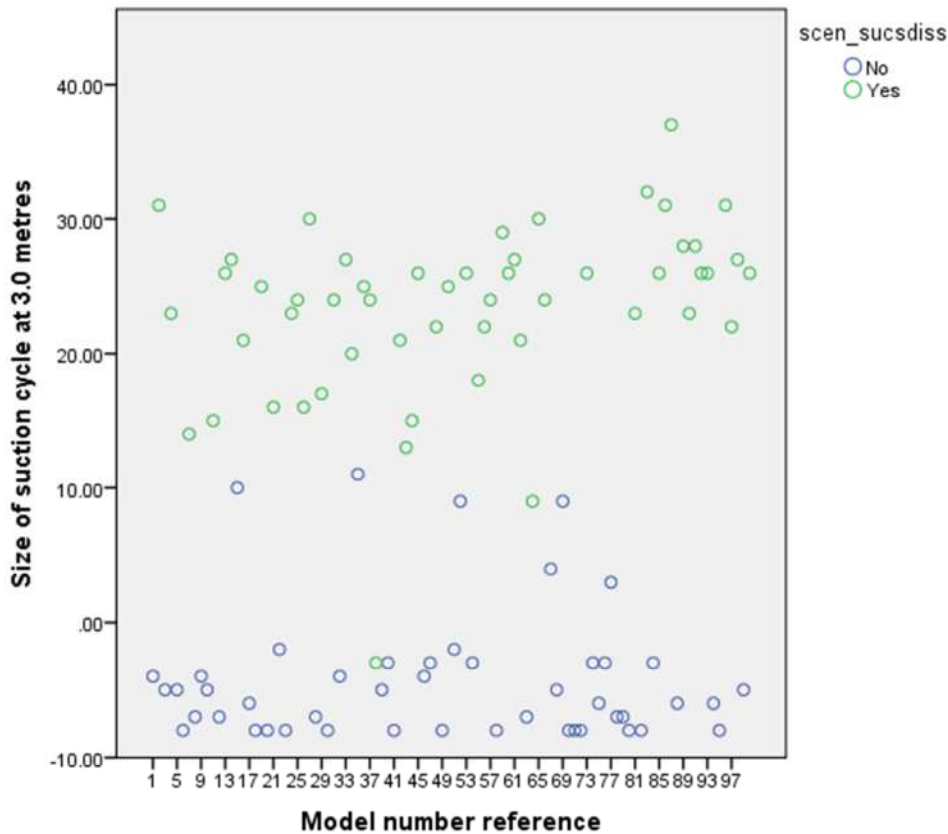
Figure 6-42: Relationship between size of suction cycle at 3.0 metres depth and whether suctions are dissipated for all scenario models.

6.6.2.5 Effect of runoff

Figure 6-43 and Figure 6-44 show the relationships between the proportion of precipitation lost as runoff after maximum suctions compared to the size of the pore water pressure cycle at 3.0 metres depth for the control and scenario models respectively. Both plots show a strong correlation between the two variables and the R^2 value for both shows that the proportion of precipitation lost as runoff explains a high percentage of the variability in the size of the pore water pressure cycle. The R^2 value can be converted to a percentage to quantify this (Field, 2005a).
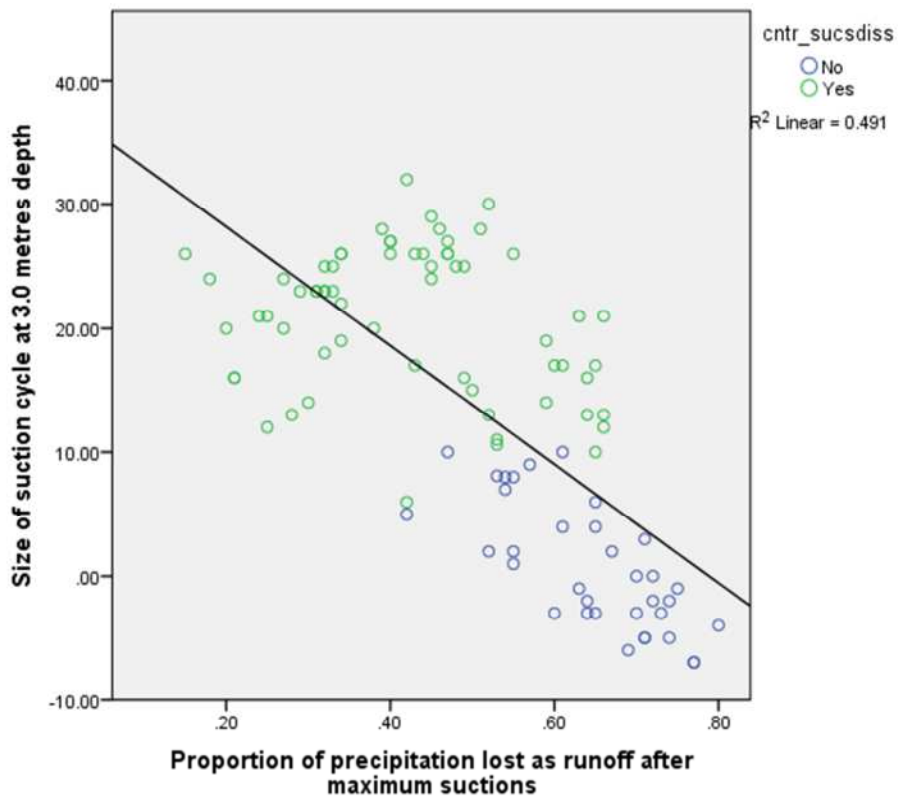
Figure 6-43: Relationship between runoff and size of pore water pressure cycle for control models.
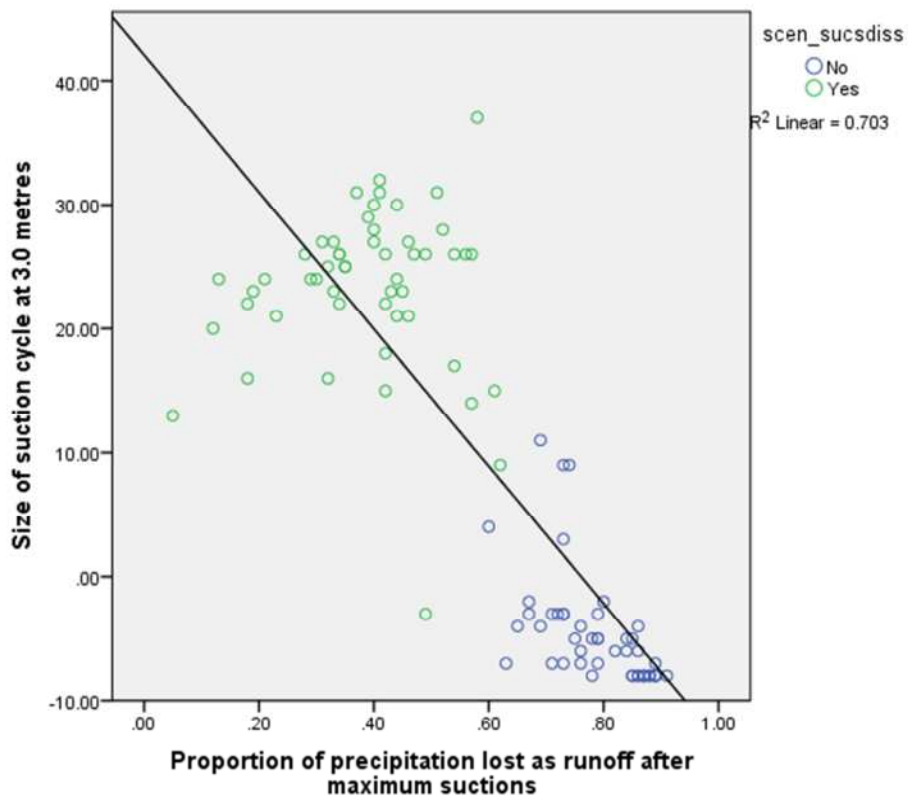
Figure 6-44: Relationship between runoff and size of pore water pressure cycle for scenario models.

The respective R^2 values show that the proportion of precipitation lost as runoff explains 49 % of variance in the size of pore water pressure cycle in the control models and 70 % in the scenario models. The increase for the scenario models could go a long way to explaining the change in hydrology affected by climate change. Another test has been carried out to identify whether there is a significant difference in the proportion of precipitation lost as runoff between the control and scenario models. Table 6-15 shows the results of the non-parametric Wilcoxon Signed Ranks Test. Significance $p < 0.05$; this shows that there is a significant difference between the mean values of proportion of precipitation lost as runoff.

Test Statistics[a]

	Proportion of precipitation lost as runoff (cntr) - Proportion of precipitation lost as runoff (scen)
Z	-2.738[b]
Asymp. Sig. (2-tailed)	.006

a. Wilcoxon Signed Ranks Test

Table 6-15: Results of Wilcoxon Signed Rank Test for proportion of precipitation lost as runoff.

Therefore, the proportion of precipitation after maximum suctions occurred was significantly higher for the scenario climate (Mdn = 0.58) than for the control climate (Mdn = 0.52), z = -2.738, $p < .05$, r = -0.19.

The amount of runoff clearly has a major part to play in the hydrology of the Newbury cutting slope. The statistical analyses have shown that the proportion of precipitation lost as runoff, and therefore not infiltrating the slope, is likely to increase in the future affecting the slope in such a way that it is likely to be less susceptible to progressive failure. Runoff occurs when the precipitation rate exceeds the infiltration capacity of the soil at the slope surface (section 2.8.3). These results suggest that precipitation rates in the scenario climate series were greater than in the control series. It is most likely that it is this, in conjunction with the higher end of summer suctions in the top of the slope which means lower hydraulic conductivity, has led to more runoff occurring in the scenario slopes.

In VADOSE/W once runoff occurs the water will not be reapplied to the model. It is assumed that this water is lost and cannot re-infiltrate the slope (Section 3.1.5.4). However, in Section 2.10.1 it was identified that one of the methods by which cracks allow infiltration into the slope is interception of runoff. It should therefore be questioned whether the VADOSE/W runoff model is sensible for a cracked soil. The results obtained in Chapter 5 support the use of VADOSE/W for a cracked soil. By including cracks the replication of pore water pressures in the Newbury cutting slope was much improved. Also in Section 5.8.2.1 it was shown that the model with bimodal properties had managed to predict the total amount of water lost as runoff very well.

Regarding the behaviour of desiccation cracks there are some facets that could influence the infiltration of runoff:

- Crack aperture – if cracks are of capillary size water may not be able to infiltrate by runoff. However, if cracks are greater than the maximum crack aperture for capillary flow then water should infiltrate through gravitational flow.
- Crack closure – it is likely that cracks close from the top upon soil saturation (Favre et al., 1997; Greve et al., 2010). If this happens then the method by which runoff infiltrates the cracks is closed off.

The relationship that crack geometry and behaviour have with the slope hydrology is extremely complex. Much more observation and testing of these are required to further develop any models that intend to include their effects.

6.6.2.6 Implications and summary

Climate change did affect the hydrology of the slope to the end of the year, but not in as much of a negative sense as was expected. Proportionally more precipitation was lost as runoff in the scenario models, which ultimately meant that suctions were dissipated less frequently and pore water pressure cycles at 3.0 metres depth were significantly smaller than the control models. This implies that in general the slope will be more stable in the future, in terms of shallow failures and deep seated, delayed failures.

Despite generally being more stable, in the extreme cases it was shown that the slope may be more unstable in the future. The minimum FOS for any model was less for the scenario models (1.023 compared to 1.199) and the largest pore water pressure cycle was much greater for the scenario models (37 kPa compared to 32 kPa).

The effect of the temporal distribution of precipitation was not clear. It seems that for dissipation of suctions to occur, heavy, persistent rainfall is required, rather than a series of extreme events. However a more detailed examination of the relationship between the hydrology and precipitation events is required, perhaps with models with precipitation defined at an hourly time frame.

Antecedent pore water pressures were found to influence the hydrology of the slope from the end of summer until the end of the year. The very large suctions that developed in the slope by the end of the summer in the scenario models impact the material properties of the soil. The conductivity of the soil is low when suctions are high; meaning that significant infiltration is required to increase the hydraulic conductivity to a point where the desiccation cracks become dominant. It is this that leads to greater proportions of runoff and the subsequent effects of slope hydrology.

6.6.3 The weather generator and the effect on the results

The aim of this chapter was to establish the possible effects of climate change on the hydrology and stability of the Newbury cutting slope when subjected to WET-DRY-WET seasonal variation in the precipitation. With the many statistical analyses carried out on the results of all the model runs, it was established that climate change will have an influence on the hydrology of the slope and probably also the stability. How much of this effect is due to changing seasonal variation has not yet been ascertained. In Section 6.4.2 the method for selecting DRY-WET-DRY years was described. This was achieved by identifying the control year exhibiting this variation then selecting the same year from the scenario output. When this part of the methodology was carried out, the scenario years that would be used in the numerical models were not looked at and therefore it was not known what variation they actually exhibited; it was assumed that they would also be WET-DRY-WET, and more

significantly so than the control years. In this section it will be shown that this assumption was erroneous.
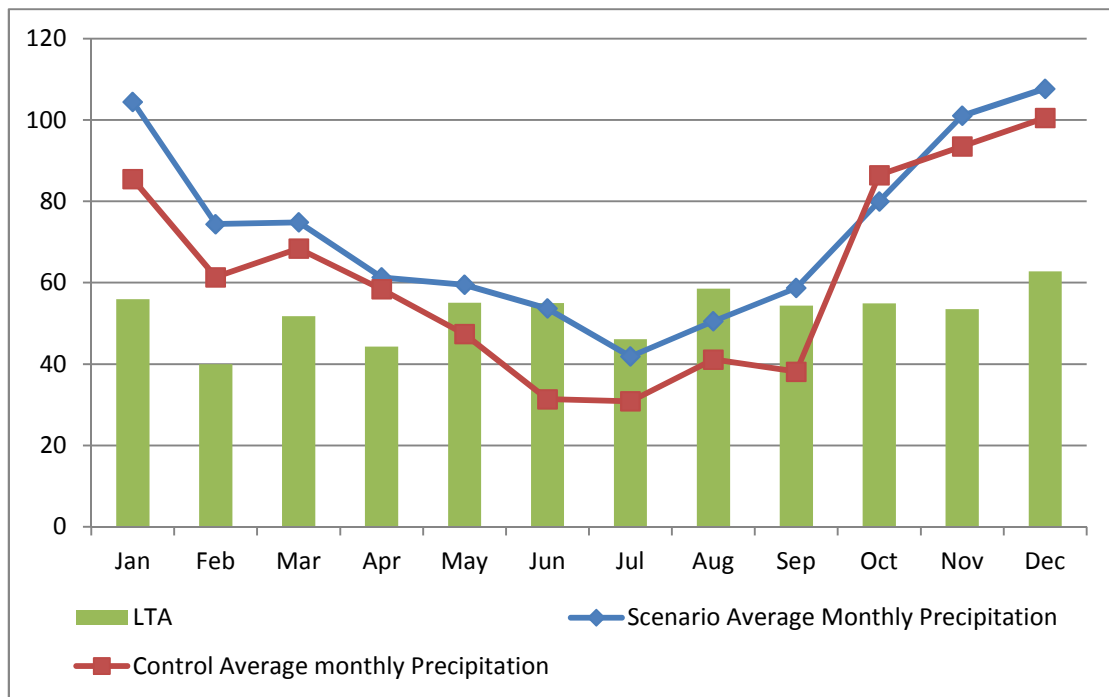
Figure 6-45: Average monthly precipitation of all control years and all scenario years used in the analyses, compared to the LTA.

Figure 6-45 shows the average monthly precipitation for all control and scenario models compared to the LTA. This graph immediately reveals that the method for selecting the desired year from the weather generator output has not worked as thought. It had been expected that the scenario years would on average have drier summers than the control years. However, Figure 6-45 reveals that the scenario summers were on average wetter than the control summers; the precipitation in May, June, July and August is either at the LTA, just below or just above. Essentially the seasonal variation that has been analysed for the scenario models is WET-AVERAGE-WET. In Appendix A, a simplified process diagram of the methodology behind the function of the weather generator is given.

This does not invalidate the findings as each year extracted from the weather generator is equally as likely to occur as any other. Ultimately what has actually been tested here are the differences occurring between WET-DRY-WET years in the control series and WET-AVERAGE-WET years in the scenario series (compared to the

LTA). It has been discovered that even though the scenario slopes are on average wetter than the control slopes they are in general more stable. This is because of increased summer drying as a result of greater evapotranspiration which generates greater summer suctions which often persist through the winter. Despite this, it cannot be assumed that these results can also lead to similar conclusions for WET-DRY-WET future years to be drawn. Some of the scenario models tested in these analyses did exhibit the WET-DRY-WET seasonal variation but resulted in dissipation of suctions and large pore water pressure cycles.

Table 6-16 shows the scenario models that exhibited actual WET-DRY-WET climate variance and the results from these models. From these results it seems that the WET-DRY-WET years have similar results to the other models tested in the scenario series. However consequences can only be implied from this as it is stressed when using the weather generator that 100 series must be tested.

Model no.	Summer precipitation (mm)	Winter precipitation (mm)	Suctions dissipated	Pore water pressure cycle (kPa)
Scen_0006	182	256	No	0
Scen_0013	172	390	Yes	26
Scen_0014	133	337	Yes	27
Scen_0018	170	245	No	0
Scen_0020	76	221	No	0
Scen_0032	170	242	No	0
Scen_0050	173	211	Yes	25
Scen_0051	179	304	No	0
Scen_0061	176	325	Yes	27
Scen_0072	159	358	No	0
Scen_0082	154	297	No	0
Scen_0084	181	274	No	0
Scen_0091	162	275	Yes	28
Scen_0095	134	241	No	0

Table 6-16: Results for scenario models showing WET-DRY-WET seasonal variance.

A major learning point from this work is that the weather generator is a very powerful tool but it must also be used very carefully. A simple misunderstanding in the use of the tool in this work, has led to a major error in carrying out the intended methodology. In Appendix C the recommended method for extracting extreme years from a Weather Generator 2.0 is provided. In addition, when deciding to use the weather generator the following should be considered:

- Large quantities of data are produced. For statistical viability at least 100 data series need to be used. Therefore, any use of the data is time consuming, especially when applied to numerical modelling.

- The data cannot be applied directly to VADOSE/W. The user must create formatted data series. Care should be taken when this is done; along with the large quantities of data this could potentially lead to some errors.

- There are some limitations of the actual data that is produced by the weather generator. Wind data is not available, and some variables, such as relative humidity, are given only as average values.

- A revised methodology for identifying and extracting desired years from the weather generator output has been developed and is shown in Appendix C. This method involves extracting years individually from each series; control and scenario.

6.7 Summary

In this chapter the effects of climate change on the hydrology of the Newbury bypass cutting slope were analysed. The VADOSE/W numerical slope hydrology model, developed throughout Chapters 4 and 5 was used, in conjunction with the UKCP09 weather generator, to run numerous models analysing the effects high seasonal variability on the slope's hydrology. The UKCP09 weather generator was used to create series of future and current weather data, which could then be manipulated such that they could be applied as VADOSE/W climate boundary conditions.

Once all models had been run, and the results compiled, it was recognised that the most efficient way to analyse and compare results, from the numerous models, was

with a statistical analysis software package. The software package IBM SPSS was chosen for this, being capable of handling large quantities of data and possessing the relevant statistical tests to analyse the data is question. Statistical tests used in this work include:

- Kolmogorov-Smirnov test for normality of data.
- Dependent t-test for parametric data used to identify significant differences between means.
- Wilcoxon signed-rank test for non-parametric data used to identify significant differences between means.
- Chi-square test to analyse significance of differences between categorical data.

These tests were used to determine whether the differences between the results obtained from the current climate model runs were significantly different from those obtained from the future climate runs and therefore establish whether climate change had statistically significant effects on the hydrology of the Newbury cutting slope.

A number of facets of the slope's hydrological behaviour were analysed, including evapotranspiration, suction magnitudes at the end of summer, depth of water table, depth of cracking and pore water pressure cycles. Of these some were found to be significantly affected by climate change. Both evaporation and transpiration were significantly higher which had repercussive effects on the magnitude of suctions at the end of summer. In the future models these were significantly higher within the top 1.0 metre of the slope, but the affect decreased with depth and by 3.0 metres depth the magnitudes of suctions were not significantly different. At the end of the year pore water pressure cycles were measured and shown to not be significantly greater for the future climate. However, these results only apply for the specific climate change that was investigated.

At the beginning of the chapter an equation to estimate the depth of desiccation cracking was introduced. This equation, suggested by Fredlund and Rahardjo (1997) uses the suction profile and material properties to estimate the maximum depth of desiccation crack. The equation was implemented in the VADOSE/W model and found to improve the modelling results for this slope. The equation was then used in later parts of the chapter to estimate the depth of desiccation cracks which were then

analysed in the statistical analysis. It is very important to note that this equation is not properly validated against actual desiccation crack measurements. This proved difficult to achieve due to the lack of recorded crack depth measurements which were accompanied by measurements of suction profiles. This equation should therefore be used with care.

7 Conclusions and recommendations

7.1 Chapter Outline

The major results and findings of this research are summarised in the chapter and recommendations for further work are suggested. In this research, a method for modelling the influence of desiccation cracking on slope hydrology was developed. The method was developed with the intention of investigating the possible effects of climate change on slope hydrology and stability of man-made slopes in the United Kingdom. A finite element model of the Newbury by-pass cutting was created and the new method was used in conjunction with measured field data to first validate the method and then investigate the effects of forecast climate change.

The stated aim at the beginning of this thesis was 'to develop a physically-based model that accounts for the temporal and spatial variability of climate and material properties. The model is developed with the intention of using it to analyse the effects of climate change on infrastructure slopes in the United Kingdom'. This would be achieved through the following objectives:-

1) Identify an infrastructure slope in the United Kingdom for which extensive pore water pressure data, material properties and climate data is available and develop a physically-based model in a suitable finite element software package and use the obtained data to validate the model.

2) Identify and review potential methods for including the effects of desiccation cracks of the hydraulic properties of soil.

3) Develop an improved soil hydraulic property model and implement into the already existing physically-based model. Again, validate the results against the observed pore water pressure data for the slope.

4) Identify the most suitable, up-to date method for generating series of future climate data. Use this to create series of temporal, present and future climate data sets for the location of the slope.

5) Combine the developed physically-based model that includes the soil properties considering the effects of desiccation, with the generated climate data to analyse the effects of climate change on infrastructure slopes in the United Kingdom.

6) From the results of these analyses draw conclusions that further the understanding of the effects of climate change on infrastructure slopes in the UK and also make recommendations for further work.

By drawing conclusions from the work carried out, results, analysis and discussion from each chapter it will be shown that the aim and each individual objective has been met in this thesis.

7.2   Chapter 4

The first chapter established the validity of using the finite element software VADOSE/W to model the interaction between the atmosphere and slope hydrology. It was found that by using comprehensive, daily climate data with well-defined vegetation properties, material properties and boundary conditions the software was able to calculate realistic trends and magnitudes of the temporal pore water pressures in the Newbury bypass cutting slope. The model performed better when calculating the maximum summer suctions compared to calculating the minimum winter suctions, perhaps due to problems with the material property model. The conclusions drawn from the findings are:

1) A model of the Newbury cutting slope, created in the finite element software VADOSE/W is able, with varying degrees of accuracy, to replicate the temporal trends and magnitudes of pore water pressures occurring throughout the year. The model must be well defined with detailed climate data measured at least at a daily time scale. The model performs better when calculating the pore water pressures at the end of the summer, compared to those at the end of the year, which is an issue that has been experienced in previous works. By analysing the water balance generated by VADOSE/W it was established that storage did not recover to the levels expected, meaning that the model had not allowed sufficient precipitation to infiltrate the slope such that pore water pressures could recover to the observed levels.

2) Incomplete material property definition by the user is responsible for the inability to replicate the winter pore water pressures. Desiccation cracking, which is generally not properly taken into account in these types of models, will affect the hydraulic properties of the soil, temporally and spatially and should be taken into account.

7.3 Chapter 5

The findings in Chapter 4 led onto the work carried out in this chapter. The temporal variance of material properties was considered, firstly by accounting for hysteresis and then by developing a method of including the effects of desiccation cracking on a soil hydraulic properties.

The effects of desiccation cracking on the hydraulic properties of the soil were accounted for by using bimodal functions for the soil water characteristic curve and the hydraulic conductivity function. The functions were created by combining van Genuchten equations for the intact soil and the cracks. Sensitivity analyses were carried out on the van Genuchten parameters of the crack part, and the crack porosity. Crack depth was also considered, and by using a crack depth more similar to that observed in the field, the replication of pore water pressure trends and magnitudes

were well replicated. The conclusions drawn from the results and analysis in this section of work are:-

1) The model developed in Chapter 4 and that of Davies et al. (2008a) cannot replicate the dissipation of suctions in the winter due to not accounting for the effects of desiccation cracks. Not including the cracks leads to an overestimation of runoff and an underestimation of infiltration.

2) Bimodal, closed form equations describing the soil water characteristic curve and hydraulic conductivity function of a cracked soil can be used to model the effects that these cracks have on the hydraulic properties of the soil. In this work, combining van Genuchten (1980) equations for the intact soil part and cracked part has been shown to be an acceptable approach.

3) By implementing these equations into a numerical hydrology model of the Newbury cutting slope, the replication of temporal trends and magnitudes in pore water pressures can be improved. The bimodal functions succeed in allowing greater infiltration of precipitation throughout winter such that pore water pressures can be recovered. By using the bimodal functions hydraulic, conductivity can be up to 2 orders of magnitude greater than when desiccation cracks are ignored. It is this capability that has the greatest effect on improving the results.

4) Results obtained when using these equations are sensitive to the parameters used to define the functions. The values used for the van Genuchten parameters *a* and *n*, and the crack saturated VWC will all affect the results. Correct definition of these parameters is important for the functions to work correctly. In this work all these parameter's values have been based on either other author's suggestions or as a result of the sensitivity analyses. The model has been validated and the approach shown to be appropriate. However to improve the model and validate the method further actual laboratory measurements of these parameters should be made.

5) Using a realistic, observed crack depth will improve the performance of the model. When the crack depth was increased in this model, the results improved at greater depths. There is currently a lack of this kind of data available. More observations and measurements of cracks in the field would further benefit the development of these models.

6) The assumption that the capillary law defines flow in the cracks need to be considered carefully if deciding to use the bimodal functions. At a certain crack width, this no longer holds true. Therefore if the soil that is to be modelled exhibits many cracks larger than this size then the use of these equations may become questionable.

7) Using temporally and spatially variable material properties is a superior approach to the traditional method of employing bulk, static material properties when modelling the hydrology of an infrastructure slope. If a slope is to be analysed for progressive failure this is particularly relevant. By using these material properties, in conjunction with detailed climate data, the influence of changing material properties on the water balance of the slope, with repercussions on slope hydrology and pore water pressure cycles, can be captured properly. This is also important to bear in mind if carrying out basic limit equilibrium analyses; the use of static pore water pressure data may lead to unsafe estimates of the minimum FOS. By using a PBM such as the one developed here in conjunction with a limit equilibrium analysis a full range of FOSs throughout the year can be calculated.

8) Hysteresis is likely to have just as significant an impact on the performance of any slope hydrology model as desiccation cracking. There can be large differences between the suctions measured on a wetting and drying curve at the same value of volumetric water content which can adversely affect modelling results.

7.4 Chapter 6

In this final chapter the bimodal soil properties were used in conjunction with the UKCP09 weather generator to study the effects of climate change on the Newbury cutting. Series of control and scenario climate data series were generated and applied as climate boundary conditions to the VADOSE/W model of the Newbury cutting. Supplemental work was carried out, including validating an analytical equation that estimates the depth of cracks occurring in a desiccated soil.

A large number of statistical analyses were carried out, comparing the results from the control and scenario models. From the results and subsequent analyses, the conclusions in this section have been made. It is noted that these conclusions apply definitely to this slope (and its location), with the emission scenario used (high), in the time slice selected (2050s). However for slopes located in other areas of the country, particularly those not in the south of England, results could differ significantly. The conclusions drawn from the work carried out in this chapter are:-

1) The amount of evaporation and transpiration from the slope in the future will be significantly greater than present. Theis will be the dominant influence changing the water balance of the slope leading to a change in the hydrology of the Newbury cutting.

2) The differing water balance behaviour and subsequent effects of the slope's hydrology will lead to significantly lager suctions developing in at least the top 1.0 metre of the slope profile; potentially leading to greater soil shrinkage throughout the summer and more of the associated serviceability problems.

3) The influence of climate change on the slope hydrology decreases with depth. This is because of the decreasing influence of evaporation and transpiration. Because of this, the maximum depth of the water table is unlikely to change significantly.

4) The equation for estimating crack depth is potentially useful. When used to estimate cracks occurring in the Newbury cutting slope the modelling results were improved. The equation was also implemented in the climate change analysis and showed that desiccation cracking will not be significantly deeper in the future. It is thought that the equation may only be applicable when the summer weather being modelled is quite dry, meaning that suctions develop through the summer with little fluctuation in magnitude.

5) Running the analyses to the end of the year showed that despite there being more precipitation falling in the winter months in the future, the size of suction cycles will actually be significantly smaller in the future, suggesting that progressive failure may in general become less of a problem. However, the analyses also showed that the worst case size of suction cycle will actually be greater than the worst case in the present climate.

6) As a proportion of the total winter precipitation falling, significantly less will infiltrate the Newbury cutting in the future, leading to more runoff and the lower pore water pressure cycles that were observed. This is due to a combination of the antecedent pore water pressures and the nature of the bimodal soil properties. High end of summer pore water pressures at the slope surface will lead to lower hydraulic conductivity.

7) In terms of the methodology used, some conclusions can be drawn. By using the weather generator, in conjunction with a numerical model, the user resolves them to a time demanding process. The weather generator is a very powerful tool, but due to its nature at least 200 models must be run for the results to be statistically viable (Section 2.11.4). Therefore, careful consideration is required before deciding to implement it in the way that has been in this chapter.

8) Statistical analysis of the results is vital. As such a large number of models are run, it is almost impossible to identify trends just by analysing the results by eye. A statistical package that can handle large amounts of data and

automatically run the required statistical tests should be used. The software package IBM SPSS that was used in this work is recommended.

9) The findings of this chapter could apply to other similar slopes, located in countries with temperate climates subject to similar levels of climate change as the United Kingdom. Despite this it is still recommended , due to the influence of material properties, to create standalone numerical hydrology models, implementing the methodology described in this chapter, of these slopes.

7.5 Recommendations for further work

The research presented in this thesis has shown that bimodal equations can be used to represent the effects of desiccation cracks on the hydraulic properties of a soil. It has also shown that climate change will effects infrastructure slopes, in terms of the hydrology and stability, although not necessarily negatively. Many facets of this work could be developed further, with potentially very interesting and important results. In this section some suggestions for further work are made.

Further development of the bimodal functions is recommended. This could be achieved in a number of ways. Perhaps the most important is validation. In this research the method has been validated against one set of pore water pressure data. More field measurements of pore water pressures, at numerous sites; similar to those used in this work in conjunction with detailed temporal climate data is vital for this. Numerical hydrology models of these slopes can be created in VADOSE/W or similar software, and the methodology developed in this work used.

The bimodal functions could be improved further with better definition of the parameters, specifically the van Genuchten parameters that in this work have either come from other authors' suggestions or assumed through the sensitivity analyses. The method of estimating crack depth also needs to be validated further, either through field observations or laboratory tests. The effects of hysteresis on soil hydrology should also be more carefully considered. Currently, most models of the

type developed in this thesis do not include such effects but it is clear that they need to be. Appropriate hysteresis models could be extremely complex and further research is required to effectively implement them into numerical models.

It is envisioned that the bimodal soil properties could be improved to the point where the model can automatically apply cracked soil properties within the model domain. This model would require functions for the crack porosity, and the van Genuchten parameters a and n such that the crack properties change with respect to the volumetric water content. The model could also identify the cracked state of the soil i.e. cracked, un-cracked or un-cracked but has previously been cracked. This last state has not been considered in the work in this thesis and is reflected by a value of K_w in the soil that is lower than cracked soil K_w but higher than the un-cracked. It is believed that this soil model could be implemented in VADOSE/W through the means of an 'add-in function', but further study is required to ascertain the best method.

In the work presented in this thesis a rather narrow view of the possible effects of climate change was considered. The intended analysis was to consider the difference between WET-DRY-WET years in the present and future, due to a high emissions scenario, at the location of the Newbury cutting and in the 2050s time slice. It transpired that what was actually analysed was the difference between WET-DRY-WET in the present climate and WET-AVERAGE-WET in the future. Despite this there were many interesting findings that provided further understanding of the effects of climate change on infrastructure slopes in the UK.

Using the methodology developed in this work many more potential analyses of the effects of climate change on infrastructure slopes are possible. These include:-
- Weather generator outputs using the other emissions scenarios (low and medium), and outputs at other time slices.
- Run models with the full 30 years of climate data applied, therefore analysing many more possible seasonal climate variations. Note that this would be exceptionally time demanding, even with a powerful computer.

- If the above suggestion is not possible, due to restrictions in computing power, then follow the method laid out in Appendix C to identify and extract different years for seasonal variability analyses.

- Analyse other slopes, in other areas of the country. The results obtained in this work apply for southern England, but other parts of the country are projected to experience different levels of climate change. It would further the understanding if other slopes were identified and analysed.

- It is believed this method could be applied in other countries, so long as weather generators are available.

The weakness of using GeoStudio VADOSE/W to carry out these analyses is that a strain-softening soil model is not available. To gain a better understanding of the behaviour of the slope and the likely effects of climate change it would be interesting to couple the hydrology model developed with a soil model of this kind.

Appendix A

A.1 VADOSE/W mathematical equations

A.2 Derivation of maximum crack width equation

A.3 Simplified weather generator 2.0 process

A.1 VADOSE/W mathematical equations

Finite element water flow equations

The governing differential equation used in the VADOSE/W finite element formulation is:

$$\frac{\delta}{\delta x}\left(k_x \frac{\delta H}{\delta x}\right) + \frac{\delta}{\delta y}\left(k_y \frac{\delta H}{\delta y}\right) + Q = m_w \gamma_w \frac{\delta(H-y)}{\delta t}$$

Where m_w is the slope of the storage curve. VADOSE/W applies the Galerkin method of weighted residuals to the governing differential equation, the finite element for two-dimensional seepage can be derived as:

$$\tau \int_A ([B]^\tau[C][B])dA\{H\} + \tau \int_A (\lambda < N >^\tau < N >)dA\{H\}, t = q\tau \int_L (< N >^\tau)dL$$

Where:

[B]	=	The gradient matrix
[C]	=	The element hydraulic conductivity matrix
{H}	=	The vector of nodal heads
<N>	=	The vector of interpolating function
q	=	The unit flux across the edge of an element
τ	=	The thickness of an element
t	=	Time
λ	=	Storage term for a transient seepage equal to $m_w \gamma_w$
A	=	A designation for summation over the area of an element
L	=	A designation for summation over the edge of an element

In abbreviated form, the finite element seepage equation can be expressed as:

$$[K]\{H\} + [M]\{H\}, t = \{Q\}$$

Where:

[K]	=	The element characteristic matrix
[M]	=	The element mass matrix
{Q}	=	The element applied flux vector

A.2 Derivation of maximum crack width equation

$$2TL = \gamma_w X_{max} \left(\frac{X_{max}}{2} L - \frac{1}{2} \frac{\pi X_{max}}{4} L \right)$$

$$\frac{2T}{\gamma_w} = X_{max} \left(\frac{X_{max}}{2} - \frac{\pi X_{max}}{8} \right)$$

$$\frac{T}{\gamma_w} = \frac{X_{max}^2}{4} - \frac{\pi X_{max}^2}{16}$$

$$\sqrt{\frac{T}{\gamma_w}} = \sqrt{0.0537 X_{max}^2}$$

$$X_{max} = \frac{\sqrt{\frac{T}{\gamma_w}}}{\sqrt{0.0537}}$$

$$X_{max} = 4.32 \sqrt{\frac{T}{\gamma_w}}$$

A.3 Simplified weather generator 2.0 process

1. Control precipitation series is created from the 1961-1990 baseline observed values.

2. Other weather variables are created from observed relationships and conditioning by rainfall considering four rainfall transitions (DD, WW, DW, WD).

4. The stochastic precipitation model is refitted using perturbed future daily rainfall statistics (by change factors) to create the scenario precipitation series.

3. Change factors at a monthly time-scale are taken from the UKCP09 probabalistic projections.

5. The remaining weather variables for the scenario series are generated, conditioned on the scenario precipitaiton series, and additionally perturbed using the change factors and the observationally based IVRs*.

*Rainfall is taken to be the primary variable, so that depending on whether the day is wet or dry other weather variables are determined by mathematical/statistical relationships with rainfall and values of the variable in question on the previous day. These IVRs maintain both the consistency between and within each of the variables.

Appendix B

B.1 Geometries and meshes for far field boundary sensitivity analyses

B.2 Geometries and meshes for inner slope region mesh density sensitivity analyses

B.3 Minimum and maximum pore water pressure profiles for 2004 and 2005

B.1 Geometries and meshes for far field boundary sensitivity analyses
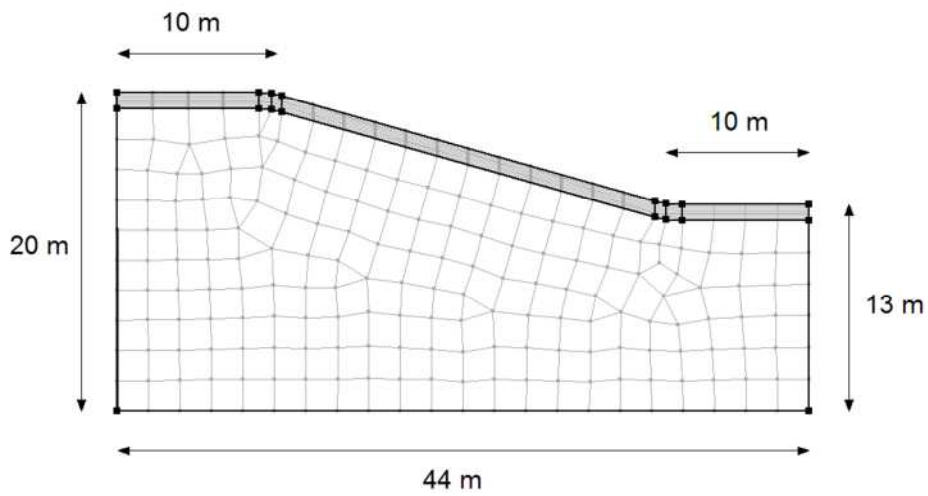
Boundaries @ 10 m - 421 elements, 458 nodes.
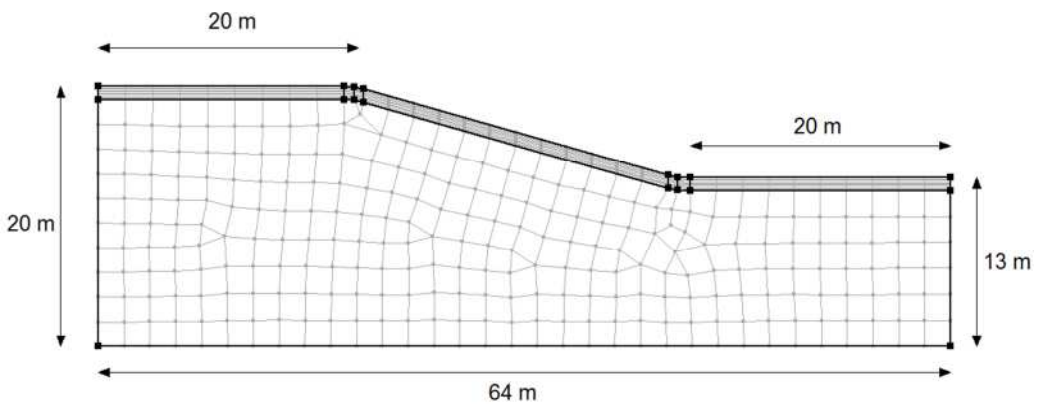
Boundaries @ 20 m - 609 elements, 658 nodes.
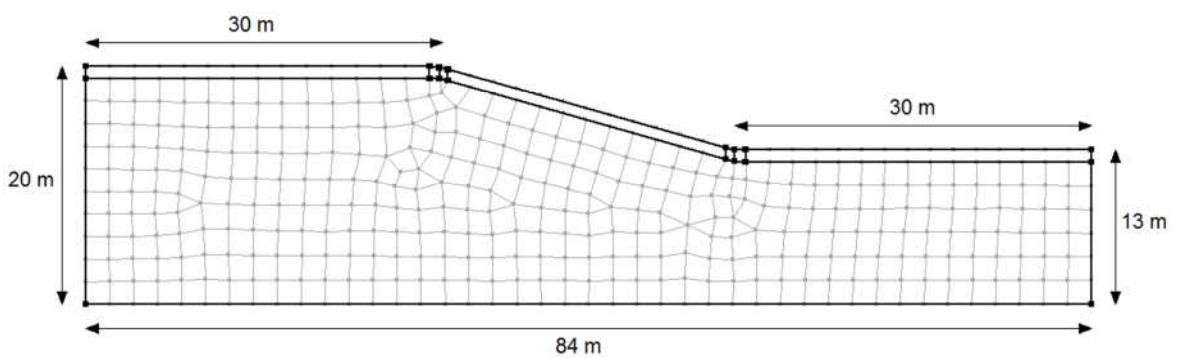
Boundaries @ 30 m - 785 elements, 842 nodes.
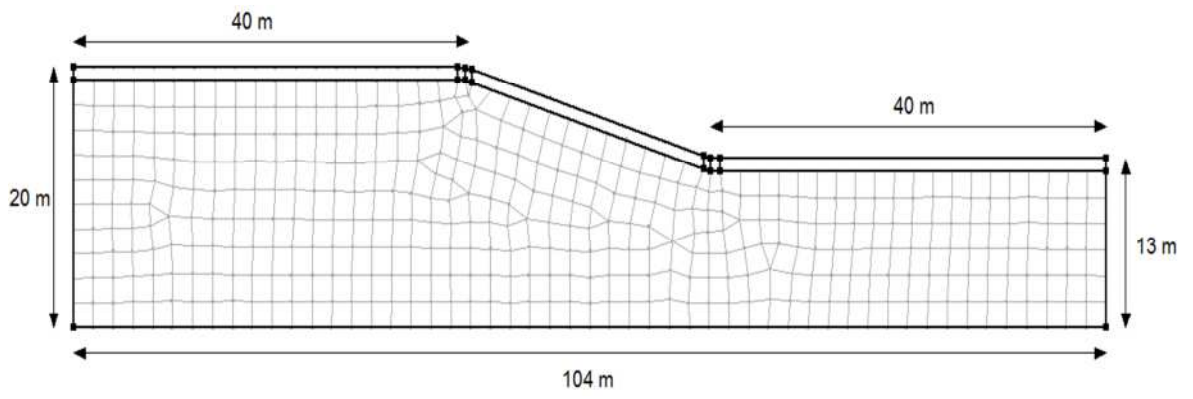
Boundaries @ 40 m - 962 elements, 1029 nodes.
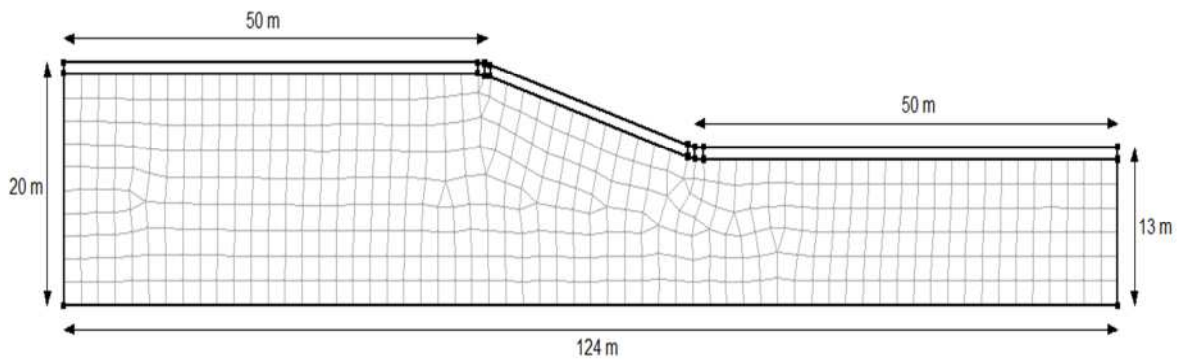
Boundaries @ 50 m - 1132 elements, 1208 nodes.

B.2 Geometries and meshes for inner slope region mesh density sensitivity analyses
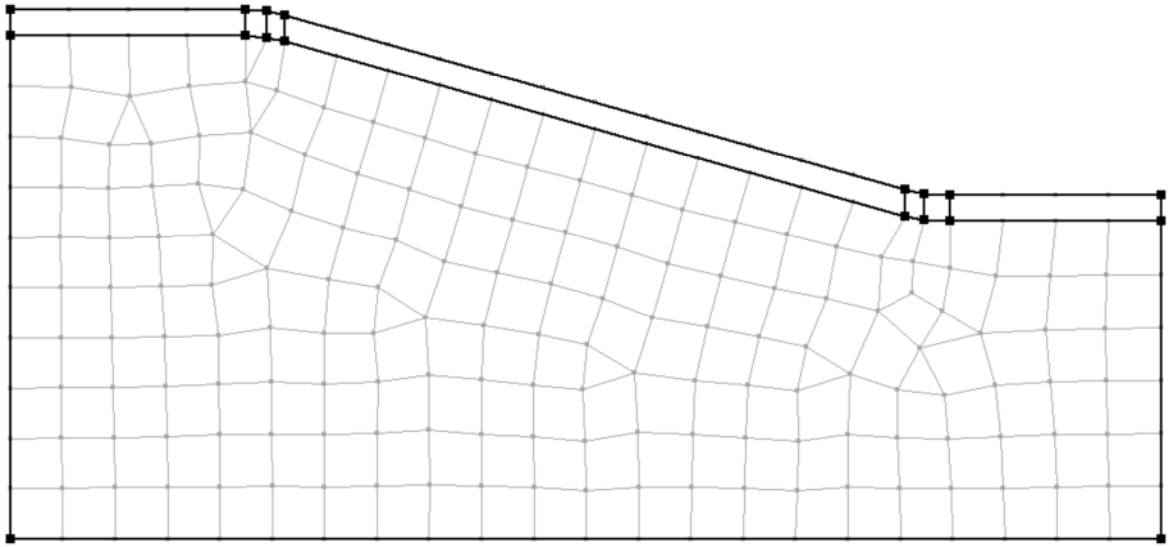
Global element size 2.0 metres - 733 elements, 783 nodes.
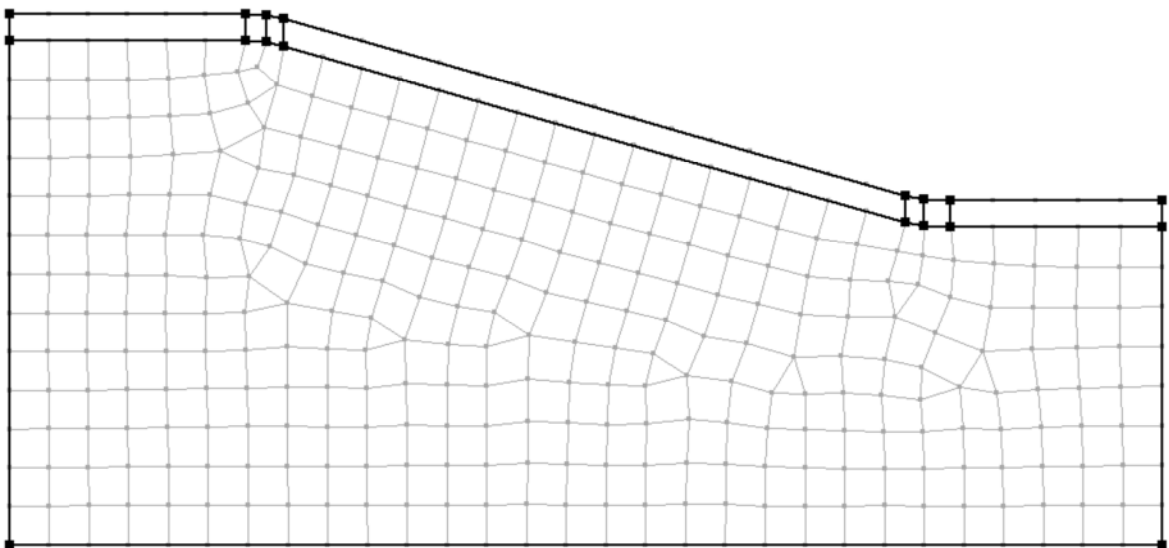
Global element size 1.5 metres - 1023 elements, 1082 nodes.
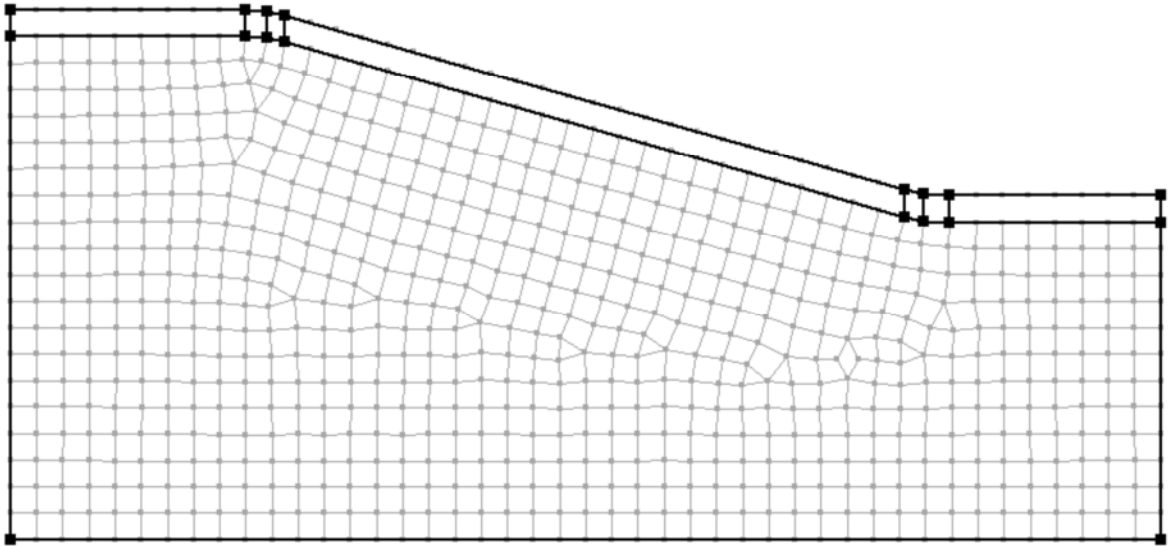
Global element size 1.0 metres - 1719 elements, 1797 nodes.
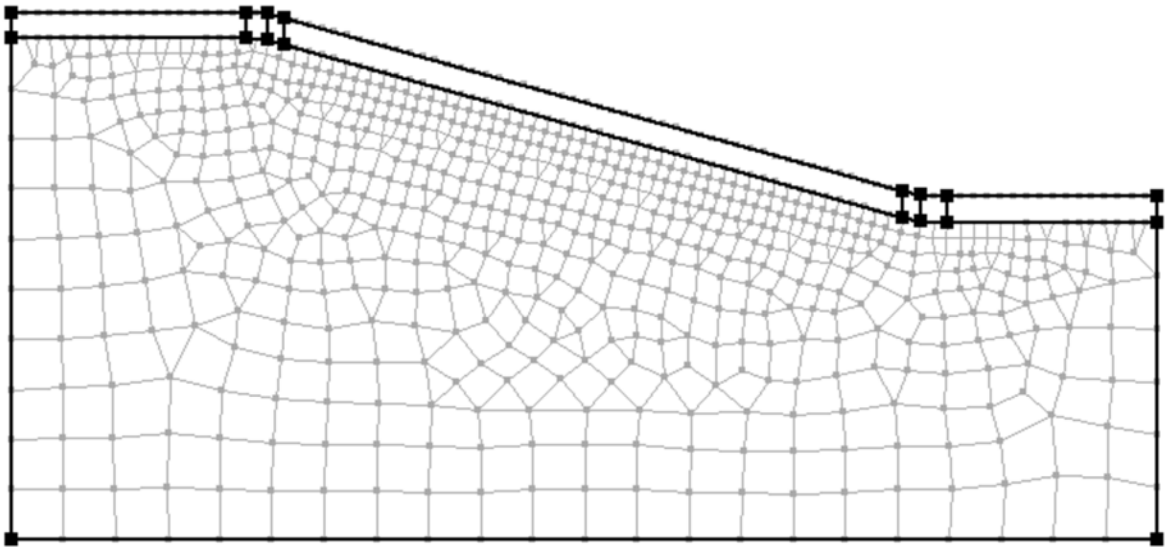
Global element size 0.5 and 2.0 metres - 2706 elements, 2753 nodes.

B.3 Minimum and maximum pore water pressure profiles for 2004 and 2005
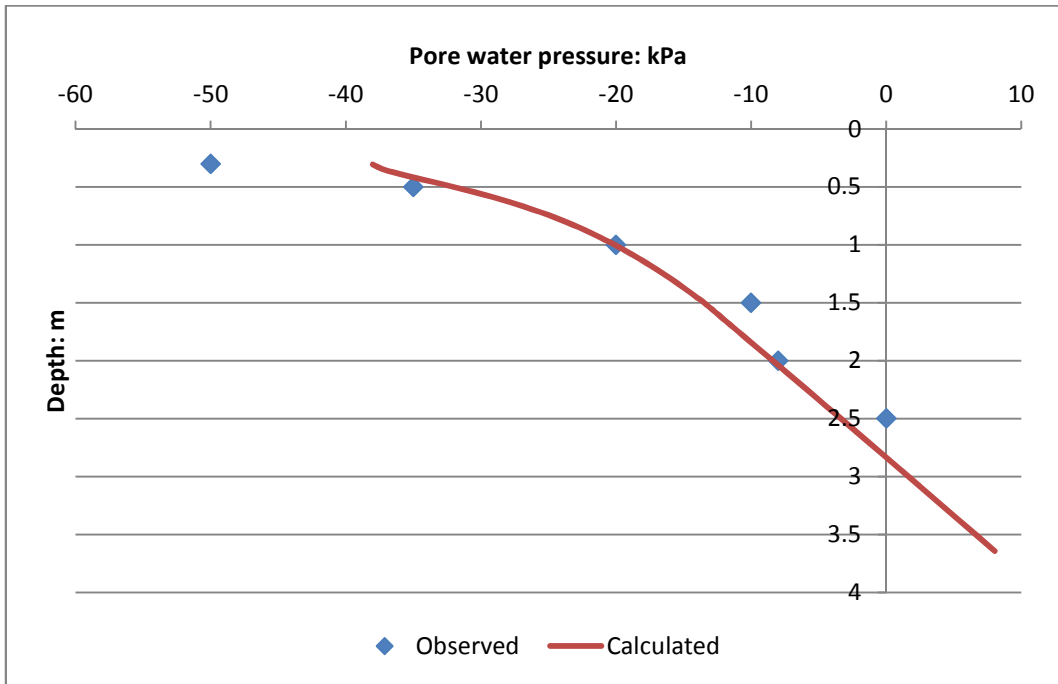
Minimum pore water pressure profiles – 2004
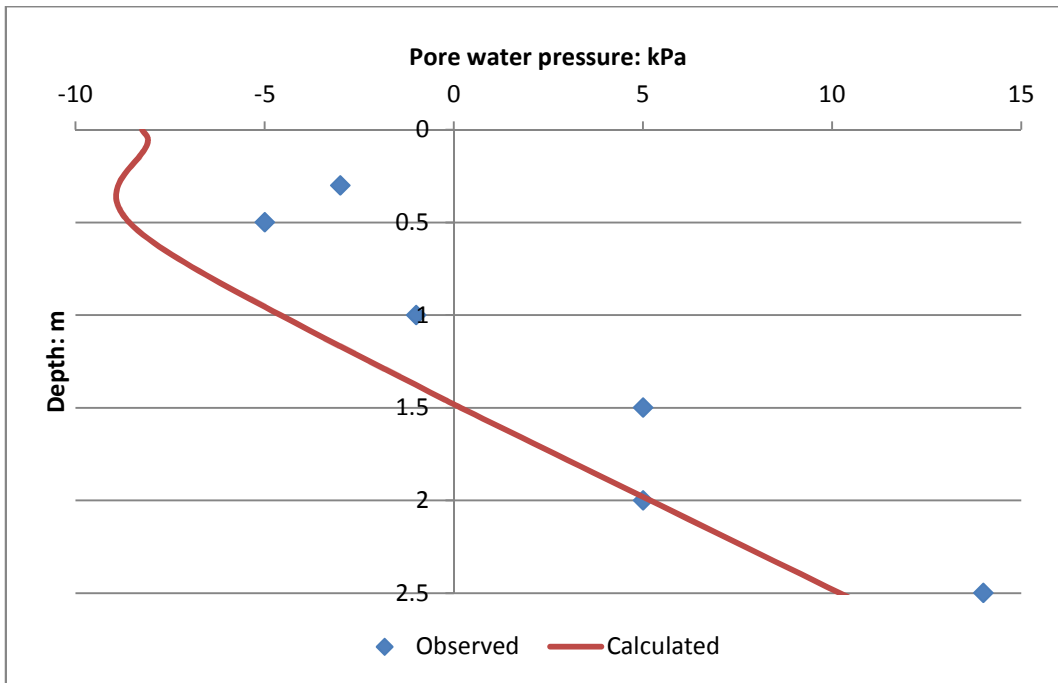
Maximum pore water pressure profiles - 2004
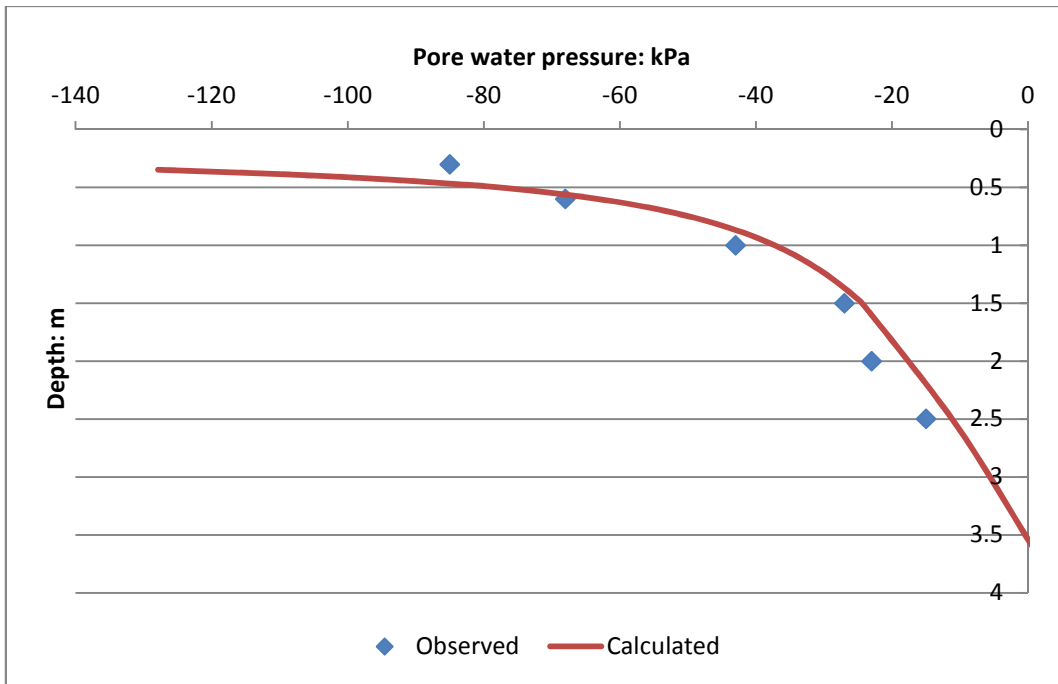
Minimum pore water pressure profiles - 2005
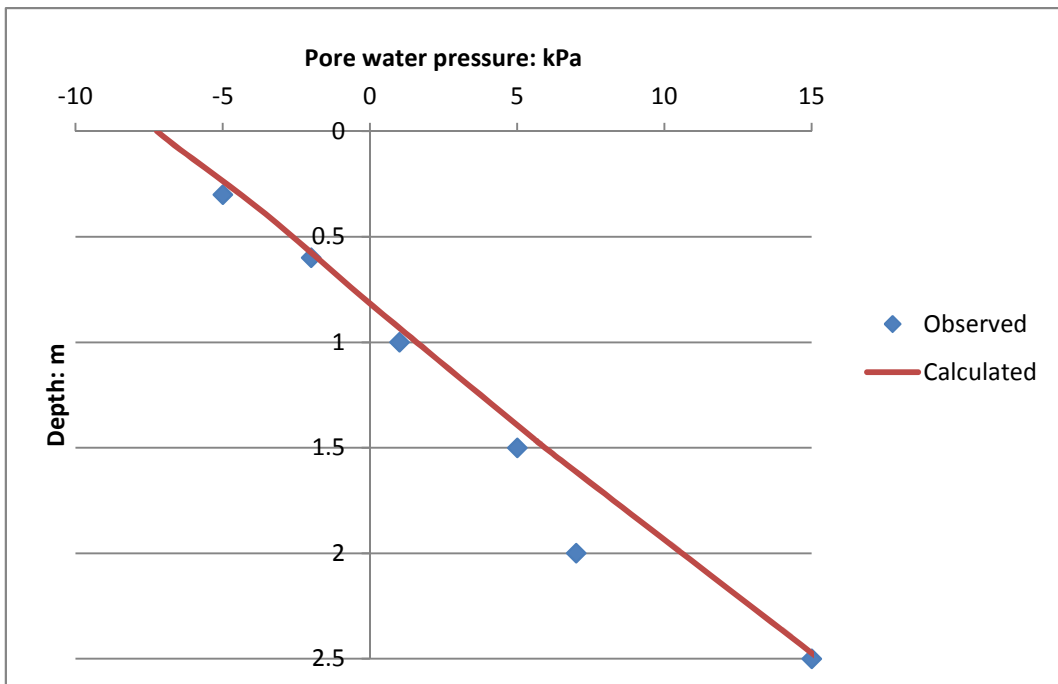
Maximum pore water pressure profiles - 2005

Appendix C

C.1 UKCP09 projections for Newbury bypass cutting location
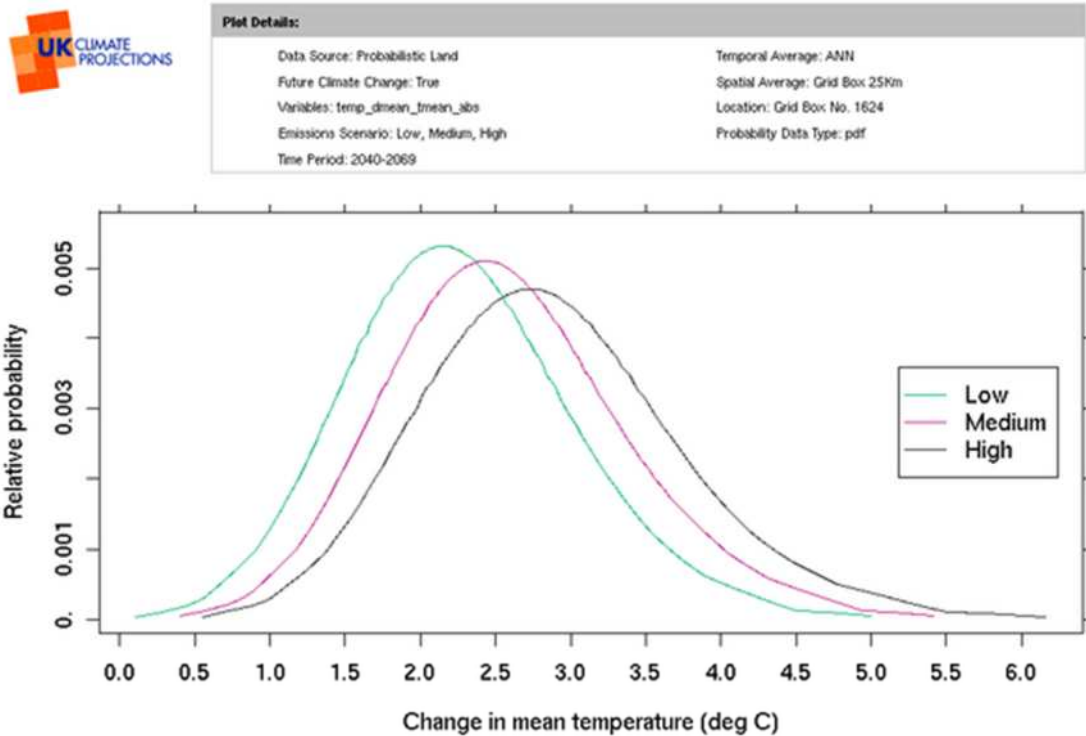
UKCP09 projections for mean annual temperature change by the 2050s at all emissions scenarios.
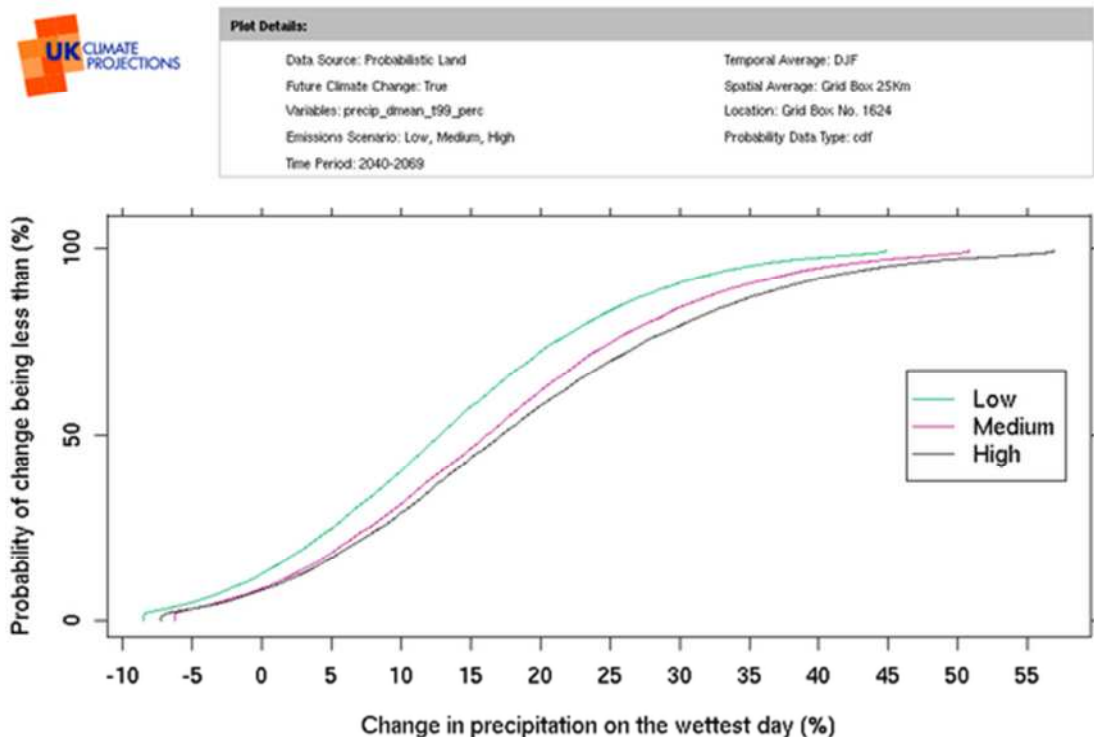
UKCP09 projections for change in precipitation on the wettest day of winter by the 2050s at all emissions scenarios

C.2 End of summer results used in SPSS analyses

Where cntr_0.5m = cntr model suctions at 0.5 m depth (kPa), scen_0.5m = scen model suctions at 0.5 m depth (kPa), cntr_1.0m = cntr model suctions at 1.0 m depth (kPa), scen_1.0m = scen model suctions at 1.0 m depth (kPa), cntr_3.0m = cntr model suctions at 3.0 m depth (kPa), scen_3.0m = scen model suctions at 3.0 m depth (kPa), cntr_evap = cumulative evaporation in cntr models (m³), scen_evap = cumulative evaporation in scen models (m³), cntr_tran = cumulative transpiration in cntr models (m³), scen_tran = cumulative transpiration in scen models (m³), cntr_WT = depth of water table in cntr models (m), scen_WT = depth of water table in scen models (m), cntr_CD = estimated crack depth in cntr models (m), scen_CD = estimated crack depth in scen models.

Model no.	Cntr 0.5m	Scen 0.5m	Cntr 1.0m	Scen 1.0m	Cntr 3.0m	Scen 3.0m	Cntr evap	Cntr tran	Scen evap	Scen tran	Cntr WT	Scen WT	Cntr CD	Scen CD
1	-247	-1083	-91	-115	-9	-11	29.4	21.6	30.2	23.5	4.01	4.1	3	3.82
2	-189	-373	-83	-103	-9	-12	26.7	20	37	24.9	3.89	3.64	3.25	2.56
3	-441	-2000	-114	-138	-12	-13	23.7	18.2	32.1	21.8	4.23	4.27	4	4.15
4	-279	-2000	-96	-142	-10	-12	27.2	21.3	30.5	22.4	4	4.1	3.86	3.68
5	-510	-289	-113	-89	-11	-9	27.7	20.1	28.3	21.7	3.26	2.81	2.88	2.68
6	-221	-830	-90	-113	-10	-12	26.8	18.7	30.7	18.1	4.03	4.24	3.4	4
7	-259	-216	-95	-90	-11	-11	24.6	18.6	28.1	21.6	4.15	4.13	3.98	4.01
8	-164	-448	-79	-103	-9	-11	27.2	20.4	26.2	18.9	3.9	4.12	3.28	3.82
9	-111	-511	-66	-114	-9	-13	29.4	22	32	19.4	3.91	4.3	2.42	4.16
10	-150	-264	-76	-99	-9	-12	26.6	19.9	26.3	20.1	3.9	4.23	2.21	4.1
11	-204	-281	-88	-94	-11	-11	28.4	18.5	28.2	19.7	4.08	4.09	3.51	3.77
12	-161	-481	-79	-105	-8	-11	29	22	26.8	19	3.85	4.14	3.46	3.96
13	-238	-1647	-93	-109	-11	-12	24.3	17.9	26.8	18.1	4.11	4.21	3.85	3.92
14	-133	-467	-60	-108	-7	-12	30	21.5	23	16.3	3.73	4.23	1.65	3.69
15	-250	-257	-97	-95	-12	-11	24.4	18.6	30.3	22.2	4.16	4.09	3.7	3.93
16	-219	-58	-90	-37	-10	-1	25.2	20.1	34.8	22.3	4.05	3.07	2.65	1.55

17	-229	-179	-92	-78	-11	-8	25.1	18.4	30.2	24.3	4.08	3.8	3.67	3.64
18	-217	-377	-88	-108	-10	-12	23.5	18.1	24.8	17.8	4.04	4.25	3.47	4.07
19	-193	-272	-84	-92	-9	-10	26.2	19.1	30.3	21.4	3.95	4.01	3.56	3.29
20	-165	-585	-78	-108	-9	-11	24.3	18.5	26.2	19.2	3.88	4.15	3.03	4
21	-205	-222	-86	-87	-10	-10	24.3	19.7	32	21.9	3.77	2.9	3.77	2.9
22	-205	-213	-83	-99	-10	-11	24.8	19	26.1	18.4	3.9	4.05	2.04	2.14
23	-271	-493	-97	-108	-11	-12	26.4	17.8	33.1	20.5	4.13	4.18	3.16	3.96
24	-168	-227	-79	-86	-9	-9	28	19.7	31.7	23.6	3.9	3.92	2.94	2.29
25	-187	-154	-83	-74	-10	-9	24	19.4	26.9	21.2	4.01	3.92	3.52	1.68
26	-222	-516	-93	-110	-11	-13	21.9	16.6	26	17.5	4.13	4.26	3.72	3.64
27	-190	-171	-83	-71	-9	-9	25.5	20.2	31	22.3	3.91	3.54	3.72	0.83
28	-173	-130	-79	-64	-9	-6	26.9	20	32.5	24.3	3.87	3.6	3.64	3.43
29	-219	-333	-90	-100	-10	-11	26.9	19.5	27.3	20.2	4.04	4.12	3.75	3.73
30	-222	-373	-89	-101	-10	-11	25.6	18.7	28.6	20.3	4.03	4.11	3.86	4
31	-292	-53	-95	-35	-11	-2	23.3	18	35.7	23.8	4.06	3.19	2.08	1.31
32	-240	-239	-92	-91	-11	-10	22.6	18.7	29.9	20	4.08	4.02	3.74	3.81
33	-242	-287	-94	-92	-11	-10	21.7	16.5	27.1	20.3	4.09	3.99	3.89	3.33
34	-221	-237	-89	-89	-10	-9	25.5	18.6	30.9	22.8	4.05	3.88	2.48	2.23
35	-185	-323	-83	-103	-9	-12	18.4	18.2	25.8	18.1	3.96	4.19	3.02	3.96
36	-192	-161	-84	-67	-9	-7	23.1	18.3	30.9	23.5	3.96	3.69	3.76	1.39
37	-334	-188	-103	-81	-12	-9	23.6	17	33.8	23.5	4.21	3.91	2.88	2.04
38	-160	-367	-78	-98	-9	-11	28.6	20.5	28.6	20.7	3.95	4.15	3.44	3.76
39	-167	-261	-79	-92	-8	-10	24.3	19.4	30.7	23	3.87	3.99	3.24	3.82
40	-180	-218	-78	-84	-10	-9	27	19.3	30	22.9	4.02	3.89	3.22	3.5
41	-228	-418	-91	-106	-10	-12	25	18.3	31	20.1	4.05	4.19	3.74	4.13
42	-164	-321	-78	-101	-9	-11	27.7	20.2	29	19.8	3.89	4.15	2.31	3.53
43	-270	-194	-94	-80	-11	-9	24.1	18.4	32	23.1	4.08	3.9	3.45	2.01
44	-153	-161	-77	-78	-9	-9	26.1	19.7	36.2	26.3	3.95	3.87	2.9	3.16
45	-254	-76	-96	-43	-11	-5	23.4	18	31.6	22.3	4.11	3.52	3.59	1.79
46	-153	-211	-76	-81	-9	-9	24.9	19.8	31.2	22.7	3.9	3.84	3.52	3.5
47	-178	-289	-81	-94	-9	-10	25.3	21.4	33.1	22.6	3.95	4.04	3.66	3.66
48	-197	-254	-84	-89	-9	-9	24.9	19	26.8	20.2	3.93	3.96	3.7	2.35

354

49	-313	-348	-104	-100	-12	-11	21.9	16.5	29.9	21	4.23	4.12	4.1	4
50	-192	-442	-82	-100	-9	-11	25.5	19.4	29.4	21.7	3.98	4.08	3.54	3.66
51	-177	-500	-82	-110	-9	-13	28.4	20.6	29.6	18.6	3.93	4.26	2.94	3.84
52	-258	-261	-94	-90	-11	-9	23.5	17.7	32.4	25	4.09	3.96	2.91	3.84
53	-206	-152	-86	-72	-10	-8	25.9	19.3	32.8	22.5	4	3.72	3.67	2.81
54	-197	-209	-83	-85	-9	-9	25.7	19.8	28.7	20.7	3.92	3.96	3.47	3.73
55	-76	-385	-47	-101	-6	-11	30.6	22.2	24	17.9	3.57	4.12	1.89	3.69
56	-240	-147	-92	-71	-10	-7	22.9	18.1	36.1	25.5	4.05	3.72	2.49	2.34
57	-243	-167	-93	-74	-11	-7	26.2	18.6	34.9	24.9	4.08	3.73	3.69	2.4
58	-168	-343	-79	-94	-9	-10	26.5	20.2	28.2	21.3	3.93	3.99	3.43	3.88
59	-176	-446	-80	-107	-9	-12	27.6	20.6	26.7	17.1	3.91	4.2	2.09	3.52
60	-225	-77	-94	-45	-11	-2	24.2	18.6	35.1	23.6	4.12	2.13	3.36	0.77
61	-222	-408	-90	-100	-10	-11	26.8	19.8	25.7	20.1	4.05	4.08	3.27	3.7
62	-251	-302	-93	-97	-11	-11	22.4	17.5	28.5	20.8	4.03	4.1	2.85	3.66
63	-220	-178	-89	-75	-10	-7	26.7	19	35.9	25.1	4.02	3.71	3.53	3.61
64	-203	-212	-84	-88	-9	-10	26	18.7	26.8	20.4	3.92	3.98	3.51	3.62
65	-178	-436	-81	-107	-9	-12	28.6	20.3	30.8	19.3	3.94	4.23	3.08	3.16
66	-200	-194	-88	-82	-10	-9	26.7	18.6	32.2	24.1	4.03	3.88	3.23	2.85
67	-224	-133	-91	-70	-10	-8	25	18.9	33.8	25.9	4.05	3.78	3.5	3.5
68	-174	-182	-86	-78	-11	-8	27.7	21.5	30.7	23.9	4.14	3.84	2.78	3.54
69	-156	-288	-76	-99	-8	-11	28.3	21	24	22.9	3.8	4.14	3.15	3.91
70	-278	-308	-99	-97	-12	-11	26.3	19.2	28.2	20.2	4.19	4.06	3.99	3.93
71	-143	-517	-72	-109	-9	-12	27.7	20.5	25.9	17.8	3.89	4.21	3.13	4.07
72	-142	-372	-72	-101	-8	-11	27.7	20	25	19	3.83	4.1	3.59	4
73	-172	-207	-79	-81	-9	-8	26.5	19.3	33.2	24.4	3.85	3.86	3.24	1.99
74	-190	-254	-83	-90	-9	-9	25.6	20.1	33.5	22.9	3.95	3.96	3.12	3.82
75	-196	-453	-88	-105	-11	-11	26.8	19.2	32.1	20.4	4.1	4.15	3.58	3.87
76	-240	-187	-93	-83	-11	-9	24.1	18.1	29.2	22.4	4.09	3.96	2.98	3.66
77	-286	-313	-95	-95	-11	-10	24	18.2	28.8	21.8	4.08	4.04	3.91	3.77
78	-167	-237	-79	-91	-9	-10	25.9	19.4	26.9	20.3	3.87	4.03	1.98	3.86
79	-160	-652	-79	-112	-9	-12	25.3	19.6	32.3	19.1	3.95	4.24	3.01	4.05
80	-155	-302	-75	-94	-8	-10	25.1	19.4	29.6	24	3.81	4.02	3.34	3.91

81	-187	-74	-81	-45	-10	-7	27.2	21.3	34	23.2	3.92	3.59	1.95	2.76
82	-168	-4273	-83	-107	-10	-11	27.3	20.8	26.2	19.3	3.99	4.1	2.83	4
83	-175	-431	-80	-106	-9	-12	25	19.8	25.9	17.8	3.89	4.17	3.64	3.42
84	-176	-243	-81	-94	-9	-11	25.2	19.4	26.4	21.2	3.91	4.11	2.96	3.88
85	-168	-268	-76	-96	-9	-11	27	20.3	31.5	22	3.9	4.09	2.08	2.71
86	-244	-65	-92	-43	-11	-4	23.6	19.1	37.9	25	4.07	3.32	3.75	1.67
87	-138	-300	-73	-95	-9	-12	27.6	21.1	27.3	19.4	3.9	3.98	1.99	2.3
88	-213	-236	-83	-92	-10	-11	26.5	20.7	27.7	21	4.02	4.08	3.64	3.89
89	-154	-204	-78	-82	-9	-9	27.9	20.6	28.6	20.8	3.91	3.93	3.43	2.15
90	-251	-222	-93	-86	-11	-9	26.9	18.4	33.3	23.9	4.09	3.94	3.16	2.96
91	-156	-369	-79	-105	-10	-12	28.3	20.3	27.7	18.7	3.98	4.23	3.42	2.42
92	-240	-287	-91	-92	-10	-10	24.5	18.4	31.7	21.7	4.04	3.93	3.64	3.43
93	-242	-559	-93	-99	-11	-11	25.5	17.8	33.3	23.6	4.01	4.1	3.3	1.91
94	-207	-256	-87	-91	-10	-10	26.9	18.1	27.1	20.6	4.02	3.98	2.1	3.77
95	-224	-315	-91	-96	-10	-11	25.4	17.4	28	19.7	4.06	4.06	2.66	3.96
96	-229	-359	-90	-95	-10	-11	26.3	19.1	29.1	19.8	4.03	4.07	3.74	2.11
97	-112	-437	-64	-109	-9	-13	28.9	22	23.7	16.1	3.89	4.26	3.32	2.91
98	-267	-291	-97	-92	-11	-10	24.8	18.6	29.5	21.7	4.12	4	2.62	3.56
99	-194	-198	-86	-80	-10	-8	25.1	19.9	28.5	21.5	4	3.79	3.83	3.55
100	-251	-246	-95	-84	-11	-9	23.7	17.9	29.1	21.5	4.13	3.81	3.39	2.22

C.3 End of year results used in SPSS analyses

Where cntr_0.5m = cntr model suctions at 0.5 m depth (kPa), scen_0.5m = scen model suctions at 0.5 m depth (kPa), cntr_1.0m = cntr model suctions at 1.0 m depth (kPa), scen_1.0m = scen model suctions at 1.0 m depth (kPa), cntr_3.0m = cntr model suctions at 3.0 m depth (kPa), scen_3.0m = scen model suctions at 3.0 m depth (kPa), cntr_diss = suctions dissipated in cntr model, scen_diss = suctions dissipated in scen model, cntr_SC3.0m = cntr models pore water pressure cycle at 3.0 m depth (kPa), scen_SC3.0m = scen models pore water pressure cycle at 3.0 m depth (kPa), cntr_MinFOS = minimum factor of safety in cntr models, scen_MinFOS = minimum factor of safety in scen models.

Model no.	Cntr 0.5m	Scen 0.5m	Cntr 1.0m	Scen 1.0m	Cntr 3.0m	Scen 3.0m	Cntr Diss	Scen Diss	Cntr SC3.0m	Scen SC3.0m	Cntr MinFOS	Scen MinFOS
1	-110	-171	-48.5	-57	-12	-15	No	No	-3	-4	2.064	2.285
2	-1	0.4	-0.7	0.2	7	19	Yes	Yes	16	31	1.883	1.423
3	0.6	-254	-3.5	-62	0	-18	Yes	No	12	-5	2.06	2.196
4	-122	0	-52	0	-10.5	11	No	Yes	-1	23	2.064	1.581
5	-153	-115	-52	-51	-8	-14	No	No	3	-5	2.07	2.126
6	-58	-154	-48	-58	-8.5	-20	No	No	1	-8	2.006	2.383
7	0	0	-0.5	-0.6	4	3	Yes	Yes	15	14	1.842	1.952
8	-4	-120	-4.5	-54	1.6	-18	Yes	No	11	-7	1.896	2.226
9	-0.6	-170	0	-59	11	-17	Yes	No	20	-4	1.548	2.257
10	-0.8	-130	0	-55	15	-17	Yes	No	24	-5	1.499	2.194
11	1	-0.6	1.4	0.2	6	4	Yes	Yes	17	15	1.935	1.778
12	-0.2	-134	-10	-55	0.1	-18	No	No	8	-7	1.917	2.235
13	-0.8	-0.5	-3.5	-2	3	14	Yes	Yes	14	26	1.868	1.758
14	-0.8	-0.8	-0.4	-0.2	16	15	Yes	Yes	23	27	1.432	1.515
15	-58	-154	-48	-58	-8.5	-20	No	No	14	10	1.77	1.843
16	-0.9	-0.7	-0.5	2	16	20	Yes	Yes	26	21	1.465	1.423
17	-0.7	-92	0	-47	10	-14	Yes	No	21	-6	1.846	2.031

18	-0.9	-141	-1	-57	15	-20	Yes	No	25	-8	1.698	2.357
19	-0.9	0	0	-0.7	12	15	Yes	Yes	21	25	1.882	1.504
20	-0.9	-141	-1.6	-56	14	-19	Yes	No	23	-8	1.515	2.279
21	-97	-0.3	-49	-2.6	-14	6	No	Yes	-4	16	2.095	1.611
22	-0.8	-101	1.6	-52	22	-13	Yes	No	32	-2	1.199	2.07
23	-0.8	-144	-0.4	-57	17	-20	Yes	No	28	-8	1.39	2.358
24	-0.1	-1	-1.6	-1.2	11	14	Yes	Yes	20	23	1.454	1.502
25	-2.1	-0.8	-1.7	-2	3	15	Yes	Yes	13	24	1.905	1.601
26	-105	-0.7	-47	-2	-8.7	3	No	Yes	2	16	2.021	1.695
27	-24	-0.7	-45	2.1	-12	21	No	Yes	-3	30	2.047	1.399
28	-71	-78	-46	-43	-10	-13	No	No	-1	-7	2.012	2.105
29	-2.1	-0.6	-0.8	-0.3	7	5.7	Yes	Yes	17	17	1.918	1.804
30	-0.6	-131	-0.1	-55	7.2	-19	Yes	No	17	-8	1.815	2.272
31	-0.7	-0.8	-1.2	2.2	16	22	Yes	Yes	27	24	1.454	1.363
32	-110	-109	-51	-51	-11	-14	No	No	0	-4	2.05	2.086
33	-5	-0.8	-3.7	0.8	-17	17	No	Yes	-6	27	2.077	1.481
34	-0.7	-0.5	1.9	0.5	20	11	Yes	Yes	30	20	1.284	1.72
35	-1	-127	-0.8	-52	17	-1	Yes	No	26	11	1.446	1.98
36	-98	-0.4	-44	0	-9	18	No	Yes	0	25	2.013	1.384
37	-0.6	-0.9	-0.8	-0.7	14	15	Yes	Yes	26	24	1.572	1.477
38	-0.5	0.7	-1.8	5	-3	-14	Yes	Yes	6	-3	1.947	1.953
39	-0.9	-110	-1	-51	5	-15	Yes	No	13	-5	1.813	2.123
40	-1.5	-101	-1.9	-48	10	-12	Yes	No	20	-3	1.543	2.068
41	-107	-140	-48	-56	-5	-20	No	No	5	-8	1.88	2.288
42	-0.8	-1	-0.5	-0.8	14	10	Yes	Yes	23	21	1.503	1.591
43	-0.6	-3.7	-2	-2.3	8	4	Yes	Yes	19	13	1.734	1.793
44	-0.8	-0.9	1.6	-0.3	4	6	Yes	Yes	13	15	1.779	1.837
45	-110	-0.9	-48	-1	-3.3	16	No	Yes	6	26	1.979	1.715
46	-0.2	-93	-9.4	-48	-4.5	-13	No	No	4	-4	1.963	2.04
47	-12	-115	-39	-52	-5	-13	No	No	4	-3	1.96	2.075
48	-98	-1.2	-47	0.5	-11	13	No	Yes	-2	22	2.033	1.454
49	-133	-128	-56	-55	-19	-19	No	No	-7	-8	2.171	2.33

50	-100	-0.8	-48	0.6	-14	14	No	Yes	-5	25	2.09	1.549
51	-0.9	-143	-0.7	-55	17	-15	Yes	No	26	-2	1.435	2.162
52	-0.9	-107	-1.2	-50	14	0	Yes	No	25	9	1.491	1.944
53	-111	-0.7	-48	-1	-12.5	18	No	Yes	-3	26	2.078	1.456
54	-1.2	-105	-1.7	-49	8	-12	Yes	No	17	-3	1.898	2.049
55	-0.8	-0.5	0	0	17	7	Yes	Yes	23	18	1.452	1.697
56	-0.1	0.2	-0.4	-2.5	18	15	Yes	Yes	28	22	1.305	1.493
57	-113	-0.6	-51	-1.3	-13	17	No	Yes	-2	24	2.068	1.476
58	-91	-117	-45	-53	-6.6	-18	No	No	2	-8	1.98	2.196
59	0.3	-0.8	-1.3	-1.5	14	17	Yes	Yes	23	29	1.507	1.479
60	-0.3	0.9	0.4	5.4	14	24	Yes	Yes	25	26	1.455	1.348
61	-1.5	-0.8	-3.6	0.5	0.8	16	Yes	Yes	11	27	1.938	1.48
62	-0.8	-0.7	-0.4	-0.6	16	10	Yes	Yes	27	21	1.409	1.763
63	-12	-89	-12	-46	-1.3	-14	No	No	9	-7	1.944	2.108
64	-1	-1.7	-0.8	-6.5	10	-0.8	Yes	Yes	19	9	1.861	1.94
65	-11	-0.9	-10	-0.2	-1.7	18	No	Yes	7	30	1.933	1.449
66	-1.7	-1.1	0	-1.6	2.2	15	Yes	Yes	12	24	1.769	1.512
67	-0.9	-78	-1.4	-41	6	-4	Yes	No	16	4	1.66	1.919
68	-0.8	-94	-2.7	-46	10	-13	Yes	No	21	-5	1.794	2.092
69	-2.8	-124	-0.9	-50	15	-1.7	Yes	No	23	9	1.432	1.973
70	-123	-123	-54	-54	-14	-19	No	No	-2	-8	2.091	2.316
71	-0.8	-145	-1.2	-57	13	-20	Yes	No	22	-8	1.672	2.361
72	-0.8	-132	-1.8	-55	2.3	-19	Yes	No	10	-8	1.839	2.334
73	-0.7	-0.8	-0.5	-1	15	18	Yes	Yes	24	26	1.493	1.432
74	-0.8	-106	-0.7	-48	17	-12	Yes	No	26	-3	1.467	2.069
75	-0.4	-133	-0.5	-54	6.6	-17	Yes	No	18	-6	1.614	2.23
76	-0.1	-94	-1.6	-46	15	-12	Yes	No	26	-3	1.485	2.067
77	-50	-115	-54	-49	-18	-7	No	No	-7	3	2.179	2.01
78	0.2	-110	1.4	-52	20	-17	Yes	No	29	-7	1.41	2.148
79	-0.9	-156	-2	-57	7	-19	Yes	No	16	-7	1.689	1.996
80	-29	-116	-33	-53	-11	-18	No	No	-3	-8	2.056	2.31
81	-0.7	-0.8	-0.3	-1.3	18	16	Yes	Yes	28	23	1.44	1.465

82	-0.8	-139	-0.6	-56	15	-19	Yes	No	25	-8	1.49	2.317
83	-94	-0.8	-48	1	-14	20	No	Yes	-5	32	2.097	1.425
84	-2.6	-115	-2.5	-52	5	-14	Yes	No	14	-3	1.734	2.075
85	-0.9	-0.9	-0.2	-1.4	17	15	Yes	Yes	26	26	1.443	1.482
86	-93	2	-51	7	-14	27	No	Yes	-3	31	2.104	1.023
87	-0.8	2.5	-0.3	7	12	25	Yes	Yes	21	37	1.724	1.399
88	-10	-114	-44	-53	-8	-17	No	No	2	-6	1.925	2.203
89	-6	0.9	-23	5.5	-1.2	19	No	Yes	8	28	1.926	1.383
90	-0.8	-0.8	-0.5	-0.4	13	14	Yes	Yes	24	23	1.694	1.693
91	-4	-0.7	-8	-1.5	-0.4	16	No	Yes	10	28	1.936	1.471
92	-3	-1	-0.5	-1.3	-1.5	16	No	Yes	8	26	1.866	1.464
93	-0.8	-0.9	-0.6	-1.4	15	15	Yes	Yes	26	26	1.546	1.485
94	-0.8	-111	0.6	-51	17	-16	Yes	No	27	-6	1.434	2.141
95	0.8	-121	-0.1	-54	15	-19	Yes	No	25	-8	1.492	2.282
96	-1	-0.8	-5	0.8	3	20	Yes	Yes	13	31	1.94	1.411
97	-0.8	-0.8	-0.2	0.1	7	9	Yes	Yes	16	22	1.865	1.765
98	-0.3	0	-1.5	-1.2	15	17	Yes	Yes	26	27	1.495	1.454
99	-106	-96	-50	-46	-15	-13	No	No	-5	-5	2.11	2.06
100	-9	-0.7	-17	-0.4	-0.9	17	No	Yes	10	26	1.962	1.448

C.4 Summary of SPSS analysis results

Variable tested	Cntr mean	Scen mean	Parametric Data	Test used	Significance, p	Effect size
End of summer evaporation	25.79 m³	29.80 m³	Yes	Dependent means t-test	0.000	0.70
End of summer transpiration	19.34 m³	21.32 m³	Yes	Dependent means t-test	0.000	0.58
Max summer suctions at 0.5 m depth	209 kPa	352 kPa	No	Wilcoxon signed ranks test	0.000	-0.38
Max summer suctions at 1.0 m depth	85.7 kPa	91.4 kPa	No	Wilcoxon signed ranks test	0.001	-0.23
Max summer suctions at 3.0 m depth	9.8 kPa	9.9 kPa	No	Wilcoxon signed ranks test	0.237	-0.08
Depth of water table	3.98 m	3.95 m	No	Wilcoxon signed ranks test	0.970	0.00
Maximum crack depth	3.21 m	3.25 m	No	Wilcoxon signed ranks test	0.274	-0.08
Dissipation of suctions	N/A	N/A	N/A	Chi-square test	0.115	0.122
Pore water pressure cycle at 3.0 m	13.8 kPa	10.2 kPa	No	Wilcoxon signed ranks test	0.043	-0.14
Minimum factor of safety	1.770	1.843	No	Wilcoxon signed ranks test	0.076	-0.13

Where $p < 0.05$ represents a statistically significant finding.

C.5 Identifying and extracting years from the weather generator output

1. Using the UKCP09 Weather Generator 2.0 create series of control and scenario weather data for the desired location, emissions scenario and time slice.

2. Modify each output series such that it can be applied as a VADOSE/W climate boundary condition. Extract the variables maximum temperature, minimum temperature, relative humidity, precipitation and potential evapotranspiration.

3. Calculate the monthly precipitation for all years of each control output. Using conditional formatting compare these values to the LTA. Select the year from the output that is the closest match to the desired seasonal variance.

4. Repeat step 3 but for all scenario outputs. Once this has been complete at least 200 years of desired seasonal variance should have been identified.

5. Each year can now be applied to VADOSE/W by calculating the start day, which is the cumulative number of days up till the start of the desired year. This day becomes the first time-step of the model run.

References

ABBASZADEH, M.M., HOUSTON, S.L., ZAPATA, C., HOUSTON, W. and WELFERT, B., 2010. Laboratory determination of soil-water characteristic curves for cracked soil, E.E. ALONSO and A. GENS, eds. In: *Proceedings of the fifth international conference on unsatuarted soils* 2010, Taylor & Francis Group, pp. 409-415.

ADU-WUSU, C., YANFUL, E.K., LANTEIGNE, L. and O'KANE, M., 2007. Prediction of water balance of two soil cover systems. *Geotechnical and Geological Engineering,* **25**(2), pp. 215-237.

ALBRECHT, B.A. and BENSON, C.H., 2001. Effect of desiccation on compacted natural clays. *Journal of Geotechnical and Geoenvironmental Engineering,* **127**(1), pp. 67-75.

ANDERSON, M.G. and KNEALE, P.E., 1980. Pore water pressure and stability conditions on a motorway embankment. *Earth Surface Processes,* **5**(1), pp. 37-46.

ANDERSON, M.G., HUBBARD, M.G. and KNEALE, P.E., 1982. The influence of shrinkage cracks on pore-water pressures within a clay embankment. *Quarterly Journal of Engineering Geology and Hydrogeology,* **15**(1), pp. 9-14.

ARNOLD, J.G., POTTER, K.N., KING, K.W. and ALLEN, P.M., 2005. Estimation of soil cracking and the effect on surface runoff in a Texas Blackland Prairie watershed. *Hydrological Processes*, **19**, pp. 598-603.

ARRHENIUS, S., 1896. On the influence of carbonic acid in the air upon temperature on the ground. *Philosophical Magazine Series 6,* **41**(251), pp. 237-276.

ATKINSON, J.H., 2007. Peak strength of overconsolidated clays. *Geotechnique,* **57**(2), pp. 127-135.

BLIGHT, G.E., 2003. The vadose zone soil-water balance and transpiration rates of vegetation. *Geotechnique,* **53**(1), pp. 55-64.

BRACEGIRDLE, A., MENKITI, C.O. and CLARK, A.R., 2007. Climate change impacts on landslide mechanisms and hazard in southern UK, R. MCINNES, J. JAKEWAYS, H. FAIRBANK and E. MATHIE, eds. In:*International Conference on Landslides and Climate Change*, 21-24 May 2007, Taylor & Francis, pp. 259-268.

BRICENO, S., BASABE, P. and BONNARD, C., 2007. Landslides and climate change: A world perspective, but a complex question, R. MCINNES, J. JAKEWAYS, H. FAIRBANK and E. MATHIE, eds. In:*Proceedings of the Internationsla Conference on Landslides and Climate Change, Ventor, Isle of Wight*, 21-24 May 2007 2007, pp. 3-6.

BRIGGS, D. and COURTNEY, F., 1985. *Agriculture and Environment the Physical Geography of Temperate Agricultural Systems.* London: Longman.

BRIGGS, K.M., 2010. Charing embankment: climate change impacts on embankment hydrology. *Ground Engineering,* June 2010, pp. 28-31.

BRIGGS, K.M., 2011. *Impacts of climate and vegetation on railway embankment hydrology*, University of Southampton.

BRITISH GEOLOGICAL SURVEY, 2011-last update, Shrink-swell hazard potential mapping [Homepage of Natural Environment Research Council], [Online]. Available:http://www.bgs.ac.uk/science/landUseAndDevelopment/shallow_geohazards/hazardPotentialMapping.html [17/11, 2011].

BRITISH GEOLOGICAL SURVEY, 2011-last update, What is subsidence? [Homepage of Natural Environment Research Council], [Online]. Available: http://www.bgs.ac.uk/science/landUseAndDevelopment/shallow_geohazards/whatisShrinkSwell.html [17/11, 2011].

BRITISH GEOLOGICAL SURVEY, 2013-last update, Lambeth Group. Available: http://www.bgs.ac.uk/science/landUseAndDevelopment/engineering_geology/lambeth_group.html [05/08, 2013].

BRITISH GEOLOGICAL SURVEY, 2013-last update, Gault formation. Available: http://www.bgs.ac.uk/science/landUseAndDevelopment/engineering_geology/GaultFormation.html [09/08, 2013].

BROOKS, R.H. and COREY, A.T., 1964. Hydraulic properties of porous media. *Hydrology Paper no.3, Civil Engineering Dep., Colorado State University, Fort Collins, Colo.*

BUMA, J. and DEHN, M., 1998. A method for predicting the impact of climate change on slope stability. *Environmental Geology,* **35**(2-3), pp. 190-196.

BURGER, C.A. and SHACKELFORD, C.D., 2001a. Evaluating dual porosity of pelletized diatomaceous earth using bimodal soil-water characteristic curve functions. *Canadian Geotechnical Journal,* **38**(1), pp. 53-66.

BURGER, C.A. and SHACKELFORD, C.D., 2001b. Soil-water characteristic curves and dual porosity of sand-diatomaceous earth mixtures. *Journal of Geotechnical and Geoenvironmental Engineering,* **127**(9), pp. 790-800.

CHANDLER, R.J. and SKEMPTON, A.W., 1974. The design of permanent cutting slopes in stiff fissured clays. *Geotechnique,* **24**(4), pp. 457-466.

CHEN, C.Y., 2007. Landslide characteristics and rainfall distribution in Taiwan, R. MCINNES, J. JAKEWAYS, H. FAIRBANK and E. MATHIE, eds. In: *Proceedings of the International Conference on Landslides and Climate Change*, 2007 2007, Taylor & Francis Group, pp. 35-39.

CHERTKOV, V.Y. and RAVINA, I., 2000. Shrinking-swelling phenomenon of clay soils attributed to capillary-crack network. *Theoretical and Applied Fracture Mechanics,* **34**(1), pp. 61-71.

CLARKE, D. and SMETHURST, J.A., 2010. Effect of climate change on cycles of wetting and drying in engineered clay slopes in England. *Quarterly Journal of Engineering Geology and Hydrogeology,* **43**, pp. 473-486.

CLARKE, G.R.T., HUGHES, D.A.B., BARBOUR, S.L. and SIVAKUMAR, V., 2006. The implications of predicted climate changes on the stability of highway geotechnical infrastructure: a case study of field monitoring of pore water pressure, 2006.

CLOKE, H.L., RENAUD, J.-., CLAXTON, A.J., MCDONNELL, J.J., ANDERSON, M.G., BLAKE, J.R. and BATES, P.D., 2003. The effect of model configuration on modelled hillslope-riparian interactions. *Journal of Hydrology,* **279**(1), pp. 167-181.

COLLISON, A., WADE, S., GRIFFITHS, J. and DEHN, M., 2000. Modelling the impact of rpedicted climate change on landslide frequency and magnitude in SE England. *Engineering Geology,* **55**(1), pp. 205-218.

CONTE, E., SILVESTRI, F. and TRONCONE, A., 2010. Stability analysis of slopes in soils with strain-softening behaviour. *Computers and Geotechnics,* **37**(5), pp. 710-722.

COSTA, S., KODIKARA, K. and THUSYANTHAN, N.I., 2008. Modelling of desiccation crack development in clay soils, *The 12th International Conference of the International Association for Computer Methods and Advances in Geomechanics*, 1-6 October, 2008 2008, IACMAG, pp. 1099-1107.

CRAIG, R.F., 2004. *Craig's soil mechanics.* 7th edn. London: Spon.

CRONEY, D., GREAT BRITAIN. DEPT. OF THE ENVIRONMENT. and H.M.S.O., 1977. *The design and performance of road pavements.* Department of the Environment : H.M.S.O.

DAVIES, O., ROUAINIA, M., GLENDINNING, S. and BIRKINSHAW, S.J., 2008a. Predicting seasonal shrink swell cycles within a clay cutting, E. ELLIS, H.S. YU, G. MCDOWELL, A. DAWSON and N. THOM, eds. In: *Proceedings of Advances in Transportation Geotechnics* 2008a, Taylor & Francis Group, pp. 481-486.

DAVIES, O.C., ROUAINIA, M. and GLENDINNING, S., 2008b. Numerical predictions of seasonal pore water pressure fluctuations using FLAC tp flow, D.G. TOLL, ed. In: *Unsaturated Soils: Advances in Geo-Engineering*, 2008 2008b, Taylor & Francis Group, pp. 817-822.

DAVIES, O., ROUAINIA, M., GLENDINNING, S. and BIRKINSHAW, S.J., 2008c. Assessing the influence of climate change on the progressive failure of a railway embankment, *The 12th International Conference of International Association for Computer Methods and Advances in Geomechanics*, 1-6 October 2008c.

DEHN, M. and BUMA, J., 1999. Modelling future landslide activity based on general circulation models. *Geomorphology,* **30**(1-2), pp. 175-187.

DEHN, M., BURGER, G., BUMA, J. and GASPARETTO, P., 2000. Impact of climate change on slope stability using expanded downscaling. *Engineering Geology,* **55**(3), pp. 193-204.

DIJKSTRA, T.A. and DIXON, N., 2010. Climate change and slope stability in the UK: challenges and approaches. *Quarterly Journal of Engineering Geology and Hydrogeology,* **43**, pp. 371-385.

DINGMAN, S.L., 2002. *Physical Hydrology.* 2nd edn. New Jersey: Prentice-Hall.

DIXON, N. and BROMHEAD, E.N., 1999. Depth-dependent permeability in London Clay measured using standpipe piezometer equilibration data. *Geotechnique,* **49**(5), pp. 651-660.

DIXON, N., DIJKSTRA, T.A., FORSTER, A. and CONNELL, R., 2006. Climate change impact forecasting for slopes (CLIFFS) in the built environment, 2006.

DIXON, N. and BROOK, E., 2007. Impact of predicted climate change on landslide reactivation: case study of Mam Tor, UK. *Landslides,* **4**(1), pp. 137-147.

DURNER, W., 1994. Hydraulic conductivity estimation for soils with heterogeneous pore structure. *Water Resources Research*, **30**(2), pp. 211-223.

ESCARIO, V. and SAEZ, J., 1986. The shear strength of partly saturated soils. *Geotechnique,* **36**(3), pp. 453-456.

EWEN, J., PARKIN, G. and O'CONNELL, P.E., 2000. SHETRAN: Distributed river basin flow and transport modelling system. *Journal of Hydrologic Engineering,* **5**(3), pp. 250-258.

FANG, H.Y., 1994. Cracking and fracture behavior of soil, L.E. VALLEJO and R.Y. LIANG, eds. In: *Fracture Mechanics Applied to Geotechnical Engineering*, 9-13 October 1994, pp. 102-117.

FAVRE, F., BOIVIN, P. and WOPEREIS, M.C.S., 1997. Water movement and soil swelling in a dry, cracked vertisol. *Geoderma,* **78**(1-2), pp. 113-123.

FIELD, A.P., 2005a. *Discovering statistics using SPSS: (and sex, drugs and rock'n'roll).* 2 edn. London: Sage.

FIELD, A.P., 2005b. *Effect sizes.* Available:
http://www.statisticshell.com/docs/effectsizes.pdf [07/03, 2014].

FIORUCCI, F., CARDINALI, M., CARLA, R., ROSSI, M., MONDIN, A.C., SANTURRI, L., ARDIZZONE, F. and GUZZETTI, F., 2011. Seasonal landslide mapping and estimation of landslide mobilization rates using aerial and satellite images. *Geomorphology,* **129**(1), pp. 59-70.

FREDLUND, D.G., 1993. *Soil mechanics for unsaturated soils.* New York ; Chichester: Wiley.

FREDLUND, D.G. and XING, A., 1994. Equations for the soil-water characteristic curve. *Canadian Geotechnical Journal,* **31**, pp. 521-532.

FREDLUND, D.G., VU, H.Q. and STIANSON, J., 2010a. Engineering protocols for the assessment of the net moisture flux at the ground surface. *Geotechnical Engineering Journal of the SEAGS & AGSSEA,* **41**(4), pp. 1-11.

FREDLUND, D.G., HOUSTON, S.L., NGUYEN, Q. and FREDLUND, M.D., 2010b. Moisture movement through cracked clay soil profiles. *Geotechnical and Geological Engineering,* **28**(6), pp. 865-888.

FREDLUND, D.G., SHENG, D. and ZHAO, J., 2011. Estimation of soil suction from the soil-water characteristic curve. *Canadian Geotechnical Journal,* **48**(2), pp. 186-198.

GAN, K.J. and FREDLUND, D.G., 1988. Multistage direct shear testing of unsaturated soils. *Geotechnical Testing Journal,* **11**(2), pp. 132-138.

GEERTSEEMA, M., EGGINTON, V.N., SCHWAB, J.W. and CLAGUE, J.J., 2007. Landslides and historic climate in northern British Columbia, R. MCINNES, J. JAKEWAYS, H. FAIRBANK and E. MATHIE, eds. In:*Proceedings of the International Conference on Landslides and Climate Change*, 2007 2007, Taylor & Francis Group, pp. 9-16.

GEO-SLOPE, 2007. *Vadose zone modelling with VADOSE/W 2007.* 3 edn. Calgary: GEO-SLOPE International Ltd.

GEO-SLOPE INTERNATIONAL LTD., 2010. Progressive failure of a cut in London Clay due to strain softening. *Banff Geotechnical Modelling Workshop,* , pp. 1-9

.

GERKE, H.H. and VAN GENUCHTEN, M.T., 1993. A dual-porosity model for simulating the preferential movement of water and solutes in structured porous media. *Water Resources Research,* **29**(2), pp. 305-319.

GERKE, H.H., 2006. Preferential flow descriptions for structured soils. *Journal of Plant Nutrition and Soil Science,* **169**(3), pp. 382-400.

GLENDINNING, S., ROUAINIA, M., HUGHES, P. and DAVIES, O., 2006. Biological and engineering impacts of climate on slopes (BIONICS): the first 18 months, *Proceedings of 10th IAEG International Congress*, 6-10 September 2006 2006, The Geological Society of London, pp. 1-12.

GLENDINNING, S., HALL, J. and MANNING, L., 2009a. Asset management strategies for infrastructure embankments. *Proceedings of the Institution of Civil Engineers: Engineering Sustainability,* **162**(2), pp. 111-120.

GLENDINNING, S., LOVERIDGE, F., STARR-KEDDLE, R.E., BRANSBY, M.F. and HUGHES, P.N., 2009b. Role of vegetation in sustainability of infrastructure slopes. Proceedings of the Institution of Civil Engineers Engineering Sustainability, 162(ES2), pp. 101-110.

GORDON, C., COOPER, C., SENIOR, C.A., BANKS, H., GREGORY, J.M., JOHNS, T.C., MITCHEL, J.F.B. and WOOD, R.A., 2000. The simulation of SST, sea ice extents and ocean heat transports in a version of the Hadley Centre coupled model without flux adjustments. *Climate Dynamics,* **16**(2), pp. 147-168.

GRECO, R., 2002. Preferential flow in macroporous swelling soil with internal catchment: model development and applications. *Journal of Hydrology,* **269**(3-4), pp. 150-168.

GREEN, R.E. and COREY, J.C., 1971. Calculation of hydraulic conductivity: a further evaluation of some predictive methods. *Soil Science Society of America Proceedings,* **35**, pp. 3-8.

GREENWOOD, J.R., NORRIS, J.E. and WINT, J., 2004. Assessing the contribution of vegetation to slope stability. *Proceedings of the Institution of Civil Engineers: Geotechnical Engineering,* **157**(4), pp. 199-207.

GREVE, A., ANDERSON, M.S. and ACWORTH, A.I., 2010. Investigations of soil cracking and preferential flow in a weighing lysimeter filled with cracking clay soil. *Journal of Hydrology,* **393**(1), pp. 105-113.

HANSEN, J., RUEDY, R., SATO, M. and LO, K., 2010. *Global surface temperature change.* New York, USA: NASA Goddard Institute for Space Studies.

HENDRIKS, M.R., 2010. *Introduction to physical hydrology.* 1st edn. New York: Oxford University Press.

HIGHWAYS AGENCY, 2013. *Repair costs, 2003-2013 - Freedom of Information Request - Available at* http://www.highways.gov.uk/foi/repair-costs-2003-2013/.

HOUGH, M.N. and JONES, R.J.A., 1997. The United Kingdom Meteorological Office rainfall and evaporation calculation system: MORECS version 2.0 - an overview. *Hydrology and Earth System Sciences,* **1**(2), pp. 227-239.

HU, L.B., HUECKEL, T., PERON, H. and LALOUI, L., 2008. Modeling evaporation, shrinkage and cracking of desiccating soils, *The 12th International Conference of the International Association for Computer Methods and Advances in Geomechanics*, 1-6 October, 2008 2008, IACMAG, pp. 1083-1090.

HUGHES, D., SIVAKUMAR, V., GLYNN, D. and CLARKE, G., 2007. A case study: delayed failure of a deep cutting in lodgement till. *Proceedings of the Institution of Civil Engineers: Geotechnical Engineering,* **160**(1), pp. 193-202.

HULME, M. and BARROW, E.C., 1997. *Climates of the British Isles present, past and future.* 1st edn. London: Routledge.

HULTEN, C., ANDERSSON-SKOLD, Y., OTTOSSON, E., EDSTAM, T. and JOHANSSON, A., 2007. Case studies of landslide risk due to climate change in Sweden, R. MCINNES, J. JAKEWAYS, H. FAIRBANK and E. MATHIE, eds. In: *Proceedings of the International Conference on Landslides and Climate Change*, 21-24 May 2007 2007, Taylor & Francis, pp. 149-157.

IBM, IBM SPSS Statistics - Predictive Analytics Software. Available: http://www-01.ibm.com/software/uk/analytics/spss/products/statistics/ [24/08, 2013].

INCI, G., 2008. Numerical modeling of desiccation cracking in compacted soils, *The 12th International Conference of the International Association for Computer Methods and Advances in Geomechanics*, 1-6 October, 2008 2008, IACMAG, pp. 1116-1125.

ITASCA, 2002. Flac - Fast Lagrangian analysis of continua - Version 4.0 users guide. Itasca Consulting Group: Minneapolis, USA.

JONES, P.D., HARPHAM, C., KILSBY, C., GLENIS, V. and BURTON, A., 2010. *UK climate projections science report: projections of future daily climate for the UK from the weather generator - available at* http://ukclimateprojections.defra.gov.uk/22588. UK Climate Projections.

KAWAGOE, S., KAZAMA, S. and SARUKKALIGE, P.R., 2009. Assessment of snowmelt triggered landslide hazard and risk in Japan. *Cold Regions Science and Technology,* **58**(3), pp. 120-129.

KHALILI, N. and ZARGARBASHI, S., 2010. Influence of hydraulic hysteresis on effective stress in unsaturated soils. *Geotechnique,* **60**(9), pp. 729-734.

KILSBY, C., JONES, P.D., BURTON, A., FORD, A.C., FOWLER, H.J., HARPHAM, C., JAMES, P., SMITH, A. and WILBY, R.L., 2007. A daily weather generator for use in climate change studies. *Environmental Modelling & Software,* **22**(12), pp. 1705-1719.

KOHNE, J.M., KOHNE, S. and GERKE, H.H., 2002. Estimating the hydraulic functions of dual-permeability models from bulk soil data. *Water Resources Research,* **38**(7), pp. 1121-1132.

KOVACEVIC, N., POTTS, D.M. and VAUGHAN, P.R., 2001. Progressive failure in clay embankments due to seasonal climate changes, *Proceedings of the 5th International Conference on Soil Mechanics and Geotechnical Engineering* 2001, AA Balkema, pp. 2127-2130.

KOVACEVIC, K., HIGHT, W. and POTTS, D.M., 2004. Temporary slope stability in London Clay - back analyses of two case histories, R.J. JARDINE, D.M. POTTS and K.G. HIGGINS, eds. In: *Proceedings of Advances in Geotechnical Engineering: The Skempton Conference*, 29-31 March 2004 2004, Thomas Telford Publishing, pp. 842-855.

KUNA, B.R., WALSH, K.D., HOUSTON, S.L., ZAPATA, C. and WELFERT, B., 2013. Full scale test of periodic irrigation infiltration in a cracked and intact clay slope, C.L. MEEHAN, D. PRADEL, M.A. PANDO and J.F. LABUZ, eds. In: *Proceedings of Geo-Congress 2013: Stability and Performance of Slopes and Embankments III*, 3-7 March 2013 2013, ASCE, pp. 828-837.

KUTILEK, M. and NIELSEN, D.R., 1994. *Soil hydrology.* Cremlingen-Destedt: Catena.

LEONG, E.C. and RAHARDJO, H., 1997. Review of soil-water characteristic curve equations. *Journal of Geotechnical and Geoenvironmental Engineering,* **123**(12), pp. 1106-1117.

LEROUEIL, S., 2001. Natural slopes and cuts: movement and failure mechanisms. *Geotechnique,* **51**(3), pp. 197-243.

LI, J.H. and ZHANG, L.M., 2010. Geometric parameters and REV of a crack network in soil. *Computers and Geotechnics,* **37**(4), pp. 466-475.

LI, J.H. and ZHANG, L.M., 2011. Study of desiccation crack initiation and development at ground surface. *Engineering Geology,* **123**(4), pp. 347-358.

LI, J.H., ZHANG, L.M. and LI, X., 2011. Soil-water characteristic curve and permeability function for unsaturated cracked soil. *Canadian Geotechnical Journal,* **48**(7), pp. 1010-1031.

LIU, H.H. and BODVARSSON, G.S., 2001. Constitutive relations for unsaturated flow in a fracture network. *Journal of Hydrology,* **252**(1), pp. 16-25.

LIU, H.H., BODVARSSON, G.S. and FINSTERLE, S., 2002. A note on unsaturated flow in two-dimensional fracture networks. *Water Resources Research,* **38**(9), pp. 1176-1185.

LOVERIDGE, F., SPINK, T.W., O'BRIEN, A.S., BRIGGS, K.M. and BUTCHER, D., 2010. The impact of climate and climate change on infrastructure slopes, with particular reference to southern England. *Quarterly Journal of Engineering Geology and Hydrogeology,* **43**, pp. 461-472.

LU, N. and LIKOS, W.J., 2004. *Unsaturated Soil Mechanics.* John Wiley & Sons.

MAATOUK, A., LEROUEIL, S. and LA ROCHELLE, P., 1995. Yielding and critical state of a collapsible unsaturated silty soil. *Geotechnique,* **45**(3), pp. 465-477.

MALET, J.-., REMAITRE, A., MAQUAIRE, O., DURAND, Y., ETCHEVERS, P., GUYOMARC'H, G., DEQUE, M. and VAN BEEK, L.P.H., 2007. Assessing the influence of climate change on the activity of landslides in the Ubaye Valley, R. MCINNES, J. JAKEWAYS, H. FAIRBANK and E. MATHIE, eds. In: *Proceedings of the International Conference on Landslides and Climate Change, Ventor, Isle of Wight*, 21-24 May 2007, pp. 195-205.

MALLANT, D., TSENG, P.H., TORDE, N., TIMMERMAN, A. and FEYEN, J., 1997. Evaluation of multimodal hydraulic function in characterizing a heterogeneous field soil. *Journal of Hydrology,* **195**, pp. 172-199.

MET OFFICE, 06/11/12, 2012-last update, The wet autumn of 2000. Available: http://www.metoffice.gov.uk/climate/uk/interesting/autumn2000.html2011.

MET OFFICE, 21/01/13, 2013-last update, Statistics for December and 2012 - Is the UK getting wetter? Available: http://www.metoffice.gov.uk/news/releases/archive/2013/2012-weather-statistics[05/08, 2013].

MET OFFICE, , Past weather events. Available: http://www.metoffice.gov.uk/climate/uk/interesting/#y2000 [14/11, 2011].

MILLINGTON, R.J. and QUIRK, J.P., 1961. Permeability of porous solids. *Trans. Faraday Soc.,* **57**, pp. 1200-1206.

MILLS, A.J., MOORE, R., CAREY, J.M. and TRINDER, S.K., 2007. Recent lanslide impacts in Scotland: possible evidence of climate change? R. MCINNES, J. JAKEWAYS, H. FAIRBANK and E. MATHIE, eds. In: *International Conference on Landslides and Climate Change*, 21-24 May 2007, Taylor & Francis, pp. 99-106.

MURPHY, J.M., SEXTON, D.M.H., JENKINS, G.J., BOORMAN, P.M., BOOTH, B.B.B., BROWN, C.C., CLARK, R.T., MA, W., BROWN, S.J., HOWARD, T.P., HUMPHREY, K.A., MCCARTHY, M.P., MCDONALD, R.E., STEPHENS, A., WALLACE, C., WARREN, R., WILBY, R. and WOOD, R.A., 2009. *UK Climate Projections Science Report: Climate Change Projections.* Exeter: Met Office Hadley Centre.

NAHLAWI, H. and KODIKARA, K., 2006. Laboratory experiments on desiccation cracking of thin soil layers. *Geotechnical and Geological Engineering,* **24**(6), pp. 1641-1664.

NAKIĆENOVIĆ, N., 2000. *IPCC Special Report on Emissions Scenarios.* Cambridge University Press.

NAM, S., GUTIERREZ, M., DIPLAS, P., PETRIE, J., WAYLLACE, A. and LU, N., 2009. Comparison of testing techniques and models for establishing the SWCC of riverbank soils. *Engineering Geology,***110**(1), pp. 1-10.

NANDAGIRI, L. and PRASAD, R., 1996. Field evaluation of unsaturated hydraulic conductivity models and parameter estimation from retention data. *Journal of Hydrology,* **179**(1-4), pp. 197-205.

NATIONAL AERONAUTICS AND SPACE ADMINISTRATION, 2010-last update, Research news - 2009: second warmest year on record; end of warmest decade. Available:http://www.giss.nasa.gov/research/news/20100121/2010].

NG, C.W.W. and SHI, Q., 1998. Influence of rainfall intensity and duration on slope stability in unsaturated soils. *Quarterly Journal of Engineering Geology and Hydrogeology,* **31**(1), pp. 105-113.

NOVAK, V., 1999. Soil-crack characteristics - estimation methods applied to heavy soils in the NOPEX area. *Agricultural and Forest Meteorology,* **98-99**, pp. 501-507.

NOVAK, V., SIMUNEK, J. and VAN GENUCHTEN, M.T., 2000. Infiltration of water into soil with cracks. *Journal of Irrigation and Drainage Engineering,* **126**(1), pp. 41-47.

NYAMBAYO, V.P., POTTS, D.M. and ADDENBROOKE, T.I., 2004. The influence of permeability on the stability of embankments experiencing seasonal cyclic pore water pressure changes, R.J. JARDINE, D.M. POTTS and K.G. HIGGINS, eds. In: *Proceedings of Advances in Geotechnical Engineering: The Skempton Conference*, 29-31 March 2004 2004, Thomas Telford Publishing, pp. 898-910.

O'BRIEN, A.S., ELLIS, E.A. and RUSSELL, D., 2004. Old railway embankment clay fill - laboratory experiments, numerical modelling and field behaviour, R.J. JARDINE, D.M. POTTS and K.G. HIGGINS, eds. In: *Proceedings of Advances in Geotechnical Engineering: The Skempton Conference*, 29-31 March 2004 2004, Thomas Telfrod Publishing, pp. 911-921.

OH, W.T. and VANAPALLI, S.K., 2010. Influence of rain infiltration on the stability of compacted soil slopes. *Computers and Geotechnics,* **37**(5), pp. 649-657.

OMIDI, G.H., THOMAS, J.C. and BROWN, K.W., 1996. Effect of desiccation cracking on the hydraulic conductivity of compacted clay liner. *Water, Air, and Soil Pollution,* **89**(1-2), pp. 91-103.

PARSONS, A.W. and PERRY, J., 1985. Slope stability problems in ageing highway earthworks, *Proceedings of the Symposium on Failures in Earthworks*, 6-7 March 1985 1985, Thomas Telford Limited, pp. 63-78.

PENMAN, H.L., 1948. Natural evaporation from open water, bare soil and grass. *Proceedings of the Royal Society of London. Series A, Mathematical and Physical Sciences,* **193**(1032), pp. 120-145.

PENNINGTON, C. and HARRISON, A., 2013. 2012 Landslide year? *Geoscientist,* **23**(5), pp. 10-15.

PERRY, J., PEDLEY, M. and REID, M., 2003a. *Infrastructure embankments - conidition appraisal and remedial treatment.* C592. London: CIRIA.

PERRY, J., PEDLEY, M. and BRADY, K., 2003b. *Infrastructure cuttings - condition appraisal and remedial treatment.* C591. London: CIRIA.

PETLEY, D., 2012. Global patterns of loss of life from landslides. *Geology,* **40**(10), pp. 927-930.

POPE, V.D., GALLANI, M.L., ROWNTREE, P.R. and STRATTON, R.A., 2000. The impact of new physical parametrizations in the Hadley Centre climate model: HadAM3. *Climate Dynamics,* **16**(2), pp. 123-146.

POTTS, D.M., KOVACEVIC, K. and VAUGHAN, P.R., 1997. Delayed collapse of cut slopes in stiff clay. *Geotechnique,* **47**(5), pp. 953-982.

RAHARDJO, H., NIO, A.S., LEONG, E.C. and SONG, N.Y., 2010. Effects of groundwater table position and soil properties on stability of slope during rainfall. *Journal of Geotechnical and Geoenvironmental Engineering*, **136**(11), pp. 1555-1564.

RAYHANI, M.H.T., YANFUL, E.K. and FAKHER, A., 2007. Desiccation-induced cracking and its effect on the hydraulic conductivity of clayey soils from Iran. *Canadian Geotechnical Journal,* **44**(3), pp. 276-283.

RAYHANI, M.H.T., YANFUL, E.K. and FAKHER, A., 2008. Physical modeling of desiccation cracking in plastic soils. *Engineering Geology,* **97**(1), pp. 25-31.

RICHARDS, L.A., 1931. Capillary conduction of liquids through porous mediums. *Physics,* **1**(5), pp. 318-333.

RIDLEY, A.M., VAUGHAN, P.R., MCGINNITY, B. and BRADY, K., 2004a. Pore pressure measurements in infrastructure embankments, *Advances in Geotechnical Engineering: The Skempton Conference* 2004, Thomas Telford Publishing, pp. 922-932.

RIDLEY, A.M., MCGINNITY, B. and VAUGHAN, P.R., 2004b. Role of pore water pressures in embankment stability. *Proceedings of the Institution of Civil Engineers: Geotechnical Engineering,* **157**(1), pp. 193-198.

ROMKENS, M.J.M. and PRASAD, S.N., 2006. Rain infiltration into swelling/shrinking/cracking soils. *Agricultural Water Management,* **86**, pp. 196-205.

ROSCOE, K.H., SCHOFIELD, A.N. and WROTH, C.P., 1958. On the yielding of soils. *Geotechnique,* **8**(1), pp. 22-53.

ROUAINIA, M., DAVIES, O.C., O'BRIEN, T. and GLENDINNING, S., 2009. Numerical modelling of climate effects on slope stability. *Proceedings of the Institution of Civil Engineers, Engineering Sustainability,* **162**(2), pp. 81-89.

SKEMPTON, A.W., 1964. Long-term stability of clay slopes. *Geotechnique,* **14**(2), pp. 77-101.

SKEMPTON, A.W., 1970. First-time slides in over-consolidated clays. *Geotechnique,* **20**(3), pp. 320-324.

SKEMPTON, A.W., 1977. Slope stability of cuttings in brown London Clay, *Proceedings of 9th International Conference on Soil mechanics and Foundation Engineering, Tokyo* 1977, pp. 261-270.

SKEMPTON, A.W., 1996. Embankments and cuttings on the early railways. *Proceedings of the Institution of Civil Engineers: Construction History,* **11**, pp. 33-49.

SMETHURST, J.A., 2003. *The use of discrete piles for infrastructure slope stabilisation*, University of Southampton.

SMETHURST, J.A., CLARKE, D. and POWRIE, W., 2006. Seasonal changes in pore water pressure in a grass-covered cut slope in London Clay. *Geotechnique,* **56**(8), pp. 523-537.

SMETHURST, J.A., CLARKE, D. and POWRIE, W., 2012. Factors affecting the seasonal variation in soil water content and pore water pressures within a lightly vegetated clay slope. *Geotechnique,* **62**(5), pp. 429-446.

SMITH, I.M. and GRIFFITHS, D.V., 2004. *Programming the finite element method.* 4th edn. Hoboken, NJ: Wiley.

SOLOMON, S., QIN, D., MANNING, M., CHEN, Z., MARQUIS, M., AVERYT, K.B., TIGNOR, M. and MILLER, H.L., 2007. *Contribution of working group I to the fourth assessment report of the Intergovernmental Panel on Climate Change 2007.* Cambridge, United Kingdom: Cambridge University Press.

STANKOVICH, J.M. and LOCKINGTON, D.A., 1995. Brooks-Corey and van Gencuhten soil-water-retention models. *Journal of the Irrigation and Drainage Division, Proceedings of the American Society of Civil Engineers,* **121**(1), pp. 1-7.

STERPI, D., 1999. An analysis of geotechnical problems involving strai softening effects. *International Journal for Numerical and Analytical Methods in Geomechanics,* **23**(13), pp. 1427-1454.

TACHER, L. and BONNARD, C., 2007. Hydromechanical modelling of a large landslide considering climate change conditions, R. MCINNES, J. JAKEWAYS, H. FAIRBANK and E. MATHIE, eds. In: *Proceedings of the International Conference on Landslides and Climate Change, Ventor, Isle of Wight*, 21-24 May 2007 2007, Taylor & Francis, pp. 131-141.

TAKE, W.A. and BOLTON, M.D., 2011. Seasonal ratcheting and softening in clay slopes, leading to first-time failure. *Geotechnique,* **61**(9), pp. 757-769.

TANG, C.S., CUI, Y.J., SHI, B., TANG, A.M. and LIU, C., 2011. Desiccation and cracking behaviour of clay layer from slurry slate under wetting-drying cycles. *Geoderma,* **166**(1), pp. 111-118.

THE INTERNATIONAL DISASTER DATABASE, [Homepage of CRED], [Online]. Available: http://www.emdat.be/2010].

TRATCH, D.J., WILSON, G.W. and FREDLUND, D.G., 1995. An introduction to analytical modelling of plant transpiration for geotechnical engineers, *48th Canadian Geotechnical Conference* 1995, pp. 771-780.

UK CLIMATE PROJECTIONS, 02/04/12, 2012-last update, About weather generator 2.0. Available: http://ukclimateprojections.defra.gov.uk/22580 [07/24, 2013].

UK CLIMATE PROJECTIONS, 11/03/2012, 2012-last update, Online climate change projections report 4.4.1 PDFs and emissions scenarios. Available: http://ukclimateprojections.defra.gov.uk/22954[29/07/2012, 2012].

UK CLIMATE PROJECTIONS, 03/05/12, 2012-last update, UK-wide key findings. Available: http://ukclimateprojections.defra.gov.uk/21730 [05/08, 2013].

UK CLIMATE PROJECTIONS, 05/07/12, 2012-last update, Why are there no estimates of wind in the weather generator but PET (which requires wind) is included?. Available:http://ukclimateprojections.defra.gov.uk/22701 [27/08, 2013].

VAN ASCH, T.W.J., BUMA, J. and VAN BEEK, L.P.H., 1999. A view on some hydrological triggering systems in landslides. *Geomorphology,* **30**(1), pp. 25-32.

VAN DAM, J.C., 2000. Simulation of field-scale water flow and bromide transport in a cracked clay soil. *Hydrological Processes,* **14**(6), pp. 1101-1117.

VAN GENUCHTEN, M.T., 1980. A closed-form equation for predicting the hydraulic conductivity of unsaturated soils. *Soil Science Society of America Journal,* **44**, pp. 892-898.

VAN GENUCHTEN, M.T. and NIELSEN, D.R., 1985. On describing and predicting the hydraulic properties of unsaturated soils. *Annales Geophysicae,* **3**(5), pp. 615-628.

VAUGHAN, P.R. and WALBANCKE, H.J., 1973. Pore pressure changes and the delayed failure of cutting slopes in overconsolidated clay. *Geotechnique,* **23**(4), pp. 531-539.

VAUGHAN, P.R., 1994. Assumption, prediction and reality in geotechnical engineering. *Geotechnique,* **44**(4), pp. 573-609.

VAUGHAN, P.R., KOVACEVIC, K. and POTTS, D.M., 2004. Then and now: some comments on the design and analysis of slopes and embankments, R.J. JARDINE, D.M. POTTS and K.G. HIGGINS, eds. In:*Advances in Geotechnical Engineering: The Skempton Conference*, 29-31 March 2004, Thomas Telford Publishing, pp. 241-290.

VOGEL, H.J., HOFFMAN, H. and ROTH, K., 2005. Studies of crack dynamics in clay soil I. Experimental methods, results, and morphological quantification. *Geoderma,* **125**(3-4), pp. 213-223.

VON TERZAGHI, K., 1936. The shearing resistance of saturated soils and the angles between the planes of shear, *First International Conference on Soil Engineering and Foundation Engineering* 1936, Harvard University, pp. 54-56.

WARRICK, A.W., LOMEN, D.O. and YATES, S.R., 1985. A gerneralized solution to infiltration. *Soil Science Society of America Journal,* **49**(1), pp. 34-38.

WASOWSKI, J., CASARANO, D. and LAMANNA, C., 2007. Is the current landslide in the Daunia region (Italy) controlled by climate or land use change? R. MCINNES, J. JAKEWAYS, H. FAIRBANK and E. MATHIE, eds. In: *Proceedings of the International Conference on Landslides and Climate Change, Ventor, Isle of Wight*, 21-24 May 2007 2007, pp. 41-49.

WILSON, G.W., FREDLUND, D.G. and BARBOUR, S.L., 1994. Coupled soil-atmosphere modelling for soil evaporation. *Canadian Geotechnical Journal,* **31**(2), pp. 151-161.

ZAPATA, C., HOUSTON, W., HOUSTON, S.L. and WALSH, K.D., 2000. Soil-water characteristic curve variability, C.D. SHACKELFORD, S.L. HOUSTON and N.N. CHANG, eds. In: , 5 - 8 August 2000 2000, American Society of Civil Engineers, pp. 84-124.

ZHANG, L. and FREDLUND, D.G., 2003. Characteristics of water retention curves for unsaturated fractured rocks, *Second Asian Conference on Unsaturated Soils*, 15-17 April 2003, pp. 425-428.

ZHANG, L. and CHEN, Q., 2005. Predicting bimodal soil-water characteristic curves. *Journal of Geotechnical and Geoenvironmental Engineering,* **131**(5), pp. 666-670.

ZHANG, L.L., ZHANG, J., ZHANG, L.M. and TANG, W.H., 2011. Stability analysis of rainfall-induced slope failure: a review. *Proceedings of the Institution of Civil Engineers: Geotechnical Engineering,***164**(5), pp. 299-316.

ZIELINSKI, M., ROMERO, E., SANCHEZ, M. and SENTENAC, P., 2011. Assessment of water retention behaviour in compacted fills. *Proceedings of the Institution of Civil Engineers: Geotechnical Engineering,* **164**(2), pp. 139-148.